BURNING VELOCITY AND THE INFLUENCE OF FLAME STRETCH

Simon Crispin Taylor BSc CPhys MInstP

Submitted in accordance with the requirements for the degree of Doctor of Philosophy

The University of Leeds
Department of Fuel and Energy
September 1991

ABSTRACT

A new technique is presented for determining burning velocities and stretch effects in laminar flames, and applied to a range of fuel/air mixtures. The speeds of expanding spherical flames, measured by high-speed schlieren cine-photography, are shown to vary with flame radius. A simple phenomenological model has been developed to analyse the data and obtain the one-dimensional flame speed by extrapolation to infinite radius.

The validity of the simple model has been tested by using it to analyse the results of detailed simulations of expanding spherical flames. The true one-dimensional flame speeds in this case are known from planar flame modelling using the same kinetic scheme. The simple model predicted flame speeds within 2% of the true values for hydrogen/air mixtures over most of the stoichiometric range. This demonstrates that the extrapolation procedure is sound and will produce reliable results when applied to experimental data.

Since the flame speeds derived from experiments are one-dimensional values, multiplying them by the density ratio gives one-dimensional burning velocities (S_u^o). Maximum burning velocities of hydrogen, methane, ethane, propane and ethylene mixtures with air were 2.85 ms^{-1}, 0.37 ms^{-1}, 0.41 ms^{-1}, 0.39 ms^{-1} and 0.66 ms^{-1} respectively. These are considerably smaller than most burner-derived values. The discrepancies can be explained by flow divergence and stretch effects perturbing burner measurements.

The rate at which the measured flame speed approaches its limiting value depends on flame thickness and flame stretch. By subtracting the flame thickness term, the influence of flame stretch, expressed as the Markstein length, can be derived. Again values are given across the whole stoichiometric range of all fuels listed above, and form the most complete set of Markstein lengths reported to date. The Markstein lengths are negative in lean hydrogen and methane and in rich ethane and propane mixtures: this means that stretch increases the burning rate. They are positive in all other mixtures, showing that stretch decreases the burning rate. The results are in line with predictions based on Lewis number considerations.

An alternative method of deriving one-dimensional burning velocities and Markstein lengths has been investigated. Burning velocities were measured at different stretch rates in flames in stagnation-point flow. Particle tracking was used to derive burning velocities referred to the hot side of the flame from the upstream values. The two

burning velocities extrapolated to different one-dimensional values, both of which differed slightly from the expanding flame results. The suggested reason is that the upstream velocity gradient is not an accurate measure of the stretch experienced by the flame. Markstein lengths were consistent with those from the expanding flame method but the uncertainties were much larger. The method in its present form is therefore useful qualitatively but not quantitatively.

To Frances, Michael and Jessica

ACKNOWLEDGMENTS

I would like to thank my supervisors, Professor Alan Williams of the University of Leeds and Dr. David Smith of the London Research Station, British Gas, for their support, advice and encouragement during the period of this research.

Thanks are due to Dr. Chris Robinson for supplying the hydrocarbon oxidation scheme and for calculating pressure-dependent reaction rates, to Pierre Laugerette for printing Figures 6 and 12, and to the Photographic Section of Watson House Research Station, British Gas, for printing Figure 7.

I would also like to thank present and former members of the Combustion Group at the London Research Station for many fruitful discussions on flames in general and on burning velocity and stretch in particular.

Finally, my thanks go to my wife, Frances, and my children, Michael and Jessica, to whom this work is dedicated. Their help and support, particularly during the writing-up period, were much appreciated. Special mention must go to my children's ability to take my mind off flames so as to concentrate on really important matters like whether whales have teeth and which dress Lucy Teddy should wear. As a means of keeping a sense of proportion, this could not be bettered.

CONTENTS

List of Tables

List of Figures

Nomenclature

A	Area
b	Flame relaxation parameter
B_k	Pre-exponential factor for reaction k
c_p	Specific heat (per unit mass) at constant pressure
D_{ij}	Binary diffusion coefficient for species i and j
$D_{T,i}$	Thermal diffusion coefficient for species i
$\mathbf{e}$	Unit vector in curvilinear coordinate system
E_k	Activation energy of reaction k
$\mathbf{f}$	Body force
g_x	Curvilinear coordinate scale factor in the x-direction
h	Coefficient of radiant emission
h_i	Enthalpy per unit mass of species i
k	Density parameter, reaction rate
ℓ	Stretch parameter = $2\sigma L$
Le	Lewis number
L	Markstein Length determined in the present work
$\mathscr{L}$	Markstein length of Clavin and Joulin
m	Total mass flow rate
M	Number of reactions, mass flux (mass flow rate per unit area)
M_r	Mass burning rate (= mass flux at the reference surface)
n	Number of moles
$\mathbf{n}$	Unit normal vector
N	Number of chemical species
p	Pressure
$\mathbf{q}$	Heat flux vector
q	Heat of reaction (energy released per unit mass of reactant mixture)
Q_C	Heat conducted by unit area of flame
Q_R	Heat released by reaction per unit area of flame
r	Radius
R	Molar gas constant, radius
s_x	Physical distance in the x-direction
S_u°	One-dimensional burning velocity
S_b°	One-dimensional ("limiting") flame speed
SS_b°	Uncertainty in S_b°
$S_{u,r}$	"Stretched" burning velocity defined as M_r/ρ_u
t	Time
T	Temperature

u Internal energy per unit mass

$\mathbf{v}, \mathbf{V}$ Gas velocity

$\mathbf{V}_i$ Diffusion velocity of species i

v, V Gas speed

V Volumetric flow rate

w Reaction rate (mass produced by chemical reactions per unit volume per unit time)

W_i Molecular weight of species i

x Cartesian coordinate

X Mole fraction

y Cartesian coordinate, independent inner variable

Y Mass fraction

z Cartesian coordinate

Greek

α Temperature rise divided by final temperature

α_k Temperature exponent for reaction k

β Zel'dovich number

Γ Dimensional flame stretch

δ Flame thickness

ϵ Emissivity

ϵ_i Mass flux fraction for species i

η Stretched inner variable, radiant heat loss coefficient, coefficient of viscosity

κ Coefficient of bulk viscosity, dimensionless flame stretch

λ Thermal conductivity

Λ Burning rate eigenvalue

μ Coefficient of shear viscosity, mass

ν' Stoichiometric coefficient for species i appearing as a reactant in reaction k

ν'' Stoichiometric coefficient for species i appearing as a product in reaction k

ξ Dimensionless distance variable

ρ Density

σ Density ratio ($= \rho_b/\rho_u$), Stefan-Boltzmann constant

τ Dimensionless temperature

ϕ Cylindrical curvilinear coordinate, equivalence ratio

χ Constant of proportionality between emissivity and radius

ω Dimensionless reaction rate

Subscripts

ad	Adiabatic
b	Burnt
dil	Dilatational contribution (to total stretch rate)
eff	Effective value
ext	Extensional contribution (to total stretch rate)
G	Gas
M	Mass diffusion zone
r	Reference surface
R	Reaction zone
rad	Radiant
$resid$	Residual
s	Sphere
t	Tangential component
T	Thermal diffusion zone
u	Unburnt

Superscripts

o	One-dimensional (1-D)
f	Heat of formation
T	Transpose

Chapter 1

INTRODUCTION

It is difficult to define flames precisely[1], but a dictionary definition[2] of flames as "gases undergoing chemical reaction with evolution of heat" covers the essential points. One might add that the reaction is localized, that light is usually produced and that the reactants need not be gases (although they are in most cases).

Flames can be produced in two essentially different ways depending upon how the reactants are brought together. In one, the reactants (usually fuel and air) are supplied separately and the flame forms where they meet. The combustion processes are then mainly determined by the rates of diffusion of fuel and air. Candle flames, fires and the flame on a Bunsen burner when the air hole is closed are examples of such nonpremixed or "diffusion" flames.

Flames can also be produced in a mixture of the reactants. Such premixed flames have an altogether different character from nonpremixed flames. They are often called combustion waves, and they do indeed have the attributes of waves[3], in particular the property of propagating in a direction normal to themselves at a (roughly) constant speed. The archetypal premixed flame is that formed on a Bunsen burner when the air hole is fully open. The blue inner cone is a region of high temperature and intense chemical reaction which is characteristic of this type of combustion.

Both diffusion and premixed flames are used in combustion equipment for water and space heating, industrial processes, transport and electricity generation. But while the design of equipment to use diffusion flames is simple, such flames produce large amounts of pollution (particularly soot) and are not easily controlled. There has therefore been a move towards the use of premixed flames.

Flames can be laminar or turbulent. Studies of laminar flames are relevant to both: provided the turbulence intensity is not too great, turbulent flames behave like perturbed laminar ones.

It follows that a study of the detailed chemistry of laminar premixed flames will provide information which is applicable to practically all premixed flames, whether

laminar or turbulent. Such studies provide insights into such flame properties as heat release rates, flammability limits, propagation rates, quenching, and emissions of nitrogen oxides, carbon monoxide, soot and other pollutants. Flame chemistry is commonly studied by performing computer simulations of laminar, one-dimensional flames. Complex chemical kinetic reaction schemes are developed for use in such simulations, and the results are compared with experiments on laminar flames. The production of accurate experimental data on laminar premixed flames therefore plays a key role in the process of understanding a large range of flames.

One distinguishing feature of laminar premixed flames is that they have a characteristic propagation rate, commonly called the burning velocity. Flames are complex systems, and no satisfactory methods exist of predicting this property. In principle the computer models described above can be used, but the chemical kinetic data used in such models are not sufficiently well known for the predictions to be used with confidence. It is more usual to use measured burning velocities to validate kinetic schemes. Since burning velocities are used in many areas of combustion science (e.g. burner design and explosion prediction), the only alternative is to measure them. Scientists have been performing such determinations for over a century.

Over the last forty years or so, there has been a gradual realization that flow nonuniformities or flame curvature can change the propagation rate. Such effects have come to be known as flame stretch. If full information about flame behaviour is required, it is therefore necessary to determine both the propagation rate of a flame and the influence of flame stretch.

The work described in this thesis is an experimental and modelling study of the propagation rates of laminar flames in a range of fuel/air mixtures, and the way these rates change when the flames are stretched.

The background to the work and the reasons for doing it are explained in this chapter. A brief historical survey of both the definition and the measurement of burning velocity is presented in the first section. The aim is to show that the concept of burning velocity has developed along with the methods used to measure it.

In the second section, the burning velocity of a fuel/air mixture is defined in terms of a one-dimensional flame. The implications of this one-dimensional definition for measurements in real flames are discussed, along with the need for an extension of the definition to cover flames which are not one-dimensional.

The organization of the thesis is described in the final section.

1.1 A BRIEF HISTORY OF BURNING VELOCITY

In this section we trace the history of the definition and measurement of burning velocity in order to provide some background for the present work. References 4 and 5 were helpful for locating early papers and putting work in context. The development of the subject is illustrated by reference to a few papers which either introduced new concepts or were influential in propagating old ones. Many of the methods described below will be reconsidered in Chapter 7 in the light of the findings of the present work.

The first recorded estimate of a burning rate of a flame appears to have been that published in 1815 by Sir Humphrey Davy[6] in his work on the development of the miners' safety lamp:

> "In exploding a mixture of 1 part of gas from the distillation of coal, and 8 parts of air in a tube of a quarter of an inch [6 mm] in diameter, and a foot [300 mm] long, more than a second was required before the flame reached from one end of the tube to the other: and this gas... consisted of carburetted hydrogen gas mixed with some olefiant gas."

In modern terms, Davy's result is that the flame speed of methane containing some unspecified amount of ethylene mixed with 8 parts of air is less than 0.3 ms^{-1}. If the far end of the tube was closed then the speed was relative to the cold gas and approximates to a burning velocity. The low value for the speed supports this idea. There is, however, no indication that Davy measured any flame speeds systematically or expected the flame speed for a given mixture to be constant.

The first systematic measurements of "the celerity with which the propagation of the ignition takes place" were published by Bunsen in Germany in 1866 and in an English translation[7] in Britain the following year. The gas mixture was made to flow through a tube and out of an orifice. A flame was ignited there and the flame speed was defined as the flow speed in the tube which was just low enough to produce lightback. The flow speed was determined from the volumetric flow rate by assuming a constant velocity across the orifice. Values of 34 ms^{-1} for "pure

hydrogen explosive mixture" (stoichiometric hydrogen/oxygen) and just less than 1 ms^{-1} for "carbonic oxide" (carbon monoxide/oxygen) were obtained.

The next stage covered the period 1875 to 1889 when Mallard, Le Chatelier, Gouy and Michelson laid the foundations for the modern view of flames. Mallard[8] reported experimental results (using essentially the same method as Bunsen) in a memoir published in 1875, along with the first theory of burning velocity. He measured burning velocities of firedamp (methane) and "lighting gas" (town gas) at a range of fuel/air mixtures. Maximum values were 0.56 ms^{-1} for 10.8% firedamp in air and 1.02 ms^{-1} for 16.7% lighting gas in air.

The next experimental determinations were by Gouy[9] in 1879. Gouy's paper was on photometry of coloured flames, but a short section dealt with the shape and size of Bunsen flames. In the theoretical section, Gouy gave the equation $V = v \sin \alpha$ where V is the burning velocity, v is the gas velocity and α is the angle between the flow direction (assumed vertical) and the flame surface. This equation is still frequently used to derive burning velocities on Bunsen burners. Gouy projected the image of a Bunsen cone onto a screen and estimated the area. His main object was to show that the burning velocity V was constant over the flame surface, by measuring the areas of flames on burners of different diameters at constant flow rate. The possibility of measuring the burning velocity by dividing this area into the volumetric flow rate was mentioned only in a footnote. Apparently the difficulty was in measuring precise flow rates. Only approximate burning velocities are quoted, and for only two mixtures of lighting gas and air. One of these was the mixture giving the maximum burning velocity, which Gouy found to be about 1 ms^{-1}.

In 1883, Mallard and Le Chatelier[10] followed up Mallard's earlier work[8] with experiments using both Bunsen's method and a new tube method. In this, the required fuel/air mixture was placed in a tube and ignited at the open end. The initial uniform speed at which the flame moved towards the closed end was measured and taken to be the burning velocity. The results were similar to those obtained using Bunsen's method. The maximum burning velocity of hydrogen/air was found to be 4.30 ms^{-1} in a mixture containing 40% hydrogen, and that of methane/air was 0.62 ms^{-1} in a mixture containing 12.2% methane. An improved theory was also proposed.

Further experimental work was reported by Michelson[11] in 1889. Michelson recognized that the burning velocity might depend on flame curvature, and implied that the "normal ignition velocity" that he defined should properly be measured in a

planar flame. However, he found that any dependence on curvature was less than the experimental error. He used Gouy's flame area method to measure burning velocities of a variety of fuel/oxidant mixtures. Maximum burning velocities included 0.71 ms^{-1} for 18% town gas in air (roughly 50% hydrogen, 30% methane, 10% carbon monoxide plus minor constituents) and 2.77 ms^{-1} for 40% hydrogen in air. Michelson pointed out that his values were much lower than those determined by previous workers, and explained why. In particular, he considered that the Bunsen method gave high results because of the assumption of constant velocity across the orifice.

Subsequent experimental work became divided into two groups. Measurements on stationary flames on Bunsen burners (see e.g. ref. 3) used the Gouy method or a derivative of it. Measurements on moving flames were made in tubes, following Mallard and Le Chatelier, and later in spherical vessels.

Starting in 1914, Wheeler and co-workers[12,13] extended Mallard and Le Chatelier's work on "the uniform movement" in tubes. While supporting the view that too narrow a tube causes a reduction in speed by heat loss, they found that too large a diameter causes an increase in speed due to turbulence. The question therefore arose about how fundamental the results were: it appeared that a particular tube diameter would have to be specified.

In 1926, Stevens[14,15] introduced the constant-pressure expanding spherical flame method. He was therefore the originator of the method used in this thesis. Stevens enclosed the flammable mixture in a spherical soap film which acted as a constant-pressure bomb. He found that the speed of the expanding spherical flame was constant, and referred to "the favourable symmetry automatically assumed by the gross mechanism of the gaseous explosive reaction". We will comment on both of these points in due course.

In 1932, Coward and Hartwell[16] measured the "fundamental speed of flame" using a tube method. They considered that prior to their work the only successful method of measuring the fundamental speed of flame was the Gouy method. They realized that tube methods can give high values unless the flame area is taken into account:

> "The flame is rarely, if ever, a flat disc at right angles to the axis of the tube; hence the axial speed of propagation is usually much greater than the normal speed of propagation (at right angles to the flame-front) of a plane flame-

front in a stationary mixture. Values for this fundamental constant have, however, been deduced..."

The maximum burning velocity for methane/air was found to be 0.27 ms^{-1} at about 10% methane in air.

Two years later, Lewis and von Elbe[17] followed Stevens' work with a description of a constant-volume method. They pointed out that Stevens' method was simple and direct, and eliminated the disadvantages of flame speed measurements in tubes. Its limitations were that it could not be used for gases that are affected by a soap film, and the gases used are always necessarily contaminated with water vapour. Their approach was therefore to measure the pressure as a function of time, and deduce the burning velocity as a function of pressure and temperature. Although this constant-volume method has become quite common, it is outside the scope of the present work. We will not consider it again except to point out some implications of the present work for such studies in Chapter 7.

Lewis and von Elbe[18] also made the next important step forward in 1943 when they introduced particle tracking in flames. The gas flowing into a burner was seeded with fine powder particles which were stroboscopically illuminated in the flame. Local measurements of gas velocities, and therefore burning velocities, could be determined from photographs. The local burning velocity was defined as the volumetric flow rate of cold gas divided by the small area of luminous zone it supplied. Lewis and von Elbe found that the burning velocity in the flame tip was high and that at the base of the flame was low, but these averaged out to give the mean value determined by the Gouy method. Particle tracking also gave valuable insights into flame stabilization.

About a decade later, Linnett, in a review of burning velocity determination[19], said that the definition of burning velocity was "easy only for an infinite plane flame". He used the example of a stationary spherical flame in a source flow to show how difficult it is to apply the definition. He claimed that

"If an attempt is made to define burning velocity strictly for such a system it is found that no definition free from all possible objections can be formulated. Moreover, it is impossible to construct a definition which will, of necessity, lead to the same value being determined for the burning velocity as would be determined in an experiment using a plane flame".

Linnett suggested that the minimum value of linear velocity in the cold gas would provide the best estimate of the burning velocity. A general principle was suggested: divide the volumetric flow rate of cold, unburnt gas by the flame area it supplies, with the area measured as close to the unburnt side as possible. This paper appears to have been influential, and many workers referred to it when they used this technique. We will return later to Linnett's claim about definitions free from all possible objections.

In 1965, Fristrom[20] compared flames in uniform and diverging flows in a similar way to Linnett but came to a different conclusion. He was the first to take account of stream tube divergence and produce an acceptable definition of a "normalized burning velocity". This was

> "the burning velocity which one would have obtained with the ideal one-dimensional flame of theory".

He introduced a surface (which in this thesis we call the reference surface) at which the mass flux (mass flow rate per unit area) should be measured. Dividing this mass flux by the cold gas density gives a suitable burning velocity. Fristrom was able to explain anomalously high burning velocities in flame tips and the change in the speed of expanding spherical flames with radius. Fristrom's definition and his explanation of the effect on expanding flames are used in the present work.

Andrews and Bradley[21] published a very influential review of burning velocity determination in 1972. They gave an explicit one-dimensional definition:

> "It is the velocity, relative to the unburnt gas, with which a plane, one-dimensional flame front travels along the normal to its surface".

They did not, however discuss how it should be applied to real flames. There was an implicit assumption (possibly following Linnett) that the burning velocity is the gas speed normal to the flame at the cold boundary.

Ten years later, Dixon-Lewis and Islam[22] used computer modelling to compare flames in uniform and divergent flows. They considered that the mass flux is the important physical quantity, and that its value is controlled by events at the hot end of the flame, where the reaction rate is high.

Shortly afterwards, Wu and Law[23] brought flame stretch into the discussion, and gave a good description of the fundamental concepts. They agreed with Dixon-Lewis and Islam that the mass flux at the hot end of the flame is the important quantity, although Law's position has since changed[24]. They also introduced a methodology for subtracting both flame stretch and flow divergence effects with a view to obtaining the true, one-dimensional burning velocity. An extended version of Law's method is studied in this thesis.

It appears that, over the century or so in which burning velocities have been measured, there has been a shift in the way they are considered. Originally, a speed was determined which was expected to correspond to a physical velocity in the flame. But later the concept of burning velocity changed: it became the speed of an ideal flame rather than the one on which the measurements were made.

At the time of Fristrom's paper[20] (1965), the connection between the real and ideal flames was very close. The mass flux of the ideal one-dimensional flame (from which the burning velocity could be derived) was simply the mass flux at the reaction zone of the real flame. The only effect of the divergent flow was "ducting". But after the effects of flame stretch had been uncovered, such a simple connection no longer existed. It was recognized that the divergent flow not only ducted the incoming gas but also changed the mass flux at the reaction zone. This led to Wu and Law's method of removing both the ducting and the stretch effects.

It is interesting to work backwards from the present to try to trace when the one-dimensional definition of burning velocity became accepted. Wu and Law in 1985, Dixon-Lewis and Islam in 1982, Andrews and Bradley in 1972 and Fristrom in 1965 all stated the definition explicitly. Linnett implied it in 1953 and Coward and Hartwell might have had it in mind in 1932. In fact, it could be argued that Michelson in 1879 was also thinking along those lines. Besides being an experimentalist, Michelson also performed some theoretical work on burning velocity (which was necessarily one-dimensional), and this may have influenced his thinking. Such considerations should also apply to Mallard and Le Chatelier, since like Michelson they performed both experimental and theoretical work. But their experimental work was always on moving flames which were too fast to be seen with the naked eye. They may have believed that their flames were close to being one-dimensional so that a carefully-worded definition was unnecessary.

It would appear that Linnett was instrumental in both introducing the one-dimensional definition and suggesting that the gas velocity should be measured at the

cold boundary to give correct results in real flames. It was only later that Fristrom, Dixon-Lewis and Islam, and Wu and Law differed from Linnett on where the burning velocity should be measured while agreeing on the one-dimensional definition.

Another interesting point is that in some theoretical work[25] the flame is considered to be a surface of discontinuity between unburnt and burnt gas. In this case, there is only one choice for where to measure the burning velocity, namely on the cold side of the discontinuity. The analogous position in a real flame might be considered to be the cold boundary, and such considerations may have suggested its use by experimentalists.

To summarize, the definition of burning velocity evolved as experimental work proceeded. There is now general agreement on the present one-dimensional definition, but a range of opinions about how it should be applied to real flames. A related point is that there is no generally-accepted extension of the burning velocity definition to flames which are not one-dimensional. An attempt is made to address these issues in the present work.

1.2 BURNING VELOCITY AND FLAME STRETCH

When the methods for measuring burning velocities which are described in the previous section were introduced, it was found that they gave different results when applied to the same combustible mixtures. Arguments about the best techniques began which have continued to the present day. In most areas of science, general agreement on the definition of the relevant physical properties comes early in the development of the subject and is followed by highly accurate measurements and good agreement among different workers. This has not happened with burning velocity. Agreement has existed on its definition for about half a century, but close agreement between results from different workers has not followed. Variations of 20% or more between different determinations still exist even for methane, the most-studied fuel.

One of the aims of the present work is to try to improve this state of affairs by considering carefully the meaning of the definition of burning velocity and its application to premixed flames.

The burning velocity of a fuel/air mixture is defined as the speed of a planar one-dimensional flame relative to the unburnt mixture[20-23]. There is general agreement on this definition, and it is used in the present work. But an examination of it is warranted, since its application to real flames is not straightforward. We will therefore consider why planar, one-dimensional flames are specified, and why measurements are relative to the unburnt mixture. A discussion of why the speed is measured (and not some other quantity) will be postponed until Chapter 3. As far as is known, no formal justification has ever been given of the definition of burning velocity. The following comments are suggestions for the rationale behind the definition.

Experiments show that nonuniformities in the approach flow can affect the speed of a flame. A reference geometry must therefore be selected for use in the definition, and the simplest possible is one-dimensional.

The flame in the definition is planar (rather than, say, spherical) because only for a planar flame in a one-dimensional geometry is the gas velocity upstream or downstream of the flame constant. This ensures that the definition is unambiguous: there is a constant flow velocity relative to which the propagation rate of the flame can be determined.

The speed is measured relative to the unburnt gas because standard upstream conditions can be specified (e.g. a temperature of 298 K); comparison of the speeds of different fuel/air mixtures is then facilitated. The speed relative to the burnt gas would not be as useful because downstream conditions depend on the flame temperature of the mixture being burned.

We can see, therefore, that the definition is a sensible one. It has its particular form because alternatives would be more complicated.

One reason for the differences among published burning velocities is the way different workers interpret the definition. The one-dimensional configuration described does not exist in nature, so it is necessary to make measurements on real flames and transform them in some way to obtain the required one-dimensional values. Different approaches to this question (including ignoring it altogether) have led to a wide spread in results.

By far the most common approach is to assume that the gas velocity at the cold boundary is equal to the one-dimensional burning velocity. An alternative method,

more common formerly than now, is to determine an average burning rate for the whole flame. This is considered to approximate to the one-dimensional value if heat loss and curvature effects are small or cancel out.

It is important to point out that, a priori, there is no reason for equating the gas velocity at first temperature rise to the one-dimensional burning velocity. We will see later that this method is incorrect: it does not give the one-dimensional value.

Studies of burning velocity have been given additional weight by a new development in combustion science: flame stretch. This is essentially a way of describing the behaviour of flames when they are not stationary, planar and one-dimensional. Since this covers *all* real flames, the range of applicability of flame stretch is very wide. Particular cases of stretched flames include Bunsen flame tips, flames in stagnation-point flow, expanding spherical flames and flames in turbulent flow. The main effect of stretch is to change the burning rate of the flame. Although there is general agreement on the definition of the burning rate of planar one-dimensional flames, there is no consensus on how the one-dimensional burning velocity definition should be extended to real, stretched flames. This point is therefore considered carefully in the present work, and a suitable definition is proposed.

If the stretch rate is small, its effect on the burning velocity is predicted to be linear. A single parameter, called the Markstein length, then characterizes the effect of stretch on a given flame. This "weak stretch" regime is the one studied in the present work. Higher stretch rates, which can cause flame extinction, are not accessible using the experimental methods developed in this thesis.

Is it necessary to take such care about defining burning velocity? I believe so, for the following reasons. First, the large scatter in the results of one-dimensional burning velocity determinations shows that there are different opinions about how to apply the definition. This begins to matter when the data are used for precise comparisons. Burning velocities are increasingly being used for the validation of chemical kinetic schemes in one-dimensional flame models, where the parameter needed for comparison is precisely the burning velocity defined above. Two- and three-dimensional models are not sufficiently well-developed to allow direct comparisons with real flames. Correct one-dimensional experimental results are therefore needed.

A second reason for the importance of careful definitions in burning velocity work is seen when flame stretch is considered. There has been only one body of work so far

in which the effect of stretch on the burning velocity has been measured systematically. In that work, by Law et al[24], the definition of burning velocity used was such that it always increases with increasing stretch - even though in certain mixtures the flame is clearly burning less intensely and is ultimately extinguished by stretch. The definition does not reflect the physical state of the flame, and it is therefore reasonable to question its suitability. In fact, Law et al found that the effect of stretch on the burning velocities of methane and propane did not change much across the stoichiometric range. They concluded that this was because the Lewis number, which will be defined later, did not deviate too much from unity. In the present work, which uses a different burning velocity, we find that these small changes in the Lewis number have a large effect. Clearly the choice of burning velocity definition is important in this case. We will see later that according to one definition the burning velocity of a flame increases with stretch, while an alternative definition shows that the burning velocity of *the same flame* decreases with stretch. It is therefore necessary to decide upon a suitable definition to prevent confusion.

Finally, the spread in the one-dimensional burning velocity data is an indication of a lack of understanding of flames which is unsatisfactory in itself.

1.3 THE ORGANIZATION OF THIS THESIS

The theory of laminar premixed flame propagation and a mathematical analysis of flame stretch are described in Chapter 2. The results derived there are used later in the work. A very full treatment is given of the theory of flame propagation. Starting with the general conservation equations for a reacting gas mixture, the equations used in the numerical modelling are derived. From these a form of the energy equation suitable for asymptotic analysis is obtained. This was done to emphasize the connection between flame modelling and asymptotic methods and to show that they are two ways of attacking the same problem. An asymptotic solution of the energy equation is included for the sake of completeness.

Comparison of the solution of the asymptotic model with that obtained from a phenomenological approach shows that the latter can yield expressions which contain the correct dependences. Since phenomenological methods are used to make several points in this work, it is useful to have this assurance.

In addition, two new pieces of work appear in Chapter 2. One is the phenomenological analysis of an expanding spherical flame. In their paper on

phenomenological analyses of stretched flames, Chung and Law[26] stated that "the phenomena [in expanding spherical flames] appear to be quite complex, so that a generalized derivation allowing for arbitrary flame curvature and Lewis number has so far eluded us". It is therefore pleasing to have succeeded in performing such a derivation. The analysis explains the far-from-obvious connection between the effect of stretch in an expanding spherical flame and that in a planar flame in a stagnation-point flow. It also explains the physics behind much of the work in this thesis. The other new piece of work is a mathematical result on the mean stretch rate of a flame. It is used at various points in the thesis to assess qualitatively the extent to which a measured burning rate is affected by stretch.

All of the subsequent work is new. Chapter 3 describes the experimental methodologies used. First, insights gained from the theory section are used to construct a definition of burning velocity which can be applied to any flame. The Markstein length, which characterizes the effect of flame stretch on the burning velocity, is then defined. The definitions of burning velocity and Markstein length are then applied to the particular experimental configurations used, namely expanding spherical flames and stationary planar flames in stagnation-point flows. For the case of expanding flames, a simple model of the radius *vs* time behaviour is derived which is used to analyse experimental data. For stagnation flow flames, the assumptions underlying the counterflow technique of Law et al[23,24,27-30], which is used in a modified form in this work, are scrutinized. Finally, an approximate method of obtaining burning velocities from button-shaped flames is described.

Chapter 4 contains descriptions of the experimental techniques used in the laboratory. The apparatus, method and data reduction techniques for expanding spherical flames and for stagnation flow flames are described. A short section at the end describes experiments on button-shaped flames.

The results of the experiments are presented in Chapter 5. Most of the results are for expanding spherical flames. The variation of flame speed with radius is shown for each set of conditions. The burning velocities and the flame relaxation parameters derived from these data are given over the stoichiometric range for hydrogen, methane, ethane, propane and ethylene. In addition, results are given for stoichiometric hydrogen/air mixtures diluted with nitrogen and for stoichiometric methane/air mixtures at various pressures. Some burning velocities and Markstein lengths are given for flames in stagnation-point flow. Finally, some burning velocities determined in button-shaped flames are presented.

Chapter 6 deals with the laminar flame modelling carried out as part of this work. The chemical schemes assembled for the work are given along with the burning velocities predicted for various compositions and for different geometries. A comparison of the structures of planar and stationary spherical flames gives information on the point in the flame where the propagation rate is controlled. The temperature at this "reference surface" is given for various conditions.

The results of the modelling are used to determine a flame thickness correction needed for the determination of Markstein lengths from the expanding flame experiments. Values of this constant and the derived Markstein lengths are given for all experimental conditions. Finally, the results of simulations of expanding spherical flames are given. The expanding flame simulations play a central role in this work because they provide a way of testing the simple model of expanding flames derived in Chapter 3. The results demonstrate the conditions under which good results can be expected.

The methods and results are discussed in Chapter 7. The two experimental approaches used in this work are compared. A list of requirements is assembled, based on the analyses in Chapters 2 and 3, which must be fulfilled if an experiment is to give true, one-dimensional results. Previous methods of determining burning velocity are compared with this specification and methods likely to give good results are indicated. The experimental Markstein lengths are compared with theory and with the few other experimental data available. Implications of the results of the work are discussed.

Finally, conclusions are drawn in Chapter 8 about the strengths and weaknesses of the different experimental approaches and the meaning of the burning velocity used in this work.

We now make some points about usage in this thesis. Equations are numbered consecutively in each chapter. References to equations within a chapter use this single number. Reference to an equation in another chapter is by prefacing the equation number with the chapter number; for example, equation (3-10) means equation (10) in Chapter 3. Figures and tables are numbered consecutively through the thesis and listed in the contents section.

The gas with the formula C_2H_4 is referred to as ethylene in this work instead of the recommended ethene; this is in line with gas industry usage.

The relative amounts of fuel and air in the combustible mixtures in this work are expressed in terms of the stoichiometry. There are several alternative names for this quantity, e.g. fraction stoichiometry, but the present name has been used for brevity. It is defined as the mole fraction of fuel in the mixture divided by the mole fraction of fuel in a stoichiometric mixture. For gases other than hydrogen, the stoichiometry is roughly equal to the equivalence ratio which is defined at the end of Section 2.1.3.2.

Nomenclature for flame propagation rates varies widely. In the present work, burning velocity is used as the standard way of expressing the flame propagation rate relative to the cold gas. Flame speed is the speed of a flame relative to laboratory coordinates. A flame on a burner therefore has a flame speed of zero. The main use of flame speed in the present work is in describing expanding spherical flames. The usage is extended to the "limiting" flame speed at infinite radius, which corresponds to the burning velocity divided by the density ratio.

Chapter 2

THEORY OF PREMIXED LAMINAR FLAMES

This chapter deals with the theory of the premixed laminar flames studied in the present work.

The subject of the first section is the theory of laminar flame propagation. A set of flame equations is derived from the general conservation equations for a reacting, multicomponent gas mixture. These are the equations which are solved numerically by the Sandia PREMIX code. By suitable simplifications, these equations are also solved by asymptotic analysis. The aim is to emphasize the link between asymptotic and full numerical solutions, and also to demonstrate the accuracy of the phenomenological analyses which are performed in this section and the next one.

The second section describes the mathematical foundations of flame stretch. An expression is derived for the flame stretch and applied to different flame configurations. A phenomenological analysis is performed of the effect of stretch on a planar flame in a stagnation-point flow. A new phenomenological analysis of the effect of stretch on an expanding spherical flame is also presented. Theories of the effect of stretch on flames are considered, and one is selected which is suitable for comparison with the results of the experiments. Finally, a new mathematical result on stretch is presented which describes the conditions necessary for the mean stretch of a region of a stationary flame surface to be zero.

2.1 CONSERVATION EQUATIONS

In this section we list the conservation equations for a multicomponent, reacting gas mixture, and then simplify them by making appropriate assumptions. Phenomenological analyses of steady planar and spherical flames are provided which give some idea of the physical processes involved, and these are followed by sections dealing with asymptotic analysis and with detailed modelling.

2.1.1 Derivation of the flame equations

We start by quoting the general conservation equations for a multicomponent, reacting ideal-gas mixture. They were derived by Williams[31] from the Boltzmann equation. A suitable set of flame propagation equations is derived from them by making appropriate simplifications.

The overall continuity (mass conservation) equation is

$$\partial\rho/\partial t + \nabla\cdot(\rho\mathbf{v}) = 0 \tag{1}$$

where ρ is density and $\mathbf{v}$ is velocity. Conservation of momentum is expressed by

$$\partial\mathbf{v}/\partial t + \mathbf{v}\cdot\nabla\mathbf{v} = -(\nabla\cdot\underline{\mathbf{P}})/\rho + \sum_{i=1}^{N} Y_i\mathbf{f}_i \tag{2}$$

where Y_i is the mass fraction of species i and $\mathbf{f}_i$ is the body force per unit mass acting on it. There are N chemical species. Conservation of energy is

$$\rho\partial u/\partial t + \rho\mathbf{v}\cdot\nabla u = -\nabla\cdot\mathbf{q} - \underline{\mathbf{P}}:(\nabla\mathbf{v}) + \rho\sum_{i=1}^{N} Y_i\mathbf{f}_i\cdot\mathbf{V}_i \tag{3}$$

where u is the internal energy per unit mass of the gas mixture. Species conservation is given by

$$\partial Y_i/\partial t + \mathbf{v}\cdot\nabla Y_i = w_i/\rho - [(\nabla\cdot(\rho Y_i\mathbf{V}_i)]/\rho, \quad i=1,\ldots,N. \tag{4}$$

In equation (2), $\underline{\mathbf{P}}$ is the stress tensor

$$\underline{\mathbf{P}} = [p + (2\mu/3 - \kappa)(\nabla\cdot\mathbf{v})]\underline{\mathbf{U}} - \mu[(\nabla\mathbf{v}) + (\nabla\mathbf{v})^T] \tag{5}$$

where p is the hydrostatic pressure, μ is the coefficient of shear viscosity, κ is the coefficient of bulk viscosity and $\underline{\mathbf{U}}$ is the unit tensor. In equation (3), the heat flux vector is

$$\mathbf{q} = -\lambda\nabla T + \rho\sum_{i=1}^{N} h_i Y_i \mathbf{V}_i + RT\sum_{i=1}^{N}\sum_{j=1}^{N}\left(\frac{X_j D_{T,i}}{W_i D_{ij}}\right)(\mathbf{V}_i - \mathbf{V}_j) + \mathbf{q}_{rad} \qquad (6)$$

where λ is the thermal conductivity, T is the temperature, R is the universal gas constant, $\mathbf{q}_{rad}$ is the radiant heat flux vector, D_{ij} is the binary diffusion coefficient for species i and j, and h_i, X_i, $D_{T,i}$ and W_i are the specific enthalpy, mole fraction, thermal diffusion coefficient and molecular weight for species i. The diffusion velocity $\mathbf{V}_i$ in equations (3) and (4) is determined by

$$\nabla X_i = \sum_{j=1}^{N}\left(\frac{X_i X_j}{D_{ij}}\right)(\mathbf{V}_j - \mathbf{V}_i) + (Y_i - X_i)\frac{\nabla p}{p} + \frac{\rho}{p}\sum_{j=1}^{N} Y_i Y_j(\mathbf{f}_i - \mathbf{f}_j)$$

$$+ \sum_{j=1}^{N}\left[\left(\frac{X_i X_j}{\rho D_{ij}}\right)\left(\frac{D_{T,j}}{Y_j} - \frac{D_{T,i}}{Y_i}\right)\right]\left(\frac{\nabla T}{T}\right), \quad i=1,\ldots,N. \qquad (7)$$

The reaction rates w_i in equation (4) are given by the phenomenological expressions of chemical kinetics,

$$w_i = W_i\sum_{k=1}^{M}(\nu''_{i,k} - \nu'_{i,k})B_k T^{\alpha_k}\exp(-E_k/RT)\prod_{j=1}^{N}\left(\frac{X_j p}{RT}\right)^{\nu'_{i,k}}, \quad i=1,\ldots,N \qquad (8)$$

where M is the number of reactions, $\nu'_{i,k}$ and $\nu''_{i,k}$ are the stoichiometric coefficients for species i appearing as a reactant ($'$) or a product ($''$) in reaction k, and B_k, α_k and E_k are the pre-exponential factor, temperature exponent and activation energy respectively in reaction k.

The $N + 5$ dependent variables in the conservation equations can be taken to be the mass fraction Y_i, the density ρ, the temperature T and the velocity $\mathbf{v}$. The other variables are related to these through the ideal-gas equation of state

$$p = \rho RT\sum_{i=1}^{N}(Y_i/W_i), \qquad (9)$$

the thermodynamic identity

$$u = \sum_{i=1}^{N} h_i Y_i - p/\rho, \tag{10}$$

the identity relating mole fraction X_i to mass fraction Y_i,

$$X_i = \frac{(Y_i/W_i)}{\sum_{j=1}^{N} (Y_j/W_j)}, \qquad i=1,\ldots,N, \tag{11}$$

and the caloric equation of state,

$$h_i = h_i^f + \int_{T_f}^{T} c_{pi}\, dT, \qquad i=1,\ldots,N, \tag{12}$$

where h_i^f is the standard heat of formation per unit mass at temperature T_f and c_{pi} is the specific heat of species i.

In equations (1) to (7), vector notation is used; bold symbols are vectors and bold underlined symbols are tensors. ∇ is the gradient operator, two dots (:) imply that tensors are to be contracted twice to form a scalar, and the superscript T denotes the transpose of the tensor.

We now make some assumptions to allow simplification. First, we neglect the radiant heat flux ($q_{rad} = 0$). A simple, phenomenological treatment of radiant heat loss from the burnt gases in expanding flames will, however, be given in Section 3.2.3. Second, the flow is taken to be one-dimensional (1-D) in the sense that the velocity is parallel to one of the orthogonal coordinate directions (taken to be x), and all properties are uniform along surfaces in the other two directions. The relations between the physical distances (s_x, s_y, s_z) and the coordinates (x, y, z) are given by

$$ds_x = g_x dx, \quad ds_y = g_y dy, \quad ds_z = g_z dz. \tag{13}$$

We take $g_x = 1$ so that x represents the physical distance in the flow direction. One-dimensional flow is then defined by $\partial/\partial y = \partial/\partial z = 0$ for all flow properties and $v_y = v_z = 0$. The only non-zero velocity is that in the x direction which we will simply denote v. We also set

$$g_2 g_3 = A, \tag{14}$$

the area of a stream tube.

We further assume that the flow is steady ($\partial/\partial t = 0$) and that there are no body forces ($\mathbf{f}_i = 0$). The Dufour effect (heat flux due to a concentration gradient), the third term in equation (6), is assumed to be negligible. But the reciprocal process, known as the Soret effect (mass diffusion due to a temperature gradient or "thermal diffusion"), is retained: it can have a large effect in hydrogen flames. Finally, the speed of the flow is assumed to be small compared with the velocity of sound - a good assumption for the low speed deflagrations of this work. The kinetic energy terms in the energy and momentum equations then disappear, leading to considerable simplification. Flames studied in this work which satisfy all the foregoing criteria include planar one-dimensional and stationary spherical deflagrations. The unsteady nature of expanding spherical flames disqualifies them from this analysis.

It can be shown using some of the results of Williams[31] that the equations reduce as follows. Continuity is

$$m = \rho v A \tag{15}$$

where m is the total mass flow rate crossing the area A. Energy conservation is

$$m \frac{dh}{dx} + \frac{d}{dx}(Aq) = 0. \tag{16}$$

Conservation of momentum reduces to

$$p = \text{constant}, \tag{17}$$

the well-known "combustion approximation". The conservation of species becomes

$$m \frac{dY_i}{dx} = A w_i - \frac{d}{dx}(\rho Y_i V_i A), \qquad i=1,\ldots,N. \tag{18}$$

Since the term containing a pressure derivative disappears, the diffusion velocities are now determined from

$$\frac{dX_i}{dx} = \sum_{j=1}^{N}\left(\frac{X_iX_j}{D_{ij}}\right)(V_j - V_i) + \sum_{j=1}^{N}\left[\left(\frac{X_iX_j}{\rho D_{ij}}\right)\left(\frac{D_{T,j}}{Y_j} - \frac{D_{T,i}}{Y_i}\right)\right]\frac{1}{T}\frac{dT}{dx},$$

$$i=1,\ldots,N. \qquad (19)$$

The heat flux vector in equation (6) reduces to

$$q = -\lambda\frac{dT}{dx} + \rho\sum_{i=1}^{N} h_iY_iV_i, \qquad (20)$$

and substituting it in equation (14) gives the energy equation

$$m\frac{dh}{dx} + \frac{d}{dx}\left(-\lambda A\frac{dT}{dx} + \rho A\sum_{i=1}^{N} h_iY_iV_i\right) = 0. \qquad (21)$$

A useful form of the energy equation is obtained by combining equations (18) and (21) as follows. Using $dh/dx = c_p dT/dx$ in equation (21), we get

$$mc_p\frac{dT}{dx} - \frac{d}{dx}\left(\lambda A\frac{dT}{dx}\right) + \rho A\sum_{i=1}^{N} Y_iV_ic_{pi}\frac{dT}{dx} + \sum_{i=1}^{N} h_i\frac{d}{dx}(\rho AY_iV_i) = 0. \qquad (22)$$

We now multiply both sides of the species equation (18) by h_i and sum over all i. The result is

$$\sum_{i=1}^{N} h_i\frac{d}{dx}(\rho AY_iV_i) = -m\sum_{i=1}^{N} h_i\frac{dY_i}{dx} + A\sum_{i=1}^{N} w_ih_i. \qquad (23)$$

It is straightforward to show that the first term on the right-hand side is zero by differentiating $h = \sum h_iY_i$ with respect to x. The two terms containing derivatives of enthalpy are zero since enthalpy is not a function of distance, so the third term, which is the sum in the first term on the right-hand side of equation (23), must also be zero. Substituting equation (23) in (22) therefore gives the modified energy equation

$$mc_p \frac{dT}{dx} - \frac{d}{dx}\left(\lambda A \frac{dT}{dx}\right) + \rho A \sum_{i=1}^{N} Y_i V_i c_{pi} \frac{dT}{dx} + A \sum_{i=1}^{N} w_i h_i = 0. \qquad (24)$$

Equations (15), (17), (18) and (24) along with the subsidiary relationships (8), (9), (11), (12) and (19) form a suitable set of flame equations, although some of the later derivations start from other points for convenience.

The boundary conditions for these equations are as follows. At $x = -\infty$ (where properties will be identified by the subscript u), all properties are uniform, i.e. $d/dx = 0$, and all variables except the total mass flow rate m are known. At $x = +\infty$ (where properties will be identified by the subscript b), all properties again become uniform, i.e. $d/dx = 0$, and chemical equilibrium is reached.

The equations can be dealt with in two different ways. First, they can be solved using asymptotic analysis. This is a mathematically rigorous technique which helps to give a good understanding of the physics of the combustion process since analytical formulae are often obtained. There are currently two disadvantages. Extreme simplification of the equations is usually needed in order to obtain tractability. Also, the large parameter around which the asymptotic expansions are built is usually the activation energy. However, the assumption of large activation energy is not always a good one for real flames. Recent work[32,33] appears to be getting round both of these difficulties.

The second way of dealing with the equations is by solving them numerically, on a digital computer. This has the advantage of providing quantitative information for comparison with experiment, but at the expense of analytical understanding.

The two methods are complementary: used together they can provide information and understanding which could be produced by neither approach by itself. Both techniques are therefore used in this work; an asymptotic analysis is performed in Section 2.1.3 and numerical modelling is described in Chapter 6. First, though, phenomenological analyses of steady planar and spherical combustion waves will be provided. These describe the main features of laminar flames and give a physical explanation for the choice of burning velocity definition used in this work.

2.1.2 **Phenomenological analysis**

We now perform phenomenological analyses of planar one-dimensional and stationary spherical flames to show the main factors affecting the burning velocity. These analyses are based on those of Williams[31] and Chung[34].

2.1.2.1 Planar one-dimensional flame

We consider a stationary, plane, one-dimensional laminar flame. By definition, the speed of the cold, unburnt gas approaching the flame is the burning velocity S_u°. Let the overall width of the combustion wave be δ and the reaction rate (mass of reactants consumed per unit volume per unit time) be $w = Y_u k$ where Y_u is the mass fraction of reactant in the unburnt gas and k is an Arrhenius-type reaction rate. Then if the reaction occurred at the same rate throughout the flame thickness, the mass of reactants consumed per unit area of the wave per unit time would be

$$M = \delta Y_u k. \tag{25}$$

However, because of the strongly temperature-dependent reaction rate, reaction is actually confined to a thin layer near to the maximum temperature. Let the thickness of this layer be $\delta_R = \delta/\beta_1$ where $\beta_1 > 1$ (and typically between 5 and 15). In addition, the mass of reactant at the reaction zone is depleted by diffusion by a factor $1/\beta_2$ ($\beta_2 > 1$). We will see in the next section that β_1 and β_2 are both equal to the Zel'dovich number. Hence the mass of reactants consumed per unit area of the wave per unit time is

$$M = \frac{\delta}{\beta_1} \frac{Y_u}{\beta_2} k. \tag{26}$$

If q is the heat of reaction (energy released per unit mass) of the fuel then the energy released per unit area of the wave per unit time is

$$Q_R = \frac{\delta}{\beta_1} \frac{Y_u}{\beta_2} kq. \tag{27}$$

The cold, incoming gas is heated to a temperature at which it reacts at an appreciable rate by means of heat conduction from the reaction zone. The rate of heat conduction upstream per unit area of the wave is roughly

$$Q_C = \lambda \frac{dT}{dx}$$

$$\approx \lambda \frac{T_b - T_u}{\delta} \tag{28}$$

where λ is the mean thermal conductivity of the gas, T is the temperature, x is distance normal to the flame and subscripts u and b identify unburnt and burnt conditions respectively.

If the wave is adiabatic and c_p is an average specific heat of the mixture then energy conservation implies that

$$Y_u q = c_p(T_b - T_u), \tag{29}$$

where the flame temperature T_b is equal to the adiabatic value T_{ad}. The rate of heat release becomes

$$Q_R = \frac{\delta}{\beta_1} \frac{k}{\beta_2} c_p(T_b - T_u). \tag{30}$$

All the heat produced by reaction must be conducted upstream, so

$$Q_R = Q_C. \tag{31}$$

Equating (28) and (30) leads to an expression for the thickness of the wave:

$$\delta = \left[\beta_1\beta_2 \frac{\lambda}{c_p k}\right]^{1/2}. \tag{32}$$

The burning velocity can be related to the flame thickness as follows. The mass of reactant entering unit area of the flame per second is $Y_u\rho_u v_u = Y_u\rho_u S_u^{\circ}$ where ρ_u is the density of the cold, unburnt mixture. This is equal to M defined in equation (26), so

$$Y_u\rho_u S_u^{\circ} = \frac{\delta}{\beta_1} \frac{Y_u}{\beta_2} k. \tag{33}$$

Substituting the flame thickness equation (32) gives

$$S_u^{\circ} = \frac{1}{\rho_u} \left[\frac{1}{\beta_1 \beta_2} \frac{\lambda k}{c_p} \right]^{1/2}. \tag{34}$$

Equation (34) shows that the burning velocity is proportional to the square root of a reaction rate and to the square root of the ratio of the thermal conductivity to the specific heat. The factor on the right-hand side with the strongest temperature dependence is usually k, which varies roughly as $\exp(-E/RT_b)$ where E is an activation energy and R is the universal gas constant. At constant temperature, λ and c_p are independent of the pressure p, $\rho_u \propto p$ according to the ideal gas law and k varies as p^n where n is the order of the reaction. Hence the pressure and temperature dependences of S_u° are given approximately by

$$S_u^\circ \propto p^{(n/2-1)} \exp(-E/2RT_b). \tag{35}$$

Eliminating k between equations (32) and (34) leads to an expression for the overall flame thickness:

$$\delta = \frac{\lambda}{\rho_u S_u^\circ c_p}. \tag{36}$$

It is interesting to note that the expression for the flame thickness is independent of β_1 and β_2.

Expressions of the form of equation (35) above can be used to define an overall (or "effective") activation energy for a flame in which there are in fact many elementary steps, each with its own activation energy. This approach is of use when the simplest possible description of the chemistry is required. At constant pressure, equation (35) can be written

$$\ln S_u^\circ = A - E/2RT_b \tag{37}$$

where A is a constant. For one-dimensional, adiabatic flames of a given fuel with constant initial temperature T_u (298 K, say), S_u° can be considered as a function only of T_b while E is a constant. Plotting $\ln S_u^\circ$ against $1/T_b$ where T_b is the calculated adiabatic flame temperature should therefore produce a straight line with a slope of

$$s = -\frac{E}{2R}. \tag{38}$$

The overall activation energy is

$$E = -2Rs. \tag{39}$$

This procedure is useful for deriving approximate overall activation energies which can be used in asymptotic theories.

Usually, the graph of $\ln S_u^{\circ}$ against $1/T_b$ is not precisely linear. Strictly, this implies that a more detailed analysis should be performed in which E is a function of temperature. But the determination of E can only be approximate since the chemistry of all real flames proceeds in a series of steps. A more thorough analysis is therefore not usually warranted.

2.1.2.2 Stationary spherical flame

A point of major importance in this thesis is the definition of the burning velocity for flames in flows which are not one-dimensional. In order to provide a physical basis for the definition of burning velocity used in this work, we now repeat the previous analysis for a stationary spherical flame in a source flow.

We first apply the continuity equation (15) to the cold and hot boundaries of the flame, giving

$$\rho_u v_u A_u = \rho_b v_b A_b. \tag{40}$$

As in the planar one-dimensional case, the heat released by reaction in the thin reaction zone must equal the heat transported upstream by conduction. Since these processes both occur at the reaction zone, the flame area does not enter the analysis and the expression for the flame thickness is the same as equation (32) obtained for the planar one-dimensional flame.

The rate at which reactant diffuses into the reaction zone must equal the rate at which it is supplied by convection up to the cold boundary. Since the rate of consumption of reactant at the reaction zone equals the rate of supply by diffusion, we have

$$\frac{\delta}{\beta_1}\frac{Y_u}{\beta_2} kA_b = Y_u \rho_u v_u A_u \tag{41}$$

Substituting equation (40) into this expression and using $M_b = \rho_b v_b$, we have

$$M_b = \frac{\delta}{\beta_1}\frac{k}{\beta_2}. \tag{42}$$

Combining with equation (32) gives an expression for the thickness of the flame

$$\delta = \frac{\lambda}{M_b c_p}, \tag{43}$$

which is identical to the one-dimensional result in equation (36), and an expression for the mass flux at the hot boundary

$$M_b = \left[\frac{\lambda k}{\beta_1 \beta_2 c_p}\right]^{1/2}. \tag{44}$$

Now k is a function only of the flame temperature which in this case equals the adiabatic value. It will be shown in the next section that β_1 and β_2 are both equal to the Zel'dovich number β which depends only on T_u and T_b. The activation energy, which appears in both k and β, the thermal conductivity λ and the specific heat c_p are constants, so M_b is a constant; in particular, it is independent of the flame radius. Comparison with equation (34) shows that it is also equal to the mass flux in a planar one-dimensional flame,

$$M_b = \rho_u S_u^{\circ} \tag{45}$$

where S_u° is the burning velocity of the corresponding one-dimensional flame. If stretch is the only factor (other than external effects like heat losses) which can perturb the burning rate of a flame then the stationary spherical flame, being unstretched, should have the same burning rate as the planar one-dimensional case. Since M_b is the same in both cases, it, or something based on it, must be the correct measure of the propagation rate in this model. Equation (45) shows that dividing the mass flux at the hot boundary by the cold gas density will give the correct burning velocity for a planar one-dimensional or a stationary spherical flame. The definition of burning velocity is examined in detail in Chapter 3, but we will anticipate the results of the analysis. We will use M_b/ρ_u as the general definition of the burning velocity, applicable to any geometry, for this model in which the reaction zone is at the hot boundary.

To make the comparison of burning velocity definitions as sharp as possible, we look at two ways of deriving a burning velocity for the spherical flame from equation (44).

The burning velocity defined in this work is denoted $S_{u,r}$. According to the above definition, it is

$$S_{u,r} = M_b/\rho_u = S_u^{\circ}; \tag{46}$$

the burning velocity equals the planar one-dimensional value.

By contrast, the "standard" approach, used by many workers, is to measure the gas velocity at the cold boundary. From equation (40), this is

$$v_u = \frac{\rho_b v_b A_b}{\rho_u A_u}. \tag{47}$$

Using $M_b = \rho_b v_b$ and equation (45) and with the radius of the cold boundary of the spherical flame denoted by r, this becomes

$$v_u = S_u^{\circ}(1 + \delta/r)^2. \tag{48}$$

The burning velocity defined at the cold boundary therefore varies with the flame radius. It always exceeds the one-dimensional value, but becomes equal to it in the limit of infinite radius.

2.1.2.3 Non-unity Lewis number

The analyses above contain the implicit assumption that the Lewis number Le is equal to 1. In this section we extend the planar analysis to the more general case of Le $\neq$ 1, in preparation for the phenomenological analyses of stretched flames in Section 2.2.2. Although the analysis is performed for the planar one-dimensional flame, the results for the spherical case are identical.

The main difference in the formulation is that the heat and mass diffusion zones now have different thicknesses, δ_T and δ_M respectively, as shown in Fig. 1. In order to perform the analysis, we define an effective mass fraction at the cold boundary

FIGURE 1

Phenomenological model of one-dimensional flame structure

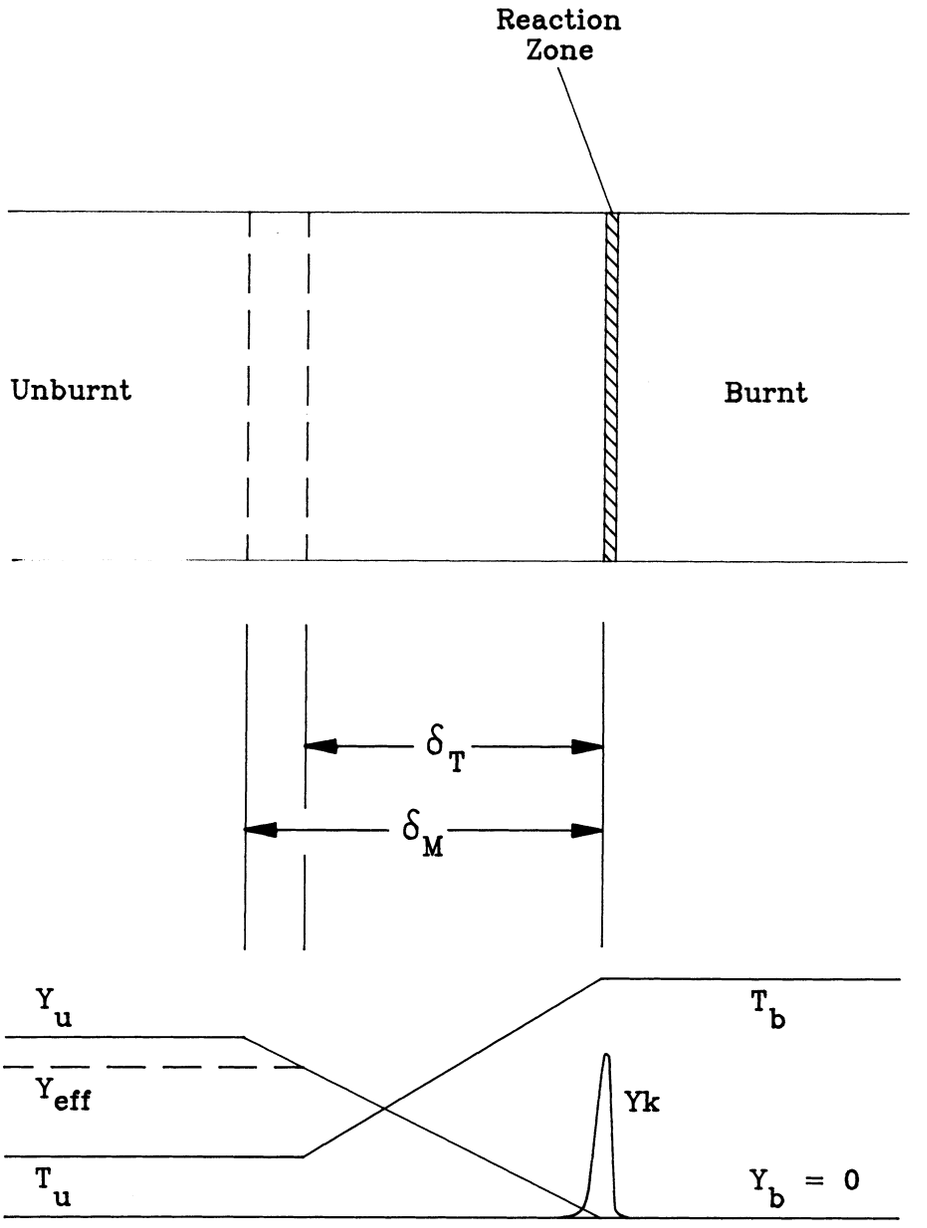

$$Y_{eff} = Y_u \delta_T / \delta_M . \tag{49}$$

The balance between heat conduction and reaction becomes

$$\lambda \frac{T_b - T_u}{\delta_T} = \frac{Y_{eff}}{\beta_1} \frac{\delta_T}{\beta_2} kq \tag{50}$$

and the balance between mass diffusion and reaction, which was not used in the previous analyses, is

$$\rho D_{12} \frac{Y_u}{\delta_M} = \frac{Y_{eff}}{\beta_1} \frac{\delta_T}{\beta_2} k. \tag{51}$$

Eliminating the right-hand sides of equations (50) and (51) and substituting equation (29) gives

$$\delta_T / \delta_M = \mathrm{Le} \tag{52}$$

where the definition of the Lewis number, $\mathrm{Le} = \lambda/(\rho D_{12} c_p)$ has been used. Substituting equations (49), (52) and (29) in (50) gives an expression for the thickness of the heat conduction or preheat zone

$$\delta_T = \left[\beta_1 \beta_2 \frac{\lambda}{c_p k \mathrm{Le}} \right]^{1/2}, \tag{53}$$

which is the same as equation (32) except for the extra factor of $\mathrm{Le}^{1/2}$ in the denominator.

Combining equation (33) (with $\delta = \delta_T$) with (52) and (53) gives

$$S_u^{\circ}(\mathrm{Le}) = \frac{1}{\rho_u} \left[\frac{\mathrm{Le}}{\beta_1 \beta_2} \frac{\lambda k}{c_p} \right]^{1/2}. \tag{54}$$

Comparison with equation (34) gives the result

$$S_u^{\circ}(\mathrm{Le}) = \mathrm{Le}^{1/2} S_u^{\circ}(\mathrm{Le} = 1). \tag{55}$$

The effect of variations of the Lewis number on the burning velocity in an unstretched flame is therefore small; this is because the flame temperature is not

affected. We will see in Section 2.2.2 that in stretched flames the effect can be considerable.

2.1.3 **Asymptotics**

Asymptotic analysis is a mathematical technique which has recently become important in combustion theory. It provides a way of obtaining analytical expressions for quantities of interest, particularly the burning velocity. This has the advantage of aiding physical understanding of the processes involved. The disadvantage of the method is that the large amount of simplification required usually prevents quantitative comparison with experiment.

The technique involves asymptotic expansions built around a large parameter. The most commonly-used parameter in combustion theory is the activation energy of a single-step reaction. The large activation energy means that the reaction rate will be strongly temperature-dependent. The result is that the premixed flame can be considered to have two zones: a wide preheat zone where the physical processes are convection and diffusion but reaction is negligible; and a narrow reaction zone where reaction and diffusion occur, with neglible convection.

In this section, a burning rate expression will be derived for the simplest possible premixed flame using activation energy asymptotics. This will introduce the method and demonstrate the main factors affecting the burning velocity. Expressions will then be quoted for more complicated systems.

2.1.3.1 Derivation of the model equations

In this section we make simplifying assumptions to make the equations derived in Section 2.1.1 tractable. By introducing the mass flux fraction we show that if the Lewis number is unity, only one equation needs to be solved. We then derive a dimensionless form of the energy equation to be solved by asymptotic methods in the next section.

We make the following assumptions in addition to those listed in Section 2.1.

1. The flame is planar, so the stream tube area A is a constant.
2. Soret effects are neglected.

3. The gas is assumed to be a binary mixture in which the unimolecular reaction $R \rightarrow P$ occurs.
4. The specific heats of both species are taken to be constant and equal.
5. The Lewis number Le (defined as the ratio of thermal diffusivity to molecular diffusivity) is equal to 1.
6. The temperature dependence of the thermal conductivity is given by

$$\lambda T^{\alpha_1 - 1} = \text{constant}$$

where α_1 is the temperature exponent in the reaction rate expression (8).

First, we introduce the mass flux fraction

$$\epsilon_i = \frac{\rho Y_i (v + V_i)}{\rho v}. \tag{56}$$

The species conservation equation (18) then reduces to

$$m \frac{d\epsilon_i}{dx} = w_i \tag{57}$$

and the neglect of thermal diffusion (the Soret effect) means that the last term disappears from the diffusion equation (19) so that it becomes

$$\frac{dX_i}{dx} = \frac{m}{\rho} \sum_{j=1}^{N} \left(\frac{X_i X_j}{D_{ij}} \right) \left(\frac{\epsilon_j}{Y_j} - \frac{\epsilon_j}{Y_j} \right), \qquad i = 1, \ldots N. \tag{58}$$

The energy equation (16) with the heat flux term given by equation (20) can be written

$$m \sum_{i=1}^{N} h_i \epsilon_i - \lambda \frac{dT}{dx} = \text{constant}. \tag{59}$$

The assumption of constant specific heats means that equation (12) reduces to

$$h_i = h_i^f + c_p (T - T_f). \tag{60}$$

We now introduce the dimensionless temperature

$$\tau = \frac{T - T_u}{T_b - T_u} \tag{61}$$

and the dimensionless distance

$$\xi = \int_0^x \frac{Mc_p}{\lambda}\, dx. \tag{62}$$

By using equations (60), (61) and (62), the boundary conditions $d/dx = 0$ at $x = \pm\infty$ and the identity $\epsilon_1 + \epsilon_2 = 1$, it can be shown that the energy equation (59) reduces to

$$\frac{d\tau}{d\xi} = \tau - \epsilon \tag{63}$$

where ϵ is the normalized mass flux fraction (or reaction progress variable) defined by

$$\epsilon = \frac{\epsilon_2 - \epsilon_{2u}}{\epsilon_{2b} - \epsilon_{2u}}. \tag{64}$$

For the present two-component mixture, the diffusion equation (58) reduces to

$$\frac{dY_i}{dx} = \frac{m}{\rho D_{12}}(Y_i - \epsilon_i) \tag{65}$$

which is Fick's law. Since the boundary conditions require that $dY_i/dx = 0$ at $x = \pm\infty$, it follows that $Y_{iu} = \epsilon_{iu}$ and $Y_{ib} = \epsilon_{ib}$, i.e. the diffusion velocities vanish far upstream and downstream. Hence, in terms of the normalized mass fraction

$$Y = \frac{Y_2 - Y_{2u}}{Y_{2b} - Y_{2u}}, \tag{66}$$

equation (65) becomes

$$\frac{1}{\mathrm{Le}} \frac{dY}{d\xi} = Y - \epsilon \tag{67}$$

where equations (62) and (64) have been used and the Lewis number is

$$\mathrm{Le} = \frac{\lambda}{\rho D_{12} c_p}. \tag{68}$$

The Lewis number is a measure of the ratio of the energy transported by conduction to that transported by diffusion. For a multicomponent mixture, Lewis numbers may be defined for each pair of species. In asymptotic theories of premixed flames, an "effective" Lewis number of a mixture is often defined as the Lewis number of the deficient reactant, or as some combination of the Lewis numbers of the two reactants[35]. For the binary mixture we are considering here there is just one Lewis number since $D_{12} = D_{21}$. The effective Lewis number is often close to 1 for combustible gas mixtures, so the assumption that $\mathrm{Le} = 1$ should provide realistic results. It is worth pointing out, though, that small differences from 1 can lead to new phenomena as we will see later in this chapter.

Putting $\mathrm{Le} = 1$ in equation (67) and subtracting from (63) gives

$$\frac{d(\tau - Y)}{d\xi} = \tau - Y \tag{69}$$

which has the general solution

$$\tau - Y = ae^{\xi}. \tag{70}$$

Since both τ and Y are bounded as $\xi \to \infty$, it follows that $a = 0$ and

$$\tau = Y. \tag{71}$$

We therefore only need to solve one equation for the model we are considering. We will solve the energy equation and obtain an expression for the burning rate and the temperature as a function of distance through the flame. The mass fractions can then be obtained by using equations (66) and (71) and the identity

$$Y_1 + Y_2 = 1. \tag{72}$$

It is possible to derive a suitable form of the energy equation from equation (63). We will take a different route, however. To emphasize the connection between the

asymptotic analysis and numerical solution, we will start with equation (24). The requirement that the flame be planar implies that the stream tube area A is constant. Dividing through by A gives

$$Mc_p\frac{dT}{dx} - \frac{d}{dx}\left(\lambda\frac{dT}{dx}\right) + \rho\sum_{i=1}^{N} Y_i V_i c_{pi}\frac{dT}{dx} + \sum_{i=1}^{N} w_i h_i = 0 \tag{73}$$

where $M = m/A$ is the constant mass flux which is equal to the mass burning rate we wish to determine.

The assumption that all the specific heats are equal means that the third term in equation (73) disappears since $\sum Y_i V_i = 0$.

For a two-component mixture with a single unimolecular reaction $R \rightarrow P$ where subscripts 1 and 2 denote reactant and product species respectively, we have

$$\nu''_{1,1} = \nu'_{2,1} = 0, \tag{74}$$

$$\nu'_{1,1} = \nu''_{2,1} = 1, \tag{75}$$

$$W_1 = W_2 = W \tag{76}$$

and

$$X_i = Y_i. \tag{77}$$

The ideal gas law equation (9) then reduces to

$$p = \rho RT/W \tag{78}$$

and the reaction rate given by equation (8) becomes

$$w_1 = -w_2 = -\frac{WpB_1T^{\alpha_1}}{RT}X_1\exp(-E_1/RT)$$

$$= -\rho B_1 T^{\alpha_1}(1 - Y_2)\exp(-E_1/RT) \tag{79}$$

where equations (72), (77) and (78) have been used. In view of equation (79), the last term in equation (73) becomes

$$\sum_{i=1}^{N} w_i h_i = w_2(h_2^f - h_1^f) = -w_2 \frac{c_p(T_b - T_u)}{Y_{2b} - Y_{2u}} \tag{80}$$

where the definition of heat of combustion as the difference between the enthalpies of formation has been used.

If, along with the above changes, the dimensionless variables defined in equations (76) and (77) (with M replacing m) are introduced, equation (73) becomes

$$\frac{d^2\tau}{d\xi^2} - \frac{d\tau}{d\xi} = -\frac{\lambda\rho B_1 T^{\alpha_1}}{M^2 c_p}(1 - \tau)\exp(-E_1/RT). \tag{81}$$

Finally, we introduce three more dimensionless variables. These are the temperature rise divided by the final temperature,

$$\alpha = \frac{T_b - T_u}{T_b}, \tag{82}$$

the Zel'dovich number (a measure of the temperature sensitivity of the overall reaction rate),

$$\beta = \frac{E(T_b - T_u)}{RT_b^2} \tag{83}$$

and the burning rate eigenvalue

$$\Lambda = \frac{\rho\lambda B T^{\alpha_1}}{M^2 c_p} \exp(-E/RT_b^2). \tag{84}$$

The energy equation then finally becomes

$$\frac{d^2\tau}{d\xi^2} - \frac{d\tau}{d\xi} = -\Lambda\omega \tag{85}$$

where

$$\omega = (1 - \tau)\exp\{-\beta(1 - \tau)/[1 - \alpha(1 - \tau)]\} \qquad (86)$$

is the dimensionless reaction rate.

Equation (85) represents a balance between dimensionless terms representing diffusion, convection and reaction respectively. This form of the equation highlights a long-standing problem in flame theory known as the "cold boundary difficulty". Upstream of the flame, i.e. as $\xi \to -\infty$, the dimensionless temperature should tend to zero smoothly such that $d^2\tau/d\xi^2$ and $d\tau/d\xi$ also tend to zero. However, the term on the right-hand side equals $\exp[-\beta/(1 - \alpha)] \neq 0$ when $\tau = 0$: there is still chemical reaction (albeit very slow) in the unburnt gas. This leads to mathematical difficulties: τ becomes negative near the cold boundary. In order to avoid such problems, an artificial "ignition temperature" was introduced in early theories as described in ref. 31 below which no reaction occurred. Other theories[36] made use of a flame holder acting as a weak heat sink. Williams[31] showed that this is mathematically equivalent to the use of an ignition temperature. In another approach, Friedman and Burke[37] used a modified reaction rate function which was zero at $\tau = 0$. The introduction of asymptotic analysis, described in the next section, made these artificial methods unnecessary for studying adiabatic flames.

2.1.3.2 Asymptotic analysis

Asymptotic analysis provides an analytical way of solving equation (85) by taking advantage of the strongly temperature-dependent reaction rate: the solution is an expansion about infinite activation energy (strictly Zel'dovich number) and the method is therefore known as activation energy asymptotics.

We consider the parametric limit in which β tends to ∞ with α of order unity and held fixed and with Λ required to vary with β in such a way that a nontrivial result is obtained.

The Zel'dovich number β is a dimensionless measure of the temperature sensitivity of the overall reaction rate; qualitatively it can be considered a measure of the strength of the dependence of the reaction rate on the extent of reaction completed. The attribute that is essential to the asymptotic approach is that the non-negative single-peaked rate function occurs at a location progressively closer to the fully burnt condition as β tends to ∞.

From equation (86) it can be seen that as β becomes large the reaction rate becomes very small ("exponentially small" since β appears inside the exponential) unless τ is very near unity. Hence for $(1 - \tau)$ of order unity, i.e. low temperatures, there is a zone in which the reaction rate is negligible and in which the convective and diffusive terms in (85) must be in balance. To describe this "convective-diffusive zone", we introduce an outer expansion

$$\tau = \tau_0(\xi) + H_1(\beta)\tau_1(\xi) + H_2(\beta)\tau_2(\xi) + \ldots, \tag{87}$$

where

$$\lim_{\beta\to\infty} [H_{n+1}(\beta)/H_n(\beta)] = 0 \tag{88}$$

with

$$H_0(\beta) = 1. \tag{89}$$

Substituting the expansion (87) into equation (85) gives

$$\sum_{n=0}^{\infty} H_n \frac{d^2\tau_n}{d\xi^2} - \sum_{n=0}^{\infty} H_n \frac{d\tau_n}{d\xi} = -\Lambda\omega. \tag{90}$$

In the limit $\beta \to \infty$ this becomes

$$\frac{d^2\tau_0}{d\xi^2} = \frac{d\tau_0}{d\xi}. \tag{91}$$

Subtracting this from equation (90), dividing by $H_1(\beta)$ and taking the limit $\beta \to \infty$ again gives

$$\frac{d^2\tau_1}{d\xi^2} = \frac{d\tau_1}{d\xi}. \tag{92}$$

and the sequence can be repeated indefinitely, giving the sequence of outer equations

$$\frac{d^2\tau_n}{d\xi^2} = \frac{d\tau_n}{d\xi}, \qquad n = 0, 1, 2, \ldots \tag{93}$$

provided

$$\lim_{\beta\to\infty} \frac{\Lambda e^{-a\beta}}{H_n(\beta)} = 0 \tag{94}$$

for any fixed a of order unity. This last restriction is satisfied by all algebraic (power-type) ordering functions, e.g. $H_n(\beta) \propto \beta^{-n}$; the reaction-rate term can contribute to equation (93) only at exponentially small orders, e.g. $H_n(\beta) \propto e^{-a\beta}$. The solutions to equation (93) satisfying the boundary condition that $\tau = 0$ at $\xi = -\infty$ are

$$\tau_n = A_n e^{\xi}, \qquad n = 0, 1, 2, \ldots \tag{95}$$

where the A_n are constants to be determined by matching conditions. Equation (95) must fail if ξ becomes sufficiently large; in fact, from equation (86) it is seen that when $(1 - \tau)$ becomes of order β^{-1}, the reaction rate term is no longer exponentially small. This observation indicates the need for a downstream zone in which $(1 - \tau)$ is of order β^{-1}. An appropriate stretched dependent variable for this zone is $y = \beta(1 - \tau)$. We now determine a suitable independent variable for use with y. If this independent variable is denoted by η, then any selection having

$$\lim_{\beta\to\infty} \frac{d\eta}{d\xi} = 0 \tag{96}$$

produces in the lowest order a first-order equation that expresses a convection-reaction balance and lacks the flexibility needed to satisfy the downstream boundary conditions and simultaneously match with equation (95). Thus the downstream zone cannot be thicker than the upstream zone. If the limit is of order unity then again matching cannot be achieved. Therefore,

$$\lim_{\beta\to\infty} \frac{d\eta}{d\xi} = \infty; \tag{97}$$

the downstream zone is thinner than the upstream zone and may reasonably be viewed as an inner zone. Any stretching of this type causes the convective term in equation (85) to become small compared with the diffusive term, and since at least two terms are needed to satisfy the matching and boundary conditions successfully, there must be a reactive-diffusive balance in the inner zone to the lowest order. The inner zone is therefore termed a "reactive-diffusive" zone. With the stretching

$$\eta = \frac{\xi - \xi_0}{s(\beta)}, \tag{98}$$

where $s \to 0$ as $\beta \to \infty$, equation (85) written in inner variables is

$$\frac{d^2y}{d\eta^2} - s\frac{dy}{d\eta} = s^2\Lambda y\exp[-y/(1 - \alpha y/\beta)], \tag{99}$$

where use has been made of equation (86).

In equation (99) an inner expansion of the form

$$y = y_0(\eta) + h_1(\beta)y_1(\eta) + h_2(\beta)y_2(\eta) + \ldots \tag{100}$$

may be introduced, where

$$\lim_{\beta\to\infty} [h_{n+1}(\beta)/h_n(\beta)] = 0 \tag{101}$$

with

$$h_0(\beta) = 1. \tag{102}$$

From equation (99) it is seen that in the limit $\beta \to \infty$ ($s \to 0$), the necessary reactive-diffusive balance with y and η of order unity will be maintained only if $s^2\Lambda$ is finite and nonzero in the limit. Therefore the expansion

$$\Lambda = (1/s^2)[\Lambda_0 + s_1(\beta)\Lambda_1 + s_2(\beta)\Lambda_2 + \ldots] \tag{103}$$

is introduced as well, where

$$\lim_{\beta\to\infty} [s_{n+1}(\beta)/s_n(\beta)] = 0 \tag{104}$$

with

$$s_0(\beta) = 1. \tag{105}$$

Following a procedure analogous to that described for the outer expansion, we then generate a sequence of inner equations, the first of which is

$$\frac{d^2y_0}{d\eta^2} = \Lambda_0 y_0 \exp(-y_0). \tag{106}$$

The downstream boundary condition, $y \to 0$ as $\eta \to \infty$, may be applied to the inner equations. The first integral of equation (106) is then

$$\frac{1}{2}\left(\frac{dy_0}{d\eta}\right)^2 = \Lambda_0 \int_0^{y_0} y' e^{-y'} dy' = \Lambda_0[1 - (1 + y_0)\exp(-y_0)]. \tag{107}$$

It is found that to achieve matching the negative square root must be taken in equation (107) when obtaining $dy_0/d\eta$. A further integration then gives

$$\eta = -\frac{1}{(2\Lambda_0)^{1/2}} \int^{y_0} \frac{dy'}{[1 - (1 + y')e^{-y'}]^{1/2}} + \text{constant}. \tag{108}$$

An expansion of this formula for large negative values of η produces

$$y_0 = -(2\Lambda_0)^{1/2}\eta + \text{constant} + \text{e.s.t.} \tag{109}$$

where e.s.t. stands for terms that go to zero exponentially in η as $\eta \to -\infty$. The higher order equations for y_n $(n = 1, 2, \ldots)$ are linear, and can be solved exactly.

Completion of a solution by matched asymptotic expansions entails using matching conditions. The method we will use here involves the investigation of a parametric limit in an intermediate variable. Thus we consider $\beta \to \infty$ with η_t held fixed, where

$$\eta_t = \frac{s(\beta)\eta}{t(\beta)}$$

$$= \frac{\xi - \xi_0}{t(\beta)}, \tag{110}$$

with $t(\beta) \to 0$ and $t(\beta)/s(\beta) \to \infty$ in the limit. The general matching condition is then written as

$$s_0 + H_1 s_1 + \ldots \sim 1 - \beta^{-1}(y_0 + h_1 y_1 + \ldots), \tag{111}$$

where ~ implies that when η_t is introduced on both sides, the two asymptotic expansions must agree. From equations (95) and (109), equation (111) may be written as

$$A_0\exp(\xi_0)(1 + t\eta_t + \ldots) + H_1A_1\exp(\xi_0) + \ldots$$

$$\sim 1 + \beta^{-1}(2\Lambda_0)^{1/2}(t/s)\eta_t + \ldots \qquad (112)$$

Equation (112) is used repeatedly at successively higher orders to evaluate constants and ordering functions. Thus we first find that $A_0\exp(\xi_0) = 1$ and next find that s must be of order β^{-1}; hence we may put $s = \beta^{-1}$, thereby obtaining the further matching requirement $(2\Lambda_0)^{1/2} = 1$. These last results provide the first approximation to the burning rate eigenvalue,

$$\Lambda \approx \Lambda_0/s^2 = \beta^2/2. \qquad (113)$$

By proceeding further with the expansion and matching, it may be shown that $H_n = \beta^{-n}$, $h_n = \beta^{-n}$, $s_n = \beta^{-n}$ and $\Lambda_1 = 3\alpha - \gamma$, where

$$\gamma = \int_0^\infty \{1 - [1 - (1 + y_0)\exp(-y_0)]^{1/2}\}\, dy_0 = 1.3440. \qquad (114)$$

With these results, the two-term expansion for Λ is

$$\Lambda = \beta^2/2 + \beta(3\alpha - \gamma). \qquad (115)$$

The flame structure calculated here is shown in Fig. 2 for a value of β of 6. ξ_0 was set to zero and the outer solution was $r = e^{\xi}$. The inner solution was obtained by numerically integrating equation (108) at various values of y_0 and with an arbitrary constant lower limit of integration using Simpson's rule. This lower limit, which is equivalent to the constant of integration, fixes the position of the resulting curve with respect to the ξ axis. The correct solution was chosen by moving the inner solution with respect to the abscissa (and therefore adjusting the constant of integration) until the slopes of inner and outer solutions matched[31]. There are two zones through which the temperature varies: a thicker upstream zone in which the reaction rate is negligible to all algebraic orders in β^{-1}, followed by a thinner reaction zone in which convection is negligible to the lowest order in β^{-1}. The reaction occurs in the downstream zone because the temperature is too low for it to

FIGURE 2

Flame structure determined by asymptotic analysis

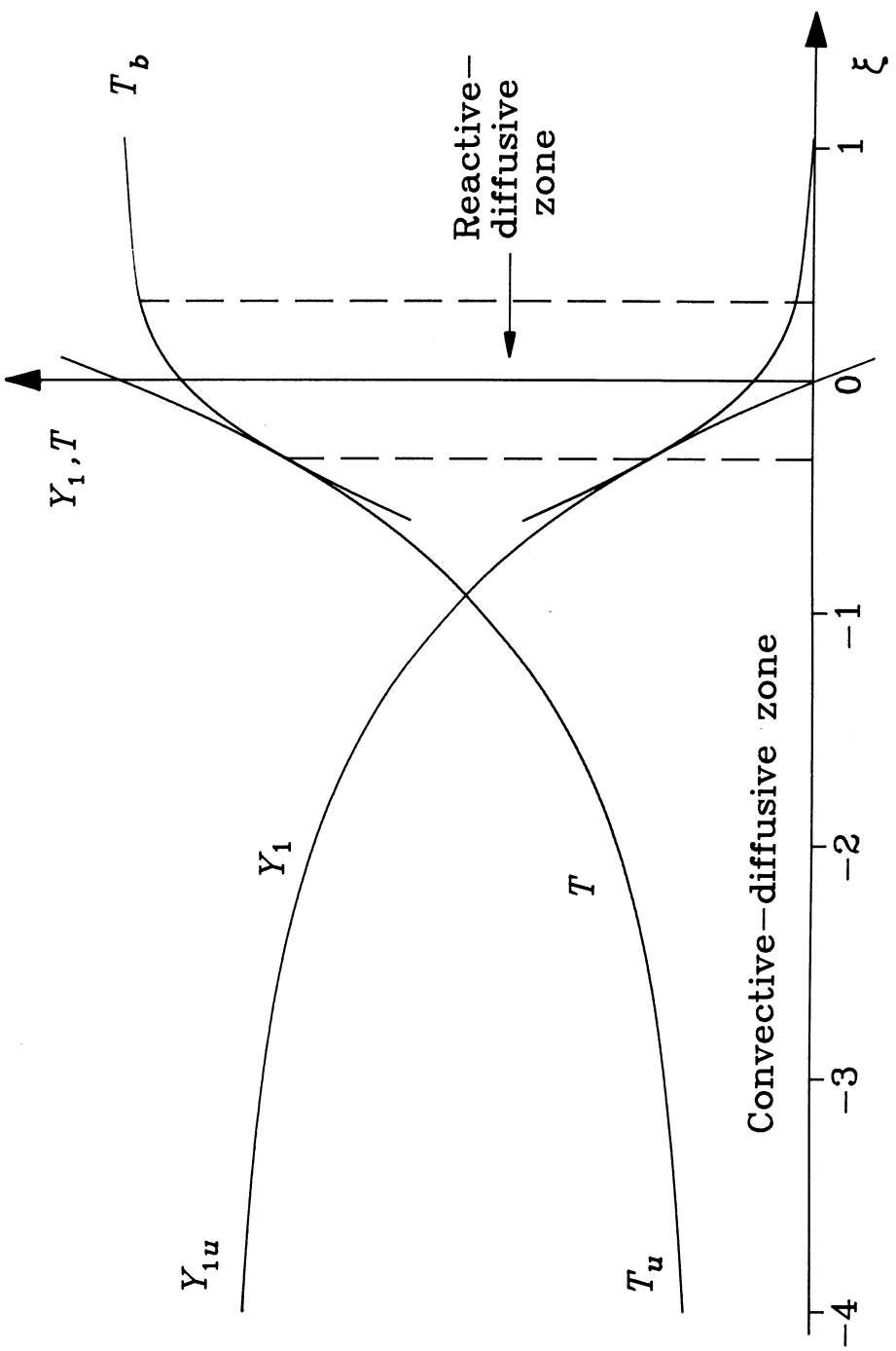

occur appreciably upstream; where the reaction is occurring, the reactant concentration has been depleted by diffusion so that it is of order β^{-1} times the initial reactant concentration.

According to equation (62), the abscissa is in units of λ/Mc_p. This is commonly used as a measure of the flame thickness, as in equation (36) for example. It is worth noting that in fact this is the distance from the reaction zone to the point where the dimensionless temperature is 1/e (about 37%) of its final value. The overall thickness is rather larger. For example, the distance between the points where the dimensionless temperature is 1% and 99% of its final value is about 5 of these "flame thicknesses".

The burning rate expression can be put in dimensional form by combining equation (115) with the definition of Λ in equation (69). The result is

$$S_u^{\,o} = \frac{1}{\rho_u}\left[\frac{2\lambda\rho BT^{\alpha_1}}{\beta^2 c_p}\right]^{1/2}\exp(-E/2RT_b)\left[1 + \frac{\gamma - 3\alpha}{\beta}\right] \qquad (116)$$

where terms of order β^{-2} have been neglected in the binomial expansion used to obtain the contents of the right-hand bracket. The parameters α and β are given by equations (67) and (68). This result has come formally from the matching condition and represents the only burning velocity for which an internally consistent asymptotic structure for the deflagration can be obtained. Retention of the second term is important at small values of β (say between 2 and 5), where it can produce corrections to the burning velocity approaching 50% in some cases[38].

Comparison of the first term of equation (116) with equation (34) produced by the phenomenological analysis in Section 2.1.2 shows that the main dependences were correctly predicted. In addition, the nature of the parameters β_1 and β_2 is now clarified. Since phenomenological analyses are used to make several important points in this work, it is useful to have this confirmation that correct results are obtained.

We close this section by quoting burning rate expressions for more realistic models. If the Lewis number is allowed to differ from 1 but all of the other assumptions are retained then the two-term expansion for Λ is found to be[38]

$$\Lambda = \beta^2/(2\mathrm{Le}) + \beta[(3\alpha - \gamma) - 2(1 - \mathrm{Le})]/\mathrm{Le}. \qquad (117)$$

When Le = 1 the expression reduces to equation (115) which was derived earlier. The corresponding expression for the burning rate is

$$S_u^{\circ} = \frac{1}{\rho_u}\left[\frac{2\mathrm{Le}\lambda\rho BT^{\alpha_1}}{\beta^2 c_p}\right]^{1/2}\exp(-E/2RT_b)\left[1 + \frac{\gamma - 3\alpha + 2(1 - \mathrm{Le})}{\beta}\right]. \qquad (118)$$

Again, all the dependences in the first term are predicted by equation (54) produced by the phenomenological analysis in Section 2.1.2.

The burning rate (to lowest order in β^{-1}) for a two-reactant flame with arbitrary Lewis numbers is[39]

$$S_u^{\circ} = \frac{1}{\rho_u}\left[\frac{2\lambda_b \nu'_{1,1}(\nu'_{2,1}/\nu'_{1,1})^m \rho_b^n B_{1,b} T_b^{\alpha_1} Y_{1u}^{n-1}}{\beta^{n+1} c_{pb} W_1^{n-1} \mathrm{Le}_1^{-k} \mathrm{Le}_2^{-m}}\right]^{1/2}$$

$$\times G^{1/2}(k,m,a)\exp(-E/2RT_b) \qquad (119)$$

where $i = 1, 2$ are the two reactants, k and m identify the reaction orders with respect to these reactants (with $n = k + m$ for clarity) and Le_1 and Le_2 are the corresponding Lewis numbers defined by $\mathrm{Le}_i = \lambda/\rho D_{iN} c_p$. D_{iN} is the diffusion coefficient of species i with respect to an inert N present in excess. The function G is defined by

$$G(k,m,a) = \int_0^{\infty} y^k (y + a)^m e^{-y}\, dy \qquad (120)$$

where $a = \beta(\phi - 1)/\mathrm{Le}_2$, with $\phi = \nu_1 W_1 Y_{2u}/\nu_2 W_2 Y_{1u}$ being the equivalence ratio. Equation (119) holds for $\phi \geq 1$ - that is, if the mixture is stoichiometric or if species 2 is in excess; for $\phi < 1$ the species definitions are interchanged.

2.2 FLAME STRETCH

The whole of Section 2.1 dealt with the theory of steady-state, one-dimensional flames, in which the flame is stationary and the flow direction is everywhere normal to the flame surface. The use of this simplification allows a good understanding of flames to be achieved; in addition, numerical modelling of such systems using computers can provide detailed predictions of flame properties for comparison with experiment.

However, no real flames are one-dimensional, and it is necessary to consider how much this matters. For the purposes of the present work, it is possible to consider the effects of non-one-dimensionality on the burning rate under two headings, "apparent effects" and "real effects".

The "apparent effects" on the burning rate are those which arise when the flow speed is measured at the wrong place. A major point of this thesis is that the burning velocity of a flame is determined in the hot part of the flame, at a position that we call the reference surface.

If flames were planar and one-dimensional, it would not matter where the burning velocity was determined. Velocity measurements at the cold boundary (or anywhere upstream of it) would give correct values for the burning velocity. But real flames are not planar and one-dimensional. Particle tracking photographs show that in almost all flames the streamlines bend outwards between the cold boundary and the luminous zone, a phenomenon known as stream tube divergence[22]. Let us assume, for the purposes of illustration, that the reference surface is at the luminous zone and that the mass flux there is the same as the planar, one-dimensional value. Then if the streamlines diverge, the speed of the gas at the cold boundary must be greater than in the planar one-dimensional case in order to supply the larger area at the reference surface at the same rate.

The foregoing was pointed out by Fristrom[20], Dixon-Lewis[40] and others, but has not yet become well accepted. The subject will be treated in more detail in Chapter 3. For the moment we can say that if the reference surface were at the cold boundary (where the burning velocity is conventionally measured) or if flow divergence corrections were made to burning velocity data as a matter of course then the "apparent effects" of non-one-dimensionality of real flames would not exist.

The "real effects" on the burning rate are those due to flame stretch, which is the subject of this section. Ideas on flame stretch have changed a little since the concept was first introduced by Karlovitz et al[41], so it will be as well to outline the usage in this thesis.

Flame stretch is a local, time-varying property of a flame. It is the rate of change per unit area of an element of flame surface, where the element is defined by points on the surface moving at the local tangential gas velocity[42]. In order to apply the definition to a real flame, a part of the flame representing the flame surface must be identified, for example an arbitrarily selected isotherm within the flame structure[43]. In the present work, the flame surface will be considered to coincide with the reference surface.

Stretch affects the propagation rate by changing the diffusive flux of reactant downstream into the reaction zone and of heat upstream out of it. Since the balance of these fluxes has an influence on the flame temperature and since the reaction rate varies strongly with temperature, flame stretch can affect the reaction rate and therefore the burning rate.

The effect of stretch on the flame depends upon the mixture composition. In particular, we will see later in this section that phenomenological and asymptotic analyses of stretched flames predict that the effective Lewis number of the reacting mixture determines whether the burning velocity increases or decreases, and to what extent. One aim of the work in this thesis is to determine the extent to which the predictions of these analyses are supported by experimental evidence.

2.2.1 **Mathematical analysis**

Flame stretch was defined by Williams[42] as

$$\Gamma = \frac{1}{A}\frac{dA}{dt} \tag{120}$$

where Γ is the stretch, A is an element of flame area and t is time. The element of area is defined by points on the flame surface moving at the local tangential velocity. A dimensionless stretch rate is commonly used in theoretical work. It is defined by

$$\kappa = \frac{\delta}{S_u^{\circ}}\Gamma = \frac{\delta}{S_u^{\circ}}\frac{1}{A}\frac{dA}{dt} \tag{121}$$

where δ/S_u° is a characteristic flow time of the flame; δ and S_u° are the flame thickness and burning velocity respectively of the unstretched one-dimensional flame.

As it stands, equation (120) can only be easily applied in a few special cases. It is useful, therefore, to derive a formulation in vector notation which can be applied generally. Such an expression was first obtained by Matalon[44], and subsequently by Chung and Law[45] using a simpler derivation. An alternative derivation was given by Candel and Poinsot[46]. The following derivation is based on Chung and Law's treatment.

The flame is considered to be a smooth, deformable surface. The position of any point on the flame surface is considered to be identifiable, such that a tangential velocity can be ascribed to the flame at any point, in addition to the more easily detected normal velocity (relative to laboratory coordinates).

Positions on the flame surface are defined by a surface curvilinear coordinate system (p,q). The evolution of the flame surface can then be represented by $\mathbf{r} = \mathbf{r}(p,q,t)$ where t is time. The arcs $d\mathbf{s}$ in the directions of p and q can be approximated by their projections on the tangent plane at $\mathbf{r}$ (see Fig. 3(a)) as

$$(d\mathbf{s})_p = \frac{\partial \mathbf{r}}{\partial p}\,dp, \qquad (d\mathbf{s})_q = \frac{\partial \mathbf{r}}{\partial q}\,dq. \tag{122}$$

The area of the parallelogram defined by these arcs is

$$A(t) = (d\mathbf{s})_p \times (d\mathbf{s})_q \cdot \mathbf{n}$$

$$= \left(\frac{\partial \mathbf{r}}{\partial p} \times \frac{\partial \mathbf{r}}{\partial q}\right)\cdot \mathbf{n}\; dpdq \tag{123}$$

where $\mathbf{n}$ is the unit vector normal to the surface. At the time $(t + \delta t)$ the flame surface can be approximated by

$$\mathbf{r}(p,q,t + \delta t) = \mathbf{r}(p,q,t) + \mathbf{v}(p,q,t)\delta t \tag{124}$$

FIGURE 3

(a) Flame surface nomenclature; (b) Bunsen flame tip in uniform flow;
(c) Bunsen flame tip in divergent flow

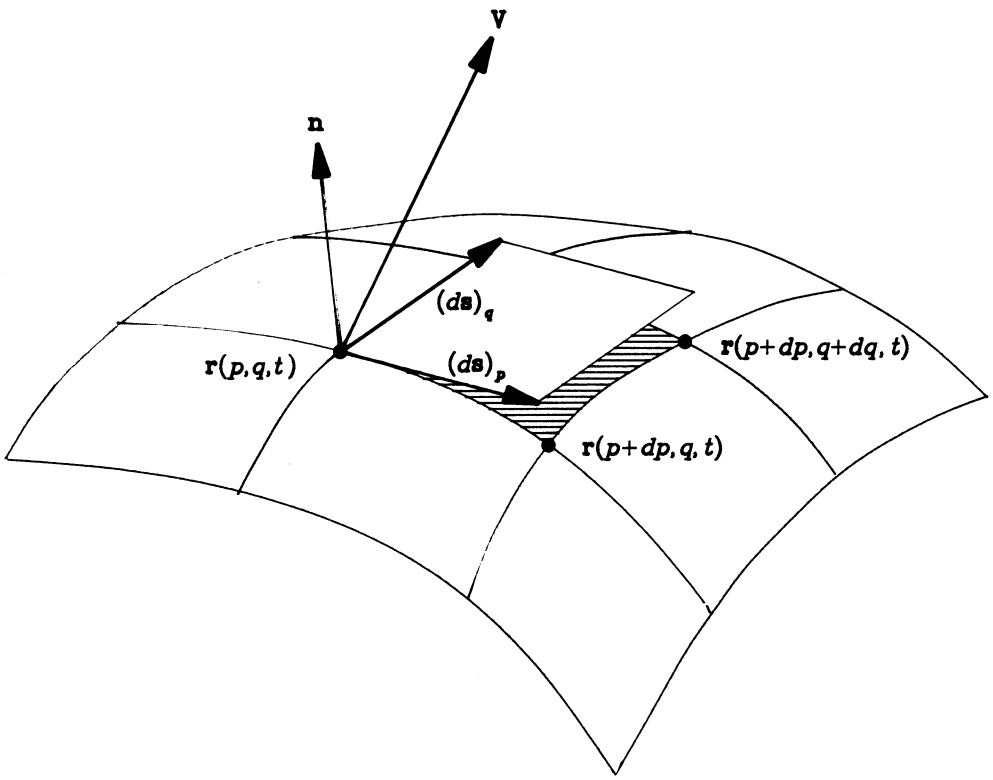

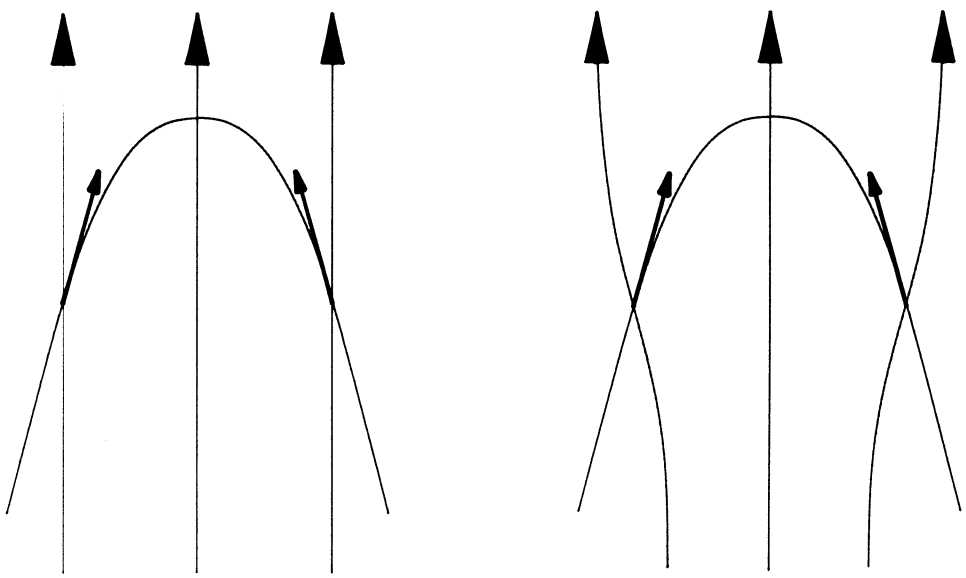

where $\mathbf{v}$ is the velocity of the flame surface relative to laboratory coordinates. The sides of the new parallelogram at $(t + \delta t)$ become

$$(d\mathbf{s})_p' = \frac{\partial \mathbf{r}}{\partial p}\, dp + \frac{\partial \mathbf{v}}{\partial p}\, dp\delta t, \quad (d\mathbf{s})_q' = \frac{\partial \mathbf{r}}{\partial q}\, dq + \frac{\partial \mathbf{v}}{\partial q}\, dq\delta t. \tag{125}$$

The new area is

$$A(t + \delta t) = \left\{\left(\frac{\partial \mathbf{r}}{\partial p} + \frac{\partial \mathbf{v}}{\partial p}\delta t\right) \times \left(\frac{\partial \mathbf{r}}{\partial q} + \frac{\partial \mathbf{v}}{\partial q}\delta t\right)\right\} \cdot \mathbf{n}\, dpdq. \tag{126}$$

Therefore from the definition of flame stretch (equation 120) we have

$$\Gamma = \frac{1}{A} \lim_{\delta t \to 0} \frac{A(t + \delta t) - A(t)}{\delta t}$$

$$= \frac{\left(\frac{\partial \mathbf{v}}{\partial p} \times \frac{\partial \mathbf{r}}{\partial p} + \frac{\partial \mathbf{r}}{\partial p} \times \frac{\partial \mathbf{v}}{\partial q}\right) \cdot \mathbf{n}}{\left(\frac{\partial \mathbf{r}}{\partial p} \times \frac{\partial \mathbf{r}}{\partial q}\right) \cdot \mathbf{n}}. \tag{127}$$

We now express the velocity of the flame as the sum of its normal and tangential velocity:

$$\mathbf{v} = (\mathbf{v} \cdot \mathbf{n})\mathbf{n} + \mathbf{v}_t. \tag{128}$$

On substituting for $\mathbf{v}$, the numerator of equation (127) becomes

$$\left(\frac{\partial \mathbf{v}_t}{\partial p} \times \frac{\partial \mathbf{r}}{\partial q} + \frac{\partial \mathbf{r}}{\partial p} \times \frac{\partial \mathbf{v}_t}{\partial q}\right) \cdot \mathbf{n} + (\mathbf{v} \cdot \mathbf{n}) \left(\frac{\partial \mathbf{n}}{\partial p} \times \frac{\partial \mathbf{r}}{\partial q} + \frac{\partial \mathbf{r}}{\partial p} \times \frac{\partial \mathbf{n}}{\partial q}\right) \cdot \mathbf{n} \tag{129}$$

where the relation $(\mathbf{n} \times \mathbf{a}) \cdot \mathbf{n} = 0$, which is true for any vector $\mathbf{a}$, has been used.

We now set all the scale factors in the curvilinear coordinate system to 1, without loss of generality. Therefore

$$\frac{\partial \mathbf{r}}{\partial p} = \mathbf{e}_p, \quad \frac{\partial \mathbf{r}}{\partial q} = \mathbf{e}_q, \quad \mathbf{e}_p \times \mathbf{e}_q = \mathbf{n} \tag{130}$$

where $\mathbf{e}_p$ and $\mathbf{e}_q$ are unit vectors in the p and q directions respectively. Thus the denominator of equation (127) is equal to unity and the stretch becomes

$$\Gamma = \left(\mathbf{e}_p \cdot \frac{\partial \mathbf{v}_t}{\partial p} + \mathbf{e}_q \cdot \frac{\partial \mathbf{v}_t}{\partial q}\right) + (\mathbf{v}\cdot\mathbf{n})\left(\mathbf{e}_p \cdot \frac{\partial \mathbf{n}}{\partial p} + \mathbf{e}_q \cdot \frac{\partial \mathbf{n}}{\partial q}\right) \tag{131}$$

where the cyclic law of scalar triple products has been used. The above expression can be expressed as the sum of two divergence terms. The final expression for the flame stretch is therefore

$$\Gamma = \nabla_t \cdot \mathbf{v}_t + (\mathbf{v}\cdot\mathbf{n})(\nabla_t \cdot \mathbf{n}). \tag{132}$$

Although the assumption was made in the derivation that tangential movement of the flame surface could be detected, in fact there is no way of doing this. The physical meaning of the tangential velocity of the flame is taken to be the tangential velocity of the gas crossing the flame. It is interesting to note that this suggests a clear physical distinction between the two terms in equation (132). The first term involves the tangential velocity of the gas crossing the flame while the other depends on the movement of the flame in space and on its curvature.

If the fluid velocity at the flame is $\mathbf{V}$ then the tangential velocity is

$$\mathbf{v}_t = \mathbf{n} \times (\mathbf{V} \times \mathbf{n}) \tag{133}$$

and the first term of equation (132) becomes

$$\nabla_t \cdot [\mathbf{n} \times (\mathbf{V} \times \mathbf{n})]. \tag{134}$$

Using the vector identity

$$\nabla\cdot(\mathbf{A} \times \mathbf{B}) = \mathbf{B}\cdot(\nabla \times \mathbf{A}) - \mathbf{A}\cdot(\nabla \times \mathbf{B}) \tag{135}$$

for any vectors $\mathbf{A}$ and $\mathbf{B}$ along with $\nabla \times \mathbf{n} = 0$, we have

$$\nabla\cdot[\mathbf{n} \times (\mathbf{V} \times \mathbf{n})] = -\mathbf{n}\cdot\nabla \times (\mathbf{V} \times \mathbf{n}). \tag{136}$$

Since we are using surface curvilinear coordinates so that $\partial/\partial n = 0$, it follows that $\nabla_t = \nabla$ and

$$\nabla_t \cdot [\mathbf{n} \times (\mathbf{V} \times \mathbf{n})] = -\mathbf{n}\cdot\nabla \times (\mathbf{V} \times \mathbf{n}). \tag{137}$$

Therefore an alternative expression for the stretch is

$$\Gamma = -\mathbf{n}\cdot\nabla \times (\mathbf{V} \times \mathbf{n}) + (\mathbf{v}\cdot\mathbf{n})(\nabla\cdot\mathbf{n}) \tag{138}$$

which is the expression derived by Matalon[44]. Equation (132) can be considered as the sum of contributions due to strain and curvature. This terminology can lead to confusion, however. Consider its application to a stationary, curved flame in a uniform flow, as in Fig. 3(b). The flame is stretched by a strain contribution although there is no hydrodynamic strain; the strain contribution is due to the flame curvature which does not provide a curvature contribution. A more precise terminology due to Buckmaster[47] will therefore be used in this work. He suggested the names "extensional" and "dilatational" stretch for the two contributions. Equation (132) can therefore be expressed as

$$\Gamma = \Gamma_{ext} + \Gamma_{dil}$$

where

$$\Gamma_{ext} = \nabla_t\cdot\mathbf{v}_t = -\mathbf{n}\cdot\nabla \times (\mathbf{V} \times \mathbf{n}) \tag{139}$$

$$\Gamma_{dil} = (\mathbf{v}\cdot\mathbf{n})(\nabla\cdot\mathbf{n}). \tag{140}$$

The subscript *ext* can sometimes refer to conditions at extinction. No confusion should arise in the present work since it only deals with weak stretch where extinction does not arise. The subdivision into extensional and dilatational contributions is convenient because in this work the two experimental configurations correspond to $\Gamma_{dil} = 0$ (stagnation flow flames) and $\Gamma_{ext} = 0$ (expanding spherical flames). These two cases will now be considered in more detail.

2.2.1.1 Extensional Stretch

In this section we examine equation (139) in more detail and apply it to the stagnation-point flow configuration used in the experiments. We also consider the relationship between flow divergence and extensional stretch.

According to equation (139), the extensional stretch is equal to the divergence of the tangential velocity vector. In a two-dimensional configuration (for example a slot

burner), it is therefore simply the rate of change of the tangential velocity with distance along the flame surface.

In an axisymmetric flame, for example a Bunsen burner, the definition of the vector operation of divergence in cylindrical coordinates (r, ϕ, z) shows that the extensional stretch is given by

$$\Gamma = \frac{1}{r} \frac{d(rv_t)}{ds} \tag{141}$$

where v_t is the tangential velocity and s is distance along the flame. By symmetry, the only component of the tangential velocity is in the ϕ = constant plane. It is interesting to look at the extensional stretch in a Bunsen flame tip in some detail. Consider a uniform flow crossing such a tip as shown in Fig. 3(b). In fact, the flow would not be uniform; this is not important at this stage, but we will return to it later. It is easy to see that there is a tangential velocity towards the tip at each point on the flame surface. This is negative flame stretch, or flame compression. The stretch here is due to the flame shape, and not to the characteristics of the flow. It is an example of how there can be flame stretch without flow divergence.

In a constant density, axisymmetric stagnation-point flow, the velocity field close to the stagnation surface but outside the boundary layer is given by[48]

$$(v_r, v_\phi, v_z) = (cr/2, 0, -cz) \tag{142}$$

where c is a constant. On the assumption that the radial velocity is unaffected by the presence of the flame, the extensional stretch is

$$\Gamma = \frac{1}{r} \frac{d(cr^2/2)}{dr}$$

$$= c$$

$$= - \frac{\partial v_z}{\partial z}. \tag{143}$$

We have therefore proved that the extensional stretch in a constant density, axisymmetric stagnation point flow is equal to minus the upstream velocity gradient.

This result will be used in the experimental methodology for stagnation flow experiments in Section 3.2.

It is worth at this point considering further the flow defined in equation (142) above. It is convenient to define this flow (sometimes known as Hiemenz flow) as "ideal" stagnation flow, because it is used in much theoretical (and implicitly in some experimental) work. It is clear that while constant density flows might approach the ideal quite closely, the same cannot be true when a flame is present. This can be seen most clearly in terms of streamlines. In Section 3.3.1, it will be shown that for ideal flow they have the form $r = a/z^{1/2}$ where a = constant. When a flame is present, the streamlines must deviate from this form. Heat release causes the gas velocity normal to the flame to increase by a factor of the density ratio (about 7 for the fastest methane flames) while, to a first approximation, the tangential velocity is unaffected. The overall effect is a "refraction" of the streamlines towards the normal. The gradual increase in the temperature of the flame means that this bending of the streamlines will occur gradually between the cold boundary and the hot end of the flame. Any calculations of flame properties which involve area ratios (like mass flux at the reaction zone calculated from cold gas properties) will therefore be in error if the ideal model is used.

We now consider flow divergence. The magnitude of the flow divergence can be determined for a stationary flame by dividing the area of the reference surface (roughly, the luminous zone) enclosed by a stream tube by the area of the cold boundary enclosed by the same stream tube. If this area ratio is greater than unity then the flow is divergent. Divergence can arise in three ways: from a straining flow, for example a stagnation-point flow; as a result of flame curvature, as in the stationary spherical flame; or by thermal expansion in the flame, which causes the streamlines to bend outwards in the approach flow. This is in addition to the streamline refraction mentioned above. It is a result of the pressure difference between the flame and the surroundings, which itself is due to the heat release.

Flow divergence is important for two reasons. First, mass is conserved within stream tubes. If a stream tube widens between the cold boundary and the reaction zone then the mass flux at the cold boundary must necessarily exceed that at the reaction zone. If the mass flux at the reaction zone is the correct measure of the rate of propagation of the flame, then burning velocities based on the gas speed at the cold boundary will be too high. This point has been made by several workers[20,40] and was also demonstrated in the phenomenological analysis in Section 2.1.2.

Second, in two of the above cases, flow divergence is related to extensional stretch. Consider a plane flame in an axisymmetric flow, with no externally-applied strain. Particle-tracking photographs show that the flow is divergent in the neighbourhood of the flame[22,49] so it must have acquired a radial velocity. It seems likely that, at least near the axis of the flame, the flow divergence will be cumulative; each element is pushing outwards by about the same amount, so the streamlines will become more oblique to the flame with distance from the axis. The tangential velocity is therefore increasing with radial distance: there is a tangential velocity gradient, so the flame is stretched. The phenomenon has been named "flame-generated stretch"[50,51]. It has not yet been studied in much detail, but may be important in explaining some results which will appear later in this thesis.

In flames which are not planar, the effect of flow divergence on the extensional stretch is less important because extensional stretch also arises as a result of the flame shape. In the Bunsen flame tip example above, the tangential velocities are modified by the flow divergence but the essential fact remains that the tip is negatively stretched as shown in Fig. 3(c).

We will consider how extensional stretch can affect the propagation rate of a flame in the phenomenological analysis of a plane flame in a stagnation-point flow in Section 2.2.2.

2.2.1.2 Dilatational stretch

In a moving flame, stretch arises because its area increases. This is the type of stretch covered in this section. A good example of a flame which is stretched solely by this mechanism is the expanding spherical flame.

In an expanding spherical flame the tangential velocity is zero everywhere, so the first term of equation (132) disappears. The remaining term in the expression is the product of the flame speed and the divergence of the unit normal, which is $2/r$ for a sphere of radius r. If the flame speed is dr/dt then the stretch is simply given by

$$\Gamma = \frac{2}{r}\frac{dr}{dt}. \qquad (144)$$

This expression can also be derived directly from the basic definition of flame stretch in equation (120) as follows. In expanding spherical flames, the spherical

symmetry means that the stretch is the same everywhere and the total flame area can be used in the expression. This is $4\pi r^2$ where r is the flame radius. The stretch is therefore

$$\Gamma = \frac{1}{4\pi r^2} \frac{d(4\pi r^2)}{dt}$$

$$= \frac{2}{r} \frac{dr}{dt}. \qquad (145)$$

This expression will be used in the simple analysis of expanding spherical flames in Section 3.1.

The physical effects of dilatational stretch will be discussed in the phenomenological analysis in the next section.

2.2.2 **Phenomenological analysis**

In this section we give phenomenological analyses of two stretched flames, to provide a physical explanation of the effects being studied in this work. The analysis of a planar flame in a stagnation-point flow is based on that of Chung[34]. The analysis of an expanding spherical flame is new. Both follow on from that of the planar flame with non-unity Lewis number in Section 2.1.2.

2.2.2.1 Planar flame in a stagnation-point flow

A diagram of a planar flame in a stagnation-point flow is given in Fig. 4. The continuity equation (15) applied to this configuration is

$$\rho_M v_M A_M = \rho_T v_T A_T = \rho_b v_b A_b \qquad (146)$$

where the subscripts M and T refer to the upstream boundaries of the mass diffusion and heat conduction zones respectively. We now apply the principle of conservation of energy to the control volume shown in the diagram. The energy in the control volume is constant, so the rate at which energy enters must equal the rate at which it leaves. The possible routes are convection at the upstream and downstream boundaries and diffusion across the streamlines.

FIGURE 4

Control volume in phenomenological model of flame in stagnation-point flow

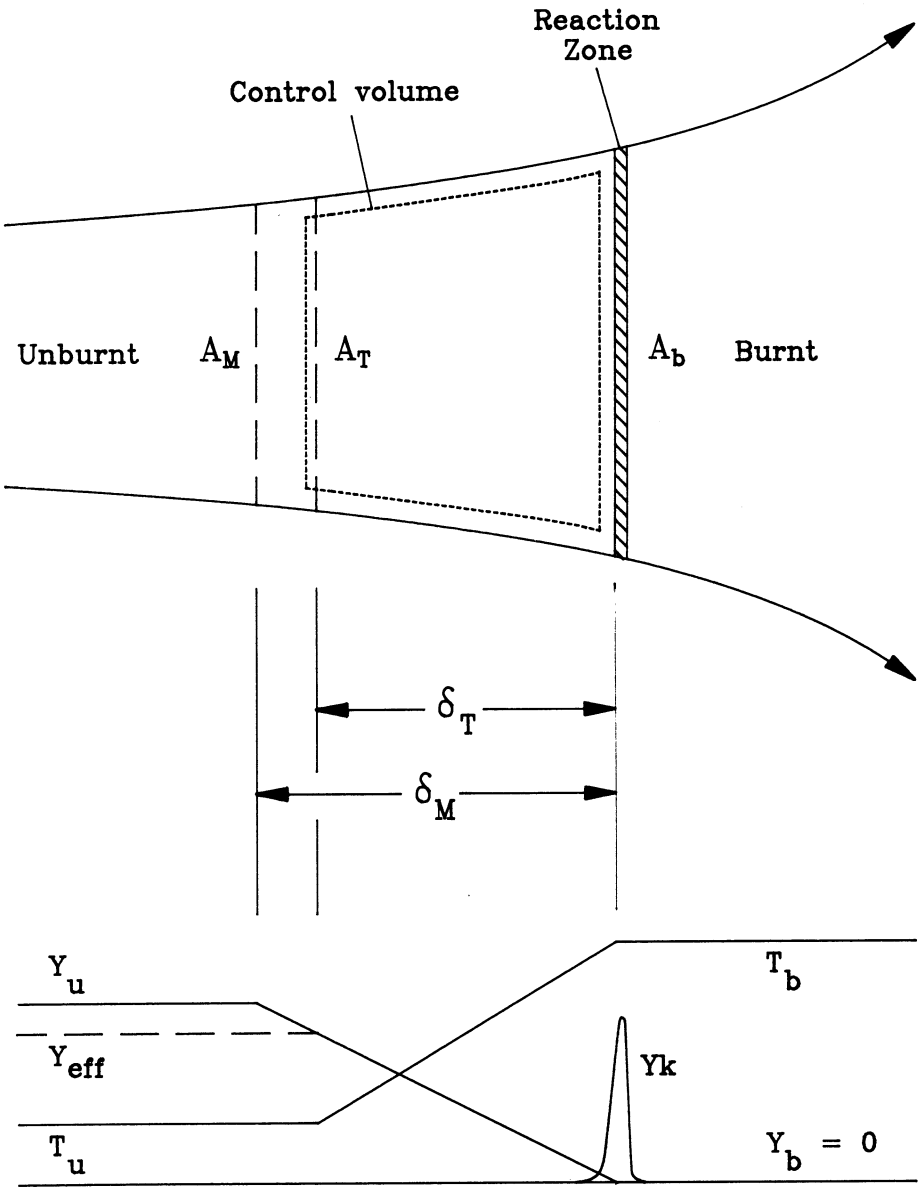

Chemical energy (in the form of reactant) and thermal energy arrive at the upstream boundary of the control volume by convection, and thermal energy is convected away at the downstream boundary. Heat from the reaction zone is conducted upstream across the streamlines and out of the control volume while reactant diffuses into the control volume in the opposite direction. The energy balance can therefore be expressed as

$$c_p(\rho_b v_b A_b T_b - \rho_T v_T A_T T_u) + \lambda \frac{T_b - T_u}{\delta_T}(A_b - A_T)$$

$$= [\rho_M v_M A_M Y_u + \rho D_{12} \frac{Y_u}{\delta_M} (A_b - A_M)]q. \tag{147}$$

Rearranging and using the provisional definition of burning velocity,

$$\rho_b v_b = M_b = \rho_u S_{u,r}, \tag{148}$$

we obtain

$$c_p(T_b - T_u)\left[1 + \frac{\lambda}{\rho_u c_p S_{u,r} \delta_T} \frac{A_b - A_T}{A_b}\right]$$

$$= Y_u q\left[1 + \frac{\rho D_{12}}{\rho_u S_{u,r} \delta_M} \frac{A_b - A_M}{A_b}\right]. \tag{149}$$

Now it will be shown in Chapter 3 that

$$\frac{A_b - A_M}{A_b} = \frac{\delta_T}{S_u^o}\Gamma = \kappa \tag{150}$$

where Γ and κ are the dimensional and dimensionless stretch rates respectively, defined in equations (120) and (121). Since the second term in each of the square brackets is the correction term we want to determine, we need only consider the leading order. Thus $S_{u,r} \approx S_u^o$, $\delta_T \approx \delta_M \approx \delta$ and $A_T \approx A_u \approx A_M$ and

$$c_p T_b = (c_p T_u + Y_u q) + Y_u q\left(\frac{1}{Le} - 1\right)\kappa. \tag{151}$$

The first term in the brackets on the right-hand side equals $c_p T_{ad}$. This expression therefore states that the flame temperature increases if Le < 1 and decreases if Le > 1 for positive stretch.

The change in flame temperature will affect the reaction rate so we examine the effect on it next. Let the reaction rate for a stretched flame with non-unity Lewis number be k_s. Then the balances between heat conduction and reaction and mass diffusion and reaction are given by equations (50) and (51) with k_s replacing k and with Y_{eff} given by equation (49). As in the case of the planar flame with non-unity Lewis number, the preheat zone thickness is given by

$$\delta_T = \left[\beta_1\beta_2 \frac{\lambda}{c_p k_s \mathrm{Le}}\right]^{1/2}. \tag{152}$$

Eliminating the right-hand sides of equations (50) and (51) and substituting (151) gives

$$\frac{\delta_T}{\delta_M} = \mathrm{Le}\left[1 + \left(\frac{1}{\mathrm{Le}} - 1\right)\kappa\right]. \tag{153}$$

Since the term in the brackets on the right-hand side of equation (147) is the total supply rate of reactant mass to the flame, it should equal equation (51) multiplied by the reaction zone area A_b. This gives

$$\rho_M v_M = \frac{1}{\beta_1}\frac{1}{\beta_2} k_s \delta_T \frac{\delta_T}{\delta_M}. \tag{154}$$

Using the continuity equation (146) and the definition of burning velocity (148) in equation (154) we obtain

$$S_{u,r} = \frac{1}{\rho_u}\frac{1}{\beta_1}\frac{1}{\beta_2} k_s \delta_T \frac{\delta_T}{\delta_M}\left(1 - \frac{A_b - A_M}{A_b}\right). \tag{155}$$

Again the area ratio term can be expressed in terms of the dimensionless stretch rate κ. The Arrhenius reaction rate term is proportional to $\exp(-E/RT_b)$ where the flame temperature T_b is in general different from the adiabatic flame temperature T_{ad}. The ratio of the reaction rate in the stretched flame to that in the unstretched one is

$$\frac{k_s}{k} = \frac{\exp(-E/RT_b)}{\exp(-E/RT_{ad})} \approx 1 + \frac{E}{R}\left[\frac{T_b - T_{ad}}{T_{ad}^2}\right]. \tag{156}$$

Using equations (150) and (151) this becomes

$$\frac{k_s}{k} = 1 + \frac{E}{R}\frac{Y_u q}{c_p T_{ad}^2}\left[\frac{1}{\mathrm{Le}} - 1\right]\kappa. \tag{157}$$

We now substitute equations (152) and (153) in (155) and divide by the burning velocity of the unstretched flame given by equation (54). For small dimensionless stretch κ, the result is

$$\frac{S_{u,r}}{S_u^{\circ}} = \left[\frac{k_s}{k}\right]^{1/2}\left\{1+\left[\left[\frac{1}{\mathrm{Le}} - 1\right] - 1\right]\kappa\right\}. \tag{158}$$

Finally, expanding equation (157) for small κ and substituting in equation (158) gives the expression for the effect of stretch on the burning velocity,

$$\frac{S_{u,r}}{S_u^{\circ}} = 1 + \kappa\left[\frac{E}{R}\frac{Y_u q}{c_p T_{ad}^2}\left[\frac{1}{\mathrm{Le}} - 1\right] + \left[\frac{1}{\mathrm{Le}} - 1\right] - 1\right]. \tag{159}$$

We will examine this equation in detail at the end of the next section.

2.2.2.2 Expanding spherical flame

We now analyse an expanding spherical flame, following a similar path to that in the previous analysis. We start by applying the principle of conservation of energy to the expanding flame. In this case the flame is not in a steady state, and we need to consider the energy balance carefully. At any instant, time t say, conservation of energy can be expressed as

$$E_{in} = E_{out} + E_{stored} \tag{160}$$

where E_{in} is the rate at which energy enters the flame, E_{out} is the rate at which it leaves and E_{stored} is the rate of change of the energy stored in the flame. For an expanding spherical flame, the only routes for energy to enter and leave are the upstream and downstream flame boundaries. E_{in} is the convection rate of thermal

and chemical energy across the upstream flame boundary and E_{out} is the rate at which thermal energy is convected away from the downstream boundary.

We now consider E_{stored} in more detail. In a premixed flame, the heat conducted upstream from the reaction zone is swept back into it a short time later by convection. If the conduction rate has increased during this time (because of an increase in flame area) then there will be an increase in the thermal energy stored in the flame. Similarly, chemical energy in the form of reactant diffuses into the reaction zone. At the same time, fresh reactant is convected across the upstream flame boundary, and replaces the mixture depleted by diffusion a short time later. If the diffusion rate has increased during this time then the chemical energy stored in the flame will be smaller. An increasing flame area therefore results in an increase in the thermal energy and a decrease in the chemical energy stored in the flame. The consequence for the reaction zone is a net loss of thermal energy and a net gain of chemical energy. In a steady-state flame the conduction and diffusion rates are constant so there is no change in the stored energy and E_{stored} is zero.

We first consider the conduction of heat. The rate of heat conduction upstream at time t is

$$\lambda \frac{T_b - T_u}{\delta_T} A_b(t) \tag{161}$$

where $A_b(t)$ is the area of the reaction zone at time t. But it was an earlier conduction rate that raised the temperature of the unburnt mixture now entering the reaction zone. The time separating a change in the rate of conduction of heat and its subsequent effect on the reaction zone is the characteristic convection time. If this is t_{conv} then the earlier conduction rate is

$$\lambda \frac{T_b - T_u}{\delta_T} A_b(t - t_{conv}). \tag{162}$$

The net rate of heat loss from the reaction zone is therefore

$$E_{heat} = \lambda \frac{T_b - T_u}{\delta_T}[A_b(t) - A_b(t - t_{conv})]. \tag{163}$$

Now

$$\frac{dA_b}{dt} \approx \frac{A_b(t) - A_b(t - t_{conv})}{t_{conv}} \tag{164}$$

and since a typical convection time in a flame is δ/S_u°, the net rate of energy gain by the flame (and therefore loss by the reaction zone) due to conduction of heat becomes

$$E_{heat} = \lambda \frac{T_b - T_u}{\delta_T} \frac{\delta}{S_u^\circ} \frac{dA_b}{dt}. \tag{165}$$

We now consider the diffusion of reactant into the reaction zone. The rate at which chemical energy in the form of reactant diffuses into the reaction zone at time t is

$$\rho D_{12} \frac{Y_u}{\delta_M} q A_b(t) \tag{166}$$

where $A_b(t)$ is the reaction zone area. This reactant was convected across the upstream flame boundary at an earlier time $(t - t_{conv})$. The rate of diffusion of chemical energy into the reaction zone at $(t - t_{conv})$ is

$$\rho D_{12} \frac{Y_u}{\delta_M} q A_b(t - t_{conv}). \tag{167}$$

The net rate of energy loss by the flame is therefore

$$E_{chem} = \rho D_{12} \frac{Y_u}{\delta_M} q [A_b(t) - A_b(t - t_{conv})]. \tag{168}$$

Now as before

$$\frac{dA_b}{dt} \approx \frac{A_b(t) - A_b(t - t_{conv})}{t_{conv}} \tag{169}$$

and since a typical convection time in a flame is δ/S_u°, the net rate of energy loss by the flame (and therefore gain by the reaction zone) due to diffusion of reactant becomes

$$E_{chem} = \rho D_{12} \frac{Y_u}{\delta_M} \frac{\delta}{S_u^\circ} \frac{dA_b}{dt} q. \tag{170}$$

Therefore the rate at which energy is stored in the expanding flame is

$$E_{stored} = E_{heat} - E_{chem}$$

$$= \lambda \frac{T_b - T_u}{\delta_T} \frac{\delta}{S_u^{\circ}} \frac{dA_b}{dt} - \rho D_{12} \frac{Y_u}{\delta_M} \frac{\delta}{S_u^{\circ}} \frac{dA_b}{dt} q. \qquad (171)$$

Substituting equation (171) in (160), along with the convective terms described earlier, gives

$$c_p \rho_T v_T A_T T_u + \rho_M v_M A_M Y_u q = c_p \rho_b v_b A_b T_b$$

$$+ \lambda \frac{T_b - T_u}{\delta_T} \frac{\delta}{S_u^{\circ}} \frac{dA_b}{dt} - \rho D_{12} \frac{Y_u}{\delta_M} \frac{\delta}{S_u^{\circ}} \frac{dA_b}{dt} q. \qquad (172)$$

Dividing by the total mass flow rate and using the continuity equation (15) and the provisional definition of burning velocity in equation (148) gives

$$c_p(T_b - T_u)\left[1 + \frac{\lambda}{\rho_u c_p S_{u,r} \delta_T} \frac{\delta}{S_u^{\circ}} \frac{1}{A_b} \frac{dA_b}{dt}\right]$$

$$= Y_u q\left[1 + \frac{\rho D_{12}}{\rho_u S_{u,r} \delta_M} \frac{\delta}{S_u^{\circ}} \frac{1}{A_b} \frac{dA_b}{dt}\right]. \qquad (173)$$

Substituting for the dimensionless stretch rate given by equation (121), expanding for small stretch and using the approximations $S_{u,r} \approx S_u^{\circ}$, $\delta_T \approx \delta_M \approx \delta$ and $A_T \approx A_u \approx A_M$ gives

$$c_p T_b = (c_p T_u + Y_u q) + Y_u q\left(\frac{1}{Le} - 1\right)\kappa \qquad (174)$$

which is identical to equation (151). It follows that the effect of stretch on the flame temperature is the same as that determined for the plane flame in a stagnation-point flow. Since the balances between thermal conduction, mass diffusion and reaction at the flame are the same as for the stagnation flow flame, equations (152), (153) and (157) are all valid.

We now consider the mass balance. The net rate of supply of reactant to the reaction zone at time t is the convection rate at the upstream boundary plus any gain by the reaction zone due to the changing diffusion rate, given by E_{chem}/q. This should equal the instantaneous rate of diffusion of mass into the flame at the reaction zone given by the product of equation (51) with the reaction zone area $A_b(t)$. This can be written

$$Y_u \rho_M v_M A_M(t) + \rho D_{12} \frac{Y_u}{\delta_M} [A_b(t) - A_b(t - t_{conv})] = \rho D_{12} \frac{Y_u}{\delta_M} A_b(t) \quad (175)$$

where E_{chem}/q was obtained from equation (168). Rearranging equation (175) and substituting the mass diffusion - reaction balance equation (51) (with Y_{eff} given by equation (49) and k_s replacing k), the continuity equation (146) and the definition of burning velocity (148) gives

$$S_{u,r} = \frac{1}{\rho_u} \frac{1}{\beta_1} \frac{1}{\beta_2} k_s \delta_T \frac{\delta_T}{\delta_M} \left[1 - \frac{A_b(t) - A_b(t - t_{conv})}{A_b(t)} \right]. \quad (176)$$

From equation (169) the contents of the bracket become

$$1 - \frac{\delta}{S_u^\circ} \frac{1}{A_b} \frac{dA_b}{dt} = 1 - \kappa \quad (177)$$

and equation (176) is identical to equation (155). The rest of the derivation follows that for the plane flame in a stagnation-point flow, and the effect of stretch on the burning velocity of both configurations is given by equation (159).

Since the stretch rate varies with radius in an expanding spherical flame, it is useful to convert equation (159) into an expression which describes more directly the change in the flame speed with radius. For the present model, $S_{u,r}/S_u^\circ = (dr/dt)/S_b^\circ$ where S_b° is the one-dimensional flame speed relative to the burnt gas. Using this result and equation (144) and rearranging gives

$$\frac{dr}{dt} = \frac{S_b^\circ}{1 + \ell/r} \quad (178)$$

where

$$\ell = -\frac{2\delta}{\sigma}\left[\frac{E}{R}\frac{Y_u q}{c_p T_{ad}^2}\left(\frac{1}{Le}-1\right)+\left(\frac{1}{Le}-1\right)-1\right]. \qquad (179)$$

A form of equation (178) containing a flame thickness term will be derived in Section 3.2.1. Equations (178) and (179) show that the propagation rate in an expanding spherical flame tends to the one-dimensional value as the radius increases. The stretch is inversely proportional to the radius, so its effect decreases as the flame grows. This would be expected on very general grounds: as the radius increases, the flame becomes less curved and more like a planar, one-dimensional (and therefore unstretched) flame.

We now use equation (159) to gain an understanding of the effect of stretch on premixed flame propagation. The discussion applies to flames in stagnation-point flow and to expanding spherical flames since the same equation was derived for both configurations. This demonstrates the universality of stretch effects, at least for weak stretch.

Equation (159) shows that stretch affects the burning rate in three ways. The first term is the effect of stretch on the flame temperature, which in turn changes the reaction rate. The high activation energy leads to large changes in reaction rate for small changes in temperature. The temperature can increase or decrease, depending on the Lewis number Le. If $Le < 1$, the rate at which reactant diffuses into the reaction zone exceeds the rate at which heat is conducted out, and positive stretch causes the temperature to increase. In the stagnation flame, the extra reactant enters the reaction zone by diffusion across the streamlines. In the expanding flame, the extra reactant enters the flame at the expense of reactant stored in the upstream mass diffusion zone. If $Le > 1$, the opposite processes occur and the temperature decreases.

The second term shows the effect of stretch on the conduction and diffusion rates via the temperature and reactant gradients in the flame. In an unstretched flame with $Le < 1$, the preheat zone is narrower than the mass diffusion zone. When the flame is positively stretched, the widths of both the preheat zone and the mass diffusion zone decrease so that the conduction and diffusion rates both increase. In an unstretched flame with $Le > 1$, the preheat zone is wider than the mass diffusion zone. Positive stretch causes both zones to widen, reducing the conduction and diffusion rates.

If the Lewis number equals 1, the flame temperature is unchanged by stretch but the burning rate still decreases. The final term gives the magnitude of the effect, which is due to the different characteristics of convectional and diffusional transport. The mass flux of reactant at the upstream boundary balances the diffusion rate at the reaction zone, whatever the subsequent flow divergence or storage rate of the convected reactant. Therefore, the greater the streamline divergence in a stagnation flame or storage rate in an expanding flame, the smaller the mass flux at the reaction zone and the slower the flame.

It is interesting that if Le = 1 the gas velocity at the cold boundary does not vary with stretch in this model. Moreover, if Le < 1 then both flame temperature and the upstream burning velocity increase with stretch, while if Le > 1 they decrease. This is one reason[52] why Law chose to define the gas velocity at the cold boundary as the true burning velocity[24,28]. Such a definition apparently makes the theory more elegant since stretch then causes Le < 1 flames to be faster and hotter and Le > 1 flames to be cooler and slower, with Le = 1 flames being unaffected. But the analysis in this chapter shows that the upstream burning velocity is not invariant even for an unstretched flame, suggesting that such a definition will be unsatisfactory. In fact it does not work for real flames. All upstream burning velocities measured by Law and co-workers were found to increase with stretch[24], including those in mixtures with Le > 1 where the temperature would have fallen.

2.2.3 **Theories**

A useful classification of theoretical work on flame stretch was given by Law[28]. Most of the analytical work on stretch has been carried out using asymptotics and can be grouped into three categories:

1. Multi-scale analyses of a general wrinkled flame in a nonuniform flow[53-55]
2. Detailed analyses of a specific flame configuration such as the flame in a stagnation-point flow[56,57] and the expanding spherical flame[58,59]
3. Analyses involving flame/flow situations characterized by some prescribed mathematical forms of stretch[60].

The first of these applies to flows in any geometry, but produces only linearized results valid for weak stretch. The second category predicts nonlinear phenomena (e.g. extinction) but only for specific geometries. The final category is less general and will not be considered further.

For the purposes of the present work, the theories in the first category are worth exploring further. The generality of the theories allows them to be applied to both expanding spherical flames and stationary flames on burners or in stagnation-point flow. Since the experimental work in this thesis has been limited to weak stretch, the linearized form of the results is not a restriction.

The theory of Clavin and Joulin[55] is particularly useful. The assumptions of their model are:

1. The Lewis number is close to 1
2. There is a single-step reaction
3. The composition is far from stoichiometric
4. The product of the density and the thermal diffusivity is a constant.

The parts of Clavin and Joulin's work which are relevant to this thesis are the expressions for the effect of stretch on the burning velocity. There are two such expressions, for the burning velocity relative to the unburnt and burnt gas:

$$u_n = S_u^\circ - \mathcal{L}\Gamma \tag{180}$$

$$u_n^b = S_b^\circ - \mathcal{L}^b\Gamma \tag{181}$$

where Γ is the flame stretch and u_n, S_u° and $\mathcal{L}$ are the stretched burning velocity, the one-dimensional burning velocity and the Markstein length respectively, relative to the unburnt gas. u_n^b, S_b° and $\mathcal{L}^b$ are the corresponding burnt gas quantities. Theoretical expressions are given for both Markstein lengths.

At first sight, equation (180) would appear to be the more useful in this thesis. But as described in more detail later, u_n is defined for an asymptotic model of a flame which differs in important respects from a real one, to such an extent that the definition of u_n in a real flame is not clear. No such problems arise with u_n^b, though, and equation (181) will be used as the basis of a suitable theoretical expression.

Because the expressions were derived on the basis of a asymptotic analysis of a flame with a single step reaction, the reaction zone is at the hot boundary as in the asymptotic analysis of a plane flame in Section 2.1.3.2. The temperature at this point is the final burnt gas temperature, so the mass flux at the hot boundary is clearly

$$M_b = \rho_b u_n^{\,b}. \tag{182}$$

Using the provisional definition of burning velocity defined in equation (148), the mass flux at the reaction zone is

$$M_b = \rho_u S_{u,r} \tag{183}$$

and it follows that

$$S_{u,r} = (\rho_b/\rho_u) u_n^{\,b}$$

$$= \sigma u_n^{\,b} \tag{184}$$

where $\sigma = \rho_b/\rho_u$ is the density ratio. Multiplying equation (181) by the density ratio gives

$$S_{u,r} = S_u^{\,o} - \sigma \mathcal{L}^b \Gamma. \tag{185}$$

and by comparison with equations (180) and (181), a suitable Markstein length for use with the burning velocity $S_{u,r}$ is

$$L = \sigma \mathcal{L}^b. \tag{186}$$

Using the expression of Clavin and Joulin for the burnt gas Markstein length, a theoretical expression for L is

$$L = \frac{\delta\sigma}{1 - \sigma}\left[\ln \sigma^{-1} + \frac{\beta(\mathrm{Le} - 1)}{2}\int_0^{(1-\sigma)/\sigma} \frac{\ln(1 + x)}{x} dx\right] \tag{187}$$

where δ is the flame thickness defined in equation (36), β is the Zel'dovich number defined in equation (83) and Le is the Lewis number defined in equation (68).

The theory of Clavin and Joulin was extended by García-Ybarra, Nicoli and Clavin[61] to include Soret (thermal diffusion) and dilution effects in the calculation of the Markstein length. Unfortunately, an expression was only provided for the unburnt gas Markstein length, and it is not clear how the burnt gas expression needed in the

present work should be derived from it. Comparison between theory and experiment will therefore be carried out using the expression for the Markstein length in equation (187).

2.2.4 The mean extensional stretch theorem

We derive here some new results on flame stretch which are of potential use in applications. They are different aspects of one principle, which could be called "the mean extensional stretch theorem". We start by defining a new quantity, the mean extensional stretch over a given region S of flame surface:

$$\langle \Gamma_{ext} \rangle_S = \frac{1}{A_S} \iint_S \Gamma_{ext} \, dS \tag{188}$$

where A_S is the area of S, given by

$$A_S = \iint_S dS. \tag{189}$$

On using Matalon's equation (138) for the stretch, equation (188) becomes

$$\langle \Gamma_{ext} \rangle_S = \frac{1}{A_S} \iint_S [\mathbf{n} \cdot \nabla \times (\mathbf{n} \times \mathbf{V})] \cdot d\mathbf{S}. \tag{190}$$

Let the boundary of the region S be a closed curve C. Then by Stokes' theorem,

$$\langle \Gamma_{ext} \rangle_S = \frac{1}{A_S} \oint_C (\mathbf{n} \times \mathbf{V}) \cdot d\mathbf{r}. \tag{191}$$

We now use this result in three different situations. First, consider a closed flame surface. This would be moving, and therefore dilatationally stretched. Here we are examining the contribution of extensional stretch to the total stretch. Any simple closed curve C divides a closed surface into two parts, P and Q. Let C_P be a circuit of C in the positive direction relative to P, and C_Q a circuit in the positive direction relative to Q. The mean extensional stretch over surface P is

$$\langle \Gamma_{ext} \rangle_P = \frac{1}{A_S} \oint_{C_P} (\mathbf{n} \times \mathbf{V}) \cdot d\mathbf{r} \tag{192}$$

with a similar result for surface Q. Hence

$$A_P\langle\Gamma_{ext}\rangle_P + A_Q\langle\Gamma_{ext}\rangle_Q$$

$$= \left[\oint_{C_P} (\mathbf{n} \times \mathbf{V})\cdot d\mathbf{r} + \oint_{C_Q} (\mathbf{n} \times \mathbf{V})\cdot d\mathbf{r}\right]. \tag{193}$$

But

$$\oint_{C_P} (\mathbf{n} \times \mathbf{V})\cdot d\mathbf{r} = -\oint_{C_Q} (\mathbf{n} \times \mathbf{V})\cdot d\mathbf{r} \tag{194}$$

so

$$A_P\langle\Gamma_{ext}\rangle_P + A_Q\langle\Gamma_{ext}\rangle_Q = 0. \tag{195}$$

Now the mean extensional stretch over the whole surface is

$$\langle\Gamma_{ext}\rangle_S = \frac{A_P\langle\Gamma_{ext}\rangle_P + A_Q\langle\Gamma_{ext}\rangle_Q}{A_P + A_Q}. \tag{196}$$

Therefore

$$\langle\Gamma_{ext}\rangle_S = 0; \tag{197}$$

the mean extensional stretch over any closed flame surface is zero.

We now consider the implications of this result for a flame subjected to weak stretch, such that the burning velocity varies linearly with Γ. This situation can be expressed by combining equations (185) and (186):

$$S_{u,r} = S_u^{\circ} - L\Gamma. \tag{198}$$

The mean burning velocity over a region S is

$$\langle S_{u,r}\rangle_S = \langle S_u^{\circ} - L\Gamma_{ext}\rangle_S$$

$$= S_u^{\circ} - L\langle\Gamma_{ext}\rangle_S \tag{199}$$

since S_u° and L are constants. If region S is defined as above then $\langle \Gamma_{ext} \rangle_S = 0$ and

$$\langle S_{u,r} \rangle_S = S_u^\circ . \tag{200}$$

Hence for a closed flame surface subjected to weak stretch, the mean burning velocity, and therefore the overall mass burning rate, is *independent of extensional stretch.*

The second application of this idea is to axially symmetric burner-stabilized laminar flames. To analyse this situation we use cylindrical polar coordinates (r, ϕ, z) with unit vectors $(\mathbf{e}_r, \mathbf{e}_\phi, \mathbf{e}_z)$. Axial symmetry implies that $\mathbf{n} \times \mathbf{V}$ in equation (191) is

$$\mathbf{n} \times \mathbf{V} = \mathbf{T} = T\, \mathbf{e}_\phi \tag{201}$$

where $T = V \sin\theta$ and θ is the angle between the velocity vector $\mathbf{V}$ and the normal to the flame surface $\mathbf{n}$. Substituting in equation (201) gives

$$\langle \Gamma_{ext} \rangle_S = \frac{1}{A_S} \oint_C \mathbf{T} \cdot d\mathbf{r} \tag{202}$$

where C is a closed path around the perimeter of the region S. By specifying that the perimeter is a circle in the z-plane (i.e. the plane normal to the axis), the integrand can be evaluated, giving

$$\begin{aligned} \mathbf{T} \cdot d\mathbf{r} &= (T\, \mathbf{e}_\phi) \cdot (dr\, \mathbf{e}_r + d\phi\, \mathbf{e}_\phi + dz\, \mathbf{k}) \\ &= T\, d\phi . \end{aligned} \tag{203}$$

Now $T \neq f(\phi)$, so the integral becomes

$$\begin{aligned} \langle \Gamma_{ext} \rangle_S &= \frac{T}{A} \oint_C d\phi \\ &= \frac{2\pi T}{A} \\ &= \frac{2\pi V \sin\theta}{A} . \end{aligned} \tag{204}$$

This is zero when $\sin\theta = 0$ and $A > 0$. This occurs when the streamlines in an axially symmetric flame cross the reaction zone normally. Such a situation occurs near the base of Bunsen flames[18,62,63]. Therefore for the case of weak stretch the same reasoning as above applies and the mean burning velocity over the area within the normal streamlines is equal to the unstretched laminar burning velocity.

The third application of this idea is to stationary flames stabilized on a multiple-slot burner. For long, thin slots, such flames have the shape of corrugated tin (as found on shed roofs) with the "trough" of the corrugation positioned over the flame strip, and the peak of the corrugation (the flame tip) above the middle of the slot. The proof is essentially a repetition of the previous one in Cartesian coordinates. Let the x, y and z directions be vertical, across the corrugations of the flame and along the corrugations of the flame respectively. There are no components of $\mathbf{n}$ or $\mathbf{V}$ in the z direction, so $\mathbf{n} \times \mathbf{V}$ in equation (191) is

$$\mathbf{n} \times \mathbf{V} = \mathbf{V}_t = \mathbf{k}V_t \tag{205}$$

where $V_t = V \sin\theta$ is the gas velocity tangential to the flame surface and θ is the angle between the velocity vector $\mathbf{V}$ and the normal to the flame surface $\mathbf{n}$. Substituting in equation (191) gives

$$\langle \Gamma_{ext} \rangle_S = \frac{1}{A_S} \oint_C \mathbf{V}_t \cdot d\mathbf{r} \tag{206}$$

where C is a closed path around the perimeter of the region S. Let C be a path defined by two straight lines in the z direction along the flame surface, connected at their ends by curves of length s along the flame surface in the x-y plane. Let the straight lines have y coordinates y_1 and y_2, and let the lines extend from z_1 to z_2. The contributions of the ends to the integral are equal and opposite, and so cancel out. For the straight line parts, $d\mathbf{r} = \mathbf{k}dz$, and the expression becomes

$$\langle \Gamma_{ext} \rangle_S = \frac{1}{A} \left[\int_{z_1}^{z_2} V_t(y_1)\, dz + \int_{z_2}^{z_1} V_t(y_2)\, dz \right]$$

$$= \frac{1}{A} \int_{z_1}^{z_2} [V_t(y_1) - V_t(y_2)]\, dz$$

$$= \frac{1}{A} [V_t(y_1) - V_t(y_2)] \int_{z_1}^{z_2} dz$$

$$= \frac{V_t(y_1) - V_t(y_2)}{s} \qquad (207)$$

since $A = s(z_2 - z_1)$. The mean extensional stretch is therefore zero between any two points which have the same tangential velocity. Now the tangential velocity at any point where the streamlines cross the reaction zone normally is zero. A useful special case of the above result is therefore that the mean extensional stretch is zero between any two points on the flame where the streamlines cross the luminous zone at right angles. In a multi-slot burner, this occurs at the trough and the tip of the flame (and possibly in between).

For the case of weak stretch the mean burning rate over this region would equal the adiabatic one-dimensional value in the absence of heat loss. However, some heat loss from the "trough" of the flame is inevitable since it plays a role in stabilization, so this result is not very useful. The utility of the result is in making qualitative estimates of stretch rates in two-dimensional flows.

These results will be used at various points in the thesis.

Chapter 3

EXPERIMENTAL METHODOLOGIES

In this chapter we derive methods of determining burning velocities and Markstein lengths experimentally. First, insights from the theory section are used to construct a consistent definition of burning velocity. The Markstein length, a measure of the effect of stretch on the burning velocity, is then defined. In subsequent sections these definitions are used to derive expressions which can be fitted to the results of experiments on expanding spherical flames and on flames in stagnation-point flow. Markstein lengths and one-dimensional burning velocities are determined from the fitted parameters. Some computations are also included of effects which are likely to cause error in the experimental methodologies used. A short section at the end describes a method of obtaining burning velocities from experiments on button-shaped flames.

3.1 DEFINITIONS OF BURNING VELOCITY AND MARKSTEIN LENGTH

In this section, definitions of burning velocity and Markstein length are developed for use in the rest of the work.

The one-dimensional burning velocity defined in Chapter 1 is the speed of a plane flame front relative to the cold gas in a one-dimensional (1-D) flow. This is the standard definition of burning velocity, and is accepted by all workers in the field. It is clear and unambiguous: the upstream velocity in a planar, one-dimensional flame is constant so there is no question about the correct value. The difficulty is that no real flames are one-dimensional. It is therefore necessary to decide what measurements to make on real flames and how to transform them so as to obtain the speed that would have been obtained if the flame had been planar and one-dimensional. In addition, it would be useful if there were a definition of the propagation rate of stretched flames. The standard definition of burning velocity clearly cannot be used since the presence of stretch implies that the flame is not planar and one-dimensional. Once a stretched burning velocity has been defined, the Markstein length can then be defined as the decrease in burning velocity per unit stretch.

The definition of burning velocity used in this work was anticipated in Chapter 2 so that the theoretical results could be derived in an appropriate form. We now present the arguments and give a formal definition.

Following Linnett[19], we consider a stationary spherical flame in a source flow. The flame is one-dimensional in the sense that the flow is everywhere normal to the flame front and all properties are constant in the other two orthogonal directions. If the radius of the flame were very small then the preheat zones would merge at the centre of the sphere and disrupt the flame. We therefore require the flame radius to be much larger than its thickness.

We now compare this stationary spherical flame with the corresponding planar one-dimensional one[64,65]. Since the spherical flame is unstretched as shown in Section 2.2.1, the propagation rates of the two flames should be the same. It is clear that the cold gas velocity profile in the spherical flame is not constant but varies as $1/r^2$. Linnett conjectured that the cold gas velocity never drops to that of the corresponding planar flame: thermal expansion at the flame's upstream boundary causes it to start increasing. It is interesting that Linnett concluded from this that the best one can do is to measure the minimum velocity. Following Fristrom[20] and Dixon-Lewis[40], we take a different view.

The first point is that the gas velocity relative to the flame is *not* a fundamental parameter in any of the flame theories presented in Chapter 2: the velocity is always derived from a mass flux or a total mass flow rate. This gives some indication that the rate of mass consumption might be the primary measure of the flame propagation rate.

Expressions for the mass fluxes in steady planar and spherical flames were derived in the phenomenological analyses in Section 2.1.2. A comparison of these expressions provides a strong argument for the way the burning velocity should be defined. The mass flux in the planar flame is constant, but in the spherical case varies with distance through the flame. Equation (2-45) shows that whatever the radius of the spherical flame, the mass flux at the reaction zone is always equal to that in the planar flame. It therefore seems clear that the burning rate in this model must be based upon the mass flux at the hot end of the flame.

In real flames, the reaction zone is rather different from that in the phenomenological and asymptotic models. Instead of just one reaction there are many, and the activation energies are not always large; indeed, some are negative.

The reaction zone of infinitesimal width at the hot boundary in the phenomenological and asymptotic models becomes in a real flame a region of finite width, though still much narrower than the preheat zone. The reaction zone temperature in the models is at the final temperature, while in a real flame it is usually well below the maximum, though still very high. Some differences between models and reality must therefore be expected. It is likely that the burning velocity is still determined at the hot end of the flame, but the controlling process (if indeed there is just one) is not obvious. It could be reaction rate, heat release rate, a radical concentration or (perhaps most likely) some combination of these.

It is possible to obtain information on where the burning velocity is determined in real flames by performing comparisons between flames in uniform and divergent flows using computer modelling. Dixon-Lewis and Islam[22] performed just such a comparison. In their case the divergent flow was not a spherically symmetric source flow but approximated to a stagnation flow. However, diffusion and heat conduction were along streamlines so that stretch effects were absent. It has been criticized on this account[28] but in fact the physics appears to be exactly that of a stationary spherical (or perhaps cylindrical) flame. In Chapter 6, modelling of true spherical flames is described. The results of the comparisons with modelled planar flames agree with those of Dixon-Lewis and Islam. The results were essentially that the varying mass flux of the stationary spherical flame becomes equal to the constant value of the planar flame in the reaction zone towards the hot end of the flame. For a stoichiometric methane/air flame, the temperature at which the mass fluxes are equal is around 1450 K.

Since this concept of equality of mass fluxes is used throughout the present work, it is useful to have a name for the point in the flame where the equality is satisfied. Dixon-Lewis and Islam used the term "reference plane" in their flat flames. We have changed this to the more general "reference surface" because many of the flames in this work are curved.

Our definition of burning velocity in real flames now becomes the mass flux at the reference surface divided by the cold gas density. It follows that burning velocities obtained by measuring the gas velocity at the position of first temperature rise will only be accurate if the reference surface coincides with the cold boundary.

The problem now is how to determine the position of the reference surface experimentally. Fristrom[20,66] considered that the reference surface was at the upstream edge of the luminous zone because that was the beginning of the reaction

zone. Dixon-Lewis and Islam[22] chose the same place because it was near the maximum reaction rate; the modelling showed that the reference surface roughly coincided with the maximum overall reaction rate, as measured by the chemical rates of disappearance of methane and molecular oxygen.

In the experimental work in this thesis it turns out that different ways of determining the reference surface position are needed. In the experiments on flames in stagnation flow, we follow Dixon-Lewis and Islam in assuming that the reference surface coincides with the upstream edge of the luminous zone. We show later (Chapter 7) that by a rather circuitous route it is possible to test experimentally whether the luminous zone is a good approximation to the reference surface position. In the expanding flame experiments the reference surface position is determined by modelling, as is the flame thickness correction that depends on it.

The definition of burning velocity given above applies to both one-dimensional and stretched flames. Since the flame structure is not expected to change when a flame is subjected to weak stretch, reference surface positions determined in unstretched flames should also be valid in the weakly stretched ones of this work. Burning velocity determination should therefore be straightforward. But in highly stretched flames the reference surface position may change, making application of the definition more difficult.

A formal definition can now be given for the burning velocity which applies to all flames, whether one-dimensional or not:

$$S_{u,r} = M_r/\rho_u \qquad (1)$$

where $S_{u,r}$ is the burning velocity, M_r is the mass flux at the reference surface and ρ_u is the density of the cold, unburnt gas. Since M_r appears frequently in this work, it is useful to give it a name. In a planar one-dimensional flame, it would be called the mass burning rate. It seems reasonable to generalize this usage so that M_r is called the mass burning rate in any flame geometry.

A final point about the burning velocity is that there is a disadvantage in adopting the definition above. In anything other than a one-dimensional flame, the burning velocity chosen does not correspond to a physical velocity anywhere in the flame. The only physical interpretation is that it is proportional to the mass flux at the reference surface, the constant of proportionality being the cold gas density. Why

not just use the mass burning rate and forget about the burning velocity? This point will be considered in the discussion in Chapter 7.

Having defined the burning velocity in a stretched flame, we are now in a position to define the other major parameter which is considered in this thesis. This is the Markstein length, a measure of the effect of stretch on the speed at which the flame propagates. In this work it is denoted by L and defined by the equation

$$S_{u,r} = S_u^{\circ} - L\Gamma. \qquad (2)$$

Some points are worth making about the Markstein length. First, the definition in equation (2) contains the assumption that the burning velocity varies linearly with the stretch rate. This assumption originally came from asymptotic analysis of stretched flames[54,55], although modelling studies[67,68] and some experimental work[24] have supported it. But it is still an assumption, and may not be true in all cases. In particular, it is predicted by asymptotic theories to be valid only in the limit of small stretch. Second, it is possible to define Markstein lengths for different definitions of burning velocity; for example, Clavin and Joulin[55] defined Markstein lengths for both their unburnt and burnt gas burning velocities. This can cause problems when comparing Markstein lengths measured with respect to differently-defined burning velocities.

Equations (1) and (2) are the fundamental relationships in this work and will be used repeatedly in the following derivations.

3.2 EXPANDING SPHERICAL FLAMES

In this section we use a phenomenological model of an expanding spherical flame to derive a simple expression for the way the radius changes with time. The expression contains two adjustable parameters which are determined by fitting it to experimental radius *vs* time records. The data obtained are a one-dimensional flame speed and a "flame relaxation parameter" containing the sum of the effects of flame stretch and flame thickness. In subsequent sections, two points of detail are elaborated. First, the form of the flame thickness correction is justified on the basis of a simple model for the density variation in the flame. Second, the effect of thermal radiation on the experimental methodology is examined.

3.2.1 Simple model of an expanding spherical flame

We now derive a simple expression for the radius as a function of time of an expanding spherical flame at constant pressure. Two effects, flame stretch and flame thickness, are included which prevent the relationship from being a simple linear one. We stress that the analysis is not intended to be a theory of spherical flame propagation; it is rather an attempt to explain phenomenologically the influence of low stretch rates on laminar flame propagation. It is a simplified approach in that we assume that the flame structure is essentially that of a one-dimensional planar flame. The analysis is therefore expected to be valid at large radii, but not at very small radii where the quasi one-dimensional assumptions will not hold. Its range of validity will be demonstrated later.

Stretch in expanding spherical flames arises from change of curvature with time. As shown in Section 2.2.1.2, the stretch rate of an expanding spherical flame is

$$\Gamma = \frac{2}{r}\frac{dr}{dt} \tag{3}$$

where r is the radius of the flame and t is time. The effect of the stretch on the burning velocity is given by equation (2) which defines the Markstein length L. The burning velocity of the flame is defined by equation (1).

For an expanding spherical flame, the mass of the gas inside the reference surface at radius r is

$$\mu = (4/3)\pi r^3 \overline{\rho}_b \tag{4}$$

where $\overline{\rho}_b$ is the mean burnt gas density. The mass flux crossing this surface is

$$\begin{aligned} M_r &= (d\mu/dt)/(4\pi r^2) \\ &= [\overline{\rho}_b + (r/3)\, d\overline{\rho}_b/dr]\, dr/dt \\ &= \rho_b^{\circ}\, f(r)\, dr/dt \end{aligned} \tag{5}$$

where ρ_b° is the one-dimensional burnt gas density and

$$f(r) = [\overline{\rho}_b + (r/3)\, d\overline{\rho}_b/dr] \;/\; \rho_b^{\circ} \tag{6}$$

is a density correction function. It is shown in the next section that, on the assumption of a linear density variation through the flame, the density function has the form

$$f(r) = 1 + k/r. \tag{7}$$

We assume that this is generally true and determine the constant k by modelling. In fact, k varies slightly with radius and we use a mean value determined over the range r = 5 to 35 mm. The standard deviation of k over this range is about 5%.

The mass flux at the reference surface differs from its one-dimensional value because of stretch. Combining equations (1), (2) and (3) and incorporating the conservation of mass, we have

$$M_r = \rho_b{}^\circ S_b{}^\circ \; - \; (2\rho_u L/r)\; dr/dt \tag{8}$$

where $S_b{}^\circ$ is the one-dimensional burnt gas value of flame speed. Equating (5) and (8) and rearranging gives

$$\frac{dr}{dt} = \frac{S_b{}^\circ}{f(r) + \ell/r} \tag{9}$$

where $\ell = 2L\rho_u/\rho_b{}^\circ$. Substituting equation (7) in (9) gives

$$\frac{dr}{dt} = \frac{S_b{}^\circ}{1 + b/r} \tag{10}$$

where

$$b = k + \ell \tag{11}$$

is called the "flame relaxation parameter" in the present work. We see later that negative values of b are obtained in lean mixtures of light fuels (hydrogen and methane) and rich mixtures of heavy fuels (ethane and propane). Equation (10) breaks down when $r \leq -b$ so the fitting procedure is limited to larger radii for these mixtures.

Integrating equation (10) gives the final expression

$$r + b \ln r = S_b^{\circ} t + \text{constant.} \qquad (12)$$

The experimentally visualized flame radius will normally be different from the reference surface radius of this analysis. But the difference is a second order effect and will be negligible when $r >> |b|$. We show later (in Chapter 5) that for all of the fuels studied in this work, $|b|$ is less than 3 mm over most of the stoichiometric range.

A common practice in previous studies has been to derive constant flame speeds from radius *vs* time data. This corresponds to the assumption that $b = 0$. On the face of it (see Fig. 5(a)), this seems entirely reasonable if the early ignition phase is ignored. However, the closer analysis in Fig. 5(b) reveals a more complex picture. (In none of the flames studied here did the r *vs* t curves appear non-linear to the casual glance.) The true S_b° is then obtained by fitting a curve of the form of equation (12) to the data, where S_b° is one of the fitted parameters. For the data in Fig. 5, this yields a value of 18.31 ms^{-1}, compared with the traditional best straight-line value of 16.36 ms^{-1}. Finally, the burning velocity S_u° is obtained by multiplying S_b° by the calculated density ratio $\sigma = \rho_b^{\circ}/\rho_u$. This is a valid procedure because S_b° is a one-dimensional value.

The other parameter obtained by fitting equation (12) to the experimental data is b. In order to derive the Markstein length, we need to subtract the density constant k. Values of k were obtained from computer modelling for each flame as explained later, and the Markstein length is determined from

$$L = (b - k)\, \sigma/2. \qquad (13)$$

It is worth stressing that although determination of L requires knowledge of the reference surface position, the method for determining burning velocity does not.

Finally, we point out that the methodology described in this section is testable: the experiments and modelling are such that it could be shown to be wrong. Tests of the expanding flame methodology will be described in Section 6.4.2.

FIGURE 5

Typical experimental data for an expanding spherical flame

(a) radius *vs* time. Points: experimental data. Curve: equation (3-12) fitted to points with S_b° = 18.31 ms^{-1}, b = 1.49 mm. 41% hydrogen/air (Stoichiometry = 1.4)

(b) flame speed *vs* radius. Points: time derivatives calculated from radius *vs* time. Curve: equation (3-10) with S_b° and b as above. Dotted line: limiting flame speed S_b°. Dashed line: flame speed obtained by fitting straight line to data in Fig. 5(a).

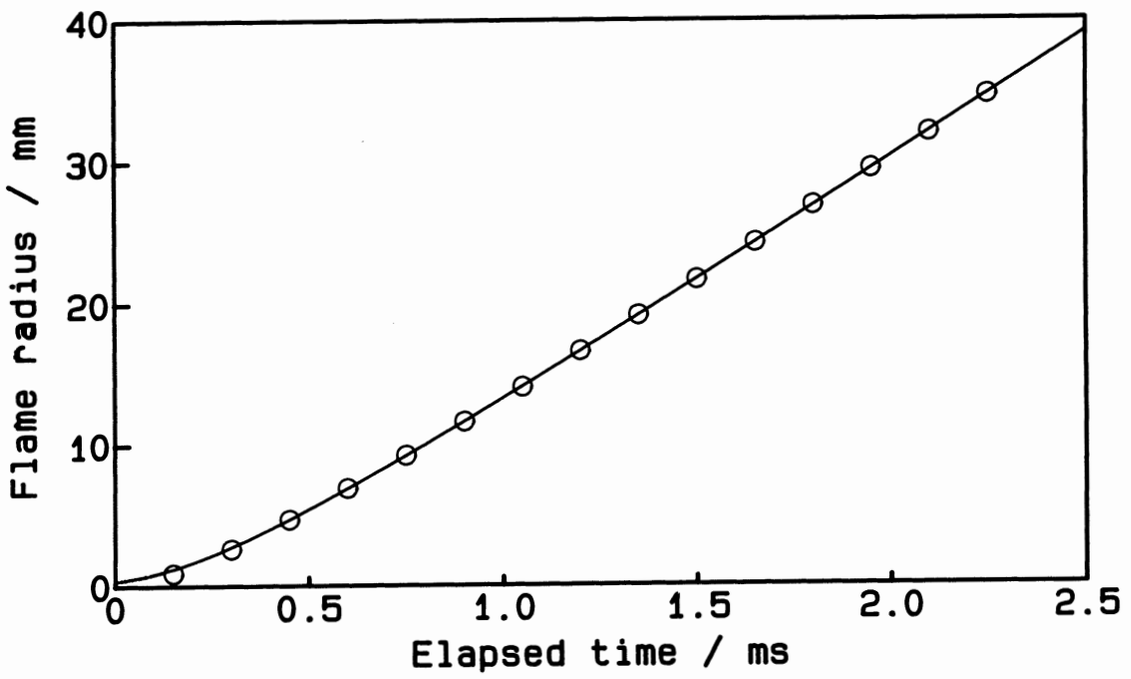

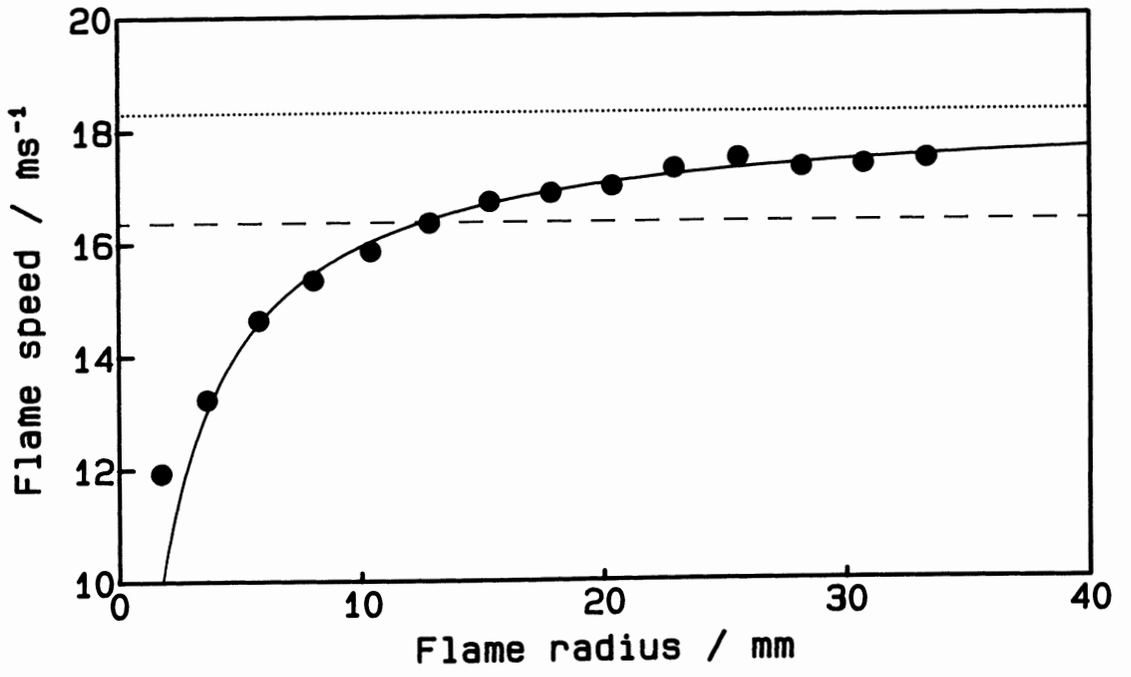

3.2.2 The effect of flame thickness

We now justify equation (7) by deriving a simple expression for the density function. We assume that the density in the expanding spherical flame varies linearly between the reference surface and the hot boundary, where the density is that of an equilibrium mixture at the adiabatic flame temperature. At some fixed time t, let the radius of the reference surface be r and that of the hot boundary $(r - \Delta r)$. The corresponding densities are ρ_b° at the hot boundary and $(\rho_b^\circ + \Delta\rho)$ at the reference surface. We want to determine the mean density inside the reference surface as a function of its radius. The mean density is the sum of the masses inside the hot boundary (μ_1) and between the hot boundary and the reference surface (μ_2) divided by the volume enclosed by the reference surface:

$$\overline{\rho} = \frac{\mu_1 + \mu_2}{V} \tag{14}$$

where

$$V = (4/3)\pi r^3 \tag{15}$$

$$\mu_1 = (4/3)\pi(r - \Delta r)^3 \rho_b^\circ \tag{16}$$

$$\mu_2 = 4\pi \int_{r-\Delta r}^{r} \rho(r')r'^2\, dr. \tag{17}$$

The linear density variation in the expression for μ_2 is

$$\rho(r') = \frac{\Delta\rho}{\Delta r} r' + \rho_b^\circ - \frac{\Delta\rho}{\Delta r}(r - \Delta r). \tag{18}$$

Evaluation of the expression for μ_2 gives

$$\mu_2 = 4\pi\left[\frac{\Delta\rho}{\Delta r}\,\frac{r^4-(r-\Delta r)^4}{4} + [\rho_b^\circ - \frac{\Delta\rho}{\Delta r}(r - \Delta r)]\frac{r^3-(r-\Delta r)^3}{3}\right]. \tag{19}$$

Since $\Delta r \ll r$, we can use the binomial theorem to expand the $(r-\Delta r)$ terms:

$$(r-\Delta r)^4 \approx r^4 - 4r^3\Delta r + 6r^2\Delta r^2 \tag{20}$$

$$(r-\Delta r)^3 \approx r^3 - 3r^2\Delta r + 3r\Delta r^2. \tag{21}$$

The expression for the mass between the hot boundary and the reference surface then becomes

$$\mu_2 = 4\pi(\Delta\rho r^2\Delta r/2 + \rho_b{}^\circ r^2\Delta r - \rho_b{}^\circ r\Delta r^2 - \Delta\rho r\Delta r^2). \tag{22}$$

Expanding the $(r - \Delta r)^3$ term in equation (16) and substituting the result along with equations (15) and (22) into the expression for the mean density inside the reference surface (equation 14) leads to

$$\frac{\bar{\rho}}{\rho_b{}^\circ} = 1 + \frac{3}{2}\frac{\Delta\rho}{\rho_b{}^\circ}\frac{\Delta r}{r} - 3\frac{\Delta\rho}{\rho_b{}^\circ}\frac{\Delta r^2}{r^2}. \tag{23}$$

Since $\Delta r \ll r$, the term in $(\Delta r/r)^2$ can be neglected so the ratio of the mean density inside the reference surface to the adiabatic burnt gas equilibrium value is

$$\frac{\bar{\rho}}{\rho_b{}^\circ} = 1 + \frac{3}{2}\frac{\Delta\rho}{\rho_b{}^\circ}\frac{\Delta r}{r}. \tag{24}$$

The density function equation (6) can be written

$$f(r) = \bar{\rho}_b/\rho_b{}^\circ + (r/3)\, d(\bar{\rho}_b/\rho_b{}^\circ)/dr. \tag{25}$$

Substituting equation (24) into this gives the final expression

$$f(r) = 1 + (\Delta\rho\Delta r/\rho_b{}^\circ)/r \tag{26}$$

which is of the form

$$f(r) = 1 + k/r \tag{27}$$

as required. Fristrom[20] quoted a similar result but with k having twice the value of the above expression. It is interesting to note that if the binomial expansions (20) and (21) are carried out to two terms instead of three, Fristrom's result is obtained.

3.2.3 **Errors due to thermal radiation**

Testing of the radius *vs* time equation (12) by fitting it to the results of detailed simulations of expanding spherical flames is described in detail in Section 6.4.2. There is one feature of real expanding flames which is not covered by such a procedure, however. The burnt gases inside real flames will emit thermal radiation and will cool as a result. We now investigate the likely magnitude of this effect.

The derivation is necessarily an approximate one because of the complexity of the phenomenon. The aim is to determine the density profile in the burnt gas inside the expanding spherical flame as a function of time. We then show the effect on the expression derived in Section 3.2.1.

It is straightforward to show the expected effect of thermal radiation. As the flame becomes larger, the volume of burnt gas increases as new "layers" of hot gas are added. At any time after ignition (during the constant pressure phase), the gas at the centre of the sphere will be coolest because it has spent the longest time radiating. Conversely, the newly-formed shell of gas immediately next to the reaction zone has lost no heat because it has not yet had an opportunity to do so. Let the constant thickness of this shell be Δr. The volume of the region which loses no heat therefore varies as $r^2\Delta r$, while the total volume of burnt gas varies as r^3. The proportion of the total volume which loses no heat therefore varies as $1/r$, and overall the expanding flame must cool. The question now becomes a quantitative one: does the expanding spherical flame cool sufficiently during the time that measurements are made to invalidate the analysis described earlier?

In order to attack this problem, we make some simplifying assumptions:

1. Thermal radiation begins only when the burnt gases have reached equilibrium.
2. The temperature drop due to thermal radiation is small, so that the properties of the whole sphere of hot gas are roughly constant and can be taken to be those of the equilibrium burnt gases.
3. Change in temperature due to other effects (e.g. flame stretch or heat loss to the electrodes) is negligible.
4. The emissivity of the sphere of burnt gas is proportional to its radius.
5. The rate of energy loss is the same from all parts of the sphere of burnt gas.
6. Absorption of thermal radiation by the burnt gas due to self-absorption, or reflection or radiation from the walls of the containing vessel, is negligible.

The rate of radiant energy loss from a sphere of burnt gas at constant temperature T is given by[69]

$$q_{rad} = \sigma A_s \epsilon_G T^4 \tag{28}$$

where σ is the Stefan-Boltzmann constant, A_s is the area of the sphere and ϵ_G is the emissivity. The energy lost from the sphere in the short time dt is therefore

$$dE = q_{rad} dt. \tag{29}$$

The temperature change resulting from the radiant emission is given by

$$dE = -c_p n dT \tag{30}$$

where

$$n = \frac{pV_s}{RT} \tag{31}$$

is the number of moles of burnt gas. Substituting equation (31) in (30) and equating to (29) gives

$$-\frac{dT}{T^5} = \frac{3\chi\sigma R}{pc_p} dt \tag{32}$$

where the area and volume of a sphere have been substituted, along with the assumed relationship

$$\epsilon_G = \chi r \tag{33}$$

where χ is the constant of proportionality between emissivity and flame radius. We now integrate between the time t_0 when the spherical shell was formed and some later time t. The corresponding temperatures are T_0 (which we will take as the adiabatic flame temperature) and T.

$$\int_{T_0}^{T} \frac{dT}{T^5} = \int_{t_0}^{t} \frac{3\chi\sigma R}{pc_p} dt \tag{34}$$

$$\frac{1}{T^4} - \frac{1}{T_0^4} = \frac{12\chi\sigma R}{pc_p}(t - t_0) \tag{35}$$

or

$$T = T_0[1 + \eta(t - t_0)]^{-1/4} \tag{36}$$

where

$$\eta = \frac{12\chi\sigma R T_0^4}{pc_p}. \tag{37}$$

According to assumption 5, equation (36) gives the temperature of any spherical shell at any time $(t - t_0)$ after it was formed. Since the aim is to include the results from this section in the derivation of the simple model described earlier, we need to convert this expression to one for the density as a function of radius. Using the approximate expressions

$$\frac{\rho}{\rho_b^\circ} \approx \frac{T_0}{T} \qquad \text{and} \qquad r \approx S_b^\circ t \tag{38}$$

we have

$$\rho(r) = \rho_b^\circ[1 + (\eta/S_b^\circ)(r - r')]^{1/4} \tag{39}$$

where r is the current flame radius and r' is the radial position in the burnt gas $(0 \leq r' \leq r)$. We expect the effect of thermal radiation on the density to be small, so η should be small and this expression can be expanded using the binomial theorem to give the final equation

$$\rho(r) = \rho_b^\circ[1 + (\eta/4S_b^\circ)(r - r')]. \tag{40}$$

This shows that the density has the adiabatic equilibrium value at the flame front but rises (i.e. the gas is cooler) towards the centre of the sphere. At the centre the density exceeds the adiabatic value (and the temperature is below the adiabatic flame temperature) by a factor of $[1 + (\eta/4S_b^\circ)r]$.

We can now use this expression to determine the mean density in a sphere of burnt gas of radius r. It is given by

$$\bar{\rho} = \frac{3}{r^3} \int_0^r \rho(r') r'^2 \, dr' \tag{41}$$

which, when evaluated using equation (40) and expressed as the ratio of the mean to the equilibrium density, becomes

$$\bar{\rho}/\rho_b^\circ = 1 + (\eta/16 S_b^\circ) r. \tag{42}$$

We now incorporate this expression into the density function equation (6). It is easy to see that the $1/r$ term in equation (24) arises from the thin shell of gas within the reaction zone of the flame which is cooler than the burnt gas. The preceding "1" in the equation is the ratio of the density of the fully-burnt gas to the equilibrium value. Clearly the "1" should therefore be replaced by $1 + (\eta/16 S_b^\circ) r$, giving the new expression for the density ratio

$$\frac{\bar{\rho}}{\rho_b^\circ} = 1 + \frac{\eta}{16 S_b^\circ} r + \frac{3}{2} \frac{\Delta\rho}{\rho_b^\circ} \frac{\Delta r}{r}. \tag{43}$$

Substituting this expression into the density function equation (6) gives

$$f(r) = 1 + hr + k/r \tag{44}$$

where

$$h = \frac{\chi \sigma R T_0^4}{p c_p S_b^\circ}. \tag{45}$$

The new expression for the flame speed is

$$dr/dt = S_b^\circ \; / \; (1 + hr + b/r). \tag{46}$$

The relative effect of thermal radiation on the flame speed can therefore be gauged by comparing hr and b/r at appropriate values of r. The comparison is performed for stoichiometric hydrogen/air and methane/air since the experimental values of b for these mixtures are of typical magnitude.

The quantities common to all mixtures in the above expression are the Stefan-Boltzmann constant σ, the molar gas constant R and the pressure p, which for all the

test cases considered here will be taken to be atmospheric. The values are therefore $\sigma = 5.671 \times 10^{-8}$ W m^{-2} K^{-4}, $R = 8.315$ J K^{-1} mol^{-1} and $p = 10^5$ Pa. The quantities which need to be determined for each mixture are the proportionality constant χ between emissivity and radius, the temperature T_0, the specific heat c_p and the flame speed S_b°.

The proportionality constant χ was determined by calculating ϵ_G at various flame radii, using the method described in ref. 69. For a sphere of gas, the mean path length of radiation L_0 is $1.2r$. It was converted to feet (for use in the tables) by dividing the value in millimetres by 304.8. The partial pressures of carbon dioxide and water vapour needed for determining the emissivity were obtained from FTEMP, a computer program for calculating adiabatic flame temperatures. T_0 and c_p were also obtained from this source, and the temperature in degrees Rankine (°R) (needed for the tables) was obtained by multiplying that in Kelvin by 1.8. S_b° was taken from the experimental results quoted later. There is no difficulty about circularity here, because only approximate values are required.

Hydrogen

The data used were: $T_0 = 2382.3$ K = 4288.1 °R, $S_b^\circ = 14.75$ ms^{-1} and $c_p = 41.795$ J K^{-1} mol^{-1}. Data calculated from ref. 69 were $p_w = 0.323$ atm and $c_w = 1.2$. The calculated radiation data are shown in Table 1.

TABLE 1

Thermal radiation data for hydrogen/air

$\frac{r}{\text{mm}}$	$\frac{L_0}{\text{ft}}$	$\frac{p_w L}{\text{ft atm}}$	ϵ_w	$\epsilon_G = c_w \epsilon_w$	$\frac{\epsilon_G / r}{\text{m}^{-1}}$
5	.0197	.0064	.0006	.0007	.140
15	.0591	.0191	.0018	.0022	.144
25	.0984	.0318	.0037	.0044	.178
35	.1378	.0445	.0054	.0065	.185

It was necessary to extrapolate the lines in the charts to obtain these data, which increased the uncertainty a little. Dixon-Lewis[70] estimated a value for the heat loss

from a 41% hydrogen/air expanding spherical flame of 20 to 30 mm radius which corresponded to an overall emissivity of just over 0.006. This fits in well with the above values.

The data in the final column show that the assumption of proportionality between the emissivity and the radius is a reasonable one. The proportionality constant was taken to be the mean of these values, so

$$\chi = 0.162 \text{ m}^{-1}.$$

Substituting the required data into equation (45) gives

$$h = 0.040 \text{ m}^{-1}.$$

For stoichiometric hydrogen/air, the experimental value of b was 1.09 mm. When r = 35 mm, the contributions of the two terms are

$$hr = 0.0014 \quad \text{and} \quad b/r = 0.0311.$$

Thus even under worst-case conditions, the effect of radiative loss is less than 5% of the changes in the flame speed due to other effects. In addition, the calculated value of h is an upper limit because two effects have been omitted from the calculation. First, some of the radiation will be reflected by the vessel back into the burnt gas where some reabsorption will occur, so that its temperature will not fall as quickly as has been calculated. Second, the change in the temperature of the burnt gas will be smaller than calculated because the "effective" specific heat is a little larger than the value quoted: at high flame temperatures, some of the chemical energy is used to dissociate the product gases and the temperature rise is limited as a result. As heat is removed, the temperature drop is limited for the same reason.

Methane

The data used were: T_0 = 2225.9 K = 4006.6 °R, S_b° = 2.671 ms^{-1} and c_p = 41.270 J K^{-1} mol^{-1}. Data calculated from ref. 69 were p_w = 0.183 atm, p_c = 0.085 atm and c_w = 1.14. The calculated radiation data are shown in Table 2.

TABLE 2

Thermal radiation data for methane/air

r mm	L_0 ft	p_cL ft atm	p_wL ft atm	ϵ_c	ϵ_w	$\epsilon_G = c_w\epsilon_w + \epsilon_c$	ϵ_G/r m^{-1}
5	.0197	.0017	.0036	.0018	.0004	.0023	.460
15	.0591	.0050	.0108	.0046	.0013	.0061	.405
25	.0984	.0084	.0180	.0074	.0023	.0100	.401
35	.1378	.0118	.0252	.0090	.0036	.0131	.374

When carbon dioxide and water vapour are present together, the total radiation is rather less than the sum of the separately calculated effects, because each gas is slightly opaque to the other. However, no correction was necessary for such "spectral overlap" in this case because the values of (p_cL+p_wL) were too small.

As in the hydrogen calculation, the right-hand column shows that the proportionality assumption is a reasonable one. The mean value of the constant of proportionality was

$$\chi = 0.410 \text{ m}^{-1}.$$

Substituting the required data into equation (45) gives

$$h = 0.431 \text{ m}^{-1}.$$

For stoichiometric methane/air, the experimental value of b was 1.80 mm. When r = 35 mm, the contributions of the two terms are

$$hr = 0.015 \quad \text{and} \quad b/r = 0.051.$$

In this case, the thermal radiation has a larger effect and more work is required to assess its influence. The extent to which the extrapolation procedure is affected was determined by fitting the integrated version of equation (46), namely

$$r + hr^2/2 + b \ln r = S_b{}^{\circ}t + \text{constant}, \qquad (47)$$

to the experimental data. The thermal radiation parameter h was assumed to have the value calculated above. The analysis program SBLS9 used for fitting the standard equation (12) to the experimental results was modified to perform this computation. It gave results for the one-dimensional flame speed S_b° and the flame relaxation parameter b which differed by only one figure in the third decimal place from those calculated assuming no heat loss. It is therefore likely that the worst-case calculations above exaggerate the importance of radiative heat loss: for most of the flame travel at radii below 35 mm the radiative effect is small, and the greater losses at larger radii appear to have a negligible effect on the extrapolation.

It is therefore safe to assume that the effect of radiative loss on the extrapolation procedure is negligible for methane. Since the compositions, flame temperatures and flame speeds of the other hydrocarbons are similar, it would appear to be reasonable to assume that heat loss by thermal radiation can be neglected generally. An exception is possible for sooting flames, where the radiative loss would be much greater. Sooting occurred in the very richest ethane and ethylene flames, and some inaccuracy can be anticipated for these mixtures. Although the present analysis could be extended to include sooting, the extra effort is probably not warranted.

3.3 FLAMES IN STAGNATION-POINT FLOW

The principle of the stagnation flow method[23,24,27-30] is, in simple terms, that measurements of burning velocity in a flame in a stagnation-point flow at different stretch rates will extrapolate to one-dimensional conditions at zero stretch. In addition, information on the effect of stretch on the burning velocity should be obtainable.

Although Daneshyar et al[48,71] had earlier studied stretch effects in a stagnation-point flow, the measurement of burning velocity by extrapolation to zero stretch conditions was introduced by Wu and Law[23]. They suggested that the same one-dimensional burning velocity would be obtained whatever definition was used for the burning velocity in the divergent flow. Their preference was for a definition based on the mass flux at the hot side of the flame as suggested by Dixon-Lewis and Islam[22] and used in the present work. However, by hypothesis the same one-dimensional result would be obtained by extrapolating the gas velocity at the cold boundary which they denoted S_{L1}. They opted to measure S_{L1} because of its experimental simplicity. We have used Law's methodology but with an important addition: as well as measuring the upstream gas velocity S_{L1}, we also determine the burning velocity referred to the

hot end of the flame. (We originally denoted this burning velocity S_{L2} by analogy with Law's nomenclature, but later changed its symbol to the more meaningful $S_{u,r}$: S for burning velocity, u for unburnt, r for reference surface).

In this section we examine two aspects of experimental work using flames in stagnation-point flow. The first is the assumption that burning velocities measured in such a flow extrapolate to the one-dimensional value at zero stretch rate. This point is examined for both the conventional, cold gas definition of burning velocity and for the definition of burning velocity used in this work. Particle tracking was used to measure the latter burning velocity in a stagnation-point flow. The second section examines the accuracy of particle tracking in this type of flow.

3.3.1 Analysis of methodology

In this section we analyse the stagnation flow methodology in order both to justify it and to clarify the discussion later in the thesis. Since we consider that $S_{u,r}$ is the fundamental measurement, we begin by listing the assumptions necessary for the $S_{u,r}$ methodology to work, and then writing down the appropriate equations. The extra assumptions required when using a burning velocity defined in the cold gas will then be introduced, followed by further analysis.

In order to analyse the method we make the following assumptions:

1. The burning velocity defined at the reference surface, $S_{u,r}$, varies linearly with the stretch rate.
2. The relevant stretch rate is that at the reference surface.
3. The upstream velocity gradient is a good measure of the stretch rate at the reference surface.

Assumption 1 is another way of expressing equation (2), namely

$$S_{u,r} = S_u^{\circ} - L\Gamma \tag{48}$$

where $S_{u,r}$ is the stretched burning velocity, S_u° is the one-dimensional value, L is the Markstein length and, by assumption 3, the stretch rate is given by

$$\Gamma = -dv_z/dz. \tag{49}$$

The Markstein length is a measure of the effect of stretch on the burning velocity, and is one of the parameters to be determined, the other being the one-dimensional burning velocity S_u°. Equation (49) was proved in Section 2.2.1.1 for a constant-density stagnation-point flow. Provided the real flow conforms to this model, measurement of the upstream velocity gradient should therefore give the stretch rate at the flame.

It is worth pointing out that although $S_{u,r}$ is considered to be the fundamental quantity, it is not easy to measure in this configuration. In fact it is obtained from S_{L1} by multiplying by an area ratio as described next. The definition of $S_{u,r}$, already given as equation (1), is

$$S_{u,r} = M_r/\rho_u \tag{50}$$

where M_r is the mass burning rate (i.e. mass flux at the reference surface) and ρ_u is the cold gas density. The mass fluxes at the cold boundary and the reference surface are related by

$$M_1 A_1 = M_r A_r \tag{51}$$

where A_1 is the area of a stream tube at the cold boundary and A_r is the area of the reference surface defined by the same stream tube. Equation (51) contains the assumption that the mass fluxes M_1 and M_r are constant over the respective areas A_1 and A_r. This is true in an ideal stagnation flow, and is probably a reasonable assumption in the real flow. Now

$$M_1 = \rho_u S_{L1} \tag{52}$$

so, combining equations (50), (51) and (52) we have

$$S_{u,r} = S_{L1} A_1/A_r. \tag{53}$$

In fact, it is not necessary to measure the gas velocity at the cold boundary; any upstream point will do just as well. Conservation of mass within a stream tube is

$$\rho v A = \text{constant} \tag{54}$$

and since the density has the constant value ρ_u anywhere upstream of the cold boundary,

$$vA = \text{constant} = S_{L1}A_1. \tag{55}$$

It is therefore possible to measure the velocity and area at several points in the cold gas and average the results to improve the accuracy.

In order to extend the analysis to include the effect of stretch on the upstream burning velocity S_{L1}, we need to make an assumption about the way the flow divergence varies with stretch. We begin with a replacement for assumption 3 above:

3a. The flow configuration is an ideal stagnation-point flow, in the sense that the normal and radial velocities v_z and v_r are $-\Gamma z$ and $\Gamma r/2$.

This supersedes assumption 3 because it was shown in Section 2.2.1.1 that equation (49) follows directly from assumption 3a. We will see later that this assumption will need to be modified.

It is straightforward to show that in an "ideal" stagnation-point flow the stream tube area is inversely proportional to the distance z from the stagnation point. The rate of change of the radius of a stream tube with distance from the stagnation surface is

$$\frac{dr}{dz} = \frac{dr/dt}{dz/dt}$$

$$= \frac{v_r}{v_z}$$

$$= -\frac{r}{2z}. \tag{56}$$

This expression can be integrated, giving

$$2\int \frac{dr}{r} = -\int \frac{dz}{z} \tag{57}$$

$$2 \ln r = -\ln z + a \tag{58}$$

where a = constant. Finally

$$r = k_1/z^{1/2} \tag{59}$$

or

$$A = k_2/z \tag{60}$$

where k_1 and k_2 are constants. Therefore

$$A_r/A_1 = z_1/z_r$$

$$= (z_r + \delta)/z_r$$

$$= 1 + \delta/z_r \tag{61}$$

where δ is the distance between the cold boundary (denoted by subscript 1) and the reference surface (subscript r). The only way that the flow could conform to the "ideal" model is for the heat release to be zero. Since we have already accepted this restriction for the purposes of this calculation, we can also make use of the corollary that

$$\Gamma = S_{u,r}/z_r. \tag{62}$$

Eliminating z_r between equations (61) and (62) and substituting for A_r/A_1 in equation (53) gives

$$S_{L1} = (1 + \delta\Gamma/S_{u,r})S_{u,r} \tag{63}$$

$$= S_u^{\circ} - (L - \delta)\Gamma. \tag{64}$$

where equation (48) has been used. Since the Markstein length L is a constant and the flame thickness δ is not expected to vary with weak stretch, it appears that on the basis of "ideal" stagnation-point flow, Law's assumption of a linear variation of S_{L1} with the upstream velocity gradient is sound.

We know, however, that the flow cannot be "ideal" in the sense described here. Heat release does occur, and the consequent thermal expansion must change the velocities in the flame and the shape of the streamlines. The usual treatment of the change in the direction of streamlines in a flame ("streamline refraction") is on the basis of a flame of infinitesimal thickness. Such an analysis is inadequate in this case; a more detailed analysis is needed because we are dealing with events within the flame,

before the maximum temperature has been reached. A simple analysis appears to be impossible because of the complexity of the phenomena, so instead we rely on the theoretical results of Tien and Matalon[72]. They determined the variation with stretch of burning velocities defined in different ways, using an asymptotic flame model which includes the effect of thermal expansion on the streamlines. They found that the burning velocity determined exactly at the cold boundary (defined as the point where the temperature had risen by 1%) did indeed vary linearly with the stretch rate. A burning velocity defined as the minimum in the upstream velocity profile, however, did not always extrapolate linearly. With this exception in mind, we accept that the linearity assumed by Law holds, and

$$S_{L1} = S_u^{\circ} - L_1\Gamma \tag{65}$$

where L_1 is an appropriate Markstein length.

3.3.2 **Particle tracking errors**

The previous section described how the burning velocity $S_{u,r}$ can be obtained from velocity measurements in the cold gas by multiplying by a stream tube area ratio.

This is determined using particle tracking[18,22,73]. The principle is that fine particles of inert powder (typically magnesium oxide) are introduced into the flow upstream of the flame. They are illuminated as they pass through the flame by a bright sheet of light passing through the diametral plane of the burner. Photographs of the flame are taken at right-angles to the sheet of light; if the correct exposure is used they show both the luminous zone of the flame and the particle tracks in the form of continuous streaks. It is also possible to "chop" the light source so as to obtain stroboscopic photographs from which the velocity can be obtained. Fig. 6 is such a photograph of the flow in a button-shaped flame.

In this section we examine the likely errors in the measurement of stream tube areas due to particles not following the flow. We are not concerned here with errors in the measurement of gas velocity in flames by laser-Doppler anemometry (LDA) and related techniques. Such errors have been dealt with by other workers[74,75]. In the present analysis the aim is to determine the error in the particle *position* due to its failure to follow the large radial accelerations in stagnation-point flow.

FIGURE 6

(overleaf)

Particle tracking photograph of button-shaped flame

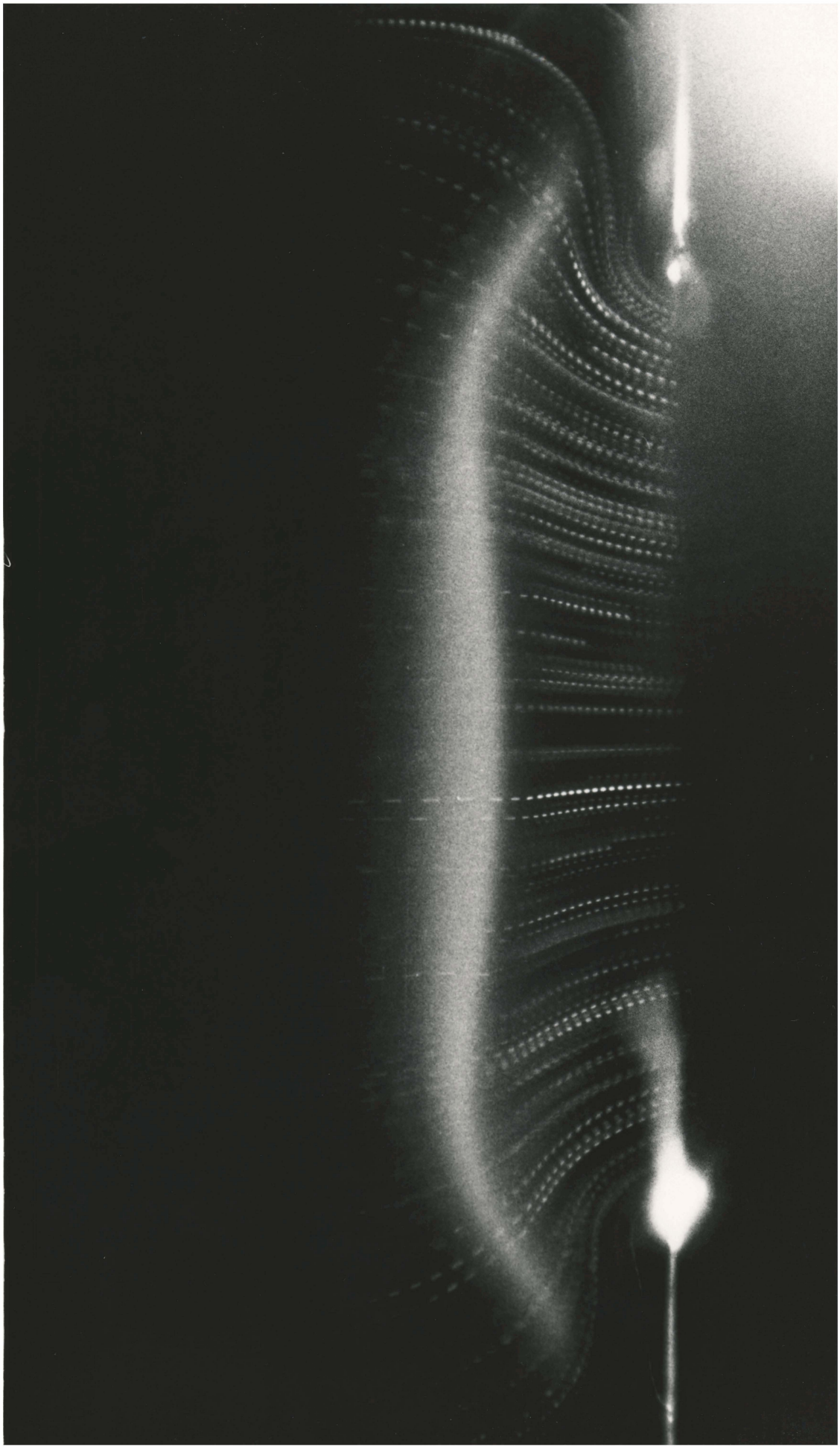

The assumptions made in the calculation are as follows:

1. Only radial accelerations are considered.
2. The particle is spherical with a force on it given by Stokes' Law.
3. The flow is an ideal stagnation-point flow.

According to Stokes' Law, the force on the particle is given by[76]

$$\mathbf{F} = 6\pi\eta R(\mathbf{v}_g - \mathbf{v}_p) \tag{66}$$

where η is the viscosity of the gas, R is the radius of the particle, $\mathbf{v}_g$ is the velocity of the gas and $\mathbf{v}_p$ is the velocity of the particle. If μ is the mass of the particle then equation (66) can be rewritten as

$$\mathbf{a} = A(\mathbf{v}_g - \mathbf{v}_p) \tag{67}$$

where $\mathbf{a}$ is the acceleration of the particle and

$$A = 6\pi\eta R/\mu \tag{68}$$

is a constant. Since the particle is spherical this becomes

$$A = \frac{9\eta}{2\rho_p R^2}. \tag{69}$$

where ρ_p is the particle density. We now restrict the analysis to radial motion. Let the radial position of the particle be r. From equation (2-142), the radial velocity of the gas at this point is

$$v_r = \Gamma r/2. \tag{70}$$

The radial velocity of the particle is dr/dt and its radial acceleration is d^2r/dt^2. Substituting in (67) gives a differential equation for the motion of the particle

$$\frac{d^2r}{dt^2} + A\frac{dr}{dt} - A\Gamma r/2 = 0. \tag{71}$$

We try as a solution

$$r = ae^{bt} \tag{72}$$

where a and b are constants. Substituting in equation (71) leads to

$$ae^{bt}(b^2 + Ab - A\Gamma/2) = 0. \tag{73}$$

Since $a \neq 0$ (otherwise we get the trivial solution of a particle on the axis) and $e^{bt} \neq 0$ for finite b and t, we have

$$b^2 + Ab - A\Gamma/2 = 0. \tag{74}$$

Solving the quadratic equation in b and substituting in equation (72) gives the general solution

$$r = \alpha\exp\{[-A + (A^2 + 2A\Gamma)]^{1/2}t/2\}$$

$$+ \beta\exp\{[-A + (A^2 + 2A\Gamma)^{1/2}]t/2\} \tag{75}$$

where α and β are constants. The first term describes r increasing with time and the second r decreasing. Only the first of these is physically acceptable, so $\beta = 0$. When $t = 0$, $r = \alpha = r_0$ say. Hence the solution is

$$r = r_0\exp\{[-A + (A^2 + 2A\Gamma)^{1/2}]t/2\}. \tag{76}$$

As $A \to \infty$ (corresponding to a particle following the flow perfectly), the contents of the square brackets tend to Γ and equation (76) reduces to the ideal stagnation-point flow solution

$$r = r_0\exp(\Gamma t/2) \tag{77}$$

as required. We now determine the particle path in space. The derivation is analogous to equations (56) to (59) in the previous section, so we just quote the result that

$$r = r_0(z_0/z)^B \tag{78}$$

where $r = r_0$ when $z = z_0$ (with z being distance from the stagnation plane) and

$$B = [(A^2 + 2A\Gamma)^{1/2} - A]/2\Gamma, \tag{79}$$

whereas for the true streamline, equation (78) holds with

$$B = 1/2. \tag{80}$$

We can now calculate the radial slippage Δr, that is the difference between the radial position of the solid particle and that of the gas particle with which it was coincident at (r_0, z_0).

$$\Delta r = r_0\left[\left(\frac{z_0}{z}\right)^{1/2} - \left(\frac{z_0}{z}\right)^{G/2}\right] \tag{81}$$

where

$$G = [(A^2 + 2A\Gamma)^{1/2} - A]/\Gamma. \tag{82}$$

We now put in some numbers. For a typical experiment, z_0 = 6.5 mm, r_0 = 2.2 mm and z = 2 mm. Let the viscosity of the fuel/air mixture be that of air at 300 K, equal to[77] 18.325 $\times$ 10^{-6} N s m^{-2}. If the particle is magnesium oxide then its density is[75,77] 3580 kg m^{-3}. Let its radius be 2 μm. Substituting these numbers in equation (69) gives A = 5759 s^{-1}. A typical stretch rate for the stagnation flow experiments described later is 200 s^{-1}, so G = 0.983. Substituting these values in equation (81) gives

$$\Delta r = 0.018 r_0 = 0.04 \text{ mm}. \tag{83}$$

It is easily shown that the error in the area ratio measurement due to such slippage is

$$E = [1 - (z/z_0)^{1-G}] \times 100\%. \tag{84}$$

The error calculated for the data above is 2% which is acceptable. But repeating the calculation for a particle radius of 5 μm leads to an area ratio error of 10% which is clearly too large.

This calculation is extremely useful because it helps to set the limits of what is possible within the experiment. It is clear from equation (81) that the particle slippage is proportional to the radius of the stream tube, so a small radius will tend to give more accurate results. But a large radius is desirable from an experimental point of view, to reduce measurement errors. Similarly, for the particles to follow

the flow accurately they should be very small. But in an experiment there is always a range of particle sizes, and the tracks that are clearest in the photographs (and whose radii can therefore be measured most accurately) are due to the largest particles because they scatter the most light. At higher flow rates the difficulties are heightened because the particles are moving so quickly that only the larger ones leave usable tracks. A further point is that the radius of the particle making a specific track is unknown, so corrections using the above derivation are not possible. Careful judgement is therefore needed when selecting particle tracks and measuring their properties.

Finally, the derivation above also gives some guidance on the application of the particle tracking technique to highly stretched flames. In the counterflow methodology[24,27-30], high stretch rates can be achieved because the flame is blown against another flame (rather than a plate as in the experiments in this thesis) and heat loss is negligible. Stretch rates of 1500 s^{-1} have been achieved for near-stoichiometric methane/air flames[24]. The calculated area ratio error for such a stretch rate using particles with a radius of 2 μm was 12%. This is clearly a serious limitation, and suggests that it would be difficult to measure $S_{u,r}$ accurately in such experiments.

3.4 BUTTON-SHAPED FLAMES

At low flow rates, flames on a constant velocity (Mache-Hebra) nozzle take on a form generally known as button-shaped. Such flames have been used by several workers for the determination of burning velocity. Usually this has been done by measuring the gas velocity at the cold boundary[23,78,79], but the present definition of burning velocity was applied by Dixon-Lewis and Islam[22]. A description will be given here of a method of determining an approximate value of S_u° in such a system.

There are three possible ways of dealing with the stretch in a button-shaped flame. These are:

1. Use the mean extensional stretch theorem described in Section 2.2.4 to eliminate stretch effects.
2. Derive the stretch from the flow divergence and correct for it using the results of other experiments.
3. Ignore the stretch since its effect is small.

The mean extensional stretch theorem would be applied to button-flame experiments by choosing an appropriate set of particle tracks from which to calculate the area ratio. The correct ones would be those which cross the luminous zone at right angles. The flame area enclosed is subjected to a zero average stretch rate so that true one-dimensional burning velocities should be obtained. Although this should produce correct results in principle, in practice it is not likely to improve the accuracy of the measurements. There are several reasons for this. First, as will be discussed in Chapter 7, there is some doubt about the existence of a normal streamline (in addition to the central one) in a button-shaped flame. Second, if such a normal streamline exists then its position is outside the strongly curved part of the flame surface, as can be seen in Fig. 6 in the present work and in Fig. 9 of ref. 63. Accurate measurement of the area of such a surface is difficult, and is likely to lead to uncertainties of the same order as the change in burning velocity produced by the stretch.

Deriving the stretch rate from the flow divergence is possible, but is not likely to help. Since there is no systematic way of removing stretch effects in a button-shaped flame, results from other experiments would be needed to make the appropriate corrections. This rather takes away the point of the experiment (since the other experiment would presumably supply values of the one-dimensional burning velocity) so it will not be considered further.

The final possibility is to ignore the stretch. We will take this course, following Wu and Law[23], after showing that the effect of stretch is usually small in button flames, while the effect of flow divergence is large. In fact, Wu and Law implicitly assumed that since the stretch rate was small, so was the flow divergence.

Particle-tracking photographs of button-shaped flames as in Fig. 6 and refs. 22 and 79 show that the streamlines diverge on approaching the luminous zone which is nearly flat on the centre line. Although there is no strain imposed by the flow, the configuration resembles a stagnation-point flow. We will therefore use the ideal stagnation flow model to relate the stretch rate to the flow divergence. According to this model, the radial velocity is

$$v_r = \Gamma r/2. \qquad (85)$$

The total radial displacement of the gas between the cold boundary and the luminous zone is found by integrating equation (85) over the typical convection time t_{conv} =

δ/S_u°. In order to give a realistic estimate of the change in the stream tube area, δ must be a true measure of the distance between cold boundary and luminous zone rather than a thermal diffusion length. The result is

$$r_2/r_1 = \exp(\Gamma t_{conv}/2), \tag{86}$$

so squaring this expression gives the area ratio between the cold and hot boundaries

$$\begin{aligned} A_2/A_1 &= \exp(\Gamma t_{conv}) \\ &= \exp(\kappa) \\ &\approx 1 + \kappa \end{aligned} \tag{87}$$

for small κ. Using the measured tangential velocities in a button-shaped flame in ref. 79, (assumed to be stoichiometric) we find that the stretch rate is[80] $\Gamma = 65\ s^{-1}$. With a burning velocity of 0.35 ms^{-1} and a flame thickness of 0.9 mm, the area ratio calculated using equation (87) is 1.19. A gas velocity measured at the cold boundary is therefore about 20% higher than the value determined on the assumption that the luminous zone is the reference surface. The effect of the stretch on the burning rate can be determined by multiplying it by the Markstein length. The value obtained from the spherical flame experiments was $L = 0.1$ mm, so the decrease in the burning velocity due to stretch is about .007 ms^{-1} or 1.9%.

A check on the flow divergence can easily be made using the particle tracking photographs in ref. 79, in Fig. 6 of the present work or the data quoted in ref. 78. In all cases the area ratio between luminous zone and cold boundary is between 1.1 and 1.2.

The effect of flow divergence on the burning velocity of button-shaped flames is therefore greater than that of stretch. It follows that correcting measured cold gas velocities for the flow divergence but not the stretch should give reasonable results.

The basic methodology is an extension of that applied earlier to stagnation flow flames and described by equation (53). As before, the mass flux is measured in the cold flow and then the mass flux at the luminous zone of the flame is determined by multiplying by the stream tube area ratio between the two points. In the case of a button-shaped flame, the velocity profile across the stream tube in the cold flow is not necessarily constant, unlike in a stagnation-point flow. It is therefore necessary

to measure the velocity as a function of radius and integrate across the stream tube radius. The result of this computation is the volumetric flow rate, which is constant at all planes of the stream tube in the cold flow. Dividing it by the area of the luminous zone enclosed by the stream tube gives the burning velocity as defined in equation (1). The methodology can therefore be represented by

$$S_{u,r} = V/A \tag{88}$$

where V is the volumetric flow rate in the selected stream tube at any point in the cold flow and A is the area of the luminous zone. This is the technique used in some of the earliest work on burning velocity measurement. The only difference from the Gouy method[9] is that in the present case the total flame area is not used; instead, the burning velocity of a region of flame area defined by a stream tube is determined. Effects of heat loss to the burner can therefore be avoided.

The volumetric flow rate is determined by measuring the vertical component of gas velocity at several points across the radius of the stream tube in some plane z_1. A polynomial function is fitted to these points. Let the variation of the vertical component of velocity with radius in a horizontal plane z_1 in the unburnt gas be given by a polynomial

$$v_z(r,z_1) = a_0 + a_1 r + a_2 r^2 + \ldots \tag{89}$$

The volumetric flow rate through a stream tube of radius R_1 is therefore

$$\begin{aligned} V(R_1) &= 2\pi \int_0^{R_1} r v_z(r,z_1)\, dr \\ &= 2\pi \int_0^{R_1} (a_0 r + a_1 r^2 + a_2 r^3 + \ldots)\, dr \\ &= 2\pi\, (a_0 R_1^{\,2}/2 + a_1 R_1^{\,3}/3 + a_2 R_1^{\,4}/4 + \ldots). \end{aligned} \tag{90}$$

For a general axisymmetric flame, it is possible to fit a function $f(r)$ to the flame profile and determine the flame area from

$$A(R_2) = 2\pi \int_0^{R_2} [1 + (df/dr)^2]^{1/2}\, dr \tag{91}$$

where R_2 is the stream tube radius at the luminous zone. For button-shaped flames, though, a less complicated procedure can be used. The flames are close to being flat, but are slightly dish-shaped. The area we wish to determine is therefore rather like an inverted spherical cap on a sphere of large radius. Using the formula for the area of a spherical cap[81] we have

$$A(R_2) = \pi(R_2^2 + h^2) \qquad (92)$$

where h is the amount by which the centre of the luminous zone dips below the level of the luminous zone at R_2. R_2 and h can be readily obtained from photographs of button-shaped flames.

The application of this method to a methane/air button-shaped flame is described in Section 4.3.

Chapter 4

EXPERIMENTAL TECHNIQUES

In this chapter the techniques used in the experimental work are described. Details are given of apparatus, method and data reduction techniques for work on expanding spherical flames and flames in stagnation-point flow. Experimental errors are covered in both cases. Finally, a method for measuring burning velocities in button-shaped flames is briefly described.

4.1 EXPANDING SPHERICAL FLAMES

4.1.1 Apparatus

The experimental apparatus consisted of a combustion bomb, a schlieren system for visualizing the expanding flames, a high-speed cine camera, and associated film development and measuring equipment. A general view of the apparatus is shown in Fig. 7.

The combustion bomb was a spherical, steel vessel with a diameter of 600 mm. It had been built some years previously for experiments on flame oscillations. Pyrex windows were fitted to opposite sides of the bomb. These were supplied by Jencons (Scientific) Ltd and were 4 inches (100 mm) in diameter and 0.75 inches (19 mm) thick. The flanges which held the windows in place limited the maximum visible flame diameter to about 70 mm. This was not a serious restriction on the work because the assumption was made that the flame propagation occurred at constant pressure. A simple calculation shows that at a final flame temperature of 2500 K (about the maximum likely to be encountered), the pressure in the vessel would have risen by about 1% when the flame radius reached 35 mm. The effect of this rise in pressure on the flame propagation rate is negligible, and the constant pressure assumption is justified. But flame radii larger than 35 mm would start to produce substantially larger pressure rises (since the pressure varies as r^3), so the present window diameter is a good compromise.

FIGURE 7
(overleaf)

General view of expanding spherical flame rig

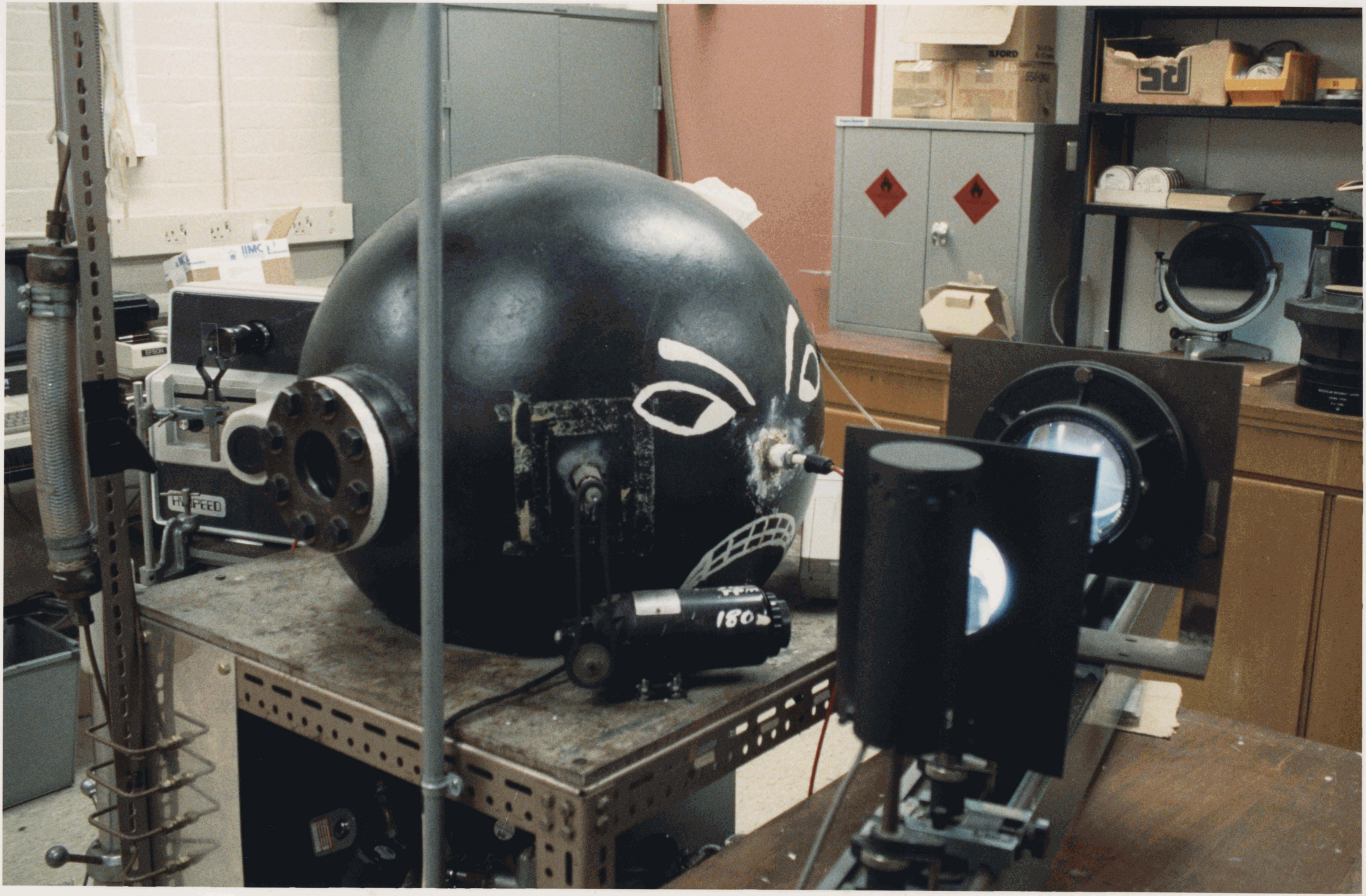
HYSPEED
180

The temperature of the bomb was measured using a K-type (chromel/alumel) thermocouple attached to a section of the bomb from which the paint had been removed, to ensure good thermal contact. The signal was processed using a temperature converter (model CE8520-OOH) supplied by the C.P. Instrument Co. Ltd. The output of this instrument was a signal in millivolts numerically equal to the temperature in degrees centigrade. Use of a digital voltmeter set to the appropriate range therefore gave a direct readout of the temperature.

The bomb was equipped with spark electrodes manufactured by K.L.G. which were screwed into the vessel walls. They had been truncated and tapped with 11 BA holes to allow small diameter silver steel electrodes, suitably threaded, to be screwed into position. Locknuts were used to secure the electrodes in place. The electrodes were of equal length (about 105 mm), giving a central spark gap. Their nominal diameter was .0125 inches or about 1.6 mm, but they were tapered for the last 8 mm to a diameter of about 0.5 mm. The use of such electrodes had two advantages. First, the small diameter gave very little flame disturbance. Second, a variable electrode gap was useful, particularly for the series of variable-pressure measurements. The usual electrode gap was about 0.7 mm.

Gas mixtures were made up in the bomb by partial pressures using the system shown in Fig. 8. The pressure in the bomb was measured using an MKS Baratron system, with a type 310 sensor head and type 270A display unit. A motorized fan fitted to the bomb was used to stir the mixtures to ensure homogeneity.

The mixtures were ignited using an electronic spark ignition system which was designed and built as part of this work. The circuit diagram is shown in Fig. 9. The design was based on that of Kono et al[82], but was modified to allow the spark to be triggered by the closure of a relay. The system worked by discharging a capacitor (which had been charged to a suitable voltage) through the primary circuit of a high tension ignition coil. The induced secondary voltage was applied to the electrode gap, causing electrical breakdown and the production of a spark. The capacitor discharge was triggered using a silicon controlled rectifier, which is essentially a solid state relay. A previous design had used an electromechanical relay, but contact bounce caused the spark energy to be delivered in a series of pulses about 1 ms apart. This was clearly unsuitable for the application since the aim was to provide just enough energy to ignite the flame; any energy supplied after about 1 ms would be unlikely to contribute to the process of ignition and would add unwanted thermal energy to the system.

FIGURE 8

Pipework of expanding spherical flame rig

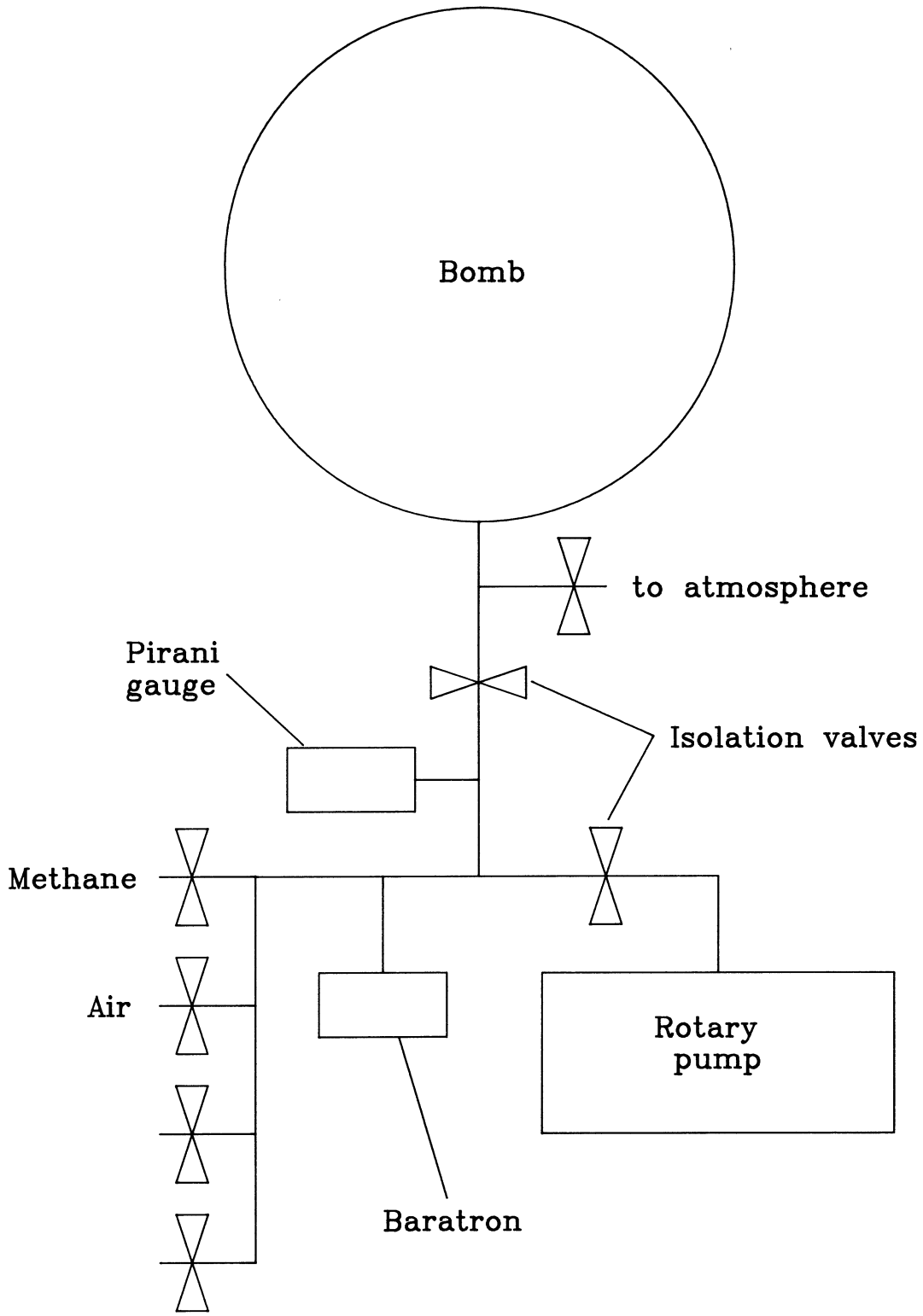

FIGURE 9

Circuit diagram of spark ignition system

Power supply

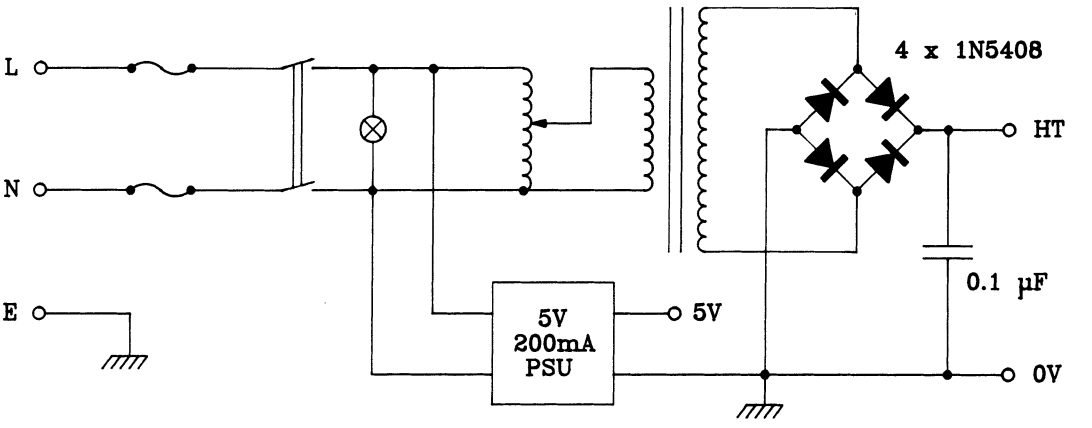

Ignition circuit

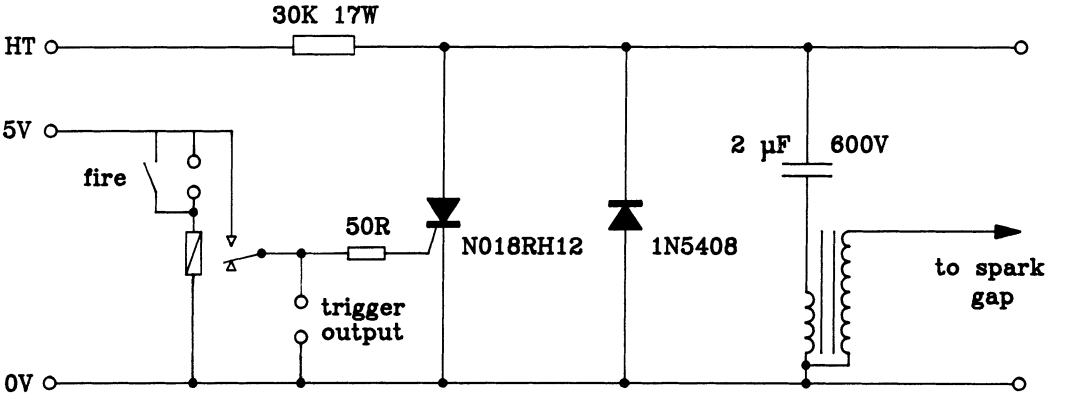

Voltage measurement

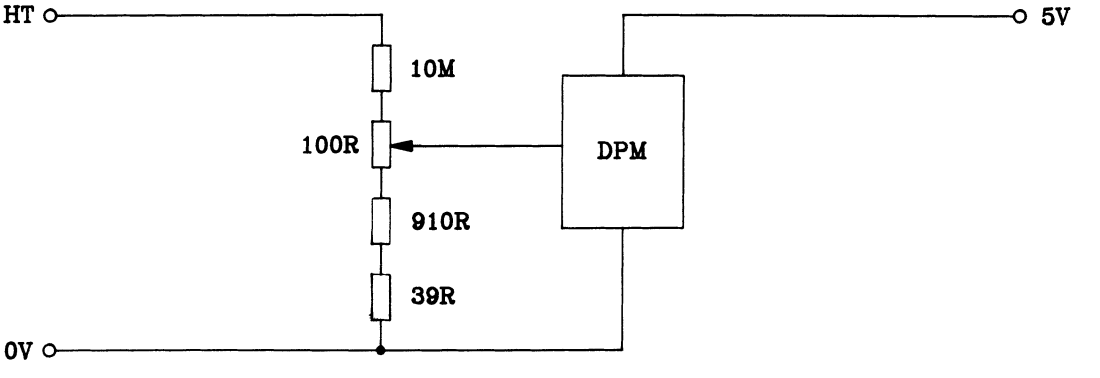

A method of visualizing the flame was necessary because the amount of light emitted from the luminous zone of an expanding flame would not be sufficient to expose the film in the time available. Shadowgraphy is a possible way of visualizing flames but in the present case would be unsatisfactory. The position of the most prominent feature of the shadow record would vary relative to the flame front as the radius of the expanding flame increased[83]. A schlieren system was therefore used to visualize the flame. The general optical arrangement is shown in Fig. 10. A 100 Watt mercury vapour lamp (Philips CS 100 W/2) was used to provide the illumination. The light was focused onto a pinhole and the divergent beam then reached a concave mirror (Optical Works Ltd type T543) of 8 inches (200 mm) diameter and 6 feet (1.829 m) focal length. It was positioned such that the rays of the reflected beam were parallel. After passing through the bomb, the beam was then reflected by an identical concave mirror onto a circular stop, which was attached to a microscope slide placed in front of the cine camera. Although a knife edge is often used in work of this sort, a circular stop was used here to take advantage of the circular symmetry of the system.

The camera was a Hyspeed motion picture camera manufactured by John Hadland (P.I.) Ltd. It was capable of film speeds up to 10 000 frames per second. A C-mount f/1.8 lens with a focal length of 75 mm (Fujinon-TV 1:1.8/75) was used with a 1.5x range extender (Fujinon CE 15-1) to provide an image of suitable size on the film. The camera had several useful features which were used in the experimental design. An internal relay could be made to switch after a certain length of film had passed through the camera. This was used to trigger the ignition system when the camera had reached its correct operating speed. A socket was provided for attaching a Timing Light Generator. The signal from the generator caused a light-emitting diode (LED) in the film path within the camera to flash at a set frequency. This produced a series of timing marks on the developed film and so provided calibration of the elapsed time. Another socket was provided for a remote switch so that the camera could be switched on from a safe distance.

Films used were Ilford HP5 type 782. They were 16 mm wide and 100 feet (30.5 m) long. They were developed automatically using a 16-35B negative processor supplied by John Hadland (P.I.) Ltd. The developer was Ilford Microphen, used in stock solution concentration. Ilford Hypam fixer was used in a mixture with an equal amount of water, along with 6.25% Ilford Rapid Hardener. Processing took 1 - 2 hours depending on the camera speed and the state of depletion of the developer.

FIGURE 10

Optical system used in expanding flame experiments

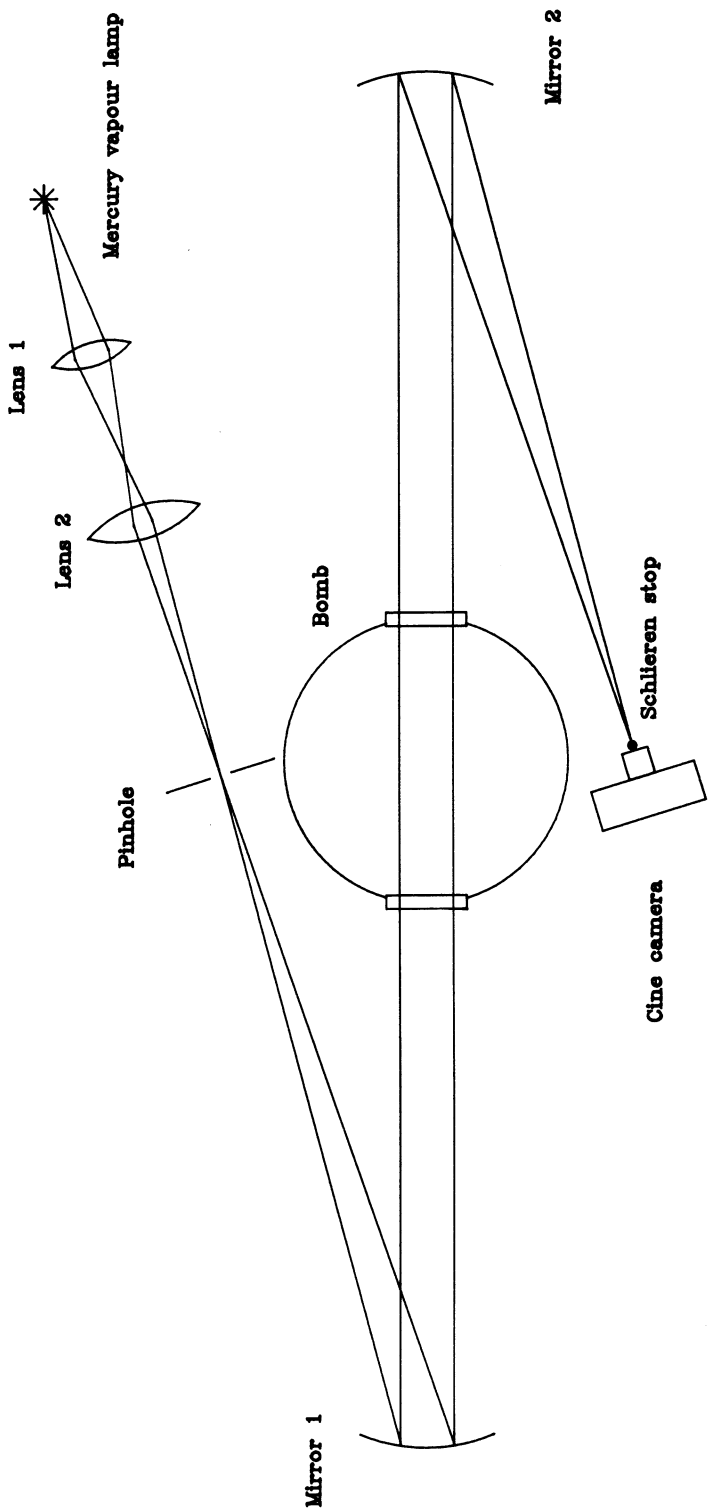

Analysis of the films was performed using an NAC Film motion analyser model PH-160B supplied by IIMC. Horizontal and vertical coordinates could be measured with crosswires, the position of which was indicated on a digital display. Apart from some initial test runs, only the vertical diameter of expanding flames was measured. This was for two reasons. First, and most important, the flames were generally very close to spherical and only one diameter was needed. Even when some departure from sphericity occurred, the rates of change of different diameters were very similar. Second, measurement of horizontal diameters was complicated by the presence of the spark electrodes which were in a horizontal plane.

4.1.2 **Method**

The aim of the experimental technique was to measure the radius of expanding spherical flames as a function of time. Details of the procedure are given in the following.

4.1.2.1 Calibration

The flame radius measurements were calibrated by running the camera with a graticule placed in the centre of the bomb. Care was taken to ensure that the graticule was normal to the light beam. When the resulting film had been developed, measurements were made using the film analyser of distances between the lines of the graticule. Since these distances were known, a scale factor could be calculated which took account of all of the magnifications in the system. The graticule consisted of a grid of vertical and horizontal lines 10 mm apart produced on transparent film using a Hewlett Packard 7550 plotter. No precision is quoted for lines drawn by the plotter, but the error is likely to be much less than its resolution of .025 mm. No error could be detected when the distance between the lines was measured using a Rabone-Chesterman ruler, implying an uncertainty of less than ±0.1 mm.

The time associated with each frame was obtained from timing marks on the edge of the film. These were produced by a flashing LED inside the camera in the film path, about 5 frames before the shutter. The LED was powered by a 1 kHz timing signal from a Timing Light Generator supplied by John Hadland (P.I.) Ltd. The quoted accuracy was ±0.01%. Any variation in the speed of the camera appeared as a change in the position of the timing mark.

4.1.2.2 Gases

Fuel gases used in the experiments were hydrogen (supplied by Air Products, with a purity of 99.95%), methane (Air Products, 99.7%), ethane (B.O.C., 99.35%), propane (B.O.C., 99.5%) and ethylene (Air Products, 99.8%). The air used in the experiments was laboratory compressed air which had been cleaned, filtered and dried. The nitrogen used to dilute some hydrogen/air mixtures was supplied by Air Products, with a purity of 99.997%.

Fuel/air compositions were expressed in terms of stoichiometry (also known as fraction stoichiometric), defined as mole fraction of fuel in the mixture divided by mole fraction of fuel in a stoichiometric mixture.

Experiments were performed across the stoichiometric range, usually in steps of 0.1 in stoichiometry, for each fuel/air mixture. The leanest and richest mixtures for which data could be obtained depended on different factors. Generally, rich mixtures of light fuels (hydrogen and methane) and lean mixtures of heavy fuels (ethane and propane) were limited by the maximum ignition energy attainable. Lean hydrogen mixtures were limited by the onset of cellularity, and lean methane and rich ethane, propane and ethylene by buoyancy. The richest ethane and ethylene flames also produced soot, which has implications for the accuracy of both the experimental method and the modelling.

4.1.2.3 Experimental procedure

Gas mixtures were made in the bomb by partial pressures. The vessel was first evacuated using a rotary pump down to a pressure of about 0.1 mbar, measured using a Pirani gauge. For most fuel/air mixtures, the proportion of fuel was much smaller than that of air. This was therefore added first in order to obtain the best precision: since the Baratron digital display provided 4 figure accuracy (so that atmospheric pressure was 760.0 torr), partial pressures up to 99.99 torr could be read to two decimal places.

In most cases the mixtures were made up to atmospheric pressure (760 torr or 101.3 kPa). In a series of variable-pressure experiments on stoichiometric methane/air, however, the final pressures were 0.25, 0.5 and 2.0 atmospheres. The lower pressures

were easily read using the Baratron, but a Bourdon tube gauge (Budenberg 0 - 15 p.s.i.g.) was fitted to measure the higher pressure. It was necessary to increase the spark gap from 0.7 mm to 4.2 mm for the lowest pressure run.

The temperature of the bomb was usually around 296 K, but varied a little depending on room temperature and the amount of heat released by the previous explosion. The mean initial temperature for all runs except diluted hydrogen/air was 296 K, with a standard deviation of about 1 K. The diluted hydrogen runs were performed during a hot spell, and the mean temperature was 298 K, again with a standard deviation of about 1 K.

After the gases had been added, a mechanical stirrer was switched on and the mixture was stirred for 20 minutes. It was then left to become quiescent for a further 10 minutes before being ignited.

The experiment was initiated from outside the laboratory for safety reasons. The run was started by closing a switch connected by a long lead to the camera. After a certain length of film had run through the camera (usually 70 feet), the ignition system was triggered. Provided the energy of the resulting spark was high enough, a spherical flame propagated outwards from the centre and its schlieren image was recorded on the remaining film.

It was decided that data from at least two runs should be obtained for each mixture. This would reduce uncertainties (by averaging) and highlight "odd" results. Spark ignition energies were to be near to the minimum value so that the flame would not be affected by excess thermal energy. It was known from earlier work that spark energies well in excess of those needed for ignition could reduce the accuracy of the experiments by changing the shape of the radius *vs* time curve. The ignition energy could be varied by charging the capacitor in the ignition circuit to different voltages. Preliminary experiments with stoichiometric methane/air showed that the minimum spark energy corresponded to a capacitor voltage of 110 V. Capacitor voltages up to 150 V produced results which were independent of the ignition energy. This led to a rule of thumb that spark energies corresponding to capacitor voltages which exceeded the minimum by 50 V or less would be considered to be acceptable.

There was no opportunity during the experiments to calibrate the ignition system precisely so that the spark energy was known from the capacitor voltage. However, measurements on an earlier version of the ignition system demonstrated an approximately linear relationship between capacitor voltage and energy delivered.

Two approaches were considered for obtaining near-minimum ignition energy runs. One would consist of making up the required mixture and then slowly increasing the capacitor voltage, attempting to ignite the mixture every 10 V say. No measurements would be taken on this trial mixture, but once the ignition energy was known, two runs would be sufficient. The second approach would involve filming all runs and gradually decreasing the capacitor voltage until the mixture failed to ignite. Runs at ignition voltages exceeding this minimum by 50 V or less would be usable.

On the face of it, the first method seems to be the better. At the expense of one "wasted" run (since no pictures would be taken during the search for the minimum ignition energy), the correct value would be known and two minimum energy runs could then be performed. But there was a disadvantage with this approach. It turned out that the mixture was harder to ignite if there had been a failure to ignite (i.e. too low an energy) immediately beforehand. The reason for this was not clear, but one might conjecture that a layer of oxidized material is produced on the electrodes by an ignition failure, leading to increased difficulty of ignition subsequently.

For this reason, the second method was used. It was not unduly wasteful of time or film, since the difference in minimum ignition energy between one mixture and the next leaner or richer was usually small. The first attempt to ignite a mixture was therefore frequently inside the 50V range of "allowed" energies.

Another choice that had to be made was the camera speed. It could be set at any value up to 10 000 frames per second (f.p.s.). However, the practical maximum using 100 foot film lengths was 7000 f.p.s. because the camera needed more than 100 feet of film to reach the higher speeds. Clearly a speed of 7000 f.p.s. could have been used in all of the runs, giving the maximum possible time resolution in all cases. But for relatively low flame speeds, the number of frames to be analysed would have been too large. For example, the highest methane/air flame speed was about 2.8 ms^{-1}. The flame therefore took about 12.5 ms to travel 35 mm. At a camera speed of 7000 f.p.s., the number of frames would be 88. Analysing this many frames would be wasteful: the extra information would be redundant and the time taken could be better spent elsewhere. In addition, the tedium of the analysis would be likely to lead to much greater operator error. Experience in earlier experiments suggested that about 35 frames for a run gave sufficient time resolution. The required camera speed was therefore about 1000 times the expected flame speed in metres per second.

For very fast mixtures (e.g. hydrogen/air) the maximum speed of 7000 f.p.s. was not high enough to provide 35 frames. In these cases a smaller number of frames had to be accepted.

The above considerations ignore a further consideration about the camera speed. The only appropriate frequency produced by the timing light generator was 1 kHz, i.e. a timing mark appeared on the film every millisecond. Choosing a camera speed of $1000n$ f.p.s. (n = integer) ensured that although the timing mark only appeared on every nth frame, it appeared at the same position on each occasion. A stationary timing mark made it easy to detect changes in camera speed and also reduced the analysis time considerably.

4.1.3 **Data reduction**

4.1.3.1 Derivation of S_b° and b

The films of the expanding spherical flames were analysed using the film motion analyser. The vertical diameter of the spherical flame was measured on each frame of the film. The position of the timing mark relative to a film perforation was measured whenever it appeared. The raw data extracted from the films therefore consisted of a flame diameter for each frame and a timing mark position for every nth frame where the nominal film speed was $1000n$ f.p.s.

A complicating issue in the case of lean hydrogen/air mixtures is the occurrence of cellular flames. For mixtures containing about 25% hydrogen, onset of cellularity occurred within the measurable range, at a radius of about 30 mm. For the leanest flame (9% hydrogen) onset was at about 11 mm. The analysis was confined to the pre-cellular region in all cases.

Since the scaling of the photographs and the frequency of the timing marker were known, it was possible to convert the raw data into radius *vs* time records. A computer program TCALC2E was written to perform this conversion. On the assumption that the flames were perfectly spherical, the flame radius was obtained by dividing the measured diameter by 2. The calculation of the elapsed time was complicated by two factors. First, the timing mark was made by an LED which was about 5 frames before the gate in the film path. Therefore the timing mark

corresponding to a particular frame was 5 frames later. This had to be taken into account both in the program and in the film analysis: measurements of the timing mark position had to be continued for 5 frames after the radius of the expanding flame had exceeded the radius of the windows. Second, for camera speeds greater than 1000 frames per second there was not a timing mark for each frame. It was therefore necessary to interpolate linearly between marks to derive a time for each frame.

Finally, the radius *vs* time records were analysed by fitting equation (3-12), i.e.

$$r + b \ln r = S_b^{\circ} t + \text{constant} \qquad (1)$$

to them; the parameters b and S_b° were varied until the best fit was obtained. A computer program SBLS9 was written to perform this calculation. The fitting procedure was based on a linear least squares analysis. An initial value of b was selected and $y = r + b \ln r$ was calculated for each value of r. A conventional linear regression computation was performed on the y *vs* t data set and the slope S_b° was determined. A measure of the goodness of fit was also calculated; in this case, the uncertainty in the slope, SS_b°, was used. A new value of b was then chosen by the program and the procedure repeated. b was varied using the Modified Regula Falsi method[84] until SS_b° was a minimum.

The procedure just outlined gave a best fit for all the points in the data set. However, from the analysis in Chapter 3 we know that the simple model is likely to break down at small values of r. More accurate data might therefore be obtained if some early points were not included in the analysis. The whole procedure was therefore repeated with the first point removed, then the first two points, and so on until there were no points left. The usual result was that the overall minimum value of SS_b° occurred when one or two points had been removed. The correct values of b and S_b° were taken to be those corresponding to this overall minimum value of SS_b°. In some cases, the number of points omitted was very large. This gave a good indication that the assumptions used to derive the simple model were reaching the limits of their validity.

It is worth mentioning that other measures of the goodness of fit were considered. In particular, test runs were carried out using the standard deviation of the points from the theoretical curve. The uncertainty in the slope, SS_b°, was chosen partly because a small uncertainty in the limiting flame speed was desirable and partly for the pragmatic reason that it had a minimum value when a small number of initial

points had been removed. Other measures simply got smaller as initial points were removed and did not provide an indication of the number of points to ignore.

The one-dimensional burning velocity S_u° was determined from the one-dimensional flame speed S_b° by multiplying by the density ratio $\sigma = \rho_b/\rho_u$ calculated using a flame temperature program FTEMP.

4.1.3.2 Experimental errors

Random errors

The uncertainties in flame radius and time measurements are estimated at 2% and 0.1% respectively. The uncertainty in the time measurement is so much smaller than that in the radius measurement that it can be ignored. True random uncertainties in radius measurement should simply cause the points to be scattered about the theoretical curve, so that the uncertainty in the burning velocity is simply that calculated from the linear regression computation. This was typically around 0.2%. The standard error calculated from the results of individual runs on the same mixture was usually larger, at around 1%. This figure includes slight variations in flame shape from one run to another, and probably represents the random uncertainty quite well. The uncertainty in the flame relaxation parameter b is harder to estimate because of the way it is used in the numerical method to determine the best fit. The value of the best-fit value of b typically changes by about 0.05 mm as initial points are removed in the fitting process. This leads to an estimated uncertainty of about 5% for a typical value of 1 mm. Again, the standard error in b determined from individual results is larger at about 10%, and since this figure contains random differences in conditions from one run to the next, it is probably the better estimate.

It is worth pointing out that the number of repeat runs was always small, so that calculated standard errors are themselves rather uncertain. The above figures are estimates of the true values.

Systematic errors

The most important source of systematic errors in the experiment is likely to be due to the difference between the behaviour of a real expanding flame and that of the

simple model fitted to the experimental results. An important feature of this work is therefore that the simple model can be tested by fitting it to the results of detailed modelling of expanding spherical flames for which the true one-dimensional burning velocity is known. The tests are described in Section 6.4.2 and show that in most cases the extrapolated burning velocity is within 3% of the true value.

Expanding flames can occasionally be non-spherical, especially in the early stages. Very non-spherical flames and ones which were not smooth were not used. Tests were performed on cases where the departure from sphericity was small. The tests showed that the rate of change of any diameter is not much affected by the shape, which helps to explain why the spherical shape is regained as the flame gets bigger. Another implication of non-sphericity is that the flame is then subjected to extensional stretch since there must be tangential velocity gradients. But the mean extensional stretch theorem (in Section 2.2.4) shows that the mean extensional stretch over the whole flame surface is zero and the net burning rate is affected only by the dilatational stretch.

4.2 STAGNATION FLOW FLAMES

4.2.1 **Apparatus**

The experimental apparatus consisted of a water-cooled burner mounted on a motorized table, a gas mixing rig and a laser-Doppler anemometry (LDA) system. A computer was used both to control the experiment and to analyse the data collected. The general arrangement is shown in Fig. 11.

The burner had been designed and built at LRS by Dr. F.G. Roper for a previous project. It consisted of a cylindrical plenum chamber about 30 mm in diameter and 80 mm long containing a flame trap and surrounded by a water-cooling jacket. Mache-Hebra nozzles of various diameters could be screwed into one end. Most of the experiments were performed using a 10 mm diameter nozzle. A thermocouple inside the burner was used to monitor the unburnt gas temperature. The temperature of the cooling water was regulated with a Churchill circulator (type 02/CTCV) such that the gas temperature was about 25°C (298 K).

Fuel/air mixtures were supplied to the burner from a gas mixing rig, also built at LRS. The flow rates were controlled by critical orifices. Upstream pressures were

FIGURE 11

Experimental set-up for stagnation flow measurements

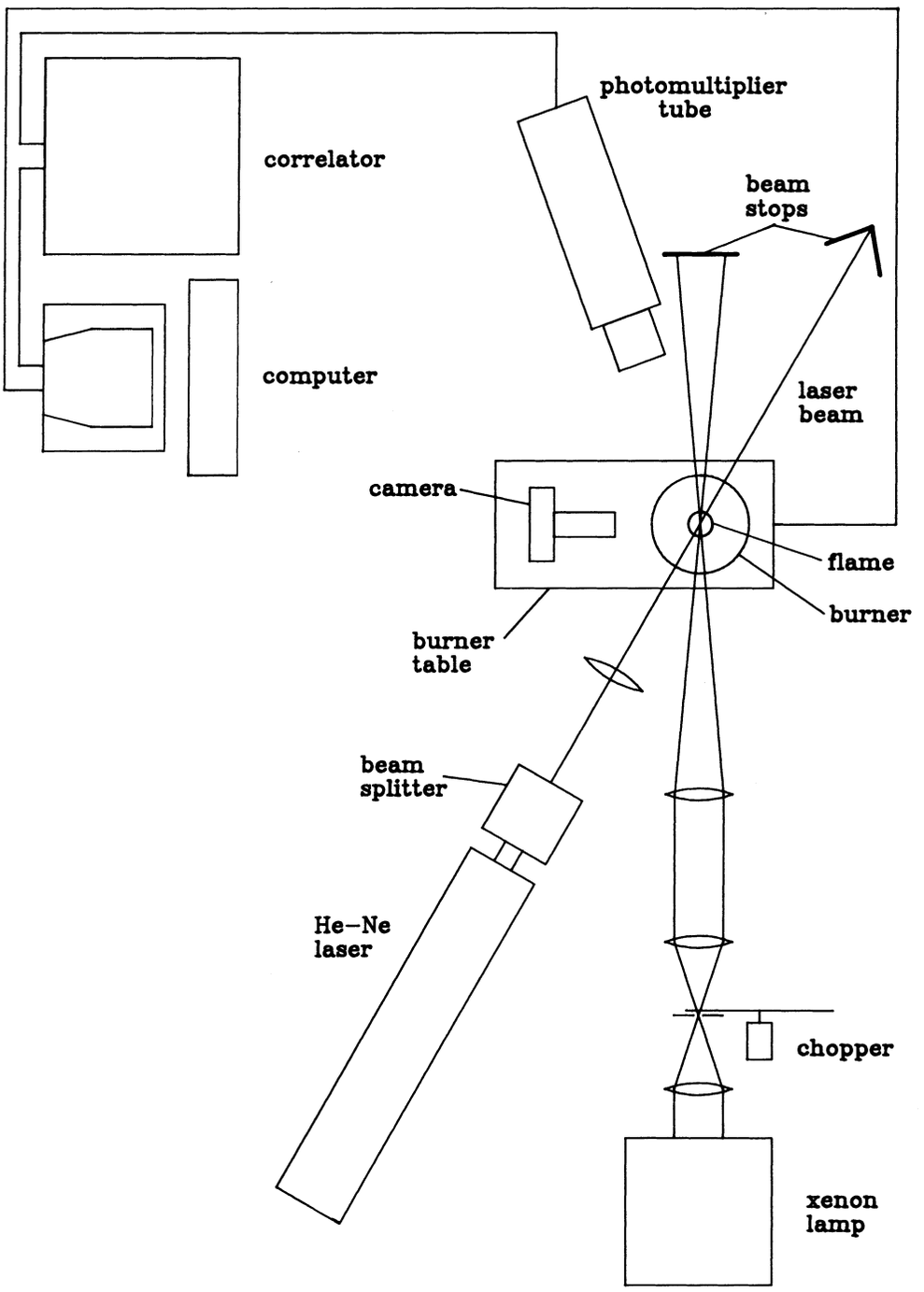

measured using Bell and Howell type 4-366-0001-01W0 pressure transducers (range 0 to 20 bar absolute). The critical orifices were ruby watch jewels, with internal diameters of 0.09 mm for fuel and 0.34 mm for air. Calibration was performed using a purpose-made soap bubble flowmeter. It was necessary in the experiment to change the flow rate while keeping the composition constant. This was achieved by routing part of the premixture (the "bypass") to a bleed burner via a rotameter. The flow rate going to the burner could then be adjusted by varying the bypass flow rate.

The premixed fuel/air mixture fed to the burner was seeded for LDA measurements with particles of magnesium oxide (MgO) with diameters of the order of 2 μm. This was accomplished by routing part of the burner gas supply through a Corning 3760/02 filter funnel which served as an elutriator. A 20 mm thick layer of MgO was placed on the 20 mm diameter sintered glass disc at the lower end of a 200 mm long vertical glass tube. The gas flow rate was adjusted so that the magnesium oxide particles formed a fluidized bed. Some of them were entrained into the flow and reached the burner where their velocity was measured. The elutriator assembly was placed in an explosion-proof enclosure for safety reasons.

The burner was mounted on a motorized table. This could be moved both vertically and horizontally under computer control. The stepper motor units (UniSlide) had resolutions of 2.5 μm horizontally and 1 μm vertically. They were driven by a Digiplan stepper motor driver under computer control via an IEEE interface. For most experiments, velocity measurements were only needed along the centre line of the flame and the burner was just moved vertically.

The gas flow velocity was measured by laser-Doppler anemometry (LDA). The beam from a 35 mW He-Ne laser (Spectra-Physics 124A) was split into two parallel beams in the same vertical plane using a Malvern RF307 beam splitter. They were then focused using a 300 mm focal length lens such that they crossed within the flame. The angle between the beams was typically about .07 rad, and with a laser wavelength of 632.8 nm the fringe spacing was about 9 μm[75].

The LDA system was operated in the forward scatter mode to maximize the intensity of scattered light. A photomultiplier tube (Malvern RR127) fitted with a 105 mm focal length lens was used to collect photons. The integral discriminator produced pulses suitable for analysis by the Malvern K7023 digital correlator. A computer program SU103I was written to control the experiment. It displayed the correlogram on the computer screen as the signals were being collected. The program also controlled the correlator via a bank of mercury relays on the IEEE bus so that a

single command typed at the keyboard would signal the correlator to stop collecting data, transfer the autocorrelation function to the computer and save it to disk along with the position where it was measured, move the burner to the next position, zero the correlator and restart data collection.

In addition to their use in LDA, the seeding particles had another function. An important part of the work on burner flames was the visualization of flow streamlines. The light for this was provided by a 1600 W xenon lamp, type XBO 1600, manufactured by AEG Telefunken. It was powered by a 95 A power supply made by Transformer and Rectifiers Ltd. The beam was focused onto a slit behind which a chopper could be mounted if stroboscopic pictures were required. The system was arranged so that the image of the slit (i.e. a thin sheet of light) was in the diametral plane of the burner. The particles illuminated by this arrangement were photographed using a Nikon F3 camera fixed to the burner table at right angles to the beam. In order to provide a suitably large image, the 50 mm f/1.4 lens was reversed and mounted on 65 mm extension tubes.

4.2.2 **Method**

4.2.2.1 Setting up

The setting-up procedure for this experiment was rather complicated, so it is best described as a series of steps. A filter was used to reduce the laser beam intensity to a very low level during the setting-up procedure.

1. The optical bench supporting the laser was positioned approximately and then levelled.
2. The beam splitter was removed from the laser and the beam was made parallel to the optical bench. This was done by adjusting the laser supports until the beam passed through an aperture fixed to a lens holder when it was placed at several points along the optical bench.
3. The beam splitter was replaced and adjusted and the beams were made parallel by a similar technique to that above.
4. The 300 mm focal length lens (used for focusing the laser) was placed close to the laser so that the crossing point occurred well before the burner. A plumb line was hung in the beam path and the beam splitter was rotated until both beams struck the plumb line. The beams were then in a vertical plane.

5. The lens was moved along the optical bench towards the burner until the crossing point was roughly on the axis of the burner.
6. The plumb line was hung on the axis of the burner.
7. The laser beams were directed onto the thread of the plumb line and the position of the focusing lens was adjusted until the two spots coincided.
8. The photomultiplier tube was focused on the laser spot on the thread.
9. The beam crossing angle was measured. A mirror was positioned in the beam path before the crossing point such that two laser spots appeared on the wall behind, about 2 m away. The distance D between the new crossing point and the wall was measured, along with the distance d between the two spots on the wall. Typical values were D = 2.2 m and d = 160 mm, giving a half angle between the beams of $\tan^{-1}(d/2D)$ = .035 rad.
10. The xenon lamp was focused on the thread.
11. The cathetometer was levelled and focused on the burner.
12. The xenon lamp was switched on, the flame was lit, and seeding particles were introduced into the flow. The camera position was adjusted until the illuminated plane of particles was in focus and then fixed in position.
13. The laser focusing lens was adjusted until the crossing point was precisely on the centre line of the flame. This was done by using the cathetometer to view the crossing point (which was made visible by the presence of seeding particles) and moving the lens until there were equal beam lengths on either side of the crossing point. The height of the crossing point above the burner surface was then measured using the cathetometer.
14. The photomultiplier tube was realigned on the crossing point by adjusting for the maximum rate of increase of the amplitude of the autocorrelation function.
15. A scaling photograph was taken of a graticule which consisted of 1 mm squares. An England Finder microscope slide supplied by Gallenkamp was used.
16. The elutriator was filled with fresh, dried magnesium oxide powder.
17. A circular steel plate was positioned just over half of the burner diameter above the burner and levelled.
18. The required mixture was set up on the flow rig and the bypass flow rate adjusted to give (i) the minimum flow rate to the burner for which the flame was reasonably flat and (ii) the maximum (without extinction). The flow rates within this range to be used in the experiment could then be determined.

4.2.2.2 Experimental procedure

Methane was the fuel used in all of the experiments described here. The same cylinder as used in the expanding flame experiments (described in Section 4.1.2.2) was used. Air, filtered and cleaned, was supplied from a cylinder of compressed atmospheric air.

The first flow rate was selected and the elutriator adjusted to give correct seeding. The axial gas velocity was then measured at different points in the flow by moving the burner vertically. Velocities were measured from close to the burner to just inside the preheat zone of the flame where the velocity starts to rise quickly. As described earlier, most of this part of the experiment was automated, and the main role of the operator was to check that the experimental conditions (burner temperature, seeding level, gas flow rates, etc) remained constant. The burner was then returned to its datum position and a check was made to ensure that no vertical slippage of the burner table had occurred. A new flow rate was selected, the seeding level adjusted and the procedure repeated.

4.2.3 **Data reduction**

4.2.3.1 Computation of burning velocities and stretch rates

The data collected in the stagnation flow experiments consisted of correlograms (autocorrelation functions) along with the positions in the flame where they were measured, and particle tracking photographs of the flame at each flow rate. For low turbulence levels, such as those encountered in this work, the Gaussian model of turbulence is appropriate[75]. A computer program LDA31 based on this model was used to analyse the autocorrelation functions. It was originally written for a Commodore PET microcomputer by Dr. F. G. Roper and was adapted for the computers used in this work (a Sirius 1 followed by an Olivetti M240). It worked by fitting an expression with five variable parameters to the measured autocorrelation function. One of the parameters is proportional to the gas velocity.

In most of the experiments, the vertical component of velocity was measured on the axis of axially symmetric flames. The above procedure therefore gave the vertical component of gas velocity in the upstream flow as a function of distance from the burner surface. The stretch rate was determined from these data by fitting a straight

line to the upstream velocity profile as described in Section 3.3.1. In the experiments, the profile was only approximately linear. The straightest part was usually that close to the upstream boundary of the flame so this was normally used.

The "conventional" burning velocity S_{L1}, namely the normal gas velocity at the upstream boundary, was taken to be the minimum in the velocity profile, following Law and co-workers[23,24]. In one set of experiments the burning velocity u_n measured by Cambray et al was measured[85-87]. This was obtained from S_{L1} by subtracting $\Gamma\delta$. Γ is the measured stretch rate and δ is the distance between cold boundary and luminous zone, with the former identified by the velocity profile and the latter by the flame photographs.

The burning velocity $S_{u,r}$ used in this work and defined by equation (3-1) was obtained by multiplying S_{L1} by a stream tube area ratio A_1/A_r obtained by particle tracking as described in Section 3.3.1. A_1 was the stream tube area in the plane where S_{L1} was measured. A_r was the area of the same stream tube at the upstream edge of the luminous zone. In some cases, several upstream velocities and areas were measured and the burning velocity was determined using equation (3-55). The stream tube areas were obtained from measurements on the negatives of the particle tracking photographs. The film analyser used in the expanding flame experiments was modified to accept 35 mm film so that it could be used for these measurements.

In order to determine the stream tube area ratio, it was necessary first to choose a suitable particle track. On the one hand this had to be clear, so that accurate measurements could be taken; on the other it had to be an accurate representation of a true streamline. Large deviations from the correct flow direction were obvious by comparison with other tracks. The selected track had to be near enough to the centre line to ensure that it supplied a flat part of the flame, but not so close that small uncertainties in measurement would lead to large errors in the area ratio. Finally, in order to locate the centre line accurately on the photograph, it was desirable that there be particle tracks on either side of the centre and close to it.

When all of the above conditions had been satisfied, measurements could be made. The data required were the radial distance of the particle track from the centre line at points in the cold flow where velocities had been measured and at the base of the luminous zone. The positions on the photograph corresponding to the velocity measurements were determined by applying the scaling data to the known height of the laser crossing point above the burner surface. Measurements were all relative to the top of the burner. The upstream edge of the luminous zone was not well

defined, but at this point the divergence of the particle tracks was small, so that errors due to the uncertainty in its position are unlikely to be large.

4.2.3.2 Determination of S_u° and L

The data obtained for each fuel/air mixture consisted of a series of stretch rates with two burning velocities measured at each one: the upstream burning velocity S_{L1} and the burning velocity defined at the reference surface $S_{u,r}$. Values of the one-dimensional burning velocity S_u° and the Markstein length L could be readily calculated for each set of data by fitting a straight line to the burning velocity *vs* stretch rate data. The one-dimensional burning velocity is the intercept of the line with the stretch = 0 axis and the Markstein length is minus the slope of the line. The results are described in Chapter 5.

4.2.3.3 Experimental errors

Random errors

For the measurement of S_{L1}, the main uncertainties were in the LDA measurement (usually estimated[75] at about 1%) and in the location of the velocity minimum. In the determination of $S_{u,r}$, these were compounded by multiplying by the measured stream tube area ratio, where the uncertainties were rather large. The uncertainty in each radius measurement is estimated at 5%, giving a net error of about 14% in the value of $S_{u,r}$. By comparison, the uncertainty due to the LDA measurement is negligible.

The other major uncertainty was in the measurement of the stretch rate. The upstream velocity gradient was often quite curved. Besides the possible systematic error due to measuring the slope at the wrong point (covered below), there must also be random error. This is estimated to be about 10%.

Systematic errors

The systematic errors in the experiment probably lie in the assumptions made about the flame behaviour. These are contained in the assumption that the experimental

flow is an ideal stagnation-point flow, which implies that (1) the upstream burning velocity S_{L1} varies linearly with stretch, (2) the upstream velocity gradient is equal to the stretch rate and (3) the vertical component of gas velocity is constant in any horizontal plane.

As described earlier, the upstream velocity profile was often nonlinear, so that systematic error in the measurement of the stretch rate is likely. In fact, it is possible that the stretch rate is systematically underestimated. Recently, flames in stagnation-point flow have been modelled by Dixon-Lewis et al[88,89] by solving the Navier-Stokes equations. This work suggests that measurements of the velocity gradient are likely to underestimate the "applied stress" (considered by Dixon-Lewis to be the important parameter).

Unlike the expanding flame case, there is no straightforward test of the correctness of the assumptions underlying the stagnation flow methodology, but we will see that the measurement of two burning velocities has interesting ramifications.

4.3 BUTTON-SHAPED FLAMES

A few experiments were also carried out using button-shaped flames and these will be described next. This section is shorter than the other two because fewer experiments were performed and much of the description in the previous section applies. The experimental methodology is described in Section 3.4. The experiment was simpler than the stagnation flow experiments in that stretch was ignored. But it was also more complicated in that the flame was no longer flat, and the cold gas velocity varied over the stream tube area.

The experimental data required were the volumetric flow rate of cold gas through a given stream tube, and the area of luminous zone supplied by the same stream tube. The volumetric flow rate was determined from measurements of the vertical component of gas velocity across the diameter of the selected stream tube. The velocities were measured using LDA as described earlier in this chapter and the streamlines were visualized by particle tracking. The necessary traverses through the flame were made by moving the burner table horizontally. A polynomial function was fitted to the velocity values and the flow rate was determined by integration across the stream tube radius using equation (3-90).

The flame area was obtained by assuming that its shape was that of a spherical cap. Particle tracking photographs of the flame were taken using a camera mounted on the burner table. After a suitable particle track had been selected, the streamline radii R_1 and R_2 in the cold flow and at the luminous zone were determined. The amount h by which the centre of the luminous zone dipped below its intersection with R_2 was measured and the area was calculated using equation (3-92).

Chapter 5

EXPERIMENTAL RESULTS

The experimental results are presented in this chapter. They are mainly in graphical form, with numerical values listed in the Appendix for reference.

5.1 EXPANDING SPHERICAL FLAMES

The results of the expanding spherical flame experiments are presented in this section. In order to give a flavour of the records being analysed, Fig. 12 shows a sequence of frames of an expanding spherical flame. The mixture was methane/air with a stoichiometry of 1.1. The first frame immediately follows ignition. Subsequent frames show the flame approximately every 1.5 ms.

The data obtained from the photographs were the radius of the expanding flame as a function of time for each run, and they could have been presented in this form. However, consideration of Fig. 5(a) shows that a plot of the experimental values of flame radius against time does not convey a great deal of information. By contrast, a graph of the same data in the form of flame speed against radius in Fig. 5(b) demonstrates clearly the variation of the speed of the expanding flame with radius and its asymptotic approach to the one-dimensional value. The experimental results are therefore presented in the latter form.

The plotted data were obtained from the experimental radius versus time values as follows. The instantaneous speed was taken to be the slope of the line segment connecting two neighbouring radius versus time points, i.e.

$$\left.\frac{dr}{dt}\right|_{(j+1/2)} = \frac{r(j+1) - r(j)}{t(j+1) - t(j)}. \qquad (1)$$

The radius corresponding to this speed was taken to be the mean radius, given by

$$r(j+1/2) = \frac{r(j+1) + r(j)}{2}. \qquad (2)$$

FIGURE 12

(overleaf)

Sequence of photographs of an expanding spherical flame

Methane/air, stoichiometry = 1.1. The flame is shown approximately every 1.5 ms

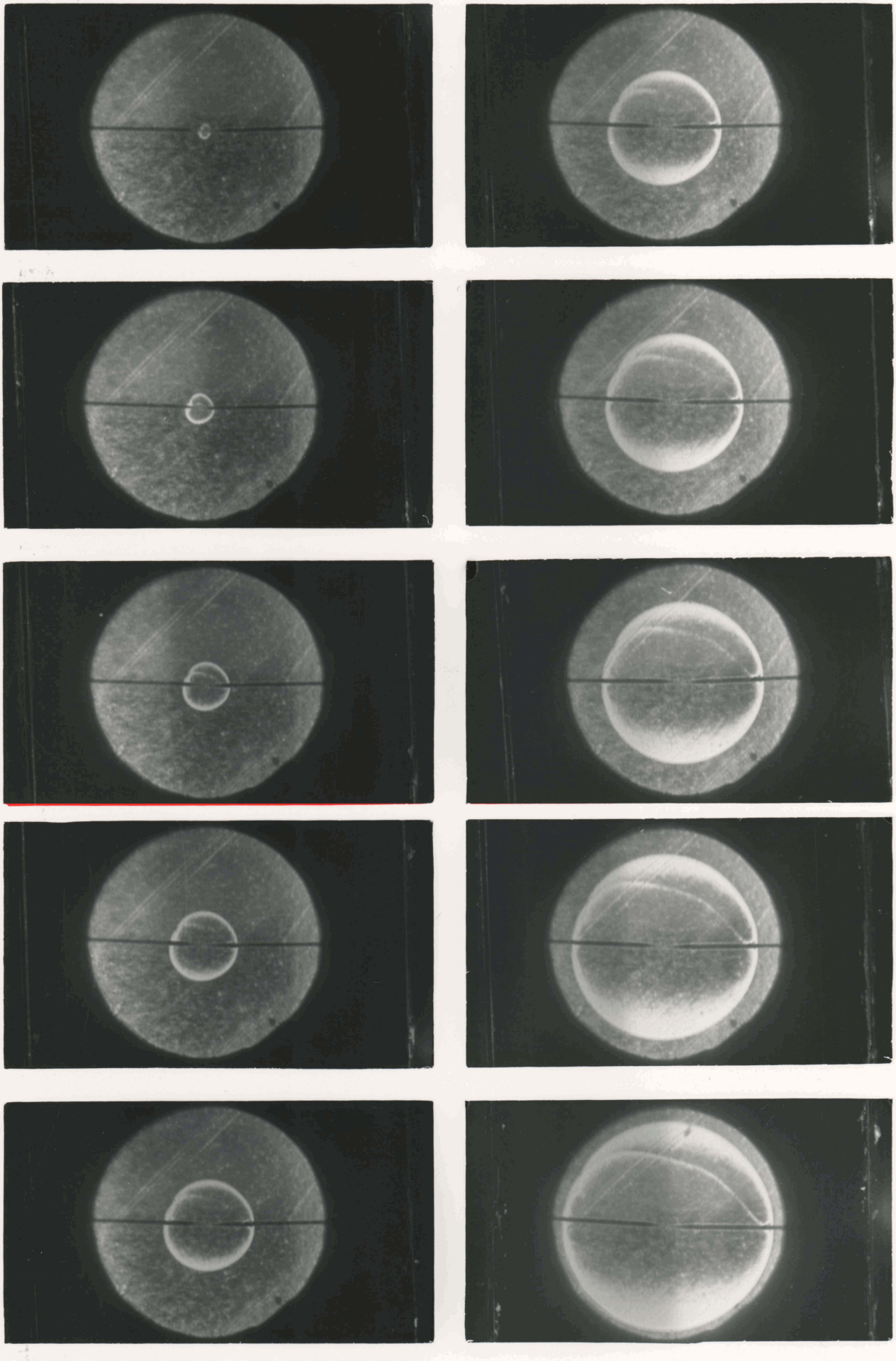

The differentiated data were necessarily rather scattered as a result of this procedure and it was difficult to perceive a clear trend. The points were therefore smoothed using a procedure called LOWESS[90], which stands for LOcally WEighted Scatterplot Smoother. A computer program which performs this operation was obtained from the publishers of ref. 90. The program requires the input of a parameter F which sets the degree of smoothing. F = 0 corresponds to no smoothing and F = 1 to complete smoothing, where the points lie on a horizontal line at the mean value. Insufficient smoothing causes the trend of the results to be obscured, while too much smoothing gets rid of real features. A value of 0.35 was found to be a good compromise between these extremes, and was used in most cases. Larger values of F were needed occasionally when the scatter was particularly large.

An unfortunate feature of smoothing techniques is that points near the minimum and maximum radii are particularly sensitive to small deviations of the end points. At small radii this is unimportant because differences from the simple model are expected there. But at large radii the effect can be an apparent systematic difference between experiment and model. This is exacerbated by larger uncertainties than usual in the largest measured radius. This increased uncertainty is due to a lack of clarity in the schlieren image on the film, and could arise from several sources. The presence of flame temperatures causes some degradation of the rubber gasket between the window and the flange of the combustion bomb. In addition, the high vacuum grease on the gasket, although only present in very small quantities, can also be affected by the adverse conditions. Material from both of these sources was found at the edge of the visible region of the windows when they were removed for cleaning.

The speed *vs* radius equation (3-10) was plotted through each data set, using the values of the parameters $S_b{}^\circ$ and b obtained by fitting equation (3-12) to the radius *vs* time data as described earlier. The level of agreement between the experimental results and the simple model used to describe them can therefore be seen.

In order to ensure that the diagrams remain clear and uncluttered, not all of the experimental data have been plotted. Displaying the results of two experiments on the same fuel/air mixture would detract from the clarity of the graph. But one example of each set of conditions has been plotted, and the numerical data derived from all runs are listed in the Appendix so that repeatability can be assessed. For measurements across the stoichiometric range, it turns out that the clearest display is produced by dividing the data into two sets. Broadly speaking, data for lean mixtures are plotted on one set of axes and data for rich mixtures on another.

The stoichiometry of each run is listed on the right-hand side opposite the corresponding data. In the case of nitrogen-diluted hydrogen mixtures, the figure given is the percentage dilution. In the variable-pressure methane/air runs, the figure is the pressure in atmospheres.

Fitting the simple model to the radius *vs* time records allows the one-dimensional burning velocity S_u° and the flame relaxation parameter b to be derived as described in Section 4.1.3.1. At least two runs were performed for each set of conditions and average values of these parameters were calculated. The mean values of S_u° are plotted against stoichiometry for each fuel and set of conditions described, along with a best-fit polynomial curve through the data. The dashed curve represents the modelling results, which will be described in Chapter 6. On a different set of axes, mean values of b are plotted against stoichiometry for the same conditions. Values of the calculated density constant k are also plotted on these axes. Again, these will be described in Chapter 6, when the determination of the Markstein lengths will be described.

To summarize, for each fuel and set of conditions the following data are plotted: dr/dt *vs* r, S_u° *vs* stoichiometry, and b *vs* stoichiometry. In addition, data for stoichiometric hydrogen/air are plotted against % nitrogen dilution and data for stoichiometric methane/air are plotted against pressure.

5.1.1 Hydrogen

5.1.1.1 Variation with stoichiometry at atmospheric pressure

The experimental flame speed *vs* radius data are plotted in Figs. 13 and 14. Two important points are worth making about the results for the lean mixtures in Fig. 13. First, at stoichiometries below 0.8 (about 25% hydrogen), the flame speed decreases with increasing radius. For all higher stoichiometries the speed increases. Second, the onset of cellularity in lean mixtures limits measurements to radii below a critical value. The critical radius decreases with decreasing stoichiometry, so that in the leanest mixture, data could only be collected up to a flame radius of 11 mm.

Fukutani et al[91] attributed the fall in flame speed with radius in lean hydrogen/air mixtures to the decreasing effect of excess ignition energy. This cannot be the

FIGURE 13

Flame speed *vs* radius of lean hydrogen flames
Points: experimental data. Curves: equation (3-10) fitted to data.
Numbers on right denote stoichiometry.

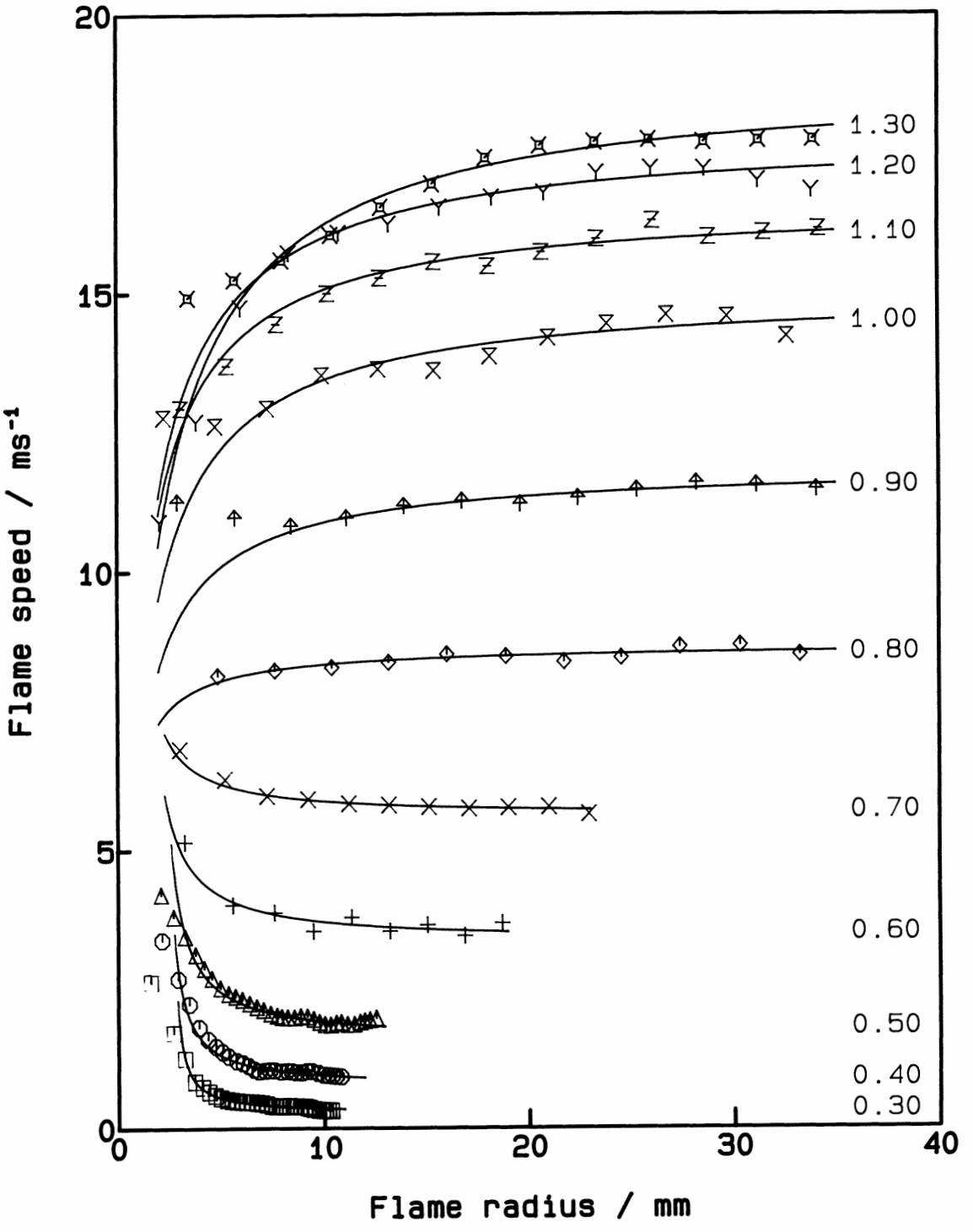

FIGURE 14

Flame speed *vs* radius of rich hydrogen flames
Points: experimental data. Curves: equation (3-10) fitted to data.
Numbers on right denote stoichiometry.

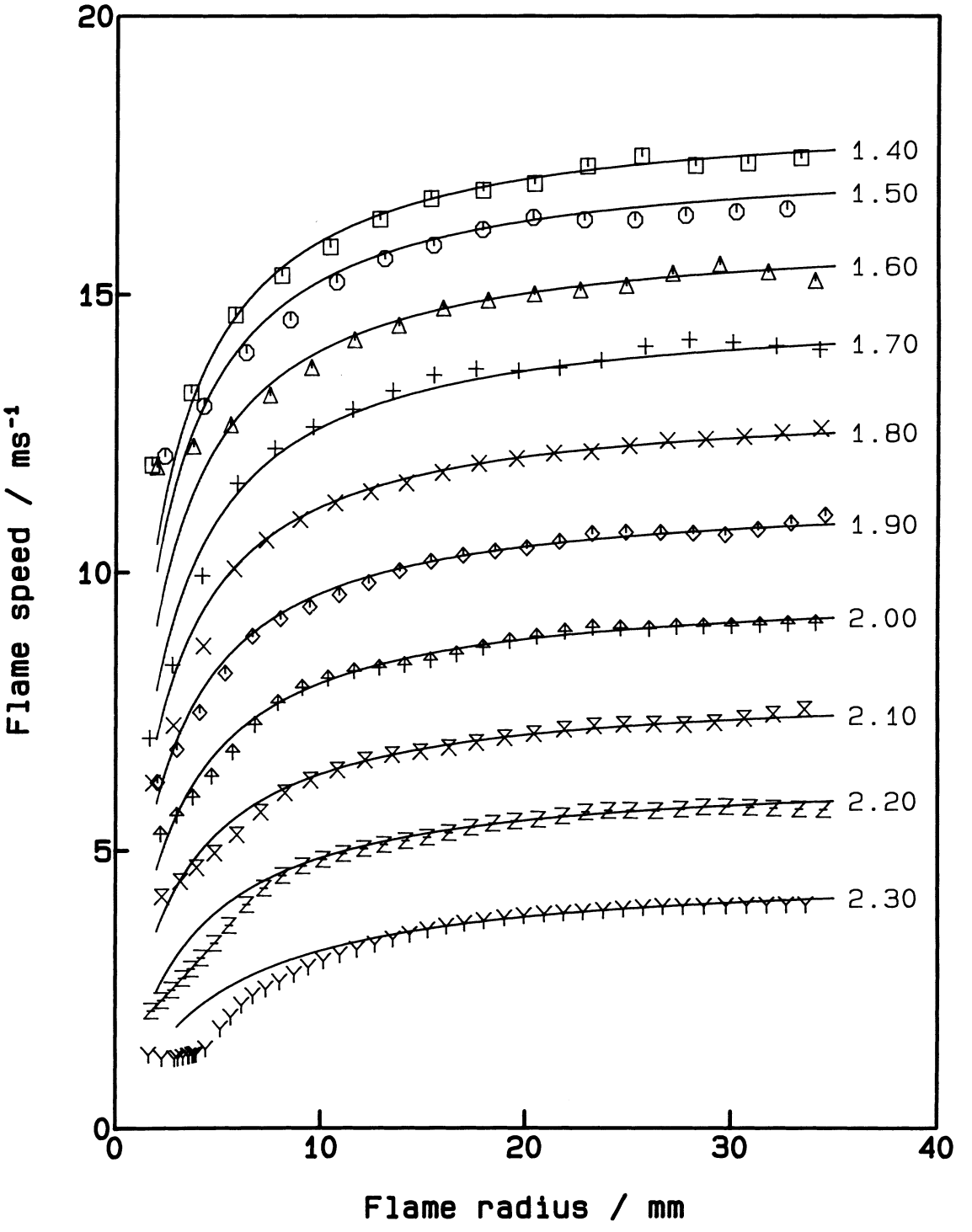

FIGURE 15

Experimental and modelled burning velocity *vs* stoichiometry for hydrogen/air flames
Points: experimental results. Solid curve: best fit polynomial curve through results.
Dashed curve: best fit polynomial curve through planar modelling results.

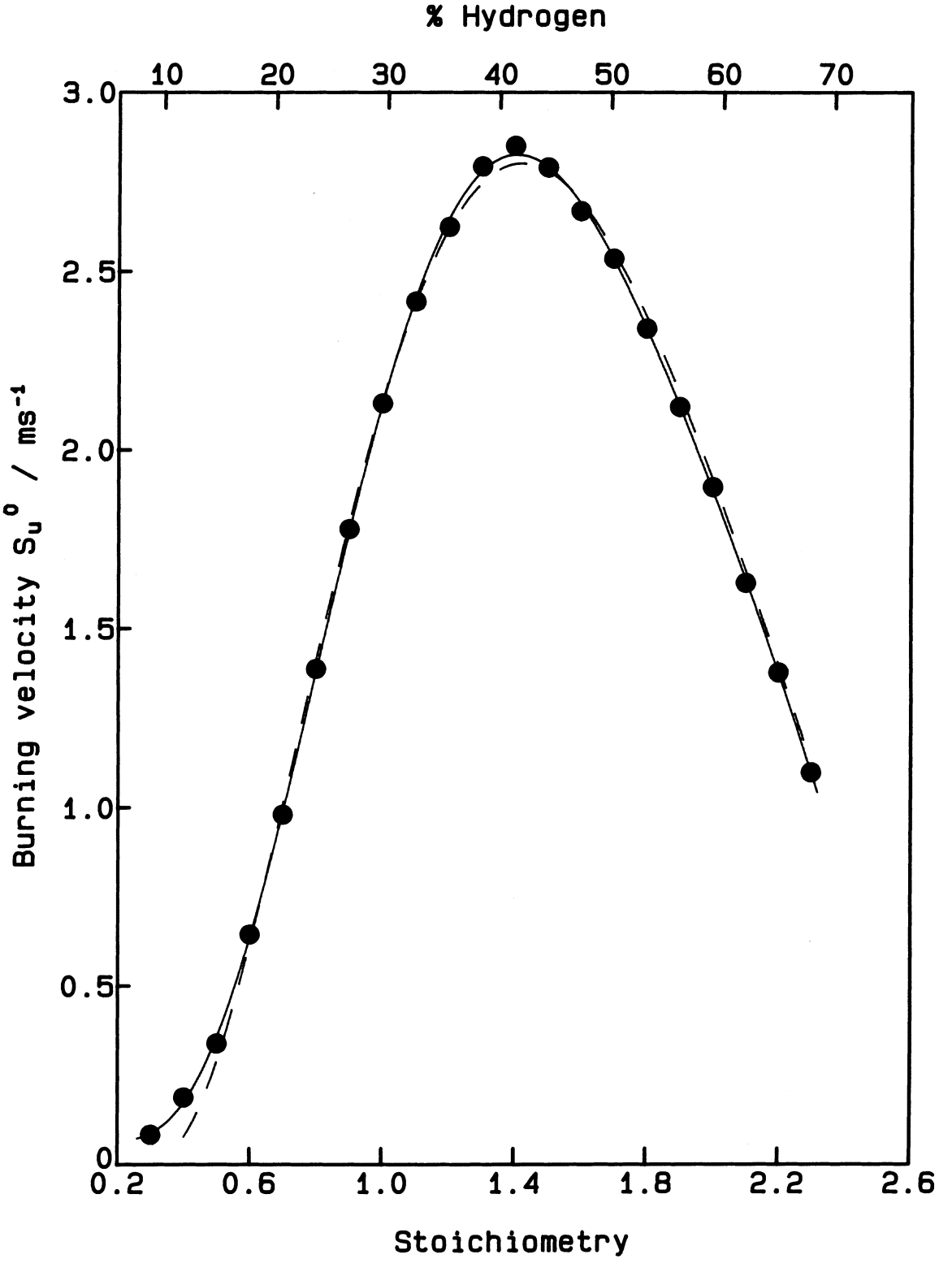

FIGURE 16

Flame relaxation and density parameters b and k *vs* stoichiometry for hydrogen/air flames

•: b derived from experiments. ○: b derived from detailed modelling of expanding spherical flames. ■ : k calculated from modelling of planar flames.

Note: the leanest k value (□) is an estimate.

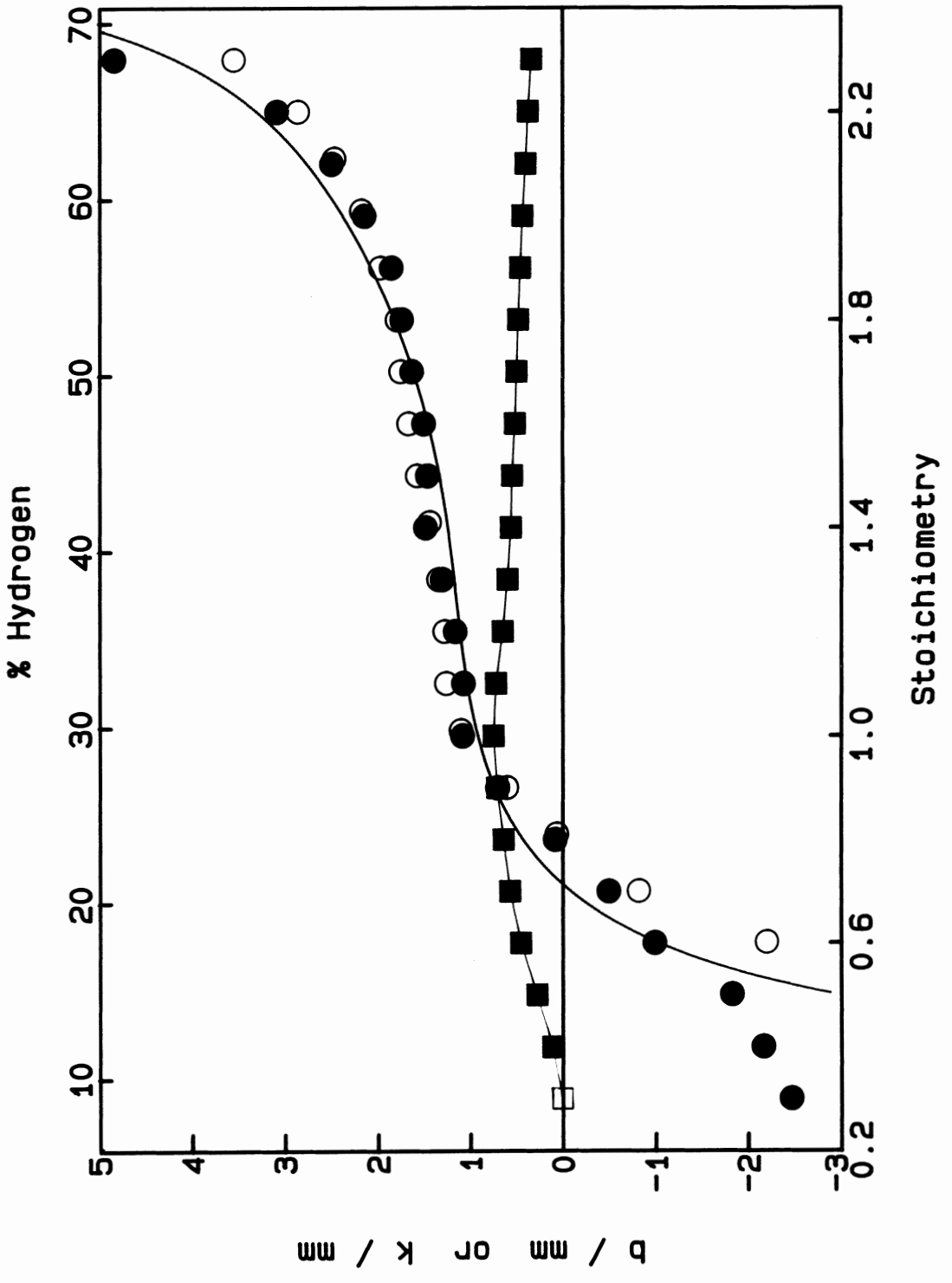

correct explanation in the present work since rich flames behave differently. The analysis in Chapter 3 shows that flame stretch is expected to be the major reason for the changes in flame speed.

In general, the fit of the simple expanding flame model is good, but differences arise in all mixtures at small radii. A systematic discrepancy can be seen in the richest mixtures in Fig. 14. This is a real effect, and is also evident in rich methane and lean ethane and propane mixtures. Similar behaviour was observed in lean propane flames by Ko et al[92]. It may be connected with the critical radius of Champion et al[59].

Hydrogen burning velocities obtained from the data in Figs. 13 and 14 are plotted in Fig. 15. The maximum burning velocity is 2.85 ms^{-1} at a stoichiometry of 1.4 (41% hydrogen). This is much higher than the maximum burning velocities of the hydrocarbons studied in this work. The reasons for this difference will be discussed in Chapter 7.

Values of the flame relaxation parameter *b* are plotted against stoichiometry in Fig. 16. As can be anticipated from the data in Figs. 13 and 14, *b* becomes negative in lean mixtures.

5.1.1.2 Effect of nitrogen dilution on stoichiometric mixtures

Flame speed *vs* radius data for all the diluted mixtures are plotted in Fig. 17. The main point of interest is that at dilutions greater than 30% the flame speed decreases with increasing radius. At dilutions of 45% and greater, the experimental flame speeds first increase and then decrease. The simple model cannot reproduce such behaviour, and the point at which it first fits the experimental data occurs at progressively larger radii.

Burning velocity as a function of nitrogen dilution is plotted in Fig. 18. An alternative way of expressing the nitrogen dilution is in terms of the proportion of oxygen in the oxidizer (consisting in this case of all of the air and added nitrogen). A scale giving this quantity has been included at the top of the graph. The main point is that burning velocity decreases as nitrogen is added.

The flame relaxation parameter *b* is plotted against nitrogen dilution in Fig. 19. It decreases monotonically with dilution, becoming negative at about 30% nitrogen.

FIGURE 17

Flame speed *vs* radius of nitrogen-diluted stoichiometric hydrogen flames
Points: experimental data. Curves: equation (3-10) fitted to data.
Numbers on right denote percent nitrogen in mixture of fuel/air + nitrogen.

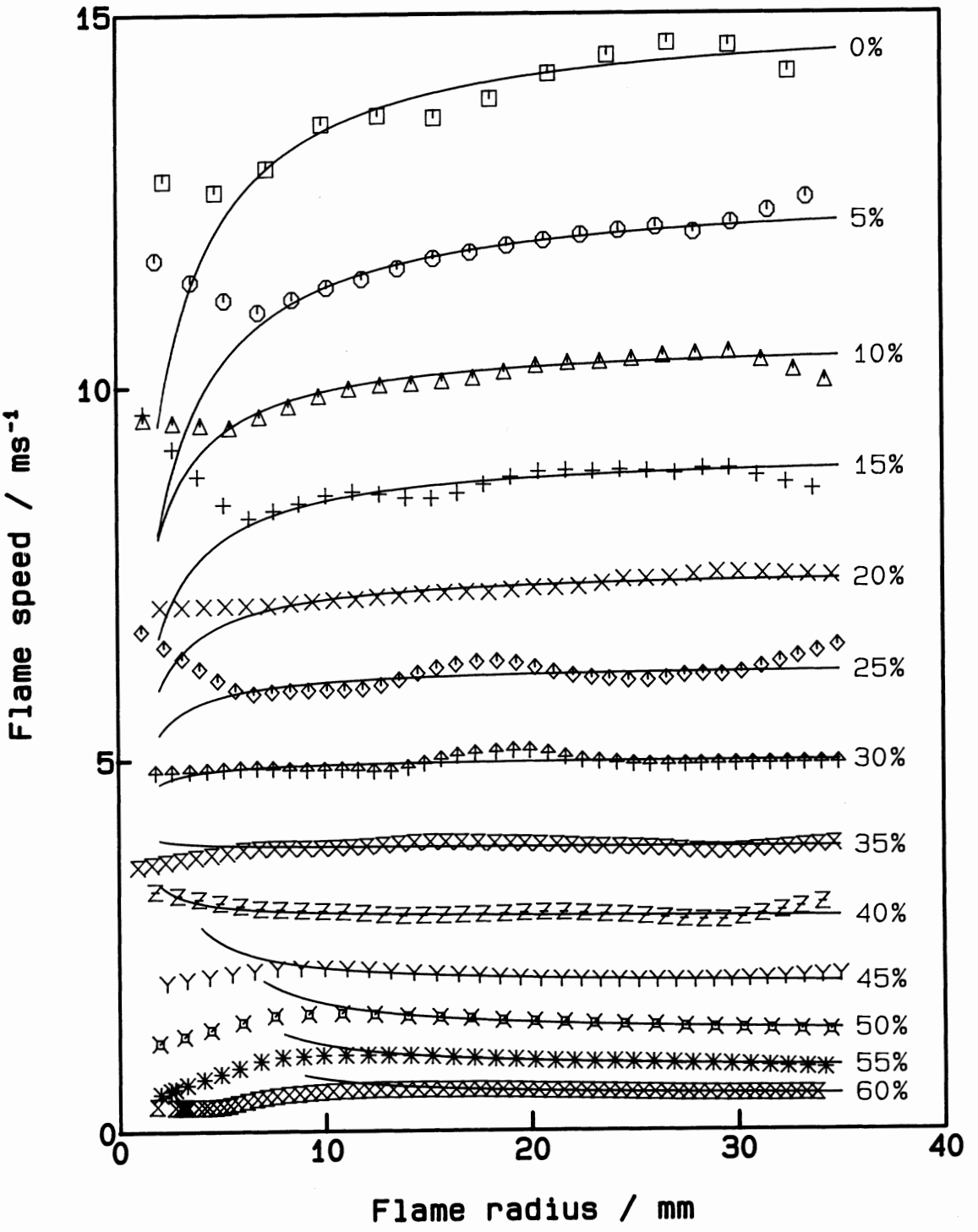

FIGURE 18

Experimental and modelled burning velocity *vs* nitrogen dilution
for stoichiometric hydrogen/air flames
Points: experimental results. Solid curve: best fit polynomial curve through results.
Dashed curve: best fit polynomial curve through planar modelling results.

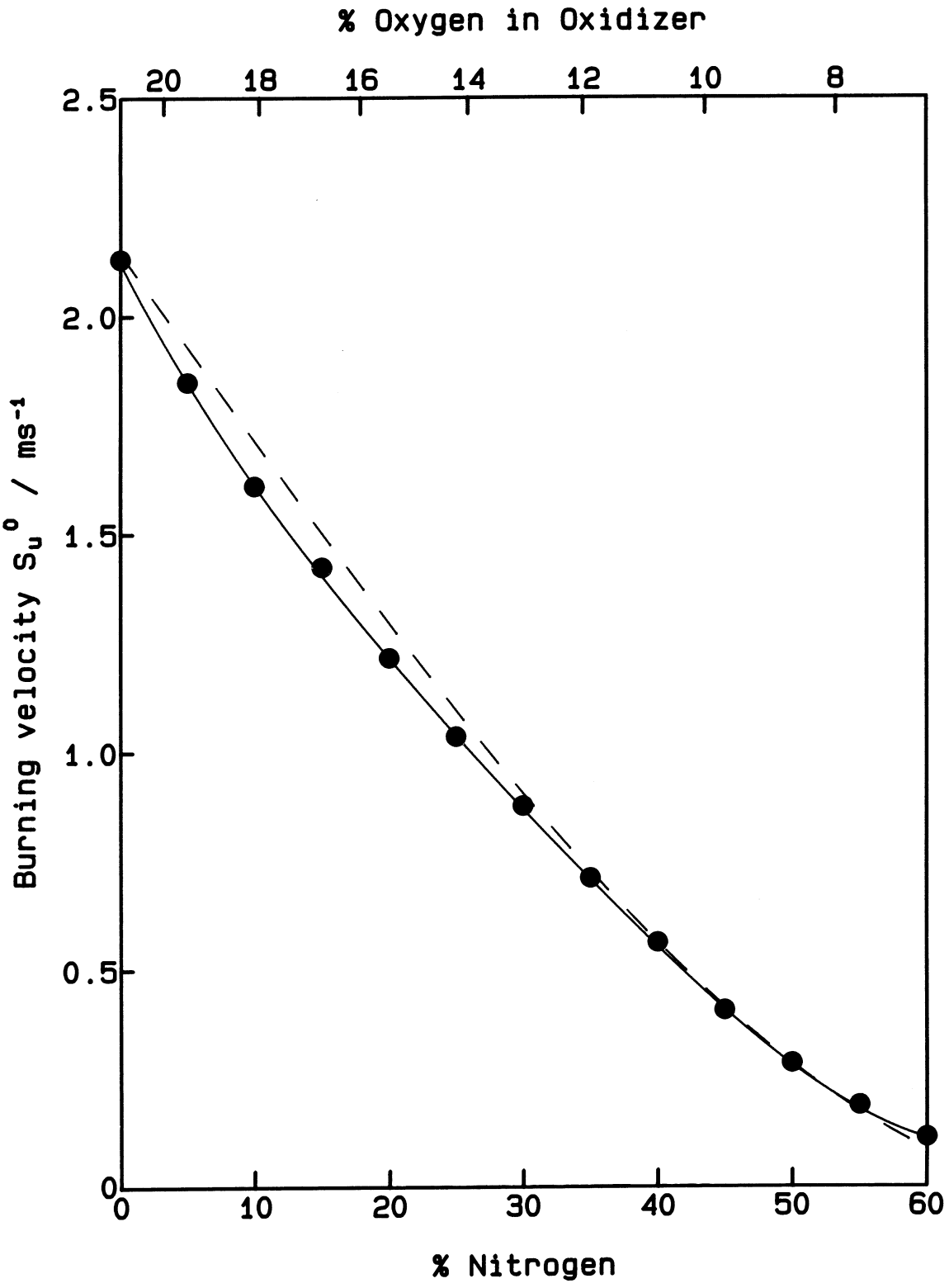

FIGURE 19

Flame relaxation and density parameters b and k *vs* nitrogen dilution for stoichiometric hydrogen/air flames

•: b derived from experiments. ○: b derived from detailed modelling of expanding spherical flames. ■ : k calculated from modelling of planar flames.

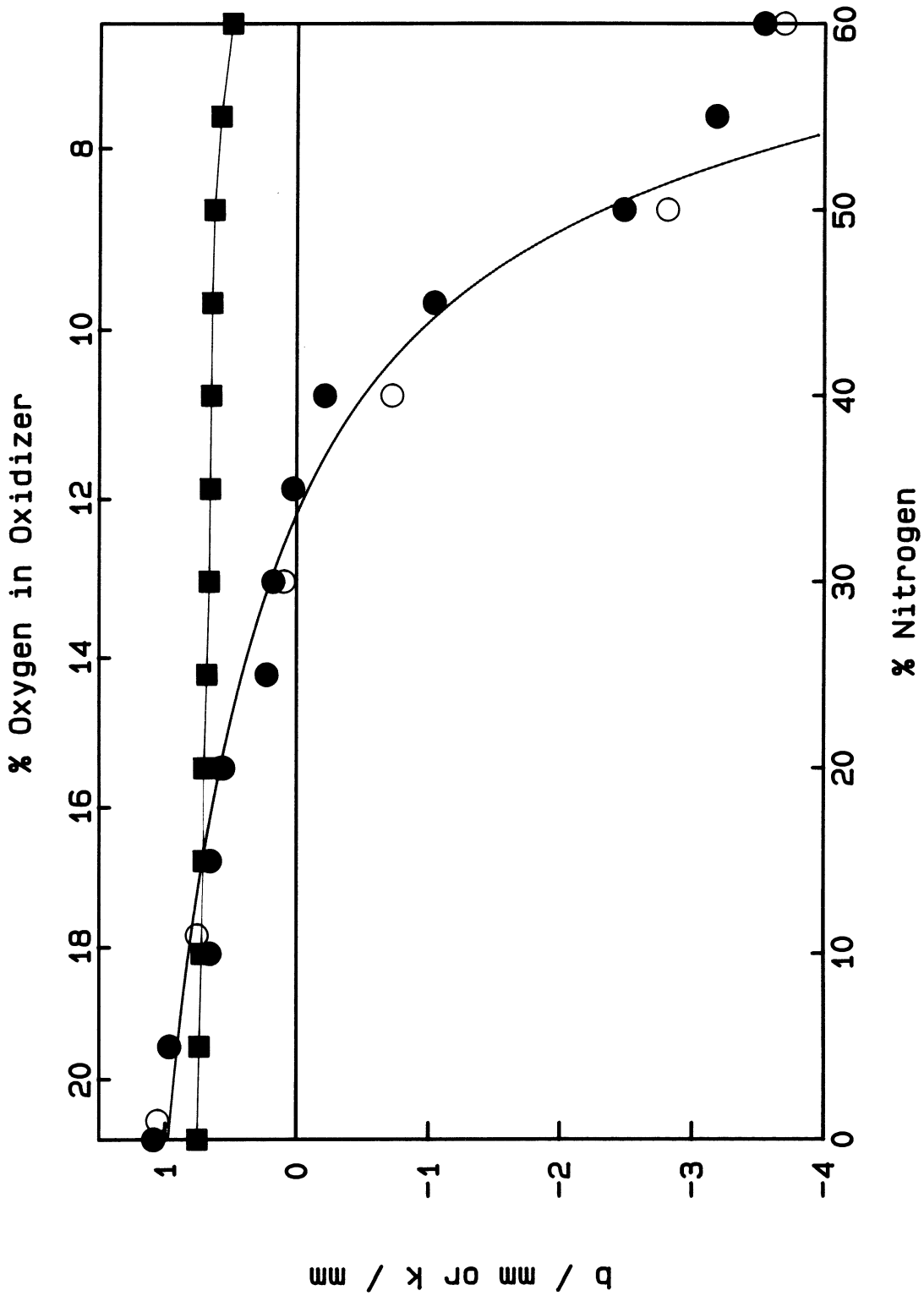

5.1.2 **Methane**

5.1.2.1 Variation with stoichiometry at atmospheric pressure

The data are plotted in Figs. 20 to 23. The flame speeds of the leanest mixtures in Fig. 20 fall as the radius increases, while the speeds rise for all other mixtures. In the richest mixtures in Fig. 21 there is a large difference between the experimental data and the behaviour of the simple model; the experimental data fall to a very low speed before recovering and returning to the model curve. The overall behaviour of methane is therefore similar to that of hydrogen.

The maximum burning velocity read from the curve fitted to the data in Fig. 22 is 0.37 ms^{-1}, a value which is considerably lower than the currently accepted value of about 0.41 ms^{-1}. Two of the experimental points in the neighbourhood of the maximum have been omitted for clarity. The aim was to pinpoint the maximum in the burning velocity curve, but in fact this did not work: the uncertainties in the measured burning velocities were of the same order as the change due to stoichiometry.

The values of the flame relaxation parameter in Fig. 23 are negative in lean mixtures and positive in rich, in qualitative agreement with the behaviour of hydrogen.

5.1.2.2 Effect of pressure variation on stoichiometric mixtures

The data are plotted in Figs. 24 to 26. Although Fig. 24 is a little messy, it shows that the effect of increasing the pressure is to decrease the limiting (one-dimensional) flame speed and to increase the rate at which this limiting speed is achieved. Reasons for this behaviour will be discussed in Chapter 7. The burning velocities determined from the radius *vs* time data are plotted against pressure in Fig. 25. In this case the solid curve through the results is of the form $S_u^{\circ}(p) = S_u^{\circ}(p=1\ \mathrm{atm})\ p^x$ where $x = -0.298 \pm 0.023$.

The flame relaxation parameter b is plotted against pressure in Fig. 26. It varies logarithmically in a similar way to the burning velocity with an exponent x of -1.041 ± 0.095.

FIGURE 20

Flame speed *vs* radius of lean methane flames
Points: experimental data. Curves: equation (3-10) fitted to data.
Numbers on right denote stoichiometry.

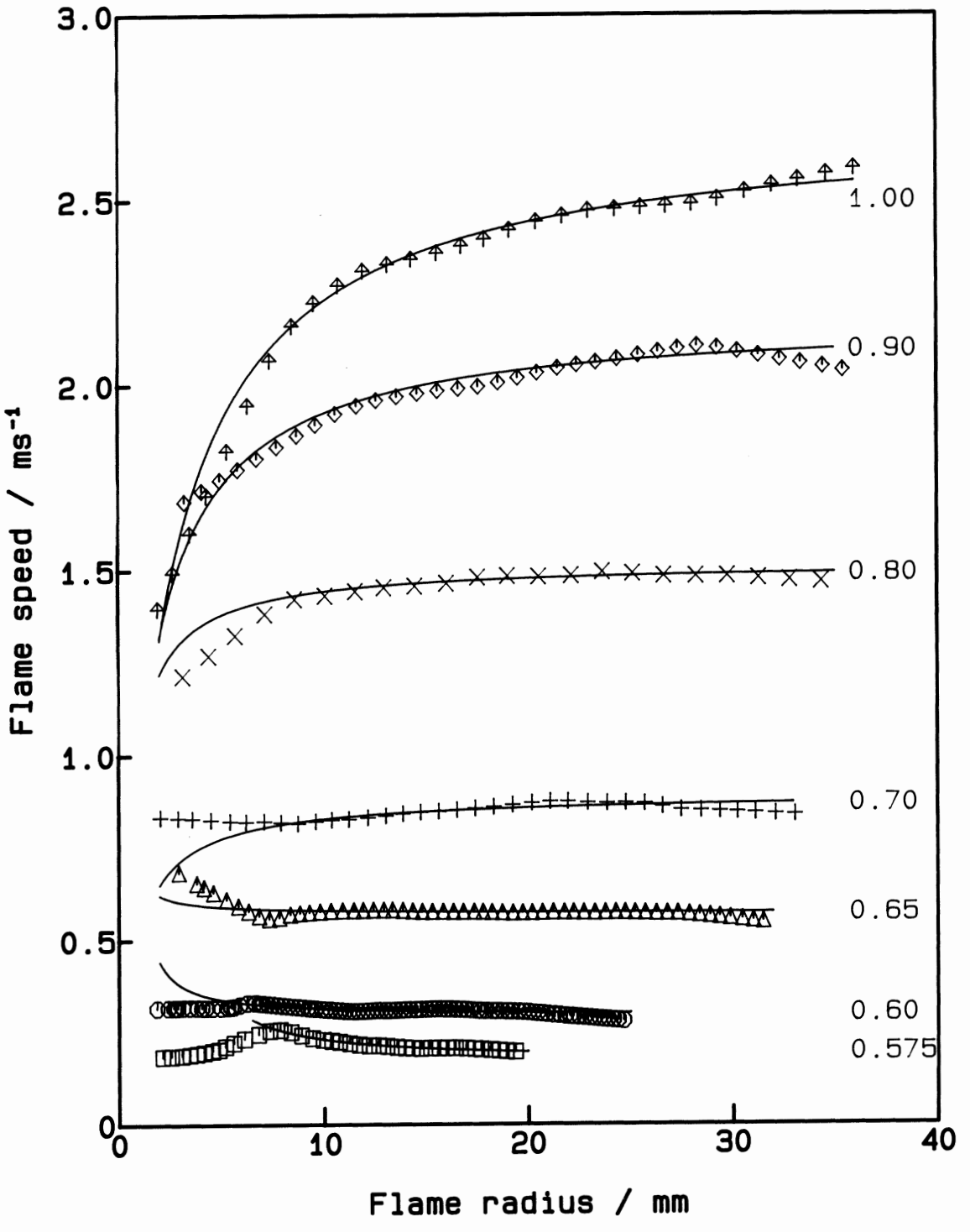

FIGURE 21

Flame speed *vs* radius of rich methane flames
Points: experimental data. Curves: equation (3-10) fitted to data.
Numbers on right denote stoichiometry.

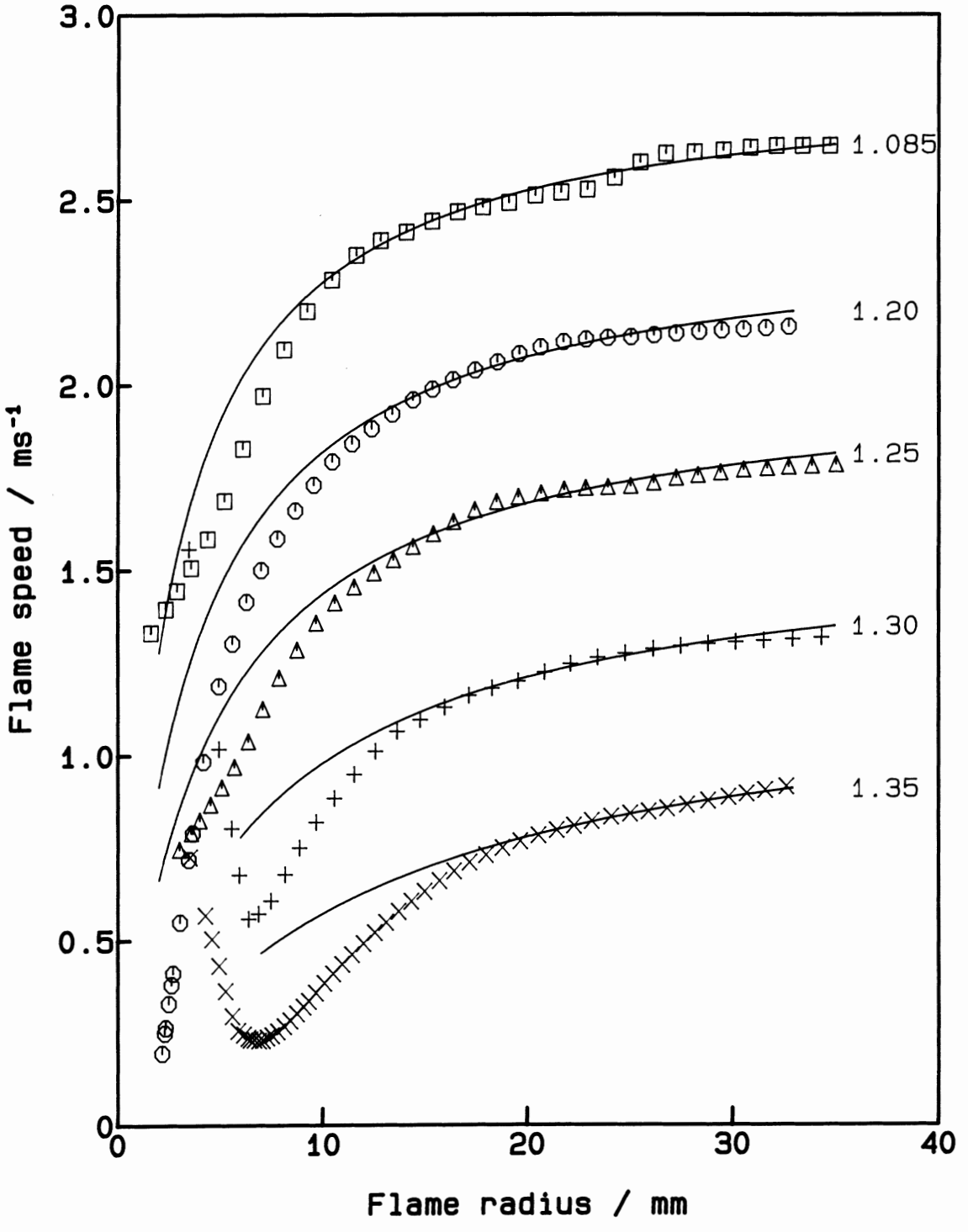

FIGURE 22

Experimental and modelled burning velocity *vs* stoichiometry for methane/air flames
Points: experimental results. Solid curve: best fit polynomial curve through results.
Dashed curve: best fit polynomial curve through planar modelling results.

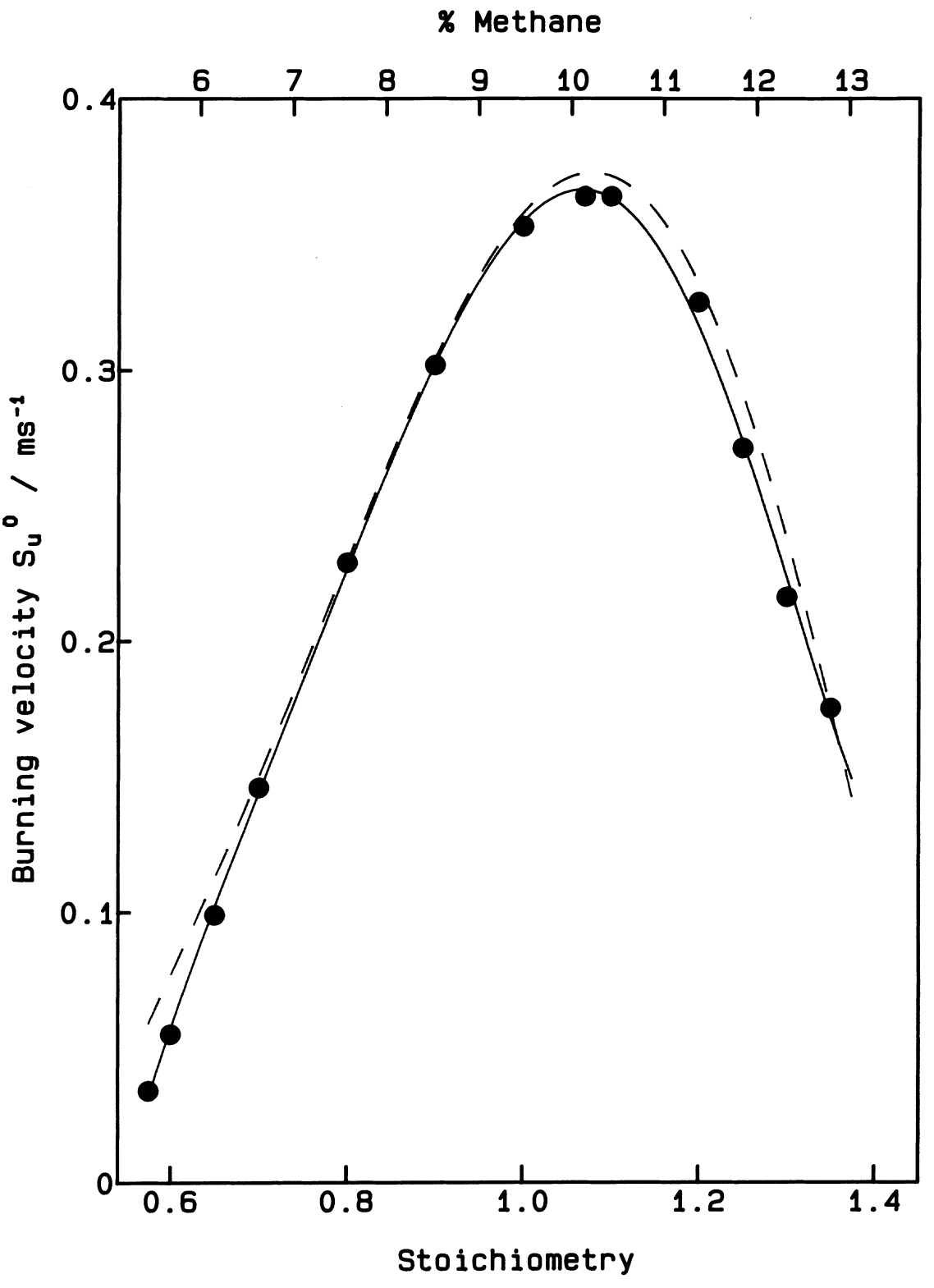

FIGURE 23

Flame relaxation and density parameters b and k *vs* stoichiometry
for methane/air flames
•: b derived from experiments. ■ : k calculated from modelling of planar flames.

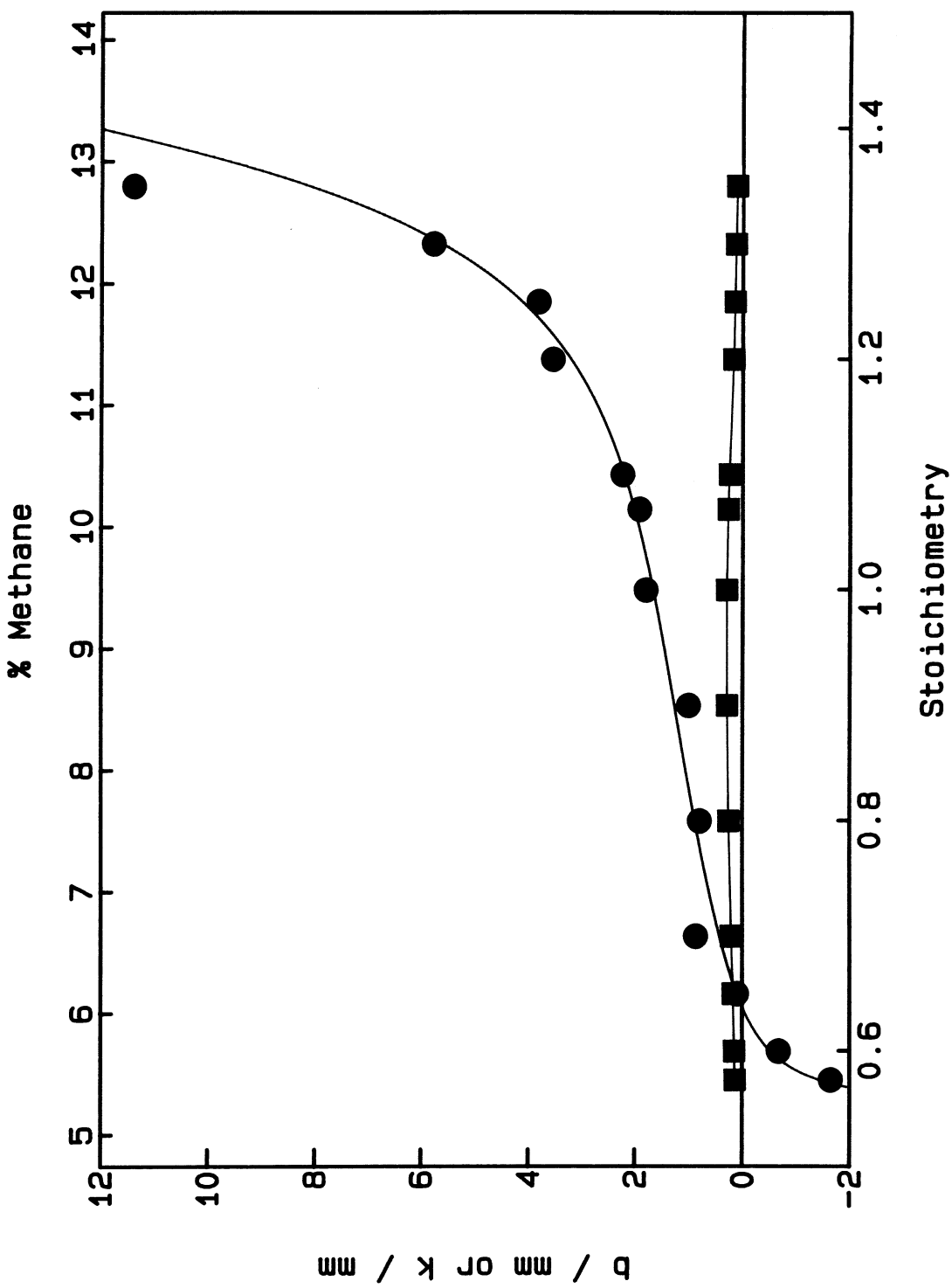

FIGURE 24

Flame speed *vs* radius of stoichiometric methane flames at various pressures
Points: experimental data. Curves: equation (3-10) fitted to data.
Numbers on right denote pressure in atmospheres.

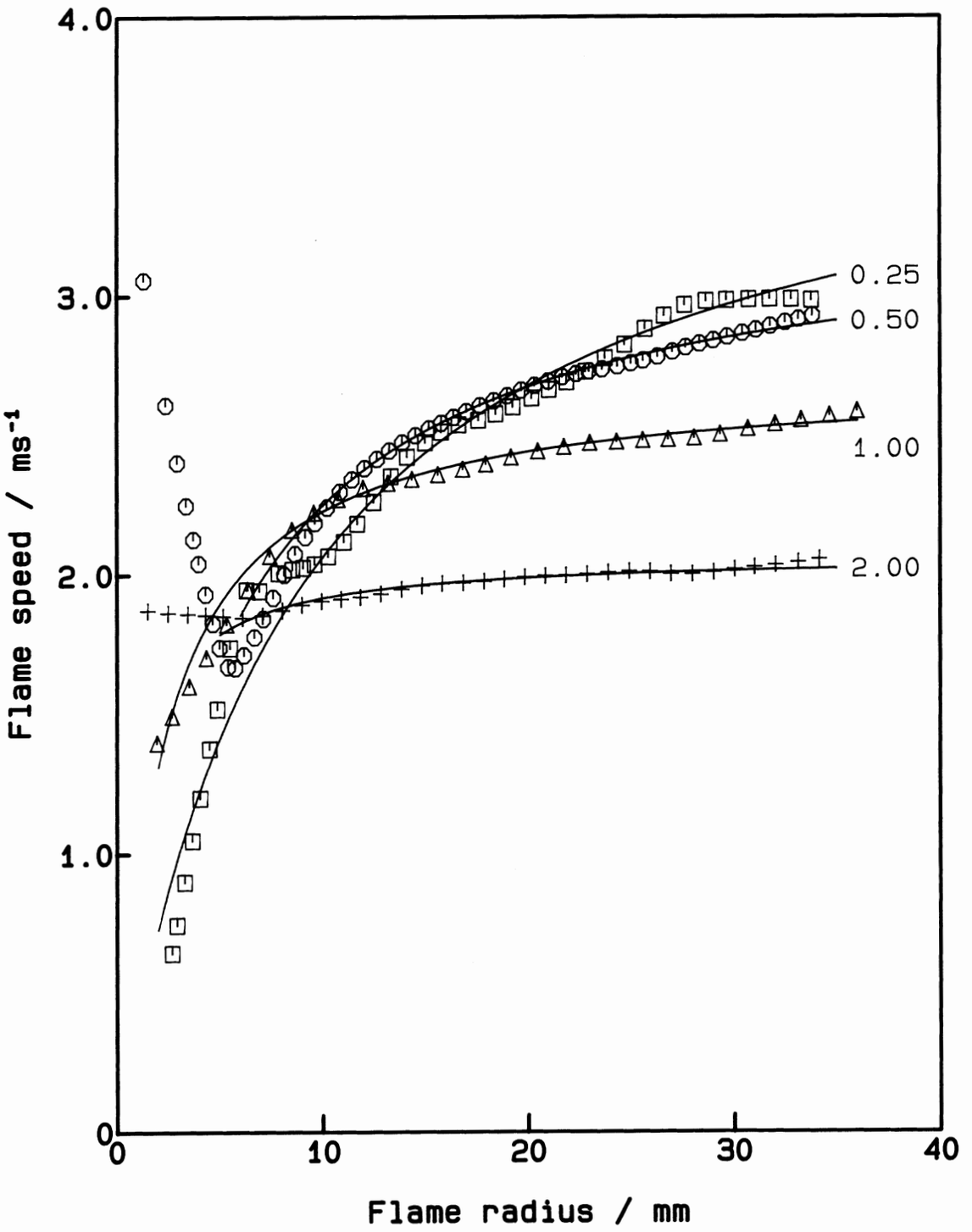

FIGURE 25

Experimental and modelled burning velocity *vs* pressure
for stoichiometric methane/air flames
Points: experimental results. Solid curve: $S_u^\circ(p) = S_u^\circ(p{=}1\ \text{atm})\ p^x$ fitted to experimental results. Dashed curve: same function fitted to planar modelling results.

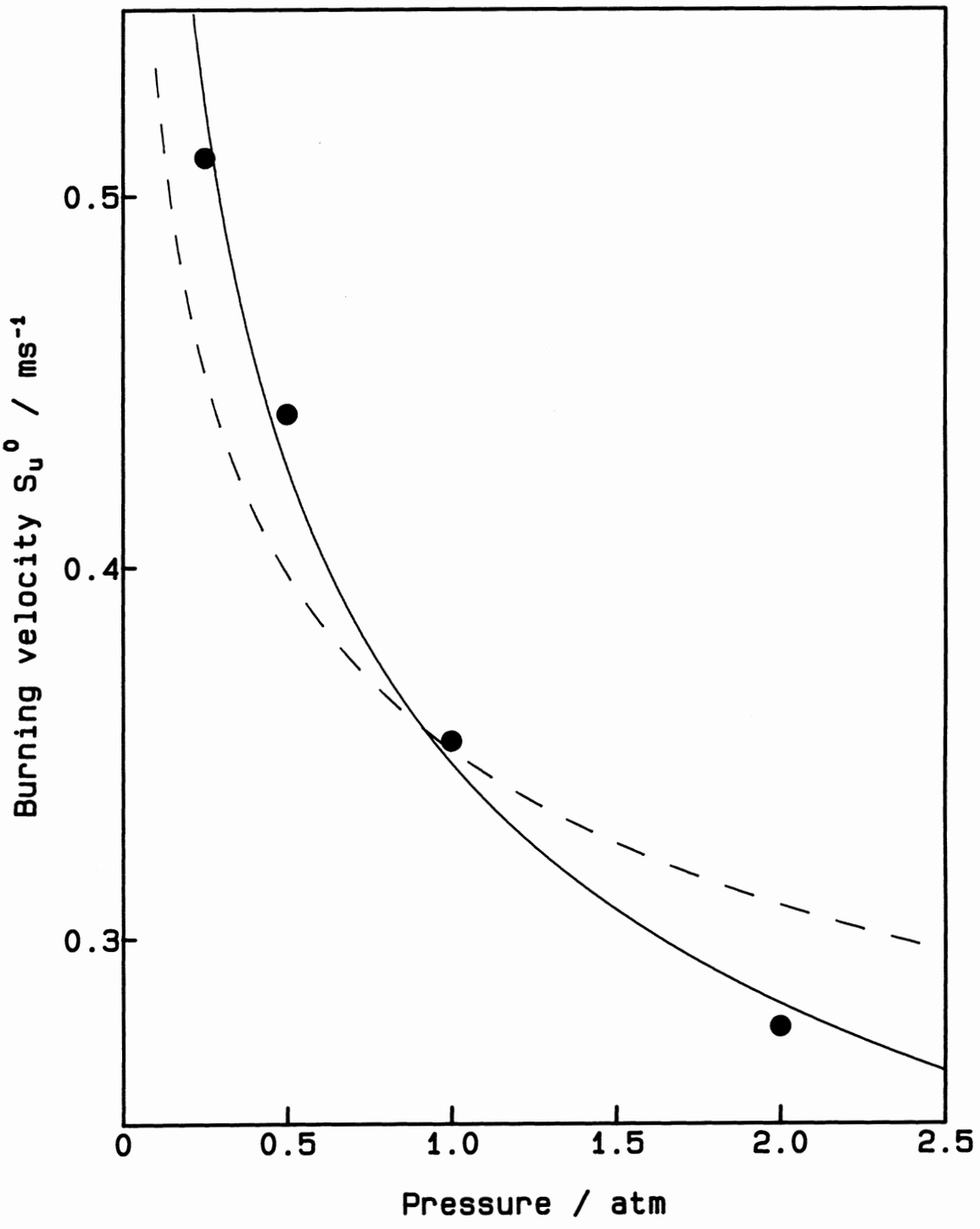

FIGURE 26

Flame relaxation and density parameters b and k *vs* pressure
for stoichiometric methane/air flames
•: b derived from experiments. ■ : k calculated from modelling of planar flames.

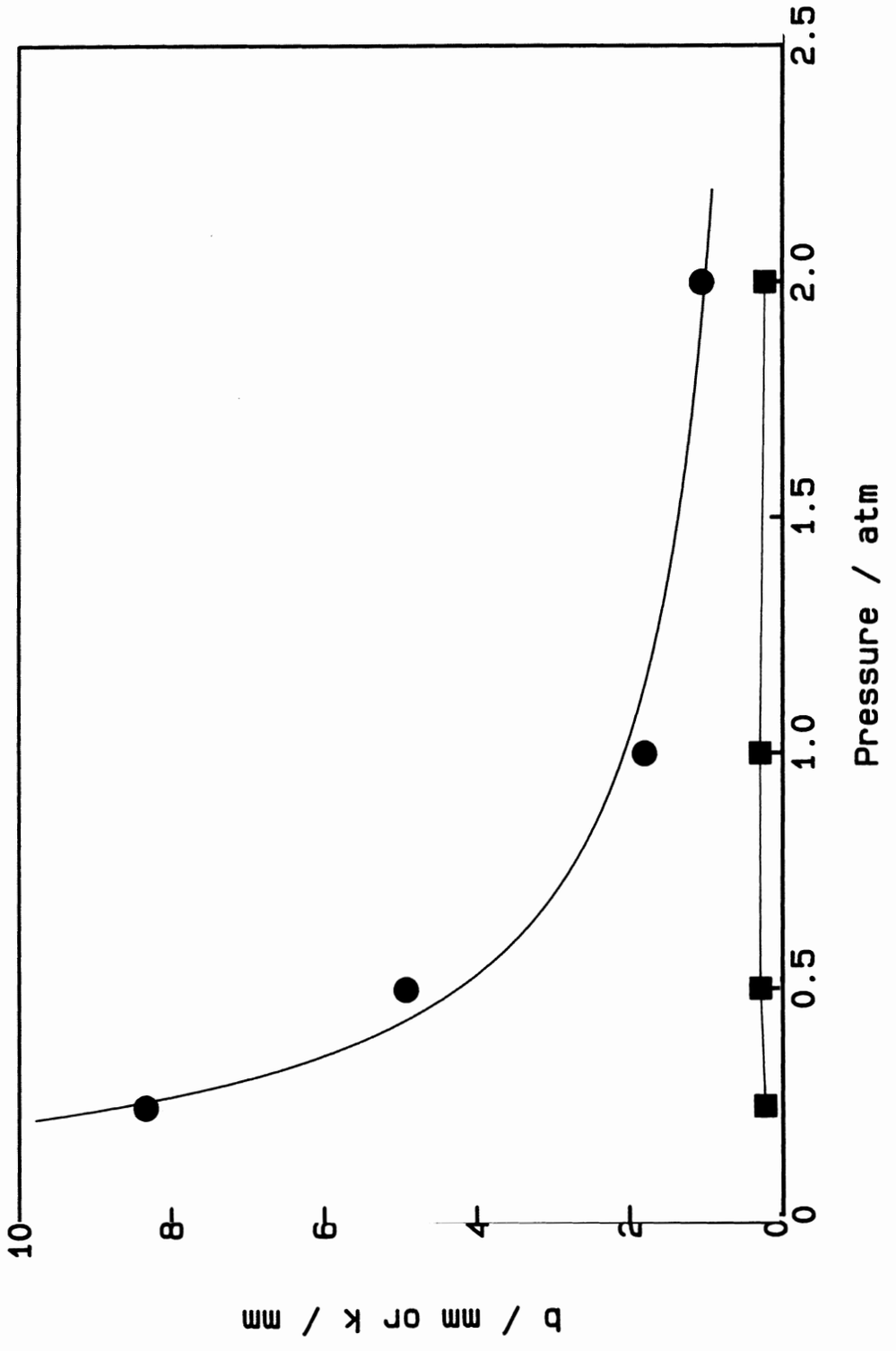

5.1.3 Ethane

The data are plotted in Figs. 27 to 30. Figure 27 shows that there is a "dip" at small radii in the flame speeds of the leanest mixtures, which is similar to that in the richest hydrogen and methane mixtures. Conversely, the rich mixtures in Fig. 28 behave like lean hydrogen and methane. In particular, at stoichiometries larger than 1.5 the flame speed decreases with increasing radius. In all other mixtures the flame speed increases.

Burning velocities determined from the radius *vs* time data are plotted in Fig. 29. The maximum value was 0.41 ms^{-1}, the largest of the saturated hydrocarbons. Values of the flame relaxation parameter *b* are plotted in Fig. 30.

5.1.4 Propane

The data are plotted in Figs. 31 to 34. Figure 31 shows that, as in ethane, there is a "dip" in the flame speeds of the leanest mixtures at small radii. Also like ethane, the flame speed decreases with increasing radius in sufficiently rich mixtures. Fig. 32 shows that the changeover happens at a stoichiometry of about 1.35, compared with 1.5 in the case of ethane. In all other mixtures the flame speed increases.

Burning velocities determined from the radius *vs* time data are plotted in Fig. 33. The maximum experimental burning velocity was 0.39 ms^{-1} at a stoichiometry of 1.08. Values of the flame relaxation parameter *b* are plotted in Fig. 34.

The experimental *b* and S_b° data can be compared with values derived from the expanding flame measurements of Palm-Leis and Strehlow[93]. In order to perform this comparison, flame speed *vs* radius data for propane/air were read from Fig. 5 of ref. 93. Since the data were in this form and not radius *vs* time, it was necessary to analyse the data in a different way from the experiments in this thesis. Accordingly, the flame speed *vs* radius equation (3-10) was fitted instead of the radius *vs* time equation (3-12). A computer program was written to perform a nonlinear least squares analysis to determine the values of S_b° and *b* giving the best fit. The results are plotted in Fig. 35. The burning velocities and flame relaxation parameters obtained are similar to the ones obtained in this thesis, but are displaced towards the rich side by a stoichiometry of about 0.1. The reason for this is not clear. No problem has been found with the gas metering or calculations of stoichiometry in the

FIGURE 27

Flame speed *vs* radius of lean ethane flames
Points: experimental data. Curves: equation (3-10) fitted to data.
Numbers on right denote stoichiometry.

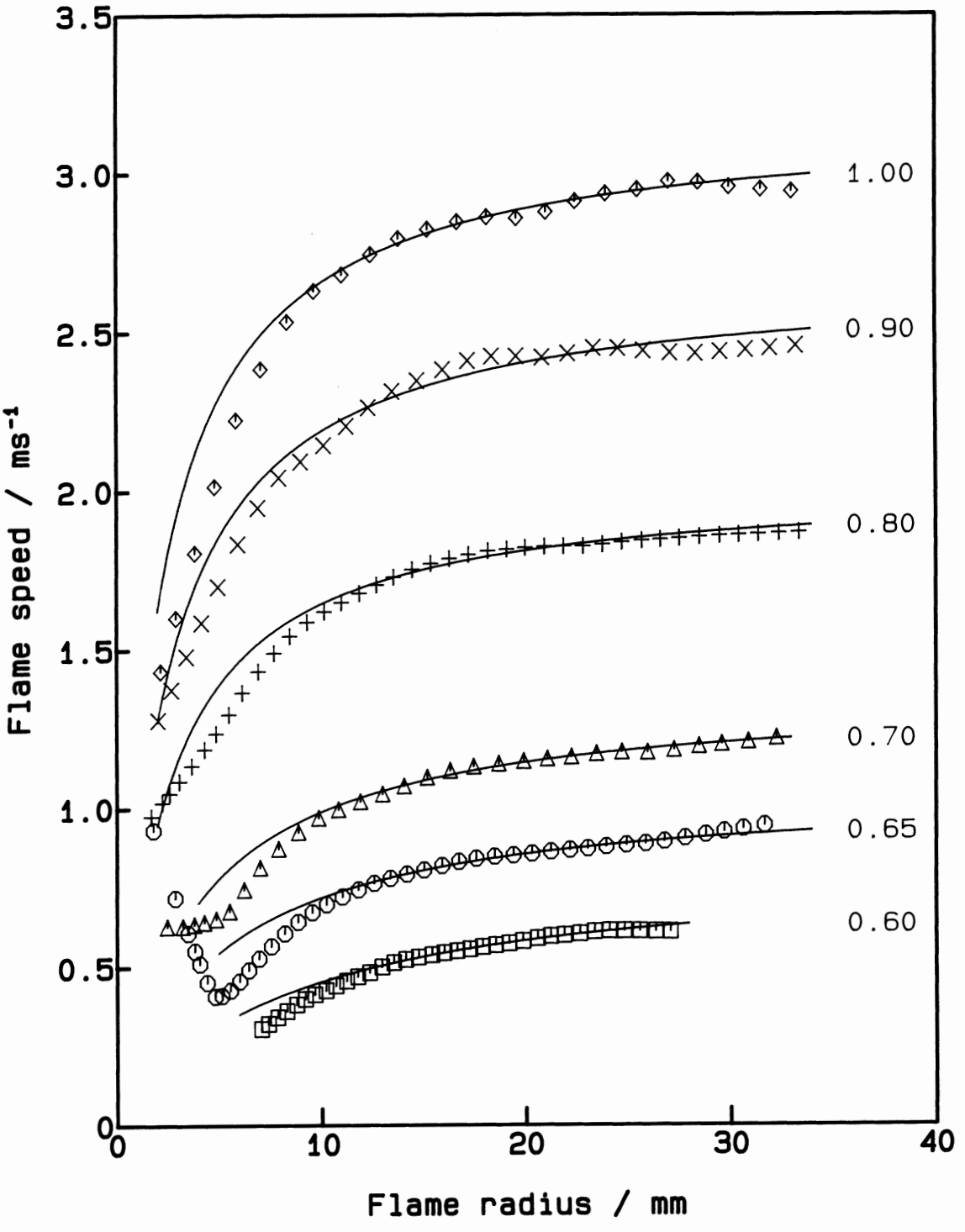

FIGURE 28

Flame speed *vs* radius of rich ethane flames
Points: experimental data Curves: equation (3-10) fitted to data.
Numbers on right denote stoichiometry.

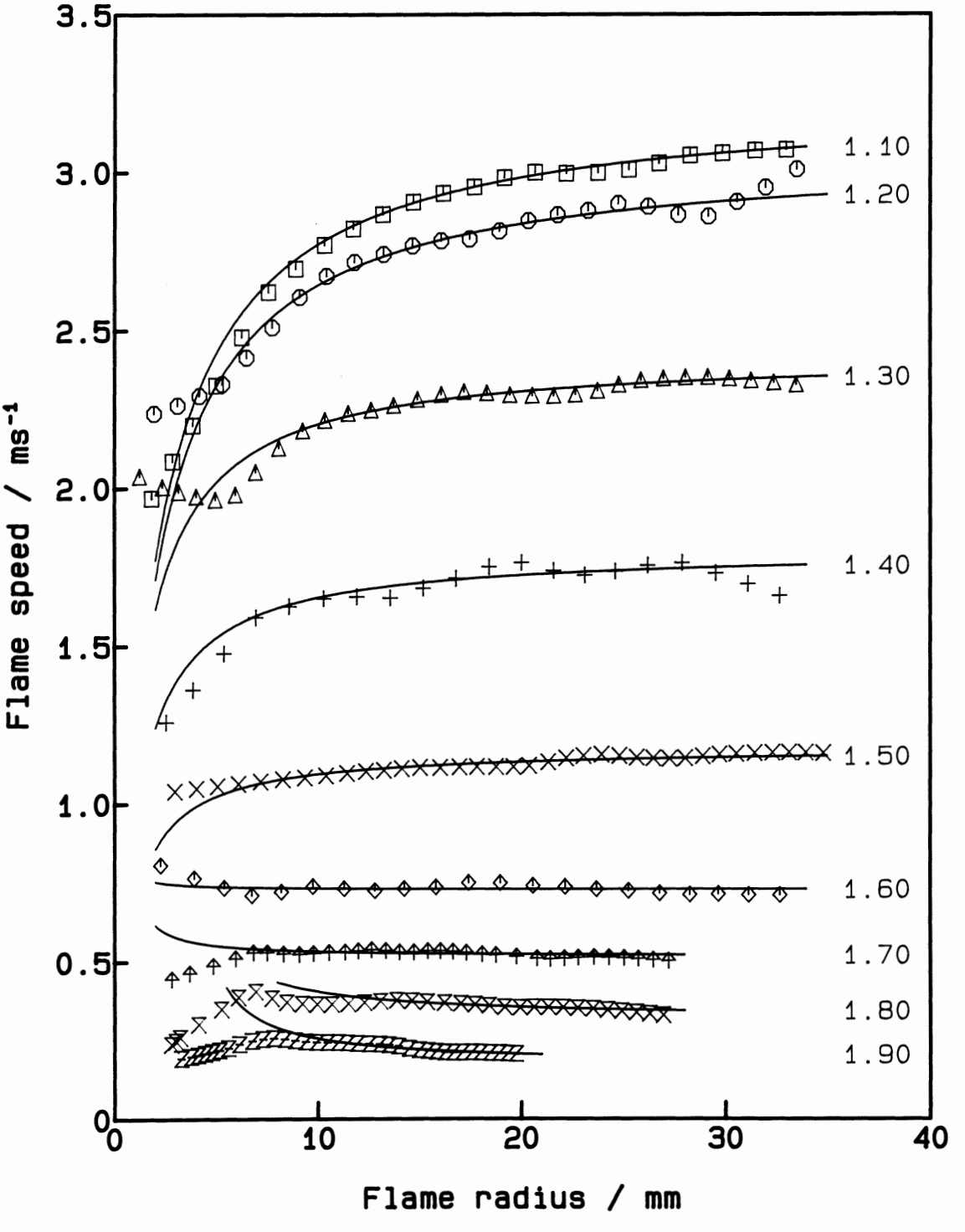

FIGURE 29

Experimental and modelled burning velocity *vs* stoichiometry for ethane/air flames
Points: experimental results. Solid curve: best fit polynomial curve through results.
Dashed curve: best fit polynomial curve through planar modelling results.

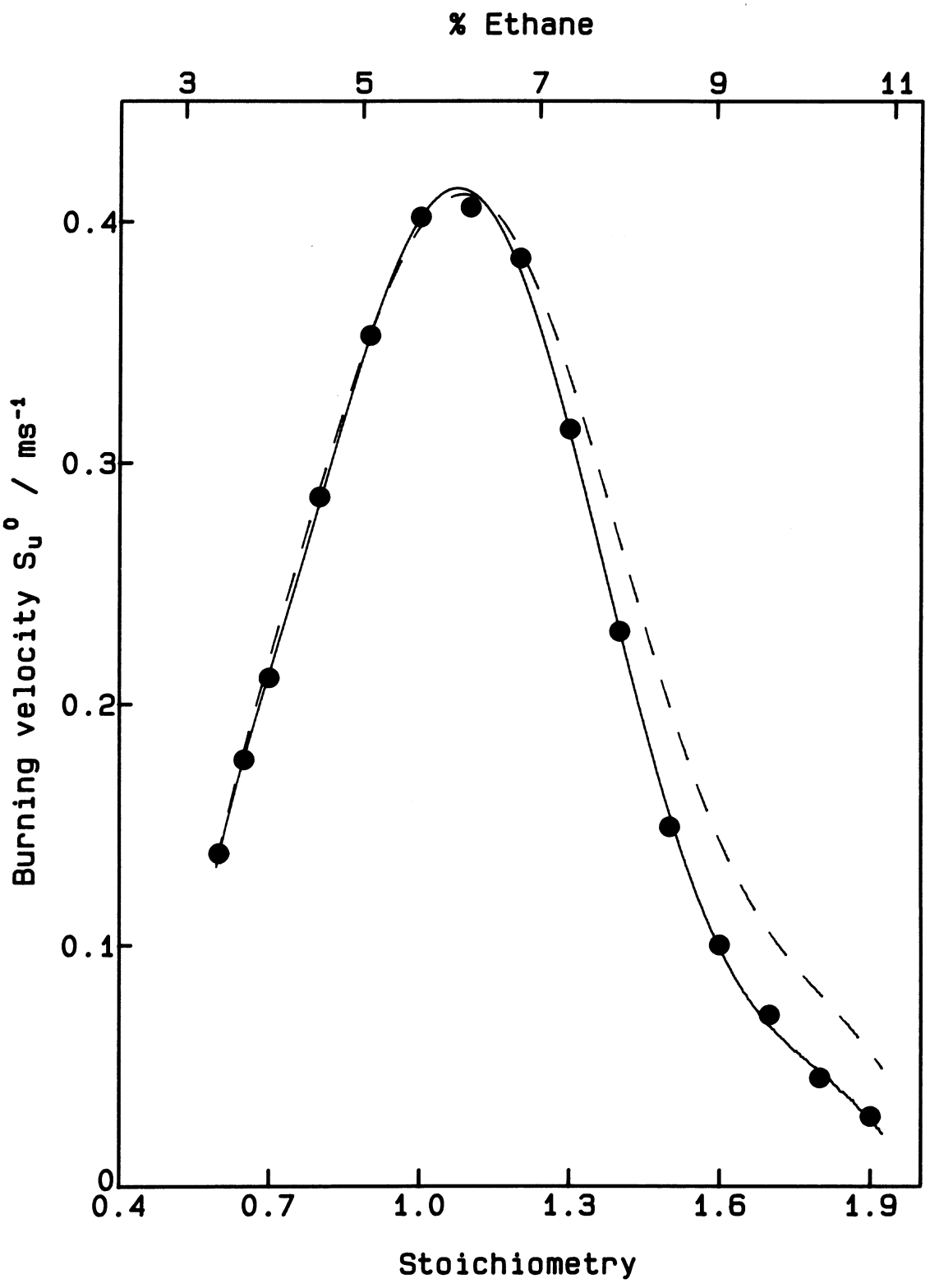

FIGURE 30

Flame relaxation and density parameters b and k *vs* stoichiometry
for ethane/air flames
•: b derived from experiments. ■ : k calculated from modelling of planar flames.

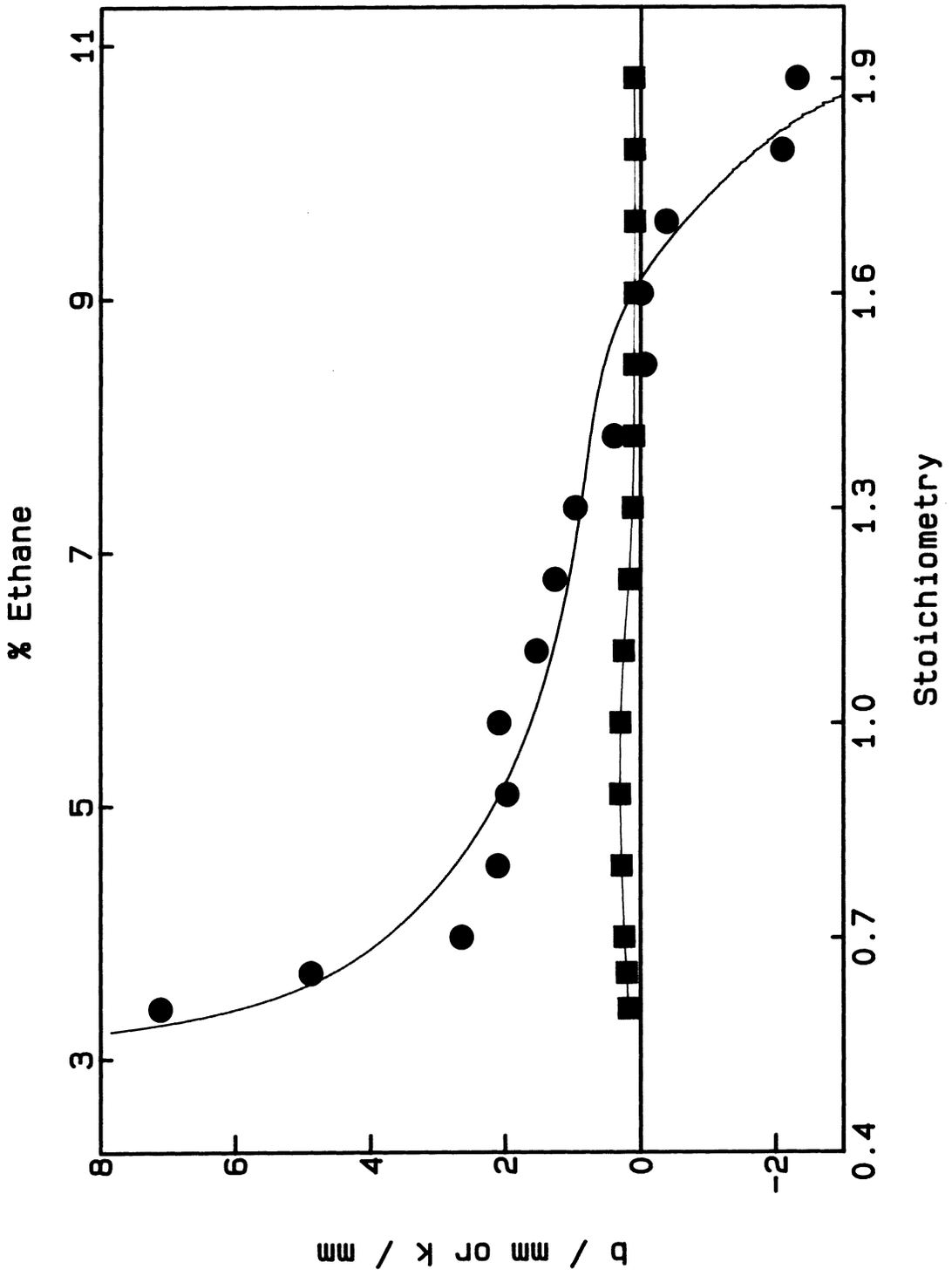

FIGURE 31

Flame speed *vs* radius of lean propane flames
Points: experimental data. Curves: equation (3-10) fitted to data.
Numbers on right denote stoichiometry.

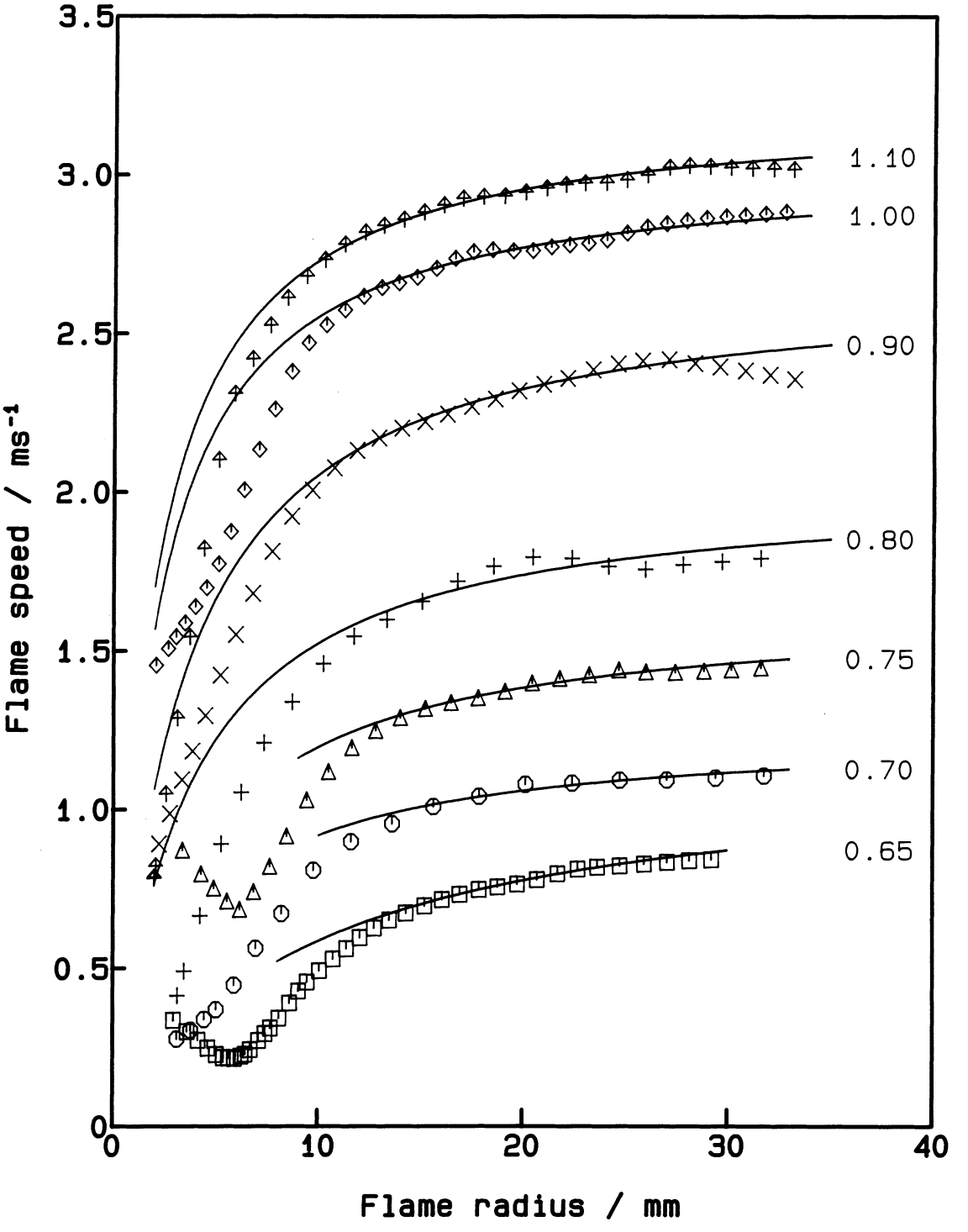

FIGURE 32

Flame speed *vs* radius of rich propane flames
Points: experimental data. Curves: equation (3-10) fitted to data.
Numbers on right denote stoichiometry.

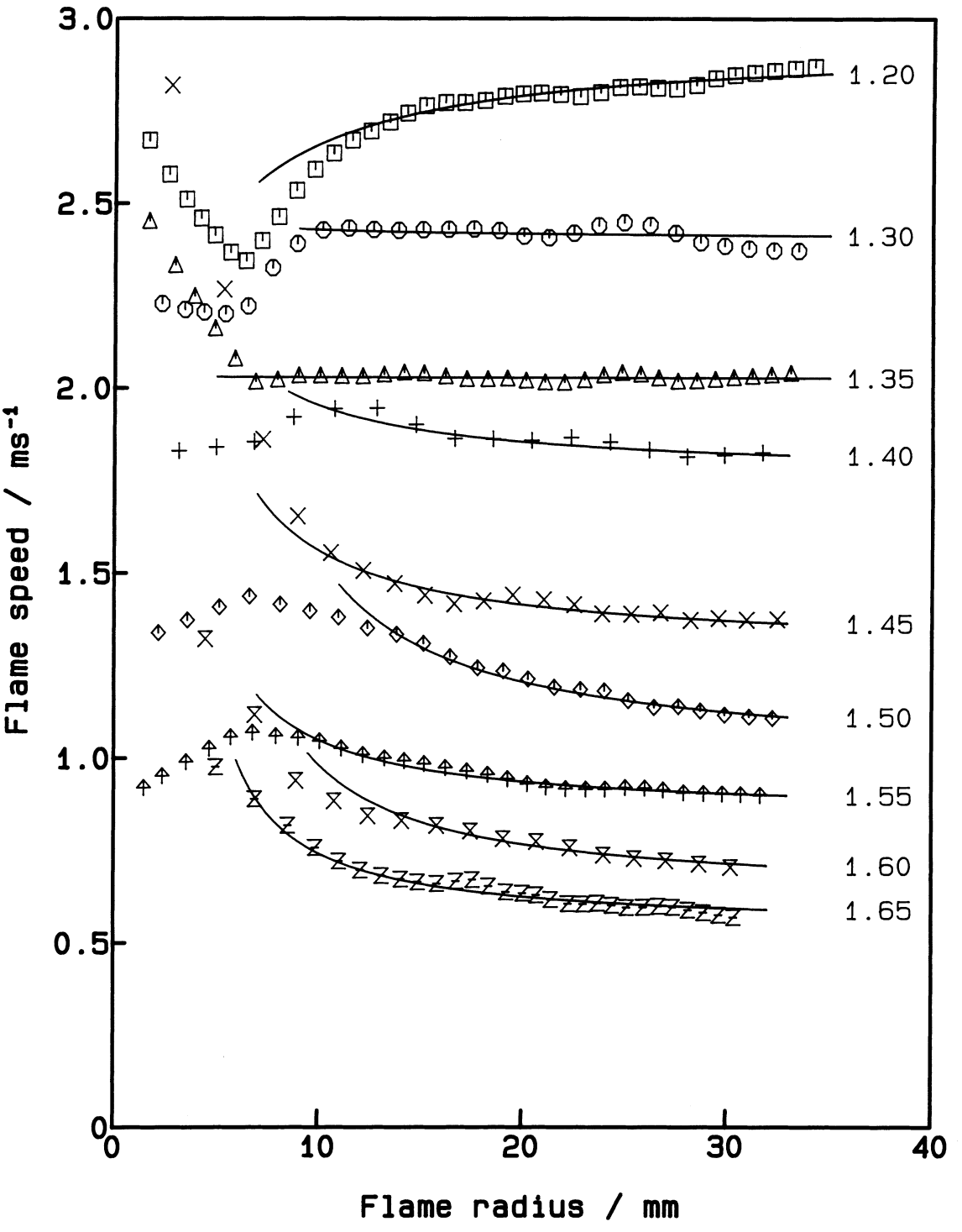

FIGURE 33

Experimental and modelled burning velocity *vs* stoichiometry for propane/air flames
Points: experimental results. Solid curve: best fit polynomial curve through results.
Dashed curve: best fit polynomial curve through planar modelling results.

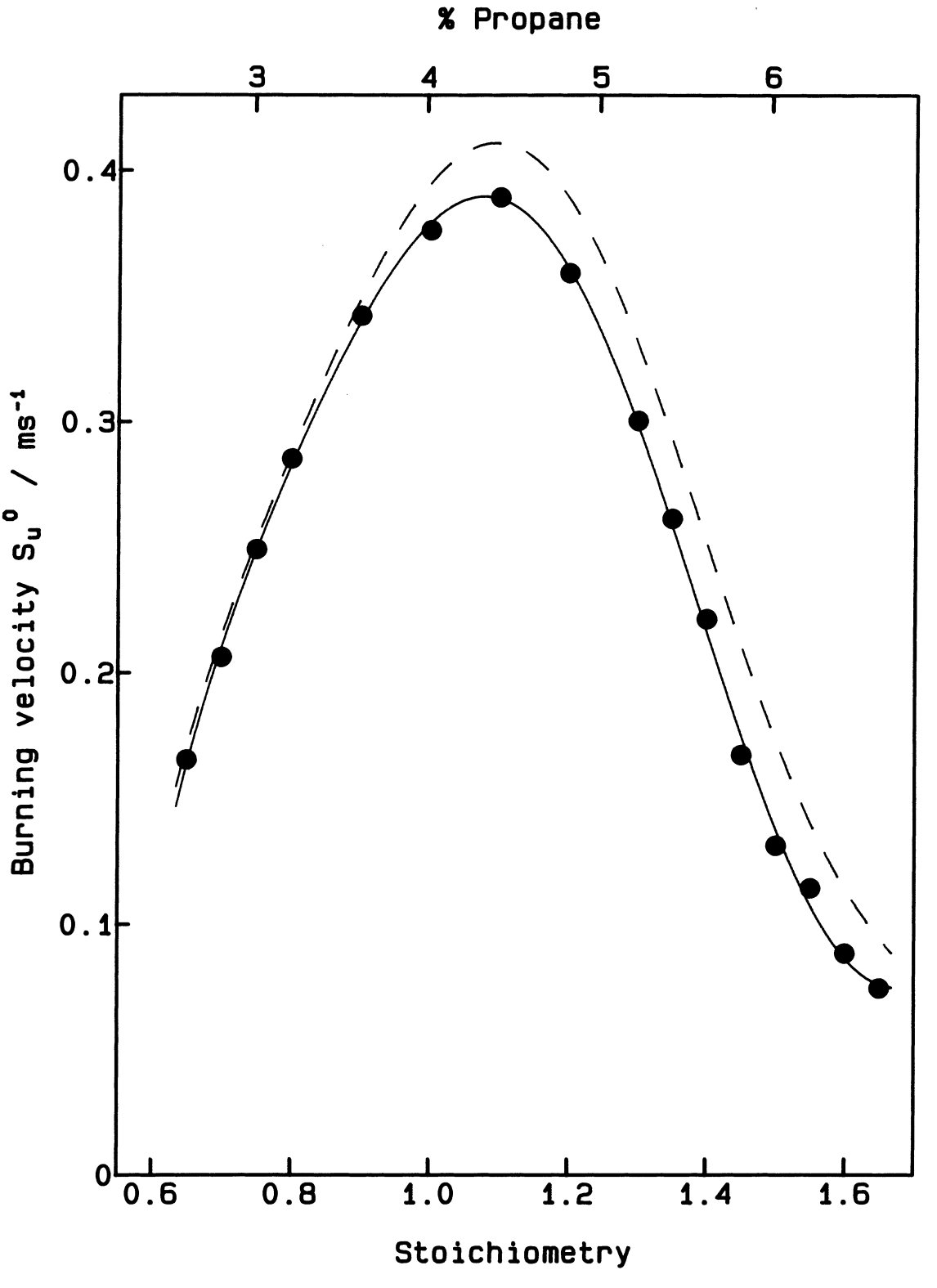

FIGURE 34

Flame relaxation and density parameters b and k *vs* stoichiometry
for propane/air flames
•: b derived from experiments. ■ : k calculated from modelling of planar flames.

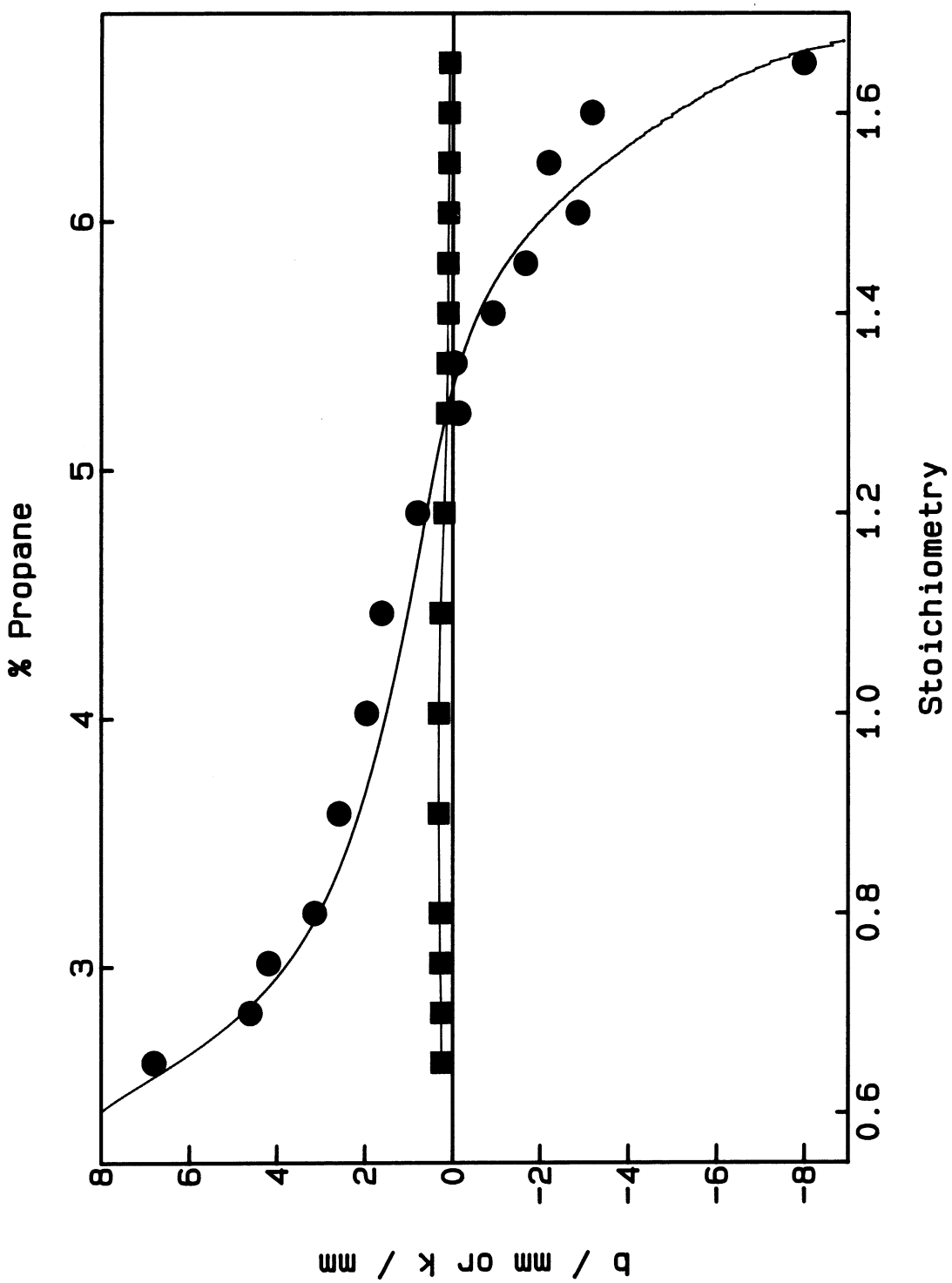

FIGURE 35

Comparison of present results for flame speed S_b°
and flame relaxation parameter b *vs* stoichiometry for propane/air flames
with values derived from work of Palm-Leis and Strehlow[93]

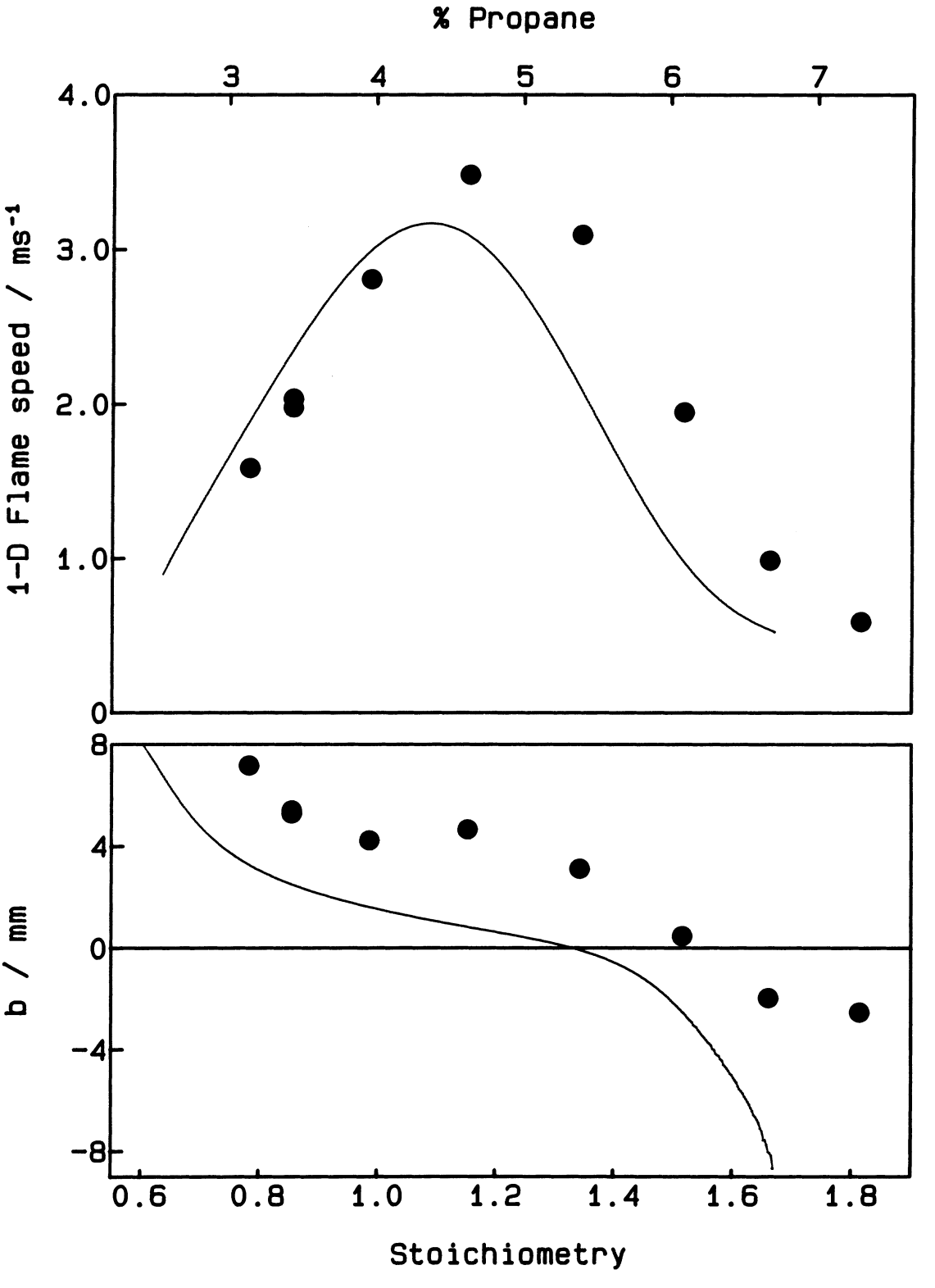

present work, and the stoichiometry corresponding to the maximum burning velocity of 1.08 is in good agreement with other work. It would therefore appear that there may have an error in the calculation of the mixture composition in ref. 93.

5.1.5 Ethylene

The data are plotted in Figs. 36 to 39. Figure 36 shows that, as in the cases of ethane and propane, there is a slight "dip" in the flame speeds of the leanest mixtures at small radii. But it can be seen from Fig. 37 that the flame speeds of rich ethylene mixtures, unlike those of rich ethane and propane, always increase with increasing flame radius.

Burning velocities determined from the radius *vs* time data are plotted in Fig. 38. The maximum burning velocity was considerably higher than that of the other hydrocarbons. It was 0.66 ms^{-1} at a stoichiometry of 1.10 (7.18% ethylene).

The flame relaxation parameter b is plotted against stoichiometry in Fig. 39. Unlike the b values of all the other fuels studied in this work it does not vary monotonically with stoichiometry. Instead it is large in both very lean and very rich mixtures, and dips to a low value at a stoichiometry of about 1.6.

5.2 STAGNATION FLOW FLAMES

The work on flames in stagnation-point flow was not as extensive as that on expanding flames so fewer results are presented in this section. The work was exclusively on methane/air mixtures.

First, data are presented which demonstrate the methodology described in Section 3.3. For a methane/air flame of stoichiometry 1.31 and stretch rate 157 s^{-1}, Fig. 40 shows the variation with distance from the burner of the normal gas velocity v, the stream tube area A and the product vA, all normalized to 1 at 1 mm from the burner. Since vA is proportional to the temperature, the diagram shows the difference between the true point of first temperature rise and the minimum in the velocity profile. The vA profile is flat to within 2% in this case, demonstrating the validity of the methodology. Dividing the constant upstream value of vA by the luminous zone area gives the stretched burning velocity defined in equation (3-53). At higher stretch

FIGURE 36

Flame speed *vs* radius of lean ethylene flames
Points: experimental data. Curves: equation (3-10) fitted to data.
Numbers on right denote stoichiometry.

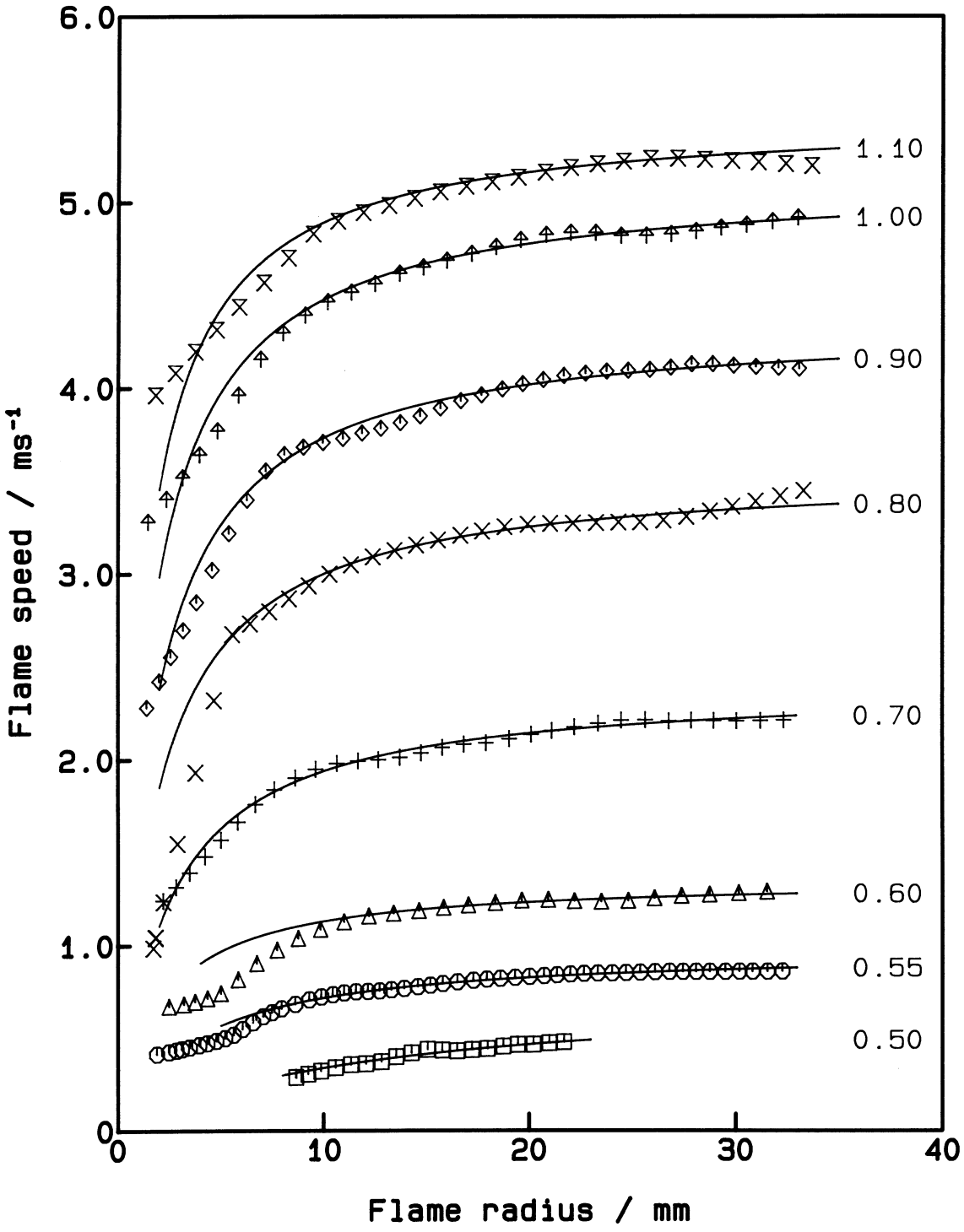

FIGURE 37

Flame speed *vs* radius of rich ethylene flames
Points: experimental data. Curves: equation (3-10) fitted to data.
Numbers on right denote stoichiometry.

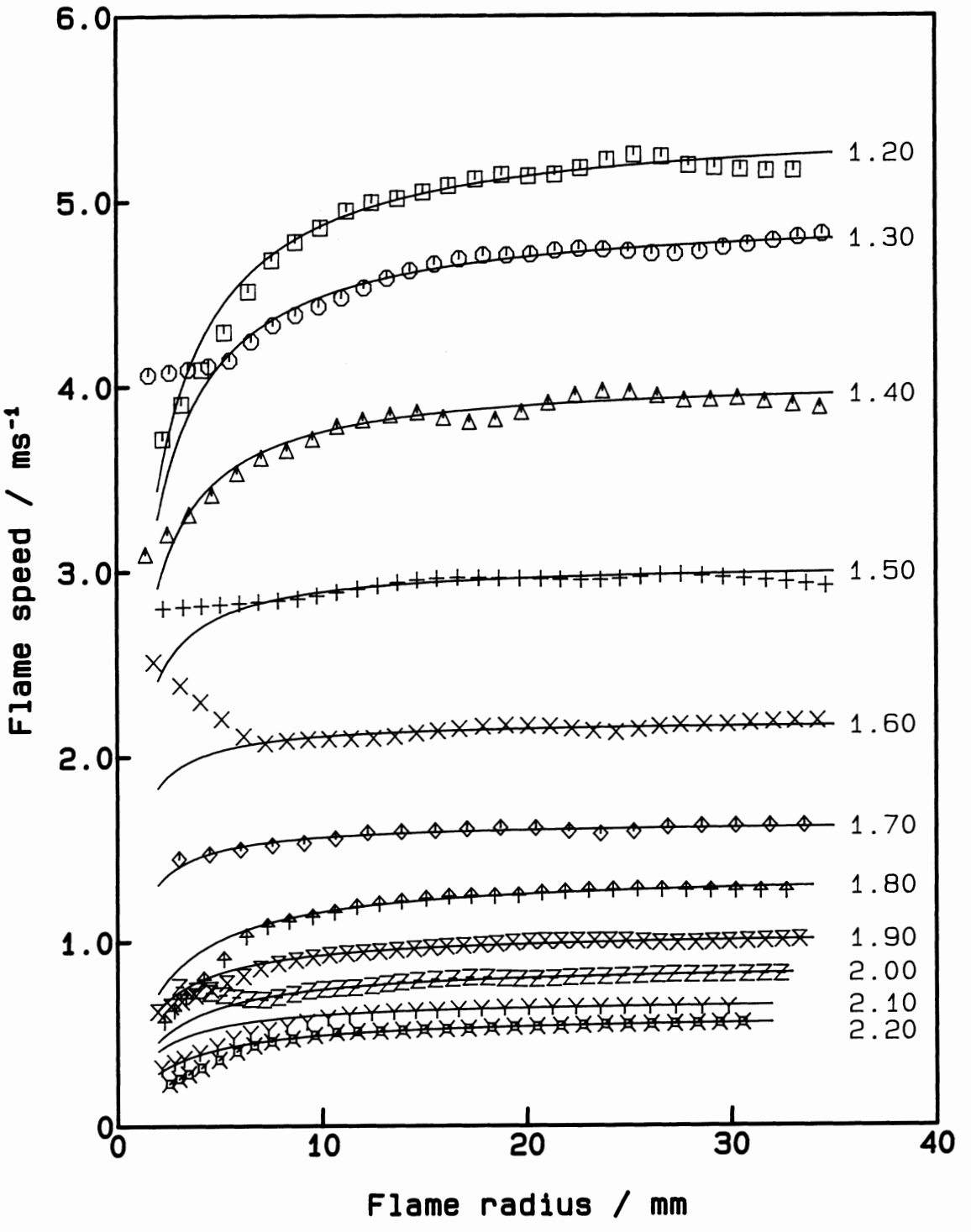

FIGURE 38

Experimental and modelled burning velocity *vs* stoichiometry for ethylene/air flames
Points: experimental results. Solid curve: best fit polynomial curve through results.
Dashed curve: best fit polynomial curve through planar modelling results.

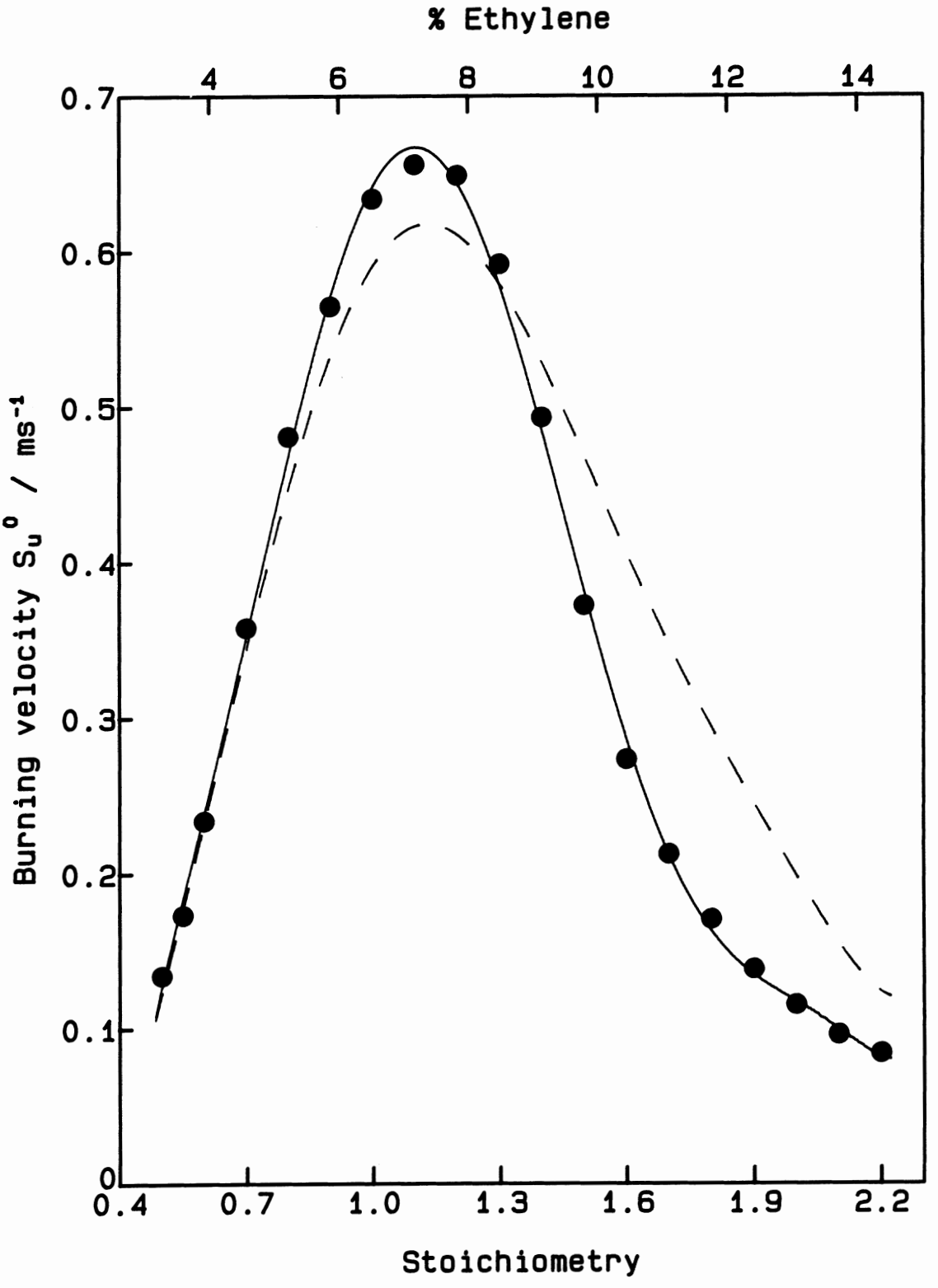

FIGURE 39

Flame relaxation and density parameters b and k *vs* stoichiometry
for ethylene/air flames
•: b derived from experiments. ■ : k calculated from modelling of planar flames.

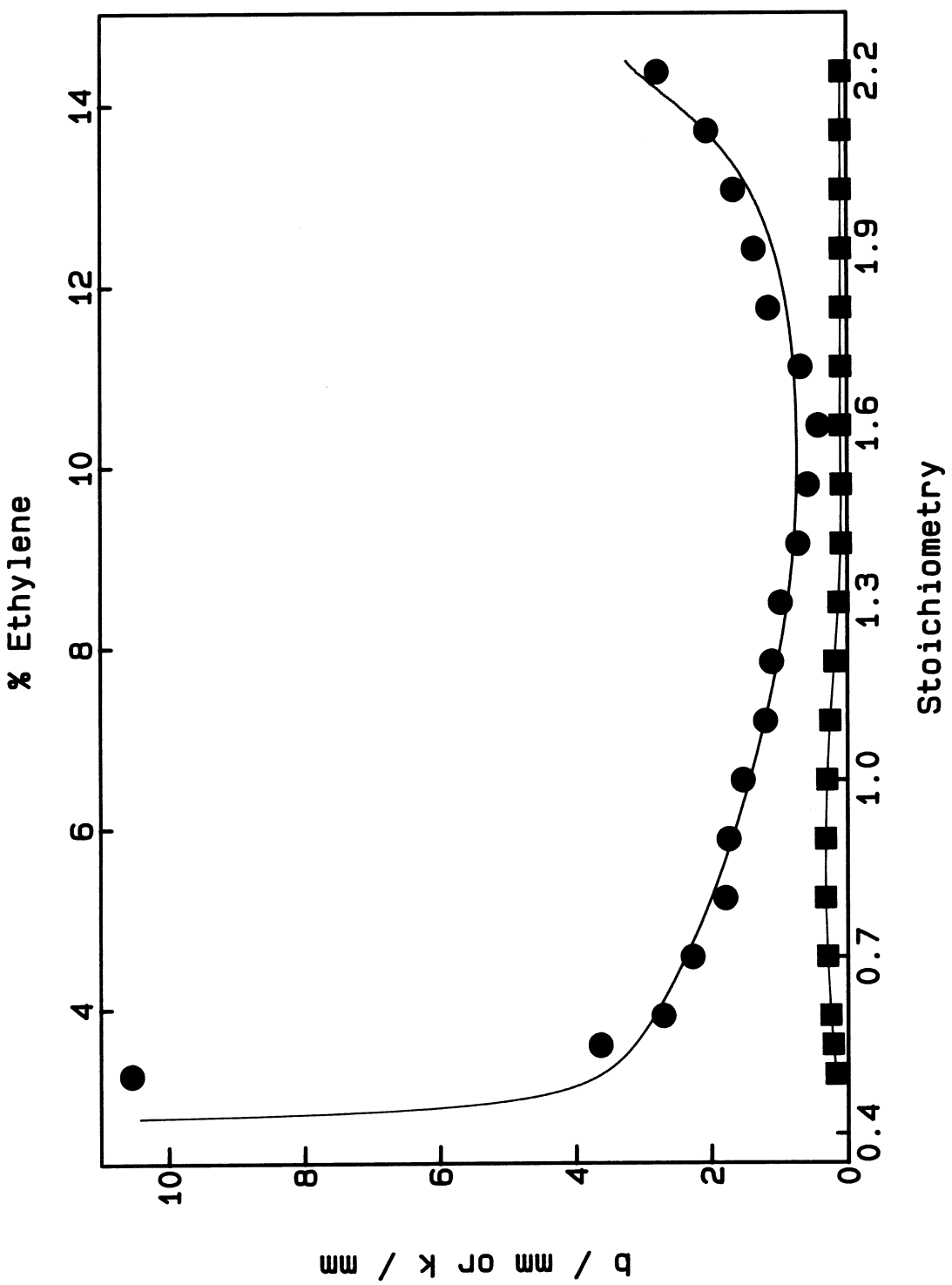

rates the *vA* profile in the cold gas becomes less flat. Reasons for this will be discussed in Chapter 7.

The data are presented as plots of burning velocity *vs* stretch for a selection of the stoichiometries studied. The data in Fig. 41 are for methane/air mixtures with stoichiometries of 0.83, 1.06 and 1.22. Those in Fig. 42(a) are for a stoichiometry of 1.31. An additional measure of burning velocity, u_n, has been included in this figure. The points to note are that in all cases the slopes of the straight lines through the $S_{u,r}$ and S_{L1} data have opposite signs and that the lines never meet at zero stretch: $S_{u,r}$ always extrapolates to a lower burning velocity than S_{L1}. u_n extrapolates to the same one-dimensional value as S_{L1} because it was defined[64,85-87] as $S_{L1} - \Gamma\delta$.

In order to investigate the relationship between $S_{u,r}$, S_{L1} and u_n the streamlines in the latter flame were traced at each stretch rate. The area enclosed by the stream tube was divided by that of the corresponding "ideal" stream tube. The resulting function was normalized to 1 at the cold boundary and plotted in Fig. 42(b) against distance from the apparent stagnation surface (i.e. where the extrapolated cold gas velocity profile intersects the velocity = 0 axis). A dotted vertical line denotes the beginning of the luminous zone. If the flow were ideal, the experimental streamlines would coincide with the horizontal line corresponding to an area ratio of 1. The differences from this ideal behaviour will be discussed in Chapter 7.

The one-dimensional burning velocities obtained by extrapolating S_{L1} and $S_{u,r}$ are listed in the Appendix and also plotted in Fig. 43 along with the best-fit curve through the results from the expanding flame method. It is interesting to note that on average the results from extrapolation of S_{L1} are higher and those from $S_{u,r}$ are lower than the expanding flame data.

The Markstein lengths obtained from the slopes of the burning velocity *vs* stretch graphs are plotted in Fig 44. The main point to note is the enormous scatter and large error bars of the stagnation-point flow results. The solid curve represents results for the Markstein length L obtained from the expanding flame work. These will be described fully in Chapter 6. The dashed curve is a best fit to Markstein lengths L_1 calculated from data presented by Law et al[24]. Within the large uncertainty, the Markstein lengths determined from stagnation flow experiments agree with the appropriate curves.

FIGURE 40

Velocity, area ratio and their product in a stagnation-point flow flame

•: Gas velocity. ○: Area ratio. Dot-dashed curve: their product.

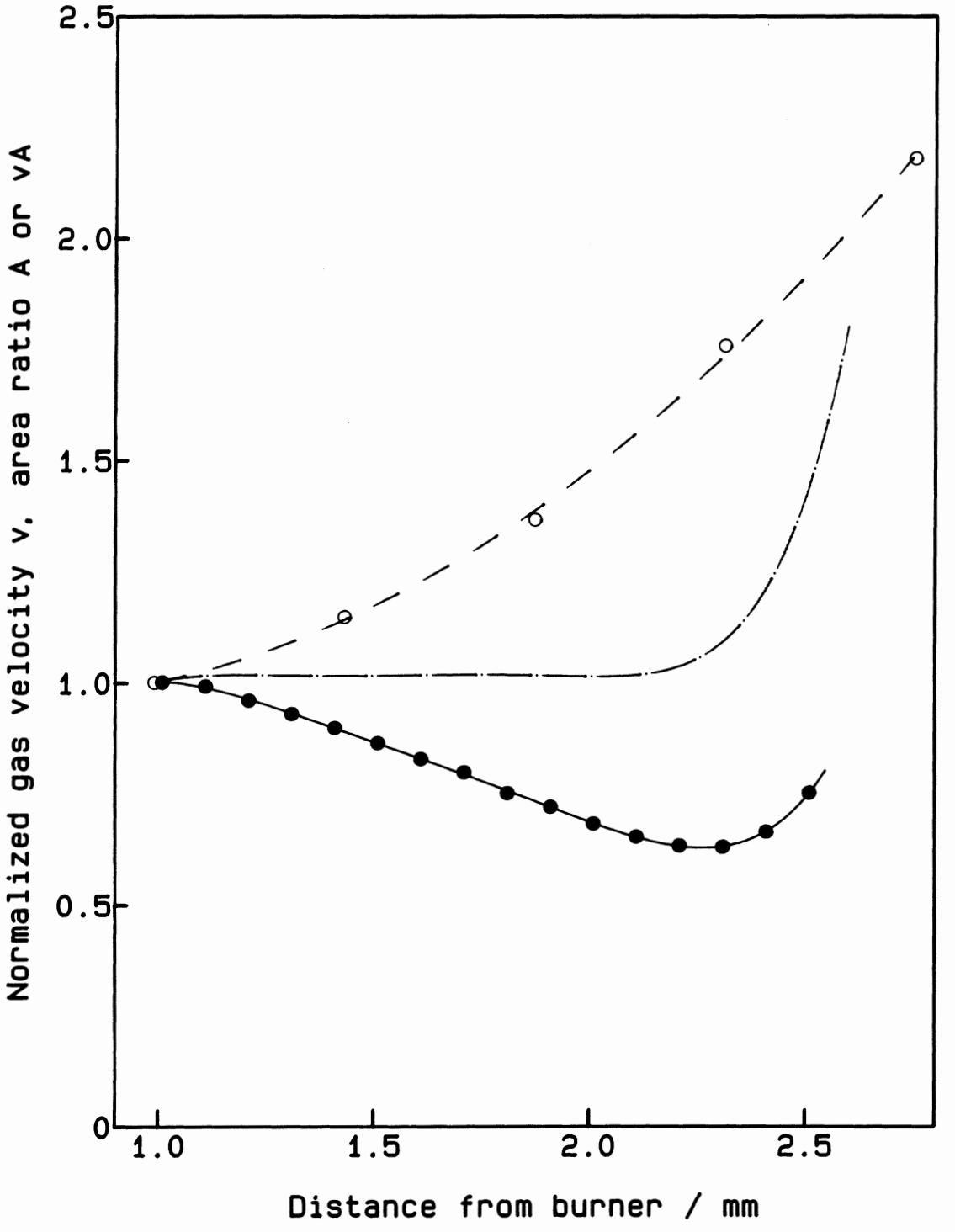

FIGURE 41

Variation of burning velocities $S_{u,r}$ (•) and S_{L1} (○) with stretch in methane/air mixtures with stoichiometries of (a) 0.83, (b) 1.06 and (c) 1.22

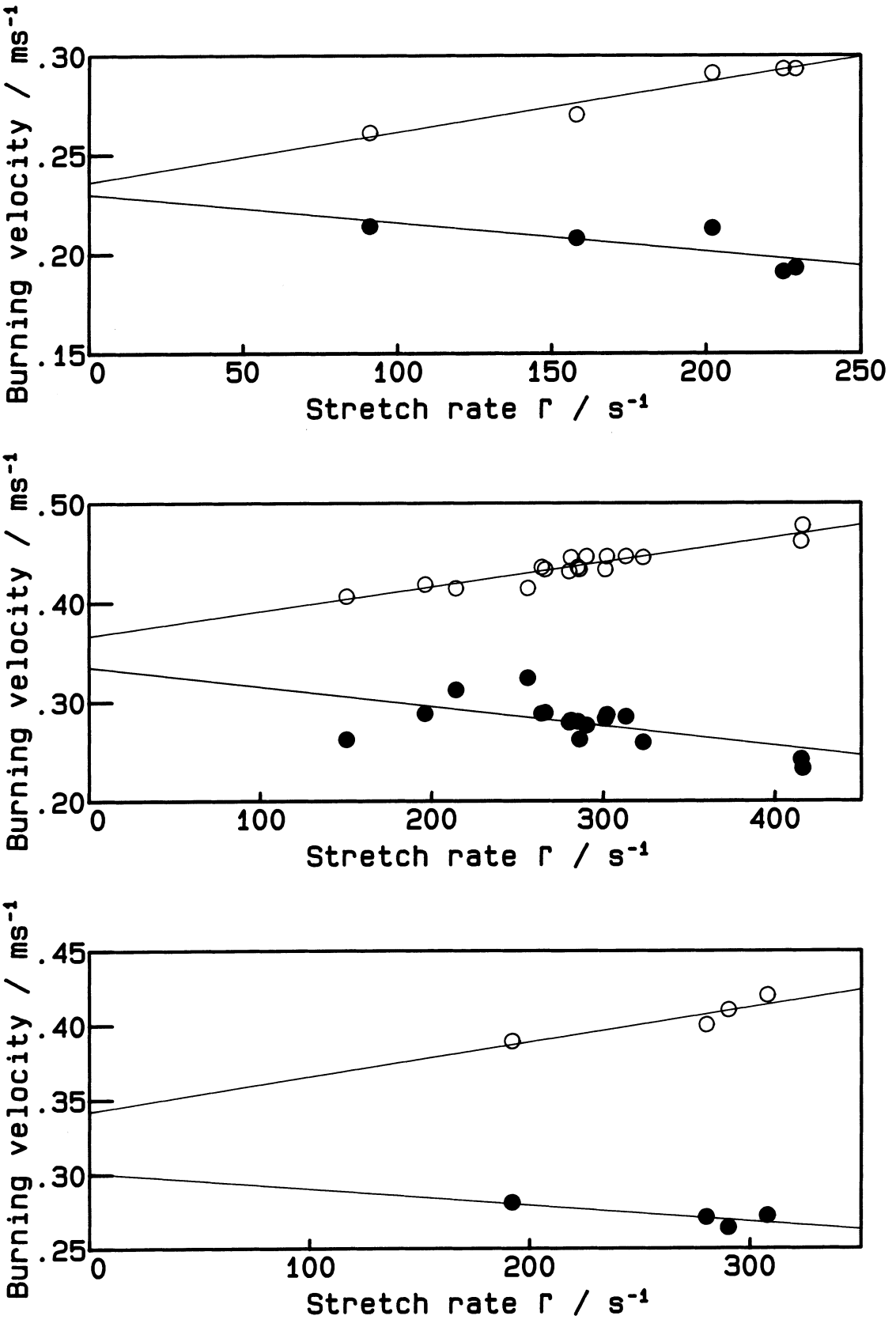

FIGURE 42

(a) Variation of burning velocities $S_{u,r}$, S_{L1} and u_n with stretch in a stagnation flow flame at a stoichiometry of 1.31

(b) Ratio of measured to ideal stream tube area for three stretch rates

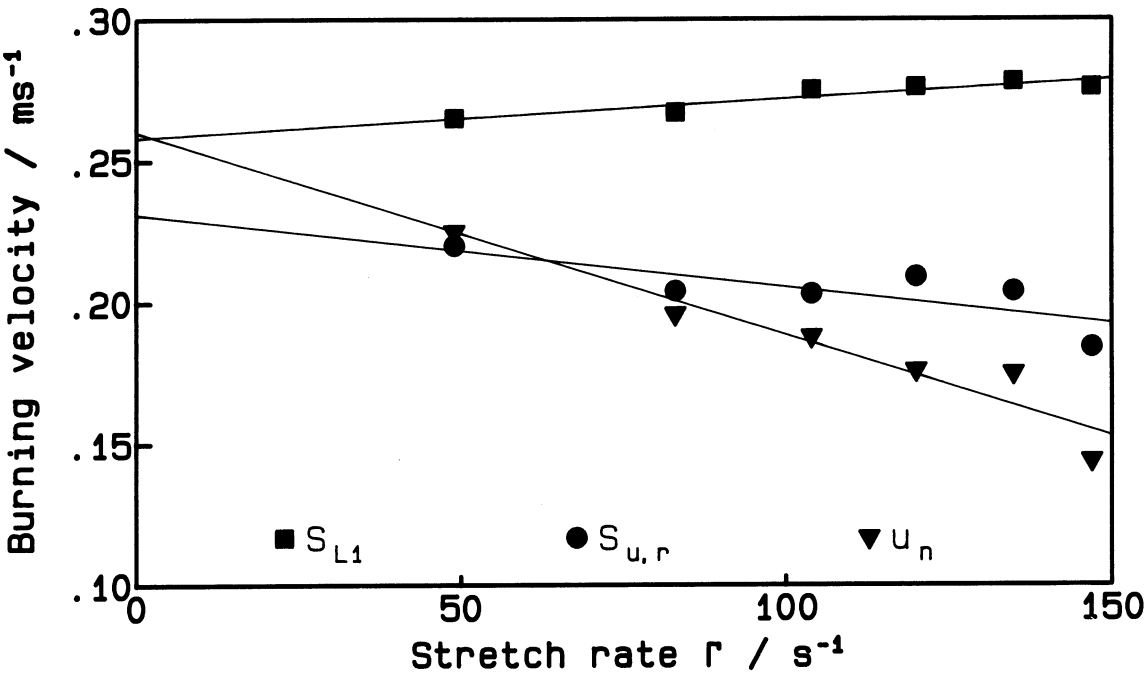

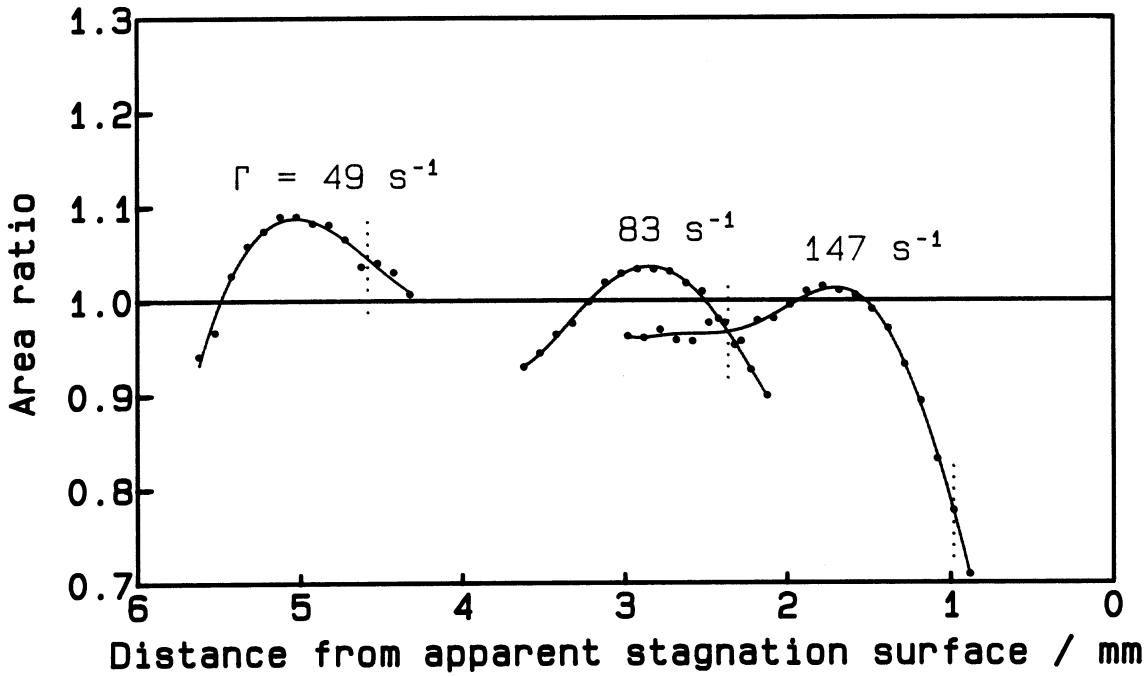

FIGURE 43

One-dimensional burning velocities derived from stagnation-point flow experiments •: Derived from $S_{u,r}$. ○: Derived from S_{L1}. Smooth curve: best fit polynomial through present expanding flame results. Dashed curve: best fit polynomial through results of Law et al[24].

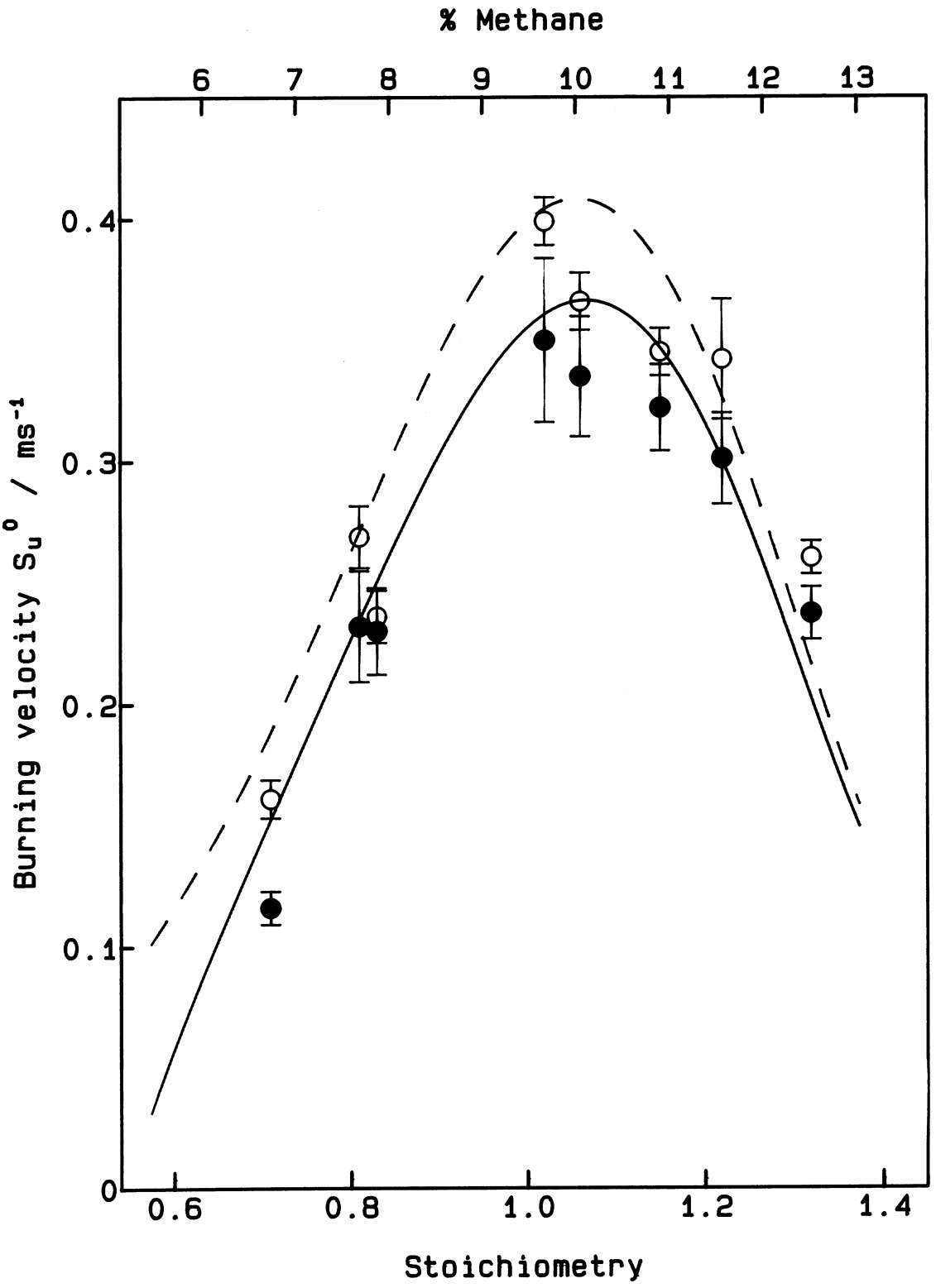

FIGURE 44

Markstein lengths derived from stagnation-point flow experiments
•: Derived from $S_{u,r}$. ○: Derived from S_{L1}. Smooth curve: best fit polynomial through present expanding flame results. Dashed curve: best fit polynomial through results of Law et al[24].

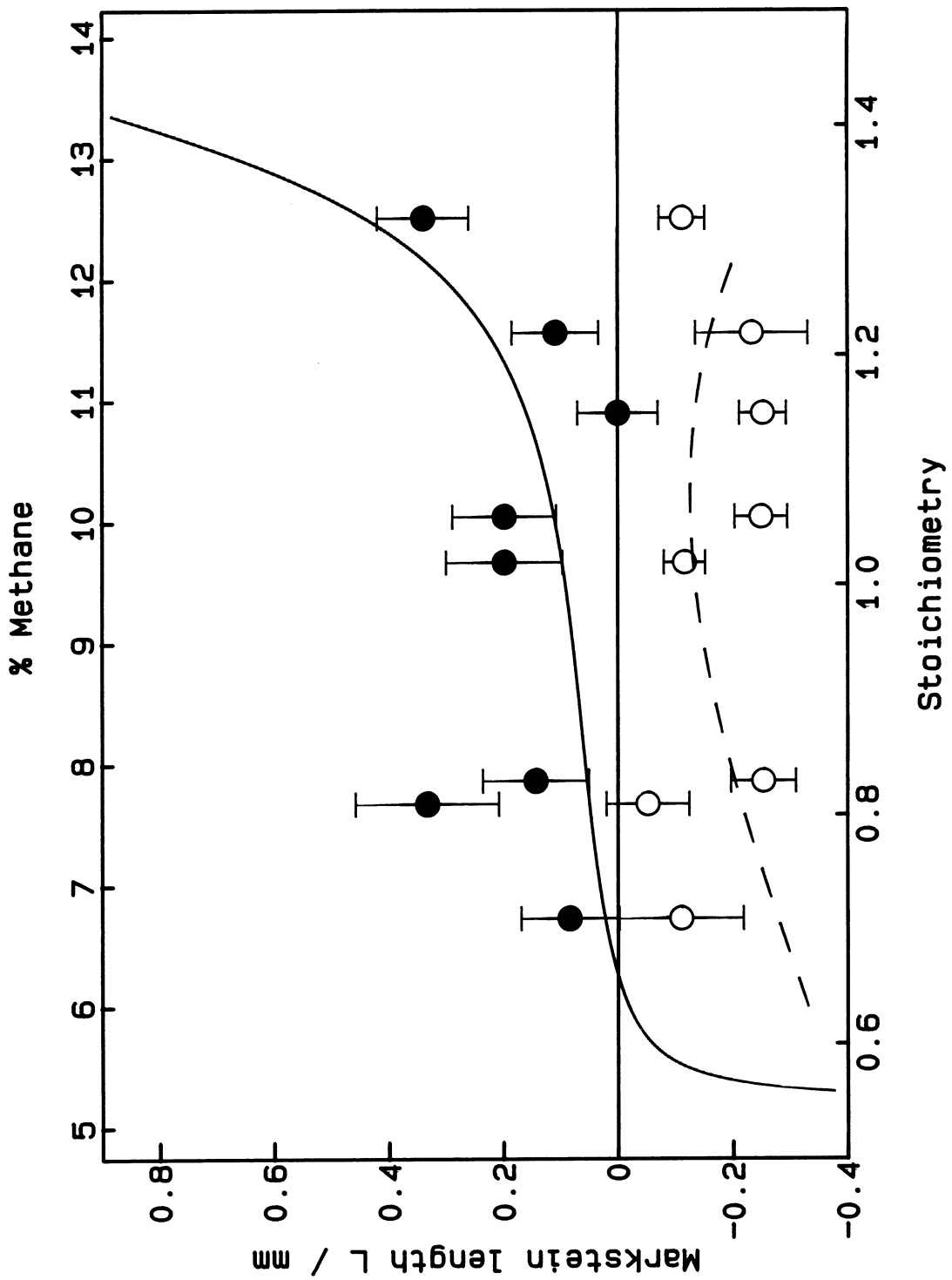

5.3 BUTTON-SHAPED FLAMES

The result of a determination of the burning velocity of stoichiometric methane/air using two different definitions is reported in this section.

According to the conventional definition, the burning velocity is the gas velocity normal to the flame at the position of first temperature rise. A good estimate of this velocity is the minimum in the upstream gas velocity profile, which is shown in Fig. 45(b). The minimum velocity is approximately 0.40 ms^{-1}.

Using the methodology described in Section 3.4, the burning velocity according to the definition used in this thesis is

$$S_{u,r} = V/A_r \tag{3}$$

where V is the volumetric flow rate in a stream tube measured at any point in the cold gas and A_r is the area of the luminous zone enclosed by the stream tube. A_r was determined for two different stream tubes and V was measured at three different planes in each stream tube. Six determinations were therefore made of the burning velocity, and the mean of all six was used to provide a final result.

Velocity profiles at each of three planes in the cold gas at distances D from the burner are shown in Fig. 45(a). These were each integrated out to radii corresponding to two different streamlines in a particle tracking photograph. There is evidence of asymmetry in the velocity profiles, so they were integrated in each direction and the volumetric flow rate determined from the average. The flame areas were determined using the spherical cap area equation (3-92). The results are shown in Table 3.

FIGURE 45

Velocity profiles in the unburnt gas in a button-shaped flame. (a) Radial, (b) Axial

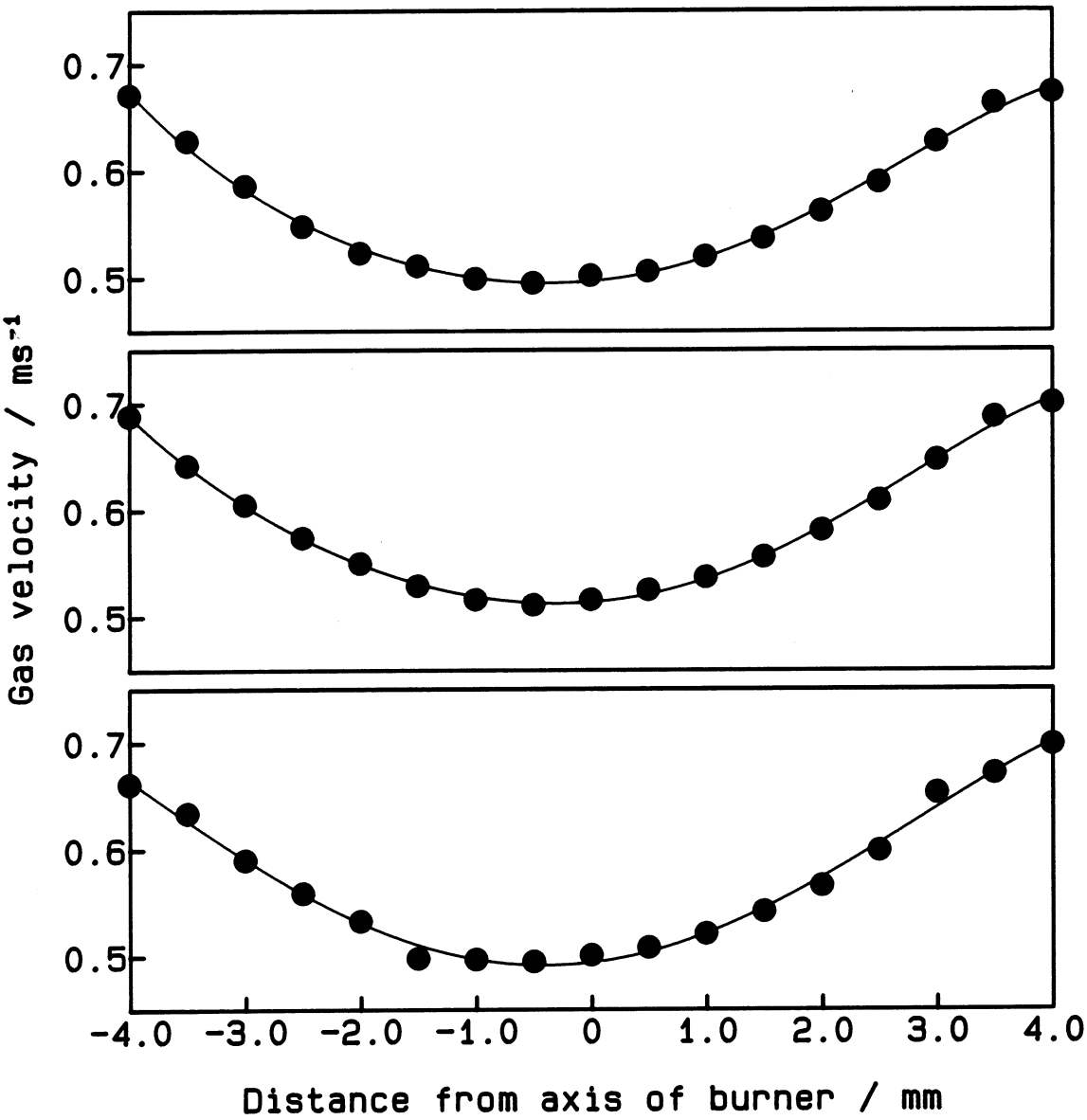

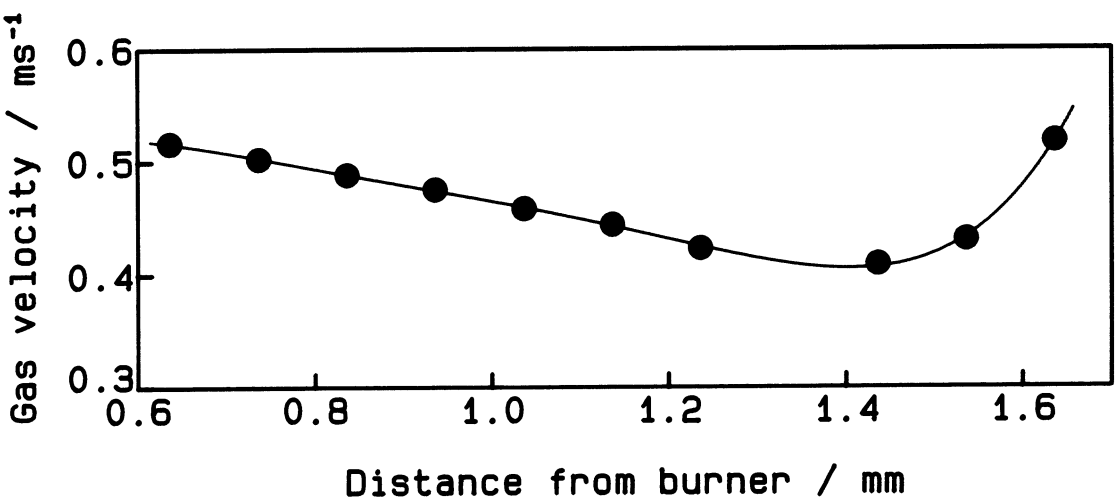

TABLE 3

Measurement of burning velocity in a button flame

Determination	1	2	3	4	5	6
D/mm	0.537	0.537	0.637	0.637	0.737	0.737
R_1/mm	3.567	4.207	3.611	4.244	3.649	4.304
$V/(10^{-6}\ m^3s^{-1})$	23.15	33.71	24.37	35.10	24.09	35.02
$A_r/(10^{-6}m^2)$	66.10	97.83	66.10	97.83	66.10	97.83
$S_{u,r}/ms^{-1}$	0.350	0.345	0.369	0.359	0.364	0.358

On the assumption that the stretch is small, the burning velocity approximates to the one-dimensional value. The final result calculated from the mean and standard error of the results in Table 3 is

$$S_u^{\circ} = 0.358 \pm 0.004\ ms^{-1}.$$

This agrees well with the expanding flame value of $0.353 \pm 0.009\ ms^{-1}$.

The area ratio between the cold boundary and luminous zone cannot be determined from the above data. It will be given approximately by the ratio of the upstream gas velocity to the burning velocity measured above, which is 0.4/0.358 = 1.14. In any case, the variation of the unburnt gas velocity with radius means that a stream tube area ratio does not fully characterize the error in burning velocity due to measuring the upstream gas velocity.

Chapter 6

LAMINAR FLAME MODELLING

In this chapter the numerical modelling performed as part of the present work is described. The subject is introduced in the first section with a brief historical survey followed by a description of the code used. The modifications which have been made to this code for use in the present work are also described.

The next section describes the chemical kinetic schemes assembled for use in the modelling. The general principles guiding the choice of reaction rate data are given, and the rate data are listed.

The last two sections contain the modelling results. First, the results for steady one-dimensional flames are given. These include planar and stationary spherical flames. The predicted burning velocities are compared with the experimental ones to demonstrate the accuracy of the model, and the structure and chemistry of the modelled flames is briefly described. Information is given on the reference surface and the flame thickness parameter k calculated from these data. Values of k are needed to determine the experimental Markstein lengths, which are therefore presented in this section.

Results of simulations of expanding flames are given in the last section. The predicted flame speed as a function of radius is compared with experimental data. The simple expanding flame model used for analysing experimental results is then applied to the results of the simulations. This provides a rigorous test of the expanding flame methodology.

6.1 DESCRIPTION OF FLAME CODE

The computation of the speed and detailed structure of premixed laminar flames began in the early 1950s. The pioneering work was performed on ozone and hydrazine decomposition flames. In 1953, Hirschfelder et al[36] solved the steady state equations for the hydrazine flame using a "shooting" technique. Downstream values of velocity and species concentrations were guessed and then the equations were integrated towards the cold boundary. The cold boundary values were

compared with the known values there and the guessed boundary conditions adjusted until agreement was obtained. Such methods become unusable when multi-step kinetics is introduced. Three years later, Spalding[94] used implicit, finite-difference methods to solve the time-dependent equations for the same system. Initial guesses for the profiles were provided and the equations were integrated forwards in time until a steady state was reached. The use of implicit methods relieved the stiffness and instability problems that caused the shooting methods to fail. Most of the subsequent work used variants of Spalding's method. Time-dependent approaches were used by Dixon-Lewis and Williams[95], Bledjian[96], Stephenson and Taylor[97], Smoot et al[98], Tsatsaronis[99], Westbrook and Dryer[100], Warnatz[101] and others.

An alternative approach was introduced by Wilde[102] in which the steady-state problem was solved directly by finite-difference boundary-value problem techniques. Both time-dependent and steady-state techniques are used in the Sandia PREMIX code used in the present work.

The aim of most of this modelling work was direct comparison with experiment, with a view to improving physical and chemical data. Most attention has been paid to chemical kinetics, since reaction rate data are less well known than the transport and thermodynamic property data which are also required. Flame geometry has been almost exclusively planar and one-dimensional up until very recently. The burning velocity predicted by such models therefore conforms precisely to the one-dimensional definition. This leads to one of the justifications for the attempts to measure the true, one-dimensional burning velocity: comparison with modelling predictions.

Recent modelling work has dealt with geometries other than planar one-dimensional, but in almost all cases the solution is still mathematically one-dimensional. Examples of such work are the planar flames in stagnation flow modelled by Rogg[68] by use of the boundary layer approximation, and by Kee et al[88] by solving the Navier-Stokes equations for the finite domain between burner and stagnation plane. True two-dimensional modelling is in its infancy, and only a few papers (e.g. refs. 103, 104) have dealt with it so far.

A major problem with two- and three-dimensional flame modelling is that the execution time and storage requirements become too large for most current machines if full chemical schemes of perhaps 25 species and 100 steps are used. There has therefore been a move towards the derivation of global or "reduced" chemical schemes in which the flame behaviour is predicted by a set of, say, 4 reactions

involving 6 species. The rates of the reactions are either determined empirically or derived from a larger set by the use of appropriate steady-state and partial equilibrium assumptions[105,106]. Such an approach is not needed in the present work because one-dimensional codes are capable of representing all of the required configurations.

Expanding spherical flames can be modelled by one-dimensional codes. Hydrogen/air flames have been modelled by Dixon-Lewis[70], Kailasanath and Oran[107] and Fukutani et al[91], while methane/air flames have been studied by Sloane and Schoene[108].

6.1.1 **Sandia code**

All of the modelling described in this thesis makes use of variants of the PREMIX flame code written by the Sandia Laboratories[109,110]. The code is part of the CHEMKIN package[111] used for solving problems in chemical kinetics. Modules are provided for reading and interpreting data from the Sandia Laboratories' thermodynamic and transport property databases and reaction rate data in the user's chemical kinetic scheme.

The program solves finite-difference approximations to the one-dimensional flame equations (2-9), (2-15), (2-18) and (2-24). The boundary value problem is thereby reduced to a system of algebraic equations. When starting a problem from scratch, a very coarse mesh with as few as six points is normally used. After a solution has been obtained, extra mesh points are added in regions where the solution or its gradient change rapidly. The initial guess for the next stage of the computation is obtained by interpolation of the coarse mesh solution. Such use of "adaptive gridding" makes optimum use of computer resources. The procedure continues until the resolution has attained the value specified by the user.

A facility for starting a run from the solution of another ("restarting") is provided. This is a very useful feature, which speeds up the calculation of a series of flames (across the stoichiometric range, say) since each run can be started from the solution of the previous one.

The other major feature of the code is the solution method for the algebraic equations. Both time-dependent and steady-state methods are used. Newton's method for solving the steady-state problem converges quickly provided the initial

guess is close to the solution, but otherwise it diverges. It is therefore used initially, but if progress is slow the program switches to time-stepping in order to get closer to the solution. Newton's method is then repeated.

A further feature of the code is the way the energy equation is used. In many experiments on burner-stabilized flames, heat losses render the flame non-adiabatic. The temperature profile is often known better than the heat losses to the burner. The code is designed to allow the solution procedure to use this experimental temperature profile. This should lead to more meaningful comparison between experiment and modelling. In such cases the energy equation is not solved and the computation ends when a converged solution has been obtained.

If a solution of the energy equation is required, the above procedure is performed first, and the energy equation is introduced in a second stage. The reason for delaying its introduction is a numerical one. The most severe nonlinearities in chemical kinetics come from the exponential dependence of the reaction rate on temperature. Eliminating temperature from the iteration in the first stage of the computation makes the flame problem easier to solve. The overall chances of obtaining a successful solution are improved by the use of this two-stage procedure.

6.1.2 **Modifications to the Sandia code**

The PREMIX code was adapted for use at the London Research Station by Dr. D. R. Dowdy. He also made some major changes in the way the code operates, and in addition produced a new code, based on this modified version of PREMIX, for modelling expanding spherical flames. These changes will be described next.

6.1.2.1 Basic changes to code

The main problem with the standard PREMIX code is the way the equations are cast in finite-difference form. If the standard differencing technique is used, conservation of mass and energy are not satisfied exactly. In many circumstances this is not very important, but for certain fuels, particularly hydrogen, the flame temperature and the burning velocity can be in error by several percent[112] for moderate numbers of mesh points (of the order of 100). If precise comparisons are being made, this disparity can matter. One way round the problem is to increase the number N of mesh points: in the limit of infinite N, correct results will be obtained.

Egolfopoulos and Law[29] found that increasing the number of mesh points to about 1000, or plotting S_u° against $1/N$ and extrapolating to $1/N = 0$, produces acceptable results. The disadvantage of these approaches is the extra use of computer resources: more memory and CPU time are required.

The differencing scheme introduced by Dr. Dowdy implements exact conservation of mass and energy. It then becomes possible to use a relatively small number of mesh points (typically about 130) and obtain the accuracy for which over 1000 points would be needed in the standard version of the code. Machine utilization is therefore much more efficient, so higher accuracy and runs over wider parameter ranges are possible for a given amount of computer time.

An alternative gridding strategy was also implemented. This differs from the standard method in that mesh points can be both added and removed in order to give the optimum resolution. In standard PREMIX, mesh points can only be added. The full advantage of this method is seen in the expanding flame code, where a grid is calculated as part of the solution.

6.1.2.2 New expanding spherical flame code

A new program was developed by Dr. Dowdy and Dr. J.K. Worrell[113] for modelling time-dependent expanding spherical flames. The program was developed from the Sandia code and retains many of its features. In particular, it preserves the use of a reference frame attached to the flame. In order to allow for changes in the structure of the flame with time, a regridding strategy is included which involves the computation of the optimum grid as part of the time-dependent solution. The main advantage of this approach is that the form of the solution changes little during the course of the calculation, resulting in high computational efficiency.

The equations solved are the same as for the steady problem except that time-dependent versions of equations (2-18) and (2-24) are used. In fact, these are already present in the code to allow time-stepping.

The modelled flames are "ignited" by the addition of heat in the form of a Gaussian temperature profile centred on zero radius. The maximum temperature and width at half height can be specified, in order to vary the ignition energy. It is also possible to specify some composition other than that of the unburnt mixture at the centre of the flame. For example, some radical species can be included to aid ignition.

The nominal radius of the expanding flame is that of the zone with a temperature TFIX specified in the input file. The output consists of the nominal radius and speed of the flame as functions of time along with composition and temperature profiles at pre-selected intervals.

6.2 CHEMICAL KINETIC SCHEMES ASSEMBLED IN THIS WORK

The approach adopted in the assembly of the reaction schemes was to start with the best (usually the most recent) available data. The initial scheme was based on a set recommended by Drs. D. B. Smith, C. Robinson and M. J. Brown following a survey by them of current rates in the literature. Also taken into account was earlier modelling work and comparison with experimental species profiles[114]. Changes in the rate data were then made based on comparisons between the modelling results and the burning velocities determined in the present work. No arbitrary changes were made: rates based on experimental data or recommendations of other workers were used. However, a different fit to experimental rate data was made in some cases. The facilities provided in the Sandia code package for performing sensitivity analyses were used for choosing for special consideration those rates which had the greatest influence on the burning velocity. Chief among these for all fuels studied in this work is the $H + O_2 \rightleftharpoons OH + O$ reaction.

The reaction schemes are listed in Tables 4, 5 and 7, with some pressure-dependent data in Table 6. The data are presented in a form consistent with equation (2-8). Three parameters are given for each reaction: a collision or pre-exponential term B_k, a temperature exponent α_k and an activation energy E_k. The units were cal, cm^3, mol, s, K. Third-body collision efficiencies are listed for some termolecular reactions; these are factors by which the reaction rate is greater (i.e. by which B_k is multiplied) for those particular collision partners. In other cases the collision efficiency is unity. The reverse reactions were included in all cases. They were computed automatically by the Sandia code from the calculated equilibrium constants.

Although the latest version of the Sandia code has the option of including the parameters for pressure-dependent reactions, the current version of the expanding flame code does not have this facility. In order to ensure consistency, the Sandia code option was not used. Instead, suitable values of the pressure-dependent rates were computed by Dr. C. Robinson using data of Tsang and Hampson[115,116].

TABLE 4

Reaction mechanism for hydrogen oxidation

	Reaction		B_k	α_k	E_k	Ref.
1.	$H+O_2$	$\rightleftharpoons O+OH$	1.92E+14	0.0	16439.0	117
2.	H_2+O	$\rightleftharpoons H+OH$	3.87E+04	2.7	6259.0	118
3.	$OH+H_2$	$\rightleftharpoons H+H_2O$	2.16E+08	1.5	3430.0	119
4.	$OH+OH$	$\rightleftharpoons O+H_2O$	1.85E+06	2.0	-956.0	120
5.	$H+OH+M$	$\rightleftharpoons H_2O+M$	2.20E+22	-2.0	0.0	115
Enhanced third-body efficiency: H_2O=6.3						
6.	$H+H+M$	$\rightleftharpoons H_2+M$	1.00E+18	-1.0	0.0	70
Third-body efficiencies: H_2=0, H_2O=0						
7.	$H+H+H_2$	$\rightleftharpoons H_2+H_2$	9.20E+16	-0.6	0.0	70
8.	$H+H+H_2O$	$\rightleftharpoons H_2+H_2O$	6.00E+19	-1.25	0.0	70
9.	$H+O_2+M$	$\rightleftharpoons HO_2+M$	2.91E+20	-1.66	0.0	121
Third-body efficiency: H_2O=0						
10.	$H+O_2+H_2O$	$\rightleftharpoons HO_2+H_2O$	1.76E+22	-2.00	0.0	121[a]
11.	$O+H+M$	$\rightleftharpoons OH+M$	6.20E+16	-0.6	0.0	70
12.	H_2O_2+M	$\rightleftharpoons OH+OH+M$	1.20E+17	0.0	45502.0	122
Enhanced third-body efficiency: H_2O=5.3						
13.	$H+H_2O_2$	$\rightleftharpoons H_2+HO_2$	3.16E+13	0.0	5258.0	120
14.	$H+H_2O_2$	$\rightleftharpoons H_2O+OH$	2.00E+13	0.0	3992.0	120
15.	$O+H_2O_2$	$\rightleftharpoons OH+HO_2$	9.60E+06	2.0	3974.0	115
16.	$OH+H_2O_2$	$\rightleftharpoons H_2O+HO_2$	2.00E+12	0.0	463.0	120
17.	HO_2+HO_2	$\rightleftharpoons H_2O_2+O_2$	1.26E+14	0.0	10038.0	123
18.	$H+HO_2$	$\rightleftharpoons OH+OH$	5.47E+13	0.0	138.0	120
19.	$H+HO_2$	$\rightleftharpoons H_2+O_2$	1.13E+13	0.0	600.0	120
20.	$O+HO_2$	$\rightleftharpoons O_2+OH$	2.00E+13	0.0	-439.0	120
21.	$OH+HO_2$	$\rightleftharpoons H_2O+O_2$	2.05E+16	-1.0	0.0	124[b]

a Modified to T^{-2} form

b Modified to T^{-1} form

TABLE 5

Reaction mechanism for C_1 and C_2 species

	Reaction		B_k	α_k	E_k	Ref.
22.	CO+OH	$\rightleftharpoons$ H+CO_2	1.50E+07	1.3	-769.6	120
23.	CO+O_2	$\rightleftharpoons$ CO_2+O	2.53E+12	0.0	47801.0	120
24.	CO+HO_2	$\rightleftharpoons$ CO_2+OH	1.50E+14	0.0	23637.7	120
25.	CO+O+M	$\rightleftharpoons$ CO_2+M	5.30E+13	0.0	-4541.1	125
26.	CHO+M	$\rightleftharpoons$ H+CO+M	1.85E+17	-1.0	17136.7	126
Enhanced third-body efficiencies: CO=1.9, H_2=1.9, CH_4=2.8, CO_2=3.0, H_2O=5.0						
27.	CHO+O_2	$\rightleftharpoons$ CO+HO_2	7.58E+12	0.0	406.3	127
28.	CHO+H	$\rightleftharpoons$ CO+H_2	1.20E+14	0.0	0.0	115
29.	CHO+OH	$\rightleftharpoons$ CO+H_2O	1.10E+14	0.0	0.0	128
30.	CHO+O	$\rightleftharpoons$ CO+OH	3.00E+13	0.0	0.0	125
31.	CHO+O	$\rightleftharpoons$ CO_2+H	3.00E+13	0.0	0.0	125
32.	HCHO+H	$\rightleftharpoons$ CHO+H_2	2.88E+13	0.0	3728.0	129
33.	HCHO+OH	$\rightleftharpoons$ CHO+H_2O	7.23E+05	2.46	-970.3	130
34.	HCHO+O	$\rightleftharpoons$ CHO+OH	1.70E+06	2.32	1481.8	131
35.	CH_4+H	$\rightleftharpoons$ CH_3+H_2	2.20E+04	3.0	8755.0	132
36.	CH_4+OH	$\rightleftharpoons$ CH_3+H_2O	5.10E+08	1.4	3398.7	133[a]
37.	CH_4+O	$\rightleftharpoons$ CH_3+OH	6.93E+08	1.56	8485.0	134
38.	CH_3+H	$\rightleftharpoons$ CH_2+H_2	1.80E+14	0.0	15392.0	135
39.	CH_3+H	$\rightleftharpoons$ CH_4	4.27E+39	-7.907	9861.4	115[b]
40.	CH_3+CH_3	$\rightleftharpoons$ C_2H_6	7.00E+56	-13.038	20640.0	137
41.	CH_3+CH_3	$\rightleftharpoons$ C_2H_4+H_2	2.10E+14	0.0	19192.2	138
42.	CH_3+OH	$\rightleftharpoons$ HCHO+H_2	4.00E+12	0.0	0.0	139
43.	CH_3+OH	$\rightleftharpoons$ HCHO+2H	2.00E+16	0.0	27500.0	135
44.	CH_3+OH	$\rightleftharpoons$ CH_2+H_2O	1.20E+06	2.1	2460.0	140
45.	CH_3+O	$\rightleftharpoons$ HCHO+H	8.40E+13	0.0	0.0	141
46.	CH_3+O_2	$\rightleftharpoons$ CH_3O+O	7.00E+12	0.0	25650.0	135
47.	CH_3+HCHO	$\rightleftharpoons$ CHO+CH_4	1.10E-12	7.4	-908.2	142
48.	CH_3+CHO	$\rightleftharpoons$ CH_4+CO	7.80E+13	0.0	0.0	143
49.	CH_3+HO_2	$\rightleftharpoons$ CH_4+O_2	2.00E+12	0.0	0.0	22
50.	CH_3+HO_2	$\rightleftharpoons$ CH_3O+OH	2.00E+13	0.0	0.0	144
51.	CH_3O+M	$\rightleftharpoons$ HCHO+H+M	4.90E+15	0.0	22780.0	145
52.	CH_3O+O_2	$\rightleftharpoons$ HCHO+HO_2	2.20E+10	0.0	1744.0	146

TABLE 5

Reaction mechanism for C_1 and C_2 species (continued)

	Reaction		B_k	α_k	E_k	Ref.
53.	CH_3O+H	$\rightleftharpoons HCHO+H_2$	6.00E+13	0.0	0.0	147[c]
54.	CH_3O+OH	$\rightleftharpoons HCHO+H_2O$	1.00E+13	0.0	0.0	148
55.	C_2H_6+H	$\rightleftharpoons C_2H_5+H_2$	5.40E+02	3.5	5210.3	132
56.	C_2H_6+OH	$\rightleftharpoons C_2H_5+H_2O$	7.77E+06	2.0	854.4	149
57.	C_2H_6+O	$\rightleftharpoons C_2H_5+OH$	2.70E+06	2.4	5831.7	150
58.	$C_2H_6+CH_3$	$\rightleftharpoons C_2H_5+CH_4$	5.50E-01	4.0	8269.6	132
59.	C_2H_5	$\rightleftharpoons C_2H_4+H$	1.64E+61	-14.5	59711.0	115
60.	$C_2H_5+O_2$	$\rightleftharpoons C_2H_4+HO_2$	2.00E+10	0.0	-191.2	151
61.	C_2H_5+H	$\rightleftharpoons CH_3+CH_3$	1.23E+14	0.0	0.0	152
62.	C_2H_5+H	$\rightleftharpoons C_2H_4+H_2$	2.00E+12	0.0	0.0	153
63.	C_2H_5+OH	$\rightleftharpoons C_2H_4+H_2O$	2.40E+13	0.0	0.0	115
64.	C_2H_5+O	$\rightleftharpoons C_2H_4+OH$	3.30E+13	0.0	0.0	154
65.	C_2H_5+O	$\rightleftharpoons HCHO+CH_3$	9.70E+13	0.0	0.0	154
66.	C_2H_4+H	$\rightleftharpoons C_2H_3+H_2$	3.16E+11	0.7	8006.7	155
67.	C_2H_4+OH	$\rightleftharpoons C_2H_3+H_2O$	2.00E+13	0.0	5951.2	156
68.	C_2H_4+O	$\rightleftharpoons C_2H_3+OH$	1.14E+15	0.0	13791.0	157
69.	C_2H_3+M	$\rightleftharpoons C_2H_2+H+M$	4.57E+43	-8.0	49924.0	115
70.	$C_2H_3+O_2$	$\rightleftharpoons C_2H_2+HO_2$	1.60E+13	0.0	10000.0	158
71.	C_2H_3+H	$\rightleftharpoons C_2H_2+H_2$	3.00E+13	0.0	0.0	159
72.	C_2H_3+HCHO	$\rightleftharpoons C_2H_4+CHO$	5.40E+02	2.81	5900.0	115[d]
73.	C_2H_3+OH	$\rightleftharpoons C_2H_2+H_2O$	3.00E+13	0.0	0.0	115
74.	C_2H_3+O	$\rightleftharpoons CH_2CO+H$	3.00E+13	0.0	0.0	159
75.	C_2H_2+H	$\rightleftharpoons C_2H+H_2$	6.00E+13	0.0	23661.6	125
76.	C_2H_2+OH	$\rightleftharpoons C_2H+H_2O$	2.71E+13	0.0	10492.3	160
77.	C_2H_2+O	$\rightleftharpoons CH_2+CO$	1.40E+04	2.8	497.1	161[e]
78.	C_2H_2+O	$\rightleftharpoons C_2H+OH$	7.59E+03	2.8	497.1	161[e]
79.	C_2H+O_2	$\rightleftharpoons CO+CO+H$	2.50E+13	0.0	0.0	163
80.	C_2H+OH	$\rightleftharpoons CH_2+CO$	1.80E+13	0.0	0.0	115
81.	C_2H+O	$\rightleftharpoons CO+CH$	1.80E+13	0.0	0.0	115
82.	CH_2+O_2	$\rightleftharpoons CO+OH+H$	9.24E+12	0.0	1505.7	164[f]
83.	CH_2+O_2	$\rightleftharpoons CO+H_2O$	3.96E+12	0.0	1505.7	164[f]
84.	CH_2+H	$\rightleftharpoons CH+H_2$	1.60E+14	0.0	0.0	166

TABLE 5

Reaction mechanism for C_1 and C_2 species (continued)

	Reaction		B_k	α_k	E_k	Ref.
85.	CH_2+OH	= HCHO+H	1.81E+13	0.0	0.0	115
86.	CH_2+O	= CO+H_2	4.05E+13	0.0	0.0	167[f]
87.	CH_2+O	= CO+H+H	4.05E+13	0.0	0.0	167[f]
88.	CH_2+CH_3	= C_2H_4+H	4.20E+13	0.0	0.0	115
89.	CH+O_2	= CO+OH	3.00E+13	0.0	0.0	168
90.	CH+O	= CO+H	6.00E+13	0.0	0.0	150
91.	CH+OH	= CHO+H	3.00E+13	0.0	0.0	169
92.	CH_2CO+H	= CH_3+CO	7.00E+12	0.0	3010.0	115
93.	CH_2CO+O	= CHO+CHO	2.00E+13	0.0	2290.0	115
94.	CH_2CO+OH	= HCHO+CHO	1.00E+13	0.0	0.0	115

a Error in scheme used in present work: B_k was 5.10E+05

b High pressure limit of ref. 115 increased by factor of 2.8 in line with ref. 136

c Rate expressed as a ratio

d Error in scheme used in present work: α_k was 0.281

e Products split between reactions 77 and 78 according to ref. 162

f Products split between reactions 82 and 83 and between 86 and 87 according to ref. 165

An Arrhenius function was fitted to the pressure-dependent rates and the resulting values of B_k, α_k and E_k were used in the scheme.

The simplest reaction scheme is that for hydrogen oxidation in Table 4. This was used for modelling hydrogen/air flames across the stoichiometric range and stoichiometric hydrogen/air flames diluted with nitrogen.

Modelling of methane, ethane and ethylene flames was performed using the C_2 scheme. This consisted of the C_1 and C_2 reactions in Table 5 along with hydrogen reactions from Table 4. Reactions 7, 8 and 12 to 17 were omitted since they are not important in hydrocarbon combustion.

Reactions 39, 40, 51, 59 and 69 in Table 5 are pressure-dependent in the range of experimental pressures used (0.25 to 2 atm). Values quoted are for 1 atm (101.35 kPa). The calculated rate data used at pressures of 0.25 atm, 0.5 atm and 2.0 atm are listed in Table 6.

TABLE 6

Reaction rate data for pressure-dependent reactions at 0.25, 0.5 and 2.0 atm

	Reaction		p/atm	B_k	α_k	E_k	Ref.
39.	CH_3+H	$\rightleftharpoons CH_4$	0.25	2.61E+39	-8.0	8956.1	115
			0.5	4.05E+39	-8.0	9418.4	
			2.0	9.12E+38	-7.6	9941.2	
40.	CH_3+CH_3	$\rightleftharpoons C_2H_6$	0.25	1.69E+58	-13.6	19979.0	137
			0.5	5.53E+58	-13.7	21048.0	
			2.0	3.86E+54	-12.3	19978.0	
51.	CH_3O+M	$\rightleftharpoons HCHO+H+M$	0.25	4.90E+15	0.0	22784.0	145
			0.5	4.90E+15	0.0	22784.0	
			2.0	1.21E+17	-0.4	24060.0	
59.	C_2H_5	$\rightleftharpoons C_2H_4+H$	0.25	3.78E+61	-14.5	53125.0	170[a]
			0.5	1.38E+64	-15.1	55329.0	
			2.0	3.34E+68	-16.1	59488.0	
69.	C_2H_3+M	$\rightleftharpoons C_2H_2+H+M$	0.25	2.61E+43	-7.9	31070.0	115
			0.5	1.60E+43	-7.9	31416.0	
			2.0	6.79E+43	-8.0	33196.0	

a Data were calculated from a different source from 1 atm values

An attempt has been made to be reasonably comprehensive (i.e. to include all relevant reactions) in both the hydrogen and the C_2 modelling. No such attempt has been made for modelling propane flames because of the complexity of the chemistry. Instead, a few reactions have been selected which are expected to be the most important. These are listed in Table 7 and were used along with the reactions listed in Tables 4 and 5 for modelling the propane flames.

TABLE 7

Reaction mechanism for C_3 species

	Reaction		B_k	α_k	E_k	Ref.
95.	$C_2H_5+CH_3$	$\rightleftharpoons C_3H_8$	7.00E+12	0.0	0.0	171
96.	C_3H_8+H	$\rightleftharpoons n\text{-}C_3H_7+H_2$	1.30E+14	0.0	9704.0	171
97.	C_3H_8+H	$\rightleftharpoons i\text{-}C_3H_7+H_2$	1.00E+14	0.0	8341.0	171
98.	C_3H_8+O	$\rightleftharpoons n\text{-}C_3H_7+OH$	3.00E+13	0.0	5760.0	171
99.	C_3H_8+O	$\rightleftharpoons i\text{-}C_3H_7+OH$	2.60E+13	0.0	4469.0	171
100.	C_3H_8+OH	$\rightleftharpoons n\text{-}C_3H_7+H_2O$	3.70E+12	0.0	1649.0	171
101.	C_3H_8+OH	$\rightleftharpoons i\text{-}C_3H_7+H_2O$	2.80E+12	0.0	860.0	171
102.	$n\text{-}C_3H_7+H$	$\rightleftharpoons C_3H_8$	2.00E+13	0.0	0.0	171
103.	$i\text{-}C_3H_7+H$	$\rightleftharpoons C_3H_8$	2.00E+13	0.0	0.0	171
104.	$n\text{-}C_3H_7+O_2$	$\rightleftharpoons C_3H_6+HO_2$	2.00E+10	0.0	-191.2	*a*
105.	$i\text{-}C_3H_7+O_2$	$\rightleftharpoons C_3H_6+HO_2$	2.75E+10	0.0	-2150.0	172
106.	$n\text{-}C_3H_7$	$\rightleftharpoons C_2H_4+CH_3$	3.40E+14	0.0	33007.0	171
107.	$n\text{-}C_3H_7$	$\rightleftharpoons C_3H_6+H$	1.00E+14	0.0	37309.0	171
108.	$i\text{-}C_3H_7$	$\rightleftharpoons C_3H_6+H$	2.00E+14	0.0	38695.0	171
109.	C_3H_6+O	$\rightleftharpoons CH_3+CH_3+CO$	5.00E+12	0.0	454.0	171
110.	C_3H_6+OH	$\rightleftharpoons CH_3CHO+CH_3$	1.00E+13	0.0	0.0	171
111.	CH_3CHO+H	$\rightleftharpoons CH_3+CO+H_2$	4.00E+13	0.0	4206.0	171
112.	CH_3CHO+O	$\rightleftharpoons CH_3+CO+OH$	5.00E+12	0.0	1793.0	171
113.	$CH_3CHO+OH$	$\rightleftharpoons CH_3+CO+H_2O$	1.00E+13	0.0	0.0	171

a as reaction 60 ($C_2H_5+O_2$)

6.3 MODELLING OF STEADY ONE-DIMENSIONAL FLAMES

The modelling results for all steady flames consisted of profiles of velocity, temperature, density, mass flux and mole fractions of chemical species through the flame. Additional data were also calculated, for example reaction and heat release rates, to aid analysis of the flame processes.

In this section, the predicted burning velocities are compared with the experimental values to demonstrate the accuracy of the modelling. A brief description is then given of the structure and chemistry of the modelled flames. The determination of

the reference surface and the flame thickness coefficient are described, and the latter parameter is then used in the determination of Markstein lengths from the experimental results.

6.3.1 **Results for planar flames**

6.3.1.1 Comparison with experiment

The main test of the success of the modelling was the agreement between the experimental and modelled burning velocities. For the purposes of the present work this is likely to be an adequate test. But more rigorous comparisons involving species profiles are usually considered to be necessary[101,173,174] before a model can be considered to be well-established.

The variation of the modelled hydrogen/air burning velocities with stoichiometry is shown in Fig. 15 along with the experimental values. The agreement is extremely good: the difference is less than 3% over most of the stoichiometric range. A systematic difference arises in very lean mixtures. This will be considered further in Section 6.4.2 and again in Chapter 7.

The modelled burning velocity of stoichiometric hydrogen/air mixtures as a function of nitrogen dilution is plotted in Fig. 18, along with the experimental results. The modelled data agree quite well with the experiments, although there is a difference of about 8% at about 10% dilution. At very high dilutions, there is a systematic difference between modelling and experiment. This is considered later along with effects in lean mixtures.

Methane burning velocities as a function of stoichiometry are shown in Fig. 22. The agreement between modelling and experiment is quite good across the stoichiometric range, although in lean mixtures the burning velocities are overpredicted. The modelled variation with pressure, though, is not so good. The data are shown in Fig. 25 and betray a systematic difference in the variation of the burning velocity with pressure. The experimental pressure dependence is much stronger. In terms of the pressure exponent, the experimental one is -0.298 while the modelled one is -0.183.

The modelled ethane, propane and ethylene burning velocities in Figs. 29, 33 and 38 can be described together. All predict the experimental burning velocity well on the

lean side but overestimate it on the rich. The errors in the C_2 scheme may have had some effect on these results. A corrected scheme gave a burning velocity for stoichiometric methane/air which was 6% lower than the present value. The consequences of these errors will be discussed in Chapter 7.

6.3.1.2 Flame structure and chemistry

We now describe briefly the structure and chemistry of the modelled flames. Hydrogen and hydrocarbon flames are qualitatively different, so they will be described separately. The descriptions are based on those of Dixon-Lewis[40,89] and Warnatz[101].

Hydrogen flames

The hydrogen flame can be considered to consist of four regions:

1. A small preheat zone where heating occurs by thermal conduction alone.
2. The major heat release zone, where radicals produced in zone 3, having diffused upstream, react with incoming gas by low activation energy steps. The gas in the early part of zone 2 also receives heat by conduction.
3. A radical production zone where the temperature is high enough and the reactant concentrations are such that the system is effectively in a chain branching condition.
4. The radical recombination region, where the system decays towards full equilibrium.

The reactions occurring in zone 2 are mainly the highly exothermic, low activation energy HO_2 steps (reactions 18 to 21). The maximum heat release rate occurs in this zone, but heat release continues through to zone 3 where the temperature has risen sufficiently for the radical production rate to become large.

The net rate of radical production in zone 3 depends on the balance between production of radicals by reactions 1, 2 and 3, and their removal, principally by reactions 19, 20 and 21. The rate of radical production can be represented by the production rate of a "radical pool" consisting of[89] ($H + 2O + OH + HO_2$). Dixon-Lewis defined the "ignition temperature" T_i as the temperature at which the production rate of this radical pool becomes positive. Values of T_i were determined

in the present work, and are plotted as open triangles in Fig. 47 for hydrogen/air flames as a function of stoichiometry and in Fig. 48 for stoichiometric hydrogen/air flames as a function of nitrogen dilution. T_i was between 900 and 1000 K in all cases.

The temperature at which the heat release is maximum is shown in the same figures as open circles. It is lower than T_i except in the leanest flames. Heat release at lower temperatures than T_i must be due to the reaction of radicals that have diffused from the high temperature region.

The driving force of the flame is the chain-branching reaction 1, which activates the dormant free valencies or unpaired electron spins present in molecular oxygen to produce two new, fully active free valencies.

Dixon-Lewis pointed out[40] that this behaviour, with heat-releasing reactions occurring at quite low temperatures, differs considerably from that of the models normally used for obtaining analytical solutions to the flame problem. A typical example of such a model is that analysed in Chapter 2. The use of a single-step reaction with high activation energy ensures that, unlike the hydrogen case, there is a preheat zone extending up to very high temperatures in which heating is purely by thermal conduction.

Hydrocarbon flames

For hydrocarbon flames, the structure is modified because radical production occurs at higher temperatures. There are two reasons for this. First, the hydrocarbon fuel can compete effectively with molecular oxygen for H atoms, thus reducing the rate of reaction 1 which is the major route for radical production. Second, the alkyl radicals resulting from the initial attack of H, O and OH radicals on the hydrocarbon participate mainly in chain-terminating reactions. The flame structure can be summarized as having three zones:

1. A large preheat zone where heating occurs by thermal conduction alone and where most of the initial radical attack on the hydrocarbon occurs.
2. The major heat release and radical production zone where radicals react with incoming gas by low activation energy steps.
3. The radical recombination and carbon monoxide oxidation region, where the system decays towards full equilibrium.

Hydrocarbon oxidation can be described[101] with reference to Fig. 46 as follows. The hydrocarbon fuel is attacked in zone 1 by H, O and OH radicals diffusing upstream. For all alkanes, the result is an alkyl radical. Larger alkyl radicals than ethyl (C_2H_5) decompose to smaller ones by fast thermal elimination of alkenes. The thermal decomposition rate of the smallest alkyl radicals, methyl (CH_3) and ethyl, is slow enough for recombination and oxidation reactions to compete. This is the rate-controlling part of the oxidation mechanism in alkanes, and explains why such flames have similar speeds and structures.

Ethylene (C_2H_4) is oxidized by O and OH to give methyl (CH_3), formaldehyde (CH_2O) and formyl (CHO). In addition, reaction with H atoms can lead back to C_2H_5 or to vinyl (C_2H_3). Subsequently, C_2H_3 is converted mainly to acetylene (C_2H_2) by thermal decomposition and by reaction with H atoms.

In zone 2, methyl radicals react only with O atoms to give formaldehyde. The formyl radical is then formed by H atom abstraction. Formyl can decompose thermally yielding CO and H atoms, or the H atom can be abstracted by H or O_2. Methyl radicals can also recombine to form ethane and also ethyl and ethylene. In rich flames, the majority of methyl radicals recombine, so in this sense methane combustion in rich flames is mainly the combustion of C_2 hydrocarbons.

Most of the ethyl radicals form ethylene by reaction with O_2 and by thermal decomposition. The remainder mainly reacts with H atoms to again give CH_3, with only a small amount reacting with O atoms.

Recombination of methyl and ethyl to form propane and butane must be considered in methane and ethane flames. For example, Warnatz[101] found that about 25% of the ethyl forms propane and butane in stoichiometric methane and ethane flames at atmospheric pressure. Strictly, therefore, the oxidation reactions of propane and butane should be considered. The fast thermal decomposition of propyl (C_3H_7), butyl (C_4H_9), etc means that the formation of higher alkanes by their recombination can be neglected.

As in the case of hydrogen, it is possible to define a radical pool. For hydrocarbons, Dixon-Lewis[89] defined it as (H + 2O + OH + CH_3 + C_2H_5 + HO_2 + CHO). As before, the temperature T_i at which its production rate becomes positive defines the

FIGURE 46

Mechanism of methane and ethane oxidation[101]

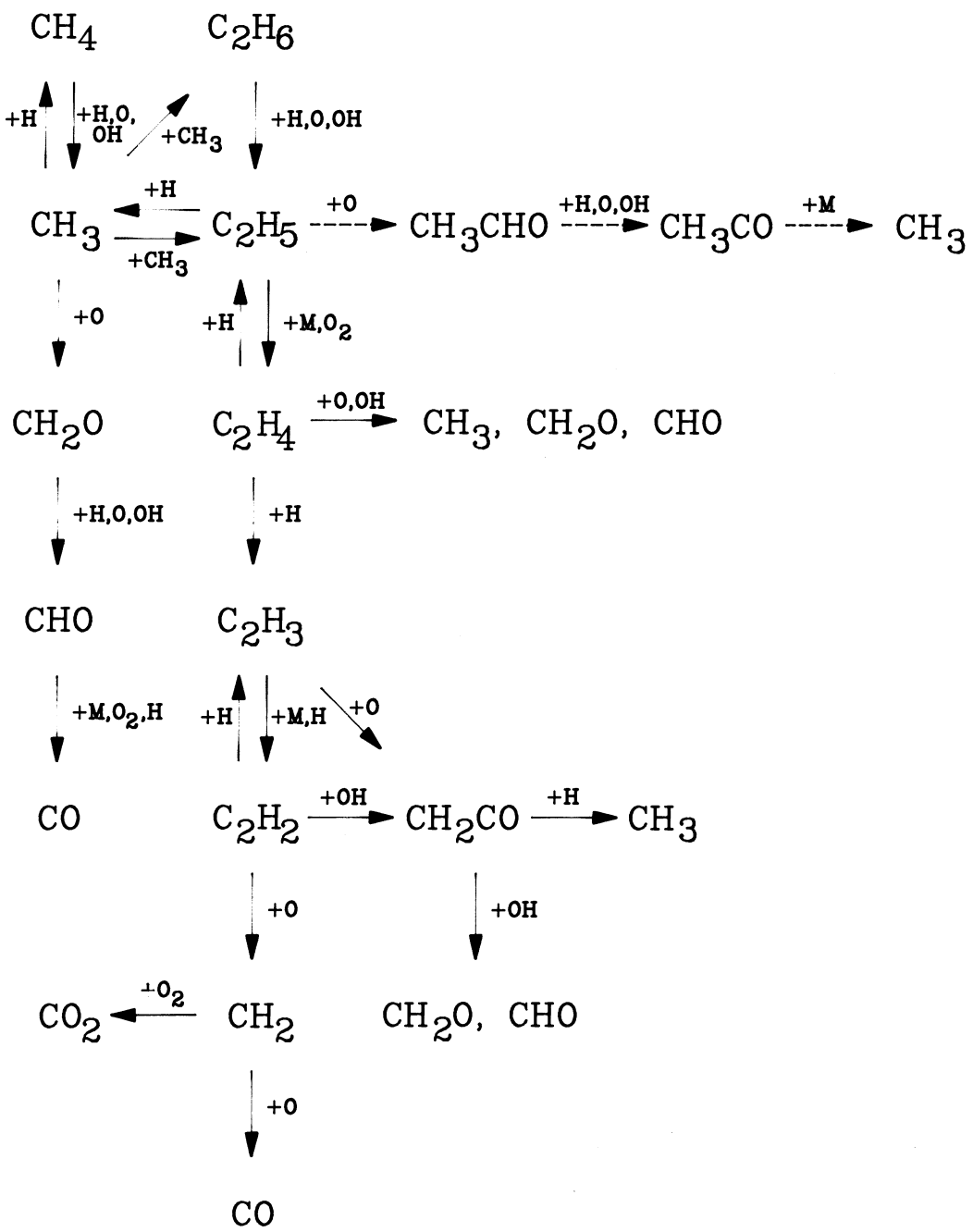

chain-branching region of the flame. Values of T_i were determined in the present work and were plotted as open triangles for methane, ethane, propane and ethylene as a function of stoichiometry in Figs. 49, 51, 52 and 53. They are plotted as a function of pressure for stoichiometric methane/air mixtures in Fig. 50. T_i for hydrocarbons varies strongly with temperature but always exceeds T_i for hydrogen. Temperatures at maximum heat release are plotted as open circles in the same figures.

The final stage of hydrocarbon oxidation is the slow oxidation of CO to CO_2 in zone 3 by reaction 14. This is a highly exothermic reaction, so the heat released at this stage of the flame is large.

Overall, the dominant reactions in hydrocarbon combustion are always 1 and 22, to the extent that lean and stoichiometric flames can be characterized as $H_2/CO/O_2$ flames fed by the hydrocarbon.

6.3.2 **Determination of the reference surface**

The reference surface is defined as the locus of points in a spherical flame where the mass flux equals that of the corresponding planar flame. It was determined by comparing flames modelled in planar and spherical geometries. The Sandia code contains an area ratio function which is set to 1 for planar flames. Spherical geometry was obtained by setting the stream tube area function equal to x^2 where x is the distance through the flame. The spherical flame modelled was one in a source flow, i.e. with the cold gas on the inside. The usual flame radius was about 21 mm. Variations in which the geometry was converted to a sink flow (hot gas on the inside) and the flame radius varied over the range 20 to 75 mm produced negligible changes in the properties of the reference surface. A comparison of the temperature profiles from planar and spherical near-stoichiometric methane/air flames showed no discernible difference when they were overlaid.

The reference surface position and temperature were easily obtained from the spherical modelling results by reading off the required properties at the zone with a mass flux equal to the planar value. Since the reference surface is usually at a point where the temperature varies very rapidly, it is more useful to quote the temperature at the reference surface position than the position itself. In any case, it is difficult to assign a meaningful position to the reference surface: relative to what should its

FIGURE 47

Temperatures of various flame surfaces *vs* stoichiometry for hydrogen/air flames ■ : Reference surface. ○: Maximum heat release. □ : Maximum fuel consumption. △ : "Ignition temperature" of Dixon-Lewis[89]. ▲ : Reference surface of Dixon-Lewis and Islam[22].

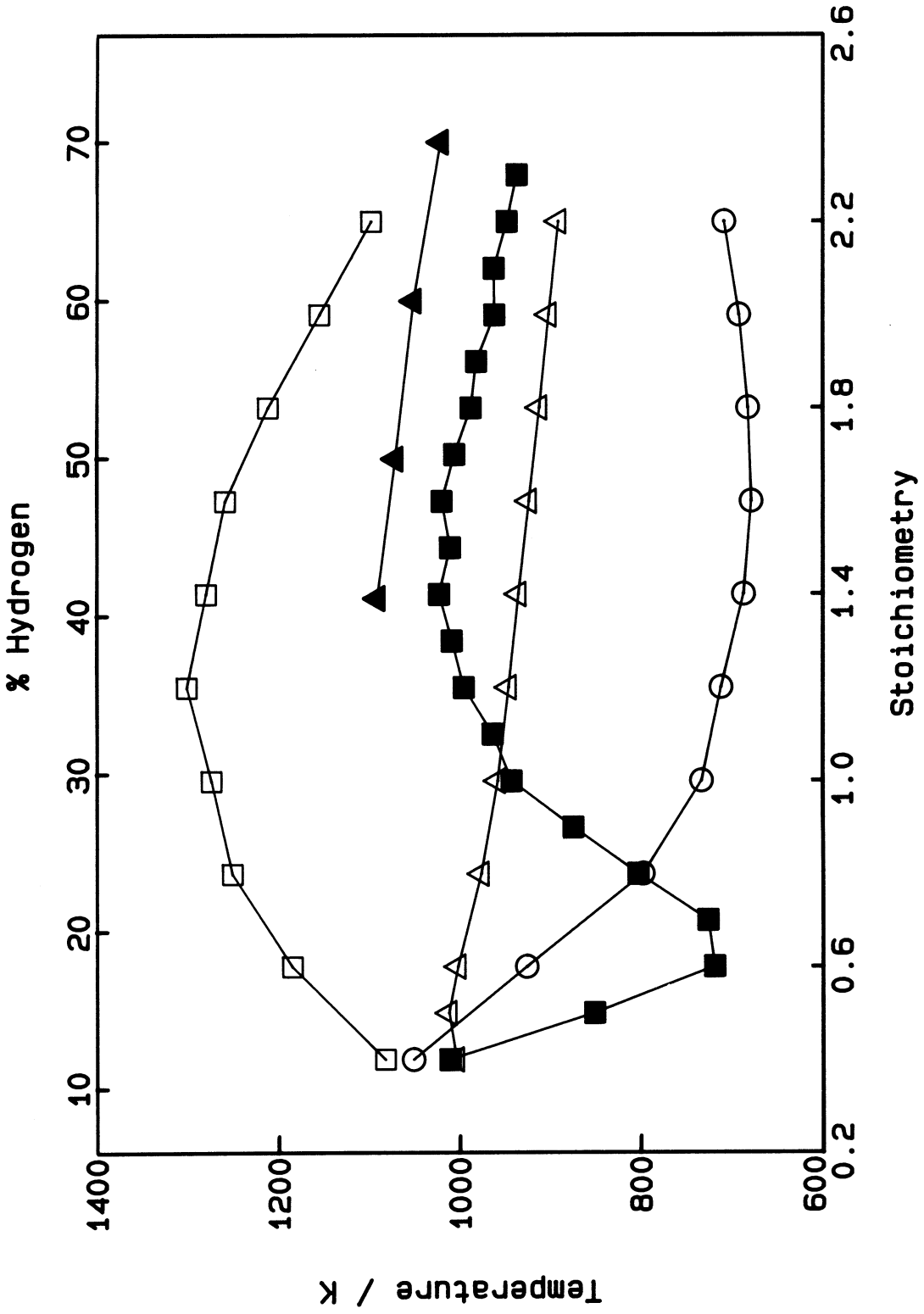

FIGURE 48

Temperatures of various flame surfaces *vs* nitrogen dilution
for stoichiometric hydrogen/air flames
■ : Reference surface. ○: Maximum heat release. □ : Maximum fuel consumption.
△ : "Ignition temperature" of Dixon-Lewis[89].

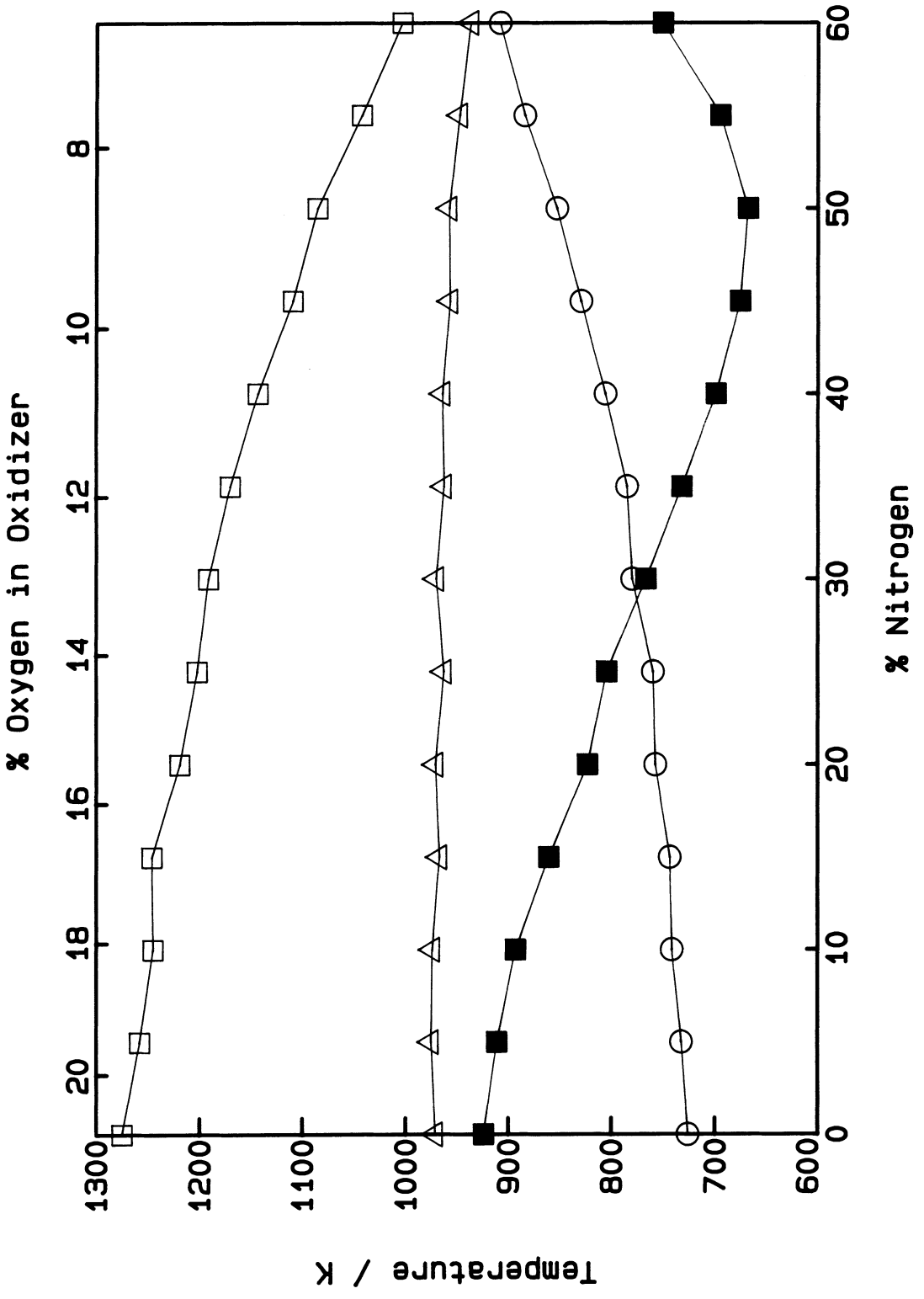

FIGURE 49

Temperatures of various flame surfaces *vs* stoichiometry for methane/air flames ■ : Reference surface. ○: Maximum heat release. □ : Maximum fuel consumption. △ : "Ignition temperature" of Dixon-Lewis[89]. ▲ : Reference surface of Dixon-Lewis and Islam[22].

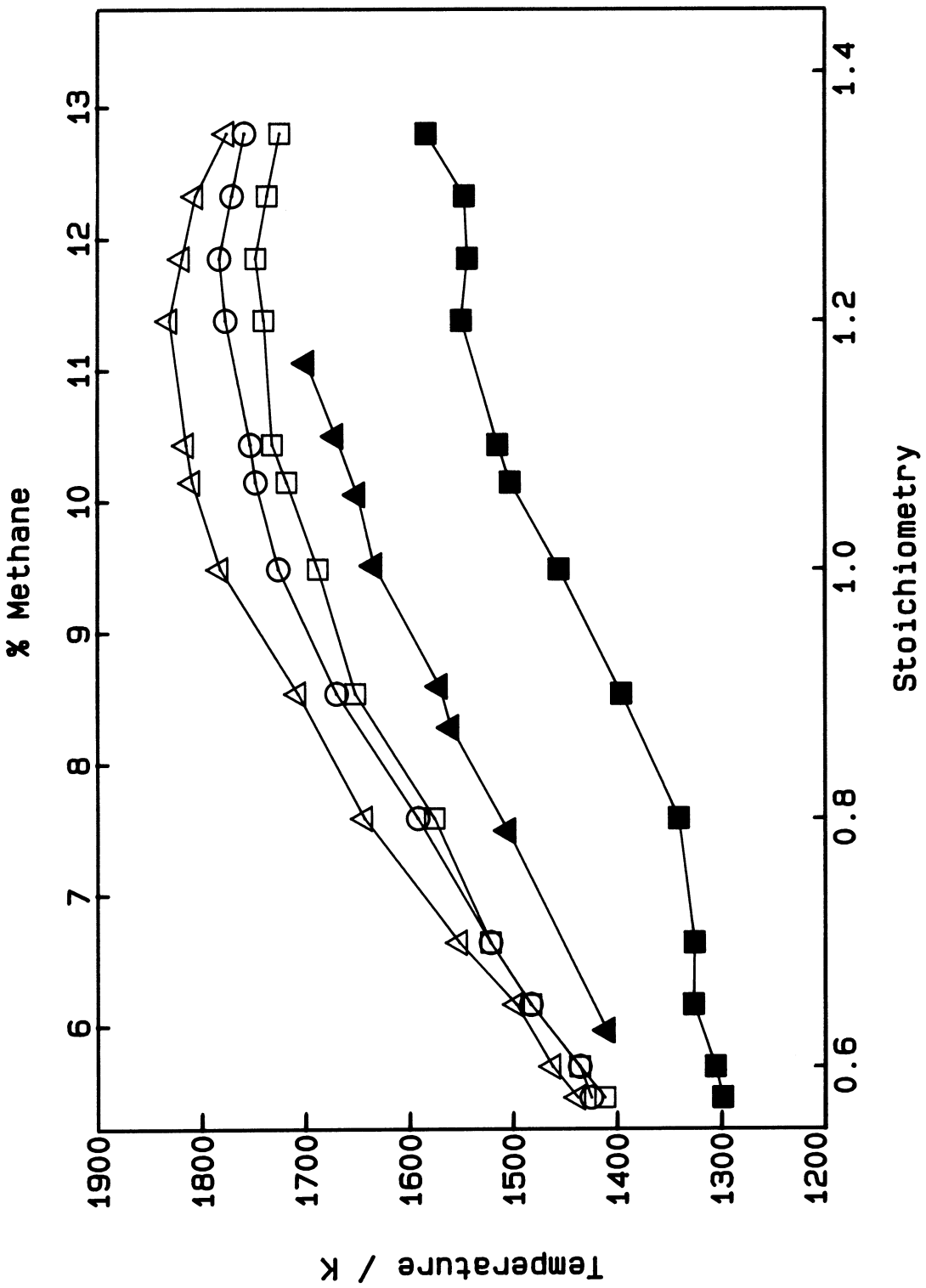

FIGURE 50

Temperatures of various flame surfaces *vs* pressure
for stoichiometric methane/air flames
■ : Reference surface. ○: Maximum heat release.
□ : Maximum fuel consumption. △ : "Ignition temperature" of Dixon-Lewis[89].

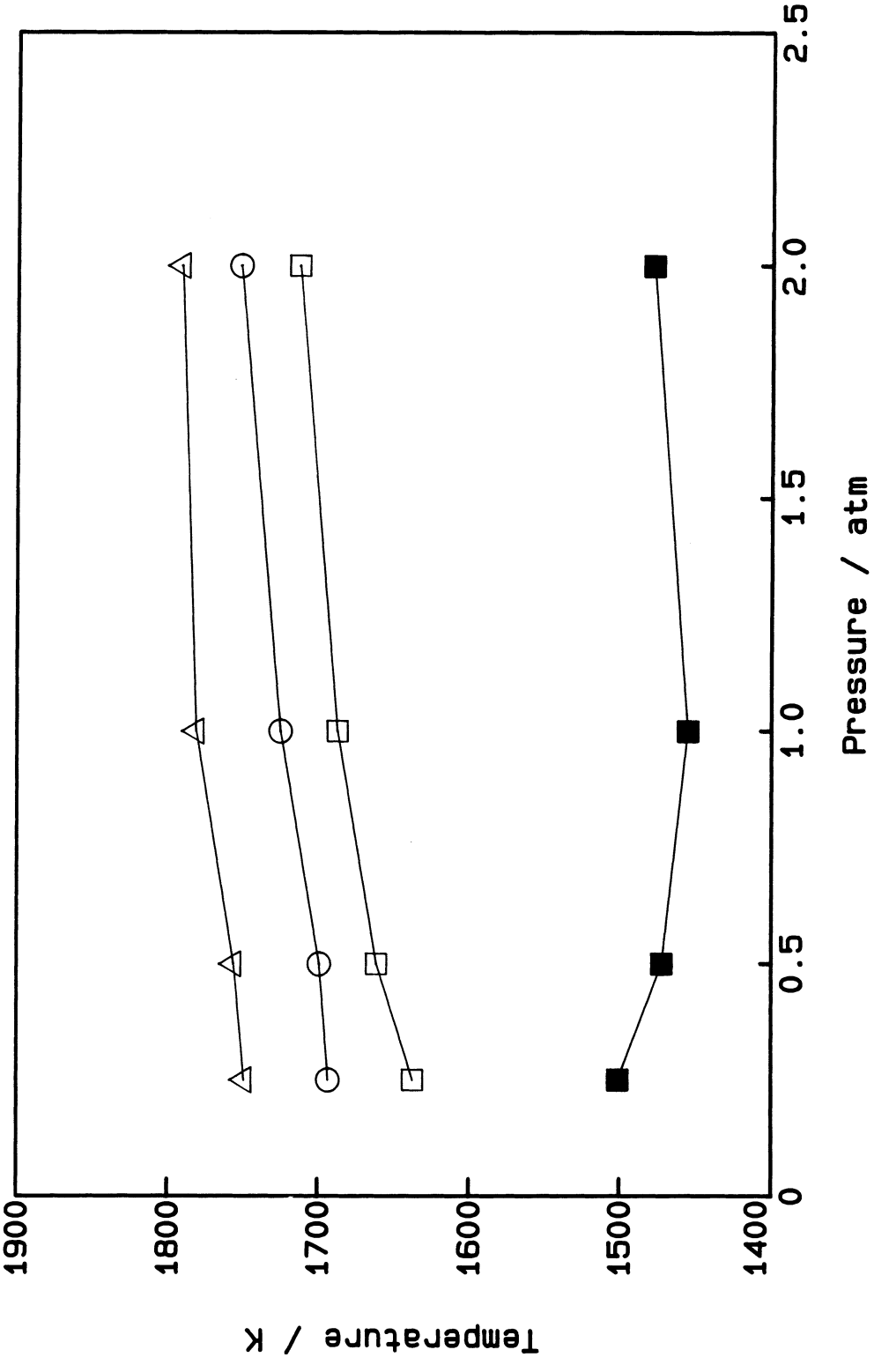

FIGURE 51

Temperatures of various flame surfaces *vs* stoichiometry for ethane/air flames

■ : Reference surface. ○: Maximum heat release.

□ : Maximum fuel consumption. △ : "Ignition temperature" of Dixon-Lewis[89].

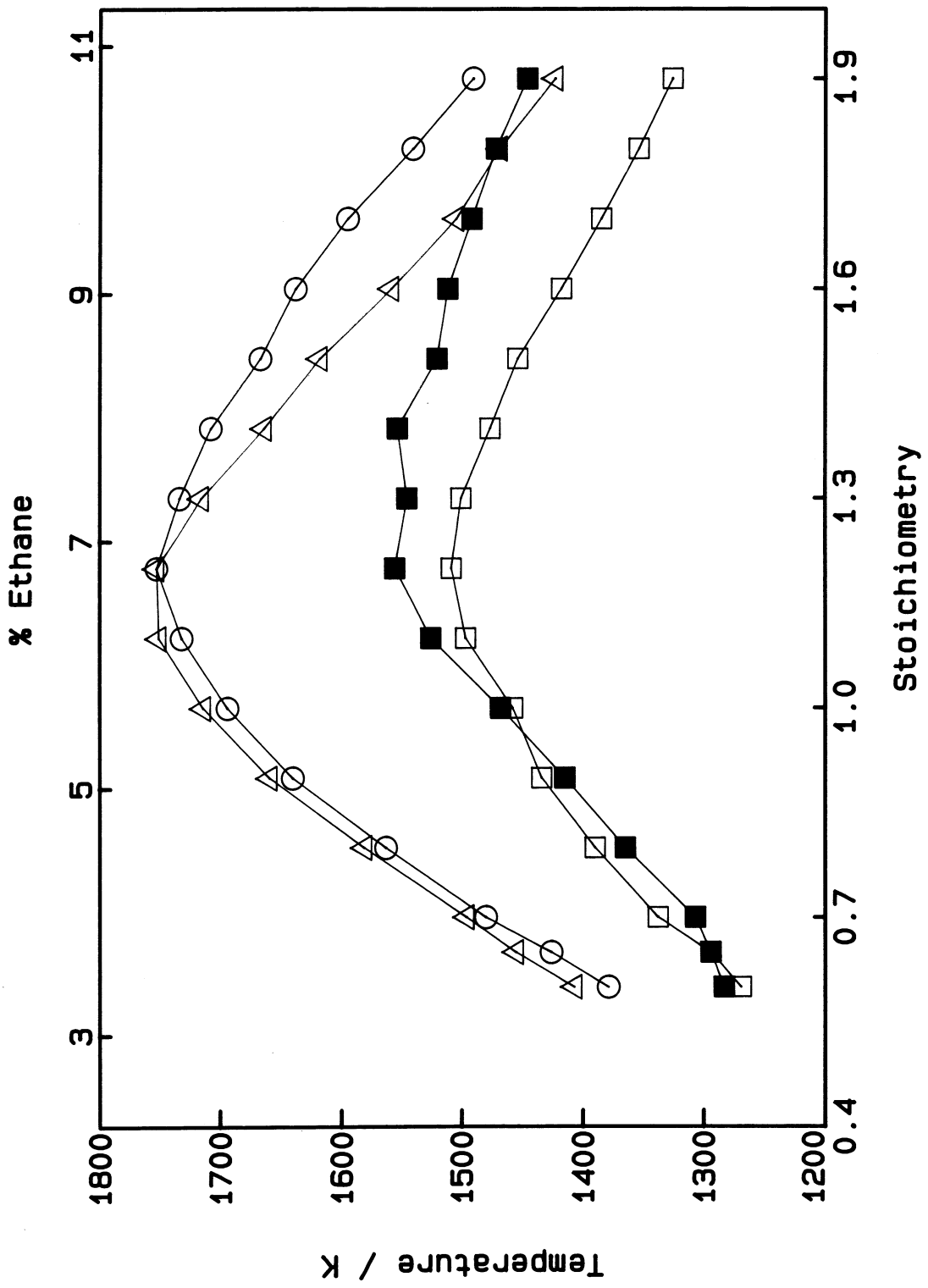

FIGURE 52

Temperatures of various flame surfaces *vs* stoichiometry for propane/air flames

■ : Reference surface. o: Maximum heat release.

□ : Maximum fuel consumption. △ : "Ignition temperature" of Dixon-Lewis[89].

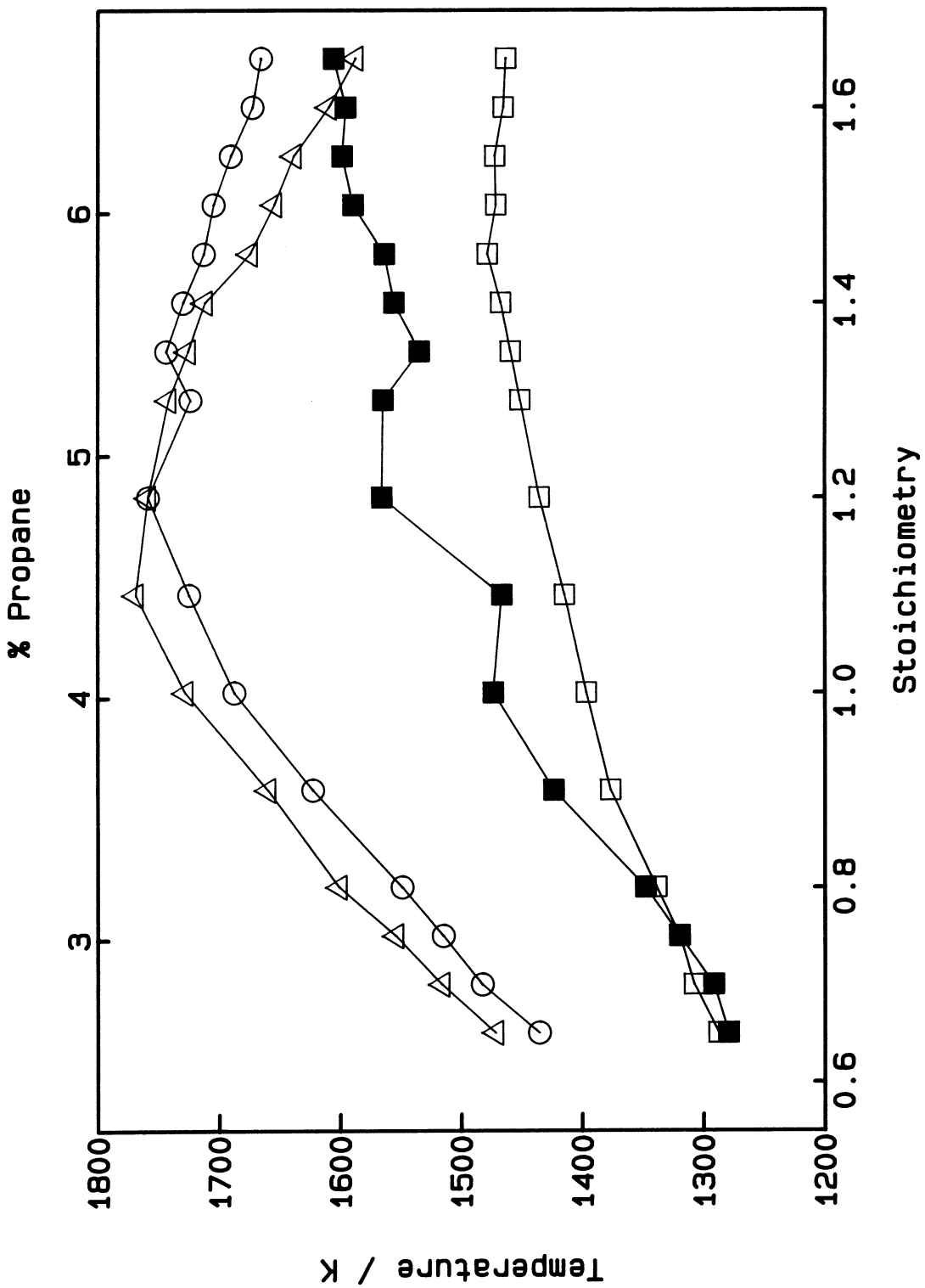

FIGURE 53

Temperatures of various flame surfaces *vs* stoichiometry for ethylene/air flames

■ : Reference surface. ○: Maximum heat release.

□ : Maximum fuel consumption. △ : "Ignition temperature" of Dixon-Lewis[89].

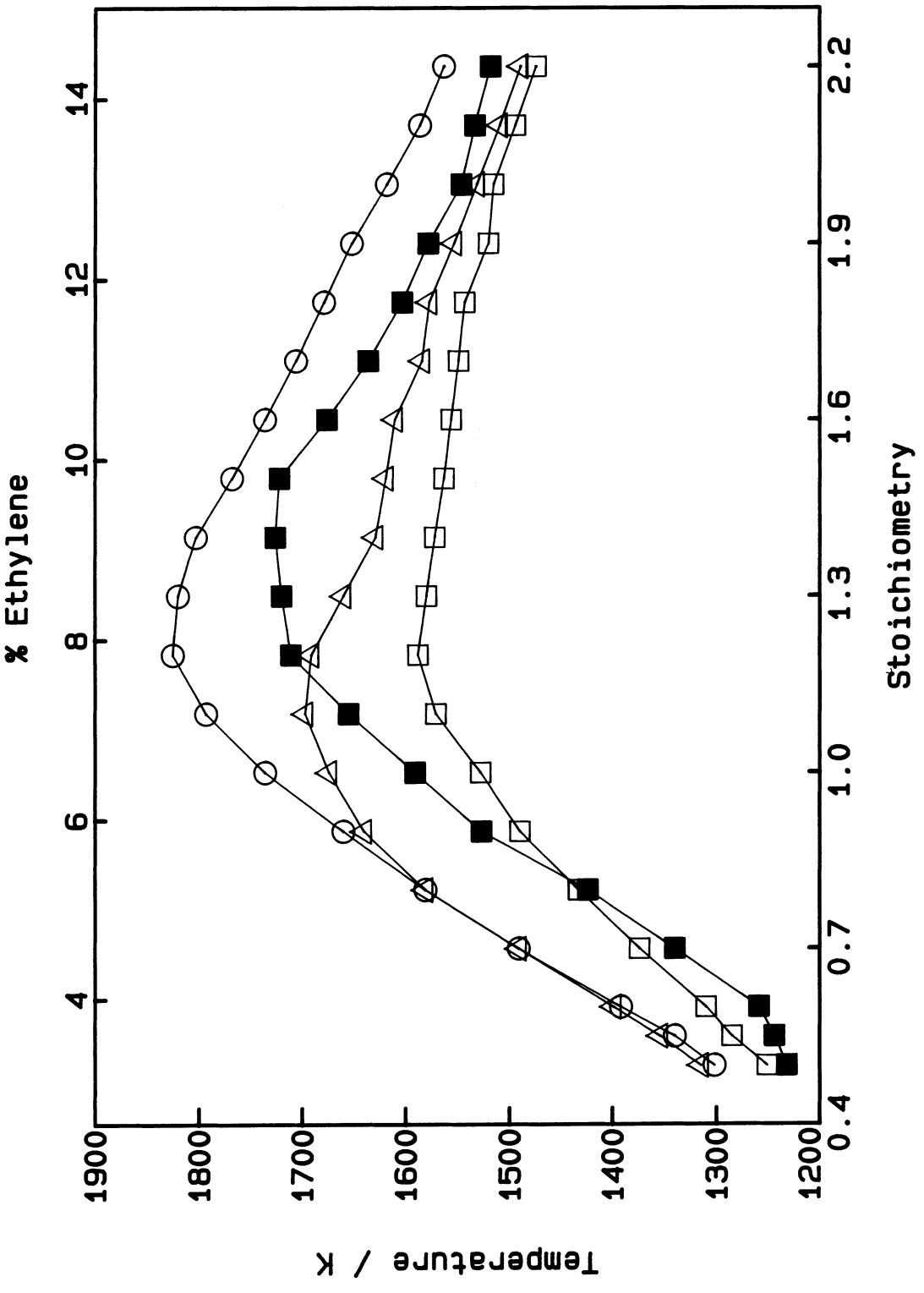

position be determined? The cold boundary, for example, is too poorly defined to provide a suitable fixed point.

The reference surface temperatures for each set of experimental conditions are plotted in Figs. 47 to 53 as filled squares. For comparison, temperatures corresponding to three other physical surfaces within the flame have been plotted on the same axes. T_i (open triangles) and the temperature at maximum heat release rate (open circles) were mentioned in the previous section. In addition, the temperature at maximum fuel consumption rate (open squares) has been included. For comparison purposes, the reference surface temperatures calculated by Dixon-Lewis and Islam[22] for hydrogen and methane flames have been plotted as filled triangles in Figs. 47 and 49.

6.3.3 Calculation of the flame thickness parameter

If flame stretch had no influence on an expanding spherical flame, its speed would still vary with radius because of a flame thickness effect. This arises from the changing mean density (due to curvature) of the burnt gas inside the reference surface. As shown in Chapter 3, the effect can be described by a density function $f(r)$ of the form $1 + k/r$. In this section we calculate the flame thickness or density constant k from the modelling results.

It turns out that the $1/r$ dependence is approximately, but not precisely, satisfied. While this does not significantly degrade the performance of the simple model, as will be shown by the tests in Section 6.4.2, it does mean that an elaborate method of computing k is not necessary.

The constant k was calculated from the modelling results for each fuel/air mixture as follows. For simplicity, we will identify the radius r of the expanding flame with the radius of its reference surface. The mean density inside the reference surface is given by

$$\overline{\rho}_b(r) = \frac{3}{r^3} \int_0^r \rho(r') r'^2 \, dr' . \qquad (1)$$

If the density profile $\rho(r')$ were known for a range of flame radii r then the mean density could be calculated at each value of r. Such detailed information is not available for all of the experimental conditions. In principle, it could be obtained

from modelling of expanding flames. But this is not currently practicable; for hydrocarbons in particular, the heavy use of computer resources would probably not be justified.

In the derivation of the simple model in Chapter 3, the expanding flame was taken to be a perturbed one-dimensional one. In the same spirit, we assume that the density profile $\rho(r')$ of the expanding flame at any radius r is that of the corresponding planar one-dimensional flame. The planar profile is mapped onto the expanding flame by fixing the density at the reference surface. As the spherical flame expands, it "drags" the profile with it. Conditions at zero radius are dealt with by truncating the profile or extending it as necessary. In terms of equation (1), the density at r' in a flame of radius r is equal to the density in the planar one-dimensional profile at $x = x_{ref} + r - r'$ where x_{ref} is the value of x at the reference surface. The negative sign arises because in the planar modelling increasing x corresponds to moving from unburnt to burnt conditions, while in an expanding spherical flame increasing r' corresponds to moving from burnt to unburnt.

The large number of zones in the computations means that the integral in equation (1) can be replaced by a summation

$$\overline{\rho}_b(r) = \frac{3}{r^3} \sum_{i=c}^{ref} \rho_i \times (x_i - x_c)^2 \times |x_i - x_{i-1}| \qquad (2)$$

where ref and c are the subscripts of the zones in the planar computation at the reference surface and at $x = x_{ref} + r$ respectively. Trial computations were performed using this modified expression at a series of values of r over the experimental range 5 to 35 mm. The calculated mean density was found to vary linearly with $1 / \text{radius}$. This is expected if the form of the density function is $f(r) = 1 + k/r$ as derived in Section 3.2.2. A consequence of this form of the expression is that the density function in equation (3-6) is given by

$$f(r) = [\overline{\rho}_b + (r/3)\, d\overline{\rho}_b/dr] \;/\; \rho_b{}^{\circ}$$

$$= (2/3)\overline{\rho}_b/\rho_b{}^{\circ}. \qquad (3)$$

Equation (3) was therefore used to determine the density function $f(r)$ at a range of radii r, with the mean density calculated using equation (2). Another consequence of

the assumption that $f(r) = 1 + k/r$ is that if $[f(r) - 1]$ is plotted against r^{-1} then the slope is equal to k. In order to provide optimum accuracy, $f(r)$ was calculated at values of r corresponding to equally spaced values of r^{-1}. Eight values of r were used over the range 5 to 35 mm and the slope of the $[f(r) - 1]$ *vs* r^{-1} plot was determined by linear regression. A computer program KCALC3 was used to perform these computations and determine k from a given density profile and reference surface position.

Values of the calculated flame thickness parameter k along with the experimentally determined values of b are plotted in Figs. 16, 23, 30, 34 and 39 for hydrogen, methane, ethane, propane and ethylene mixtures with air respectively. Figs. 19 and 26 contain the data for nitrogen-diluted stoichiometric hydrogen/air mixtures and stoichiometric methane/air mixtures at different pressures. It is noticeable that hydrogen-containing mixtures have larger k values than hydrocarbons. While the mean value of k for the hydrogen mixtures was around 0.57 mm, that for the rest of the mixtures studied was about 0.19 mm.

6.3.4 Determination of Markstein lengths

It is now possible to determine the Markstein lengths for all the expanding spherical flames studied. This was done using equation (3-13), reproduced below.

$$L = (b - k)\ \sigma/2. \qquad (4)$$

Values of b were obtained from the experiments and k from the modelling, as described in the previous section. The density ratio σ was calculated using the flame temperature program FTEMP.

The Markstein lengths determined using this procedure are plotted in Figs. 54 to 60. In all cases except the variable-pressure methane results, the smooth curve through the points was obtained by fitting equation (2-187) to the data by using the best low-degree polynomial fit to the $\beta(\mathrm{Le} - 1)$ term. The good fit of the curves therefore does not have any quantitative significance, but it does demonstrate that the theory has the correct qualitative form. Regions where the curve does not pass through the points (e.g. lean hydrogen/air mixtures) are suggestive of systematic error in the experiments.

Markstein lengths for hydrogen/air mixtures as a function of stoichiometry are plotted in Fig. 54. The main point to notice is that the Markstein lengths are negative in lean mixtures (stretch increases the burning velocity) and positive in rich mixtures (stretch decreases the burning velocity).

Markstein lengths for stoichiometric hydrogen/air mixtures diluted with nitrogen are shown in Fig. 55. They become negative at a dilution of about 15%, suggesting that a Lewis number effect is operating. This is covered in Chapter 7.

Methane/air Markstein lengths as a function of stoichiometry are plotted in Fig. 56. The data are qualitatively similar to hydrogen: they are negative in lean mixtures and positive everywhere else.

Figure 57 shows that the Markstein length of a stoichiometric methane/air mixture increases as the pressure is decreased. The curve fitted through the data has the form

$$L = L(p = 1 \text{ atm})\ p^{x} \qquad (5)$$

where $x = -1.16 \pm 0.11$. The Markstein length is therefore roughly inversely proportional to pressure. This behaviour will be discussed in Chapter 7.

Ethane/air Markstein lengths are plotted in Fig. 58. The most important point is that the behaviour is qualitatively opposite to that of methane and hydrogen. The data are positive in lean and stoichiometric mixtures and become negative in rich mixtures.

Markstein lengths for propane/air mixtures are plotted in Fig. 59. The data are qualitatively similar to those of ethane and opposite to those of methane and hydrogen: they are positive in lean and stoichiometric mixtures and negative in rich.

Ethylene/air Markstein lengths are plotted in Fig. 60. Unlike all of the other mixtures, they do not vary monotonically with stoichiometry. Ethylene therefore appears to be an intermediate case between the light gases hydrogen and methane and the heavy gases ethane and propane.

FIGURE 54

Markstein length *vs* stoichiometry for hydrogen/air flames

Points: Experimental results. Curve: Theory of Clavin and Joulin[55] fitted to results.

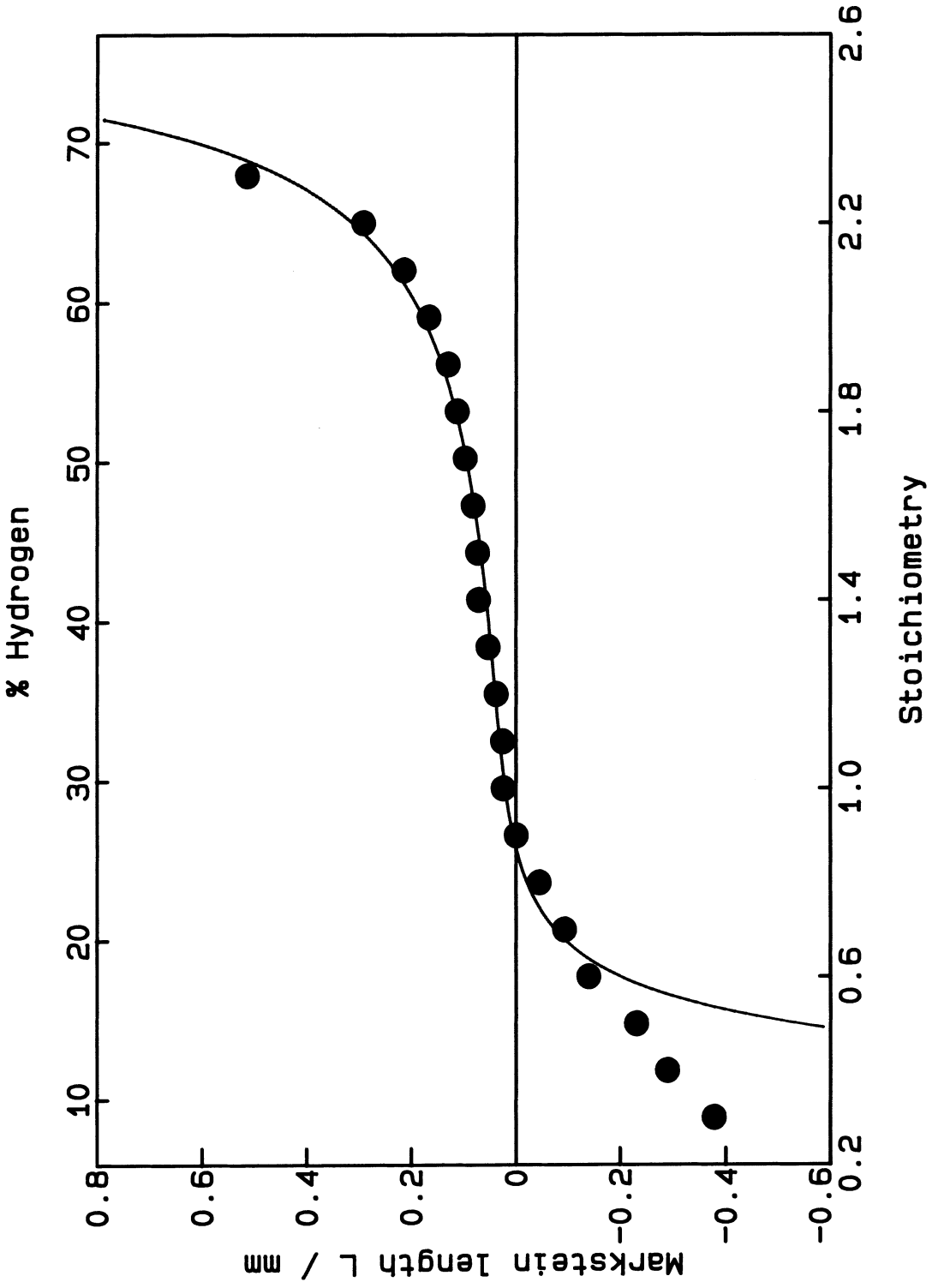

FIGURE 55

Markstein length *vs* nitrogen dilution for stoichiometric hydrogen/air flames
Points: Experimental results. Curve: Theory of Clavin and Joulin[55] fitted to results.

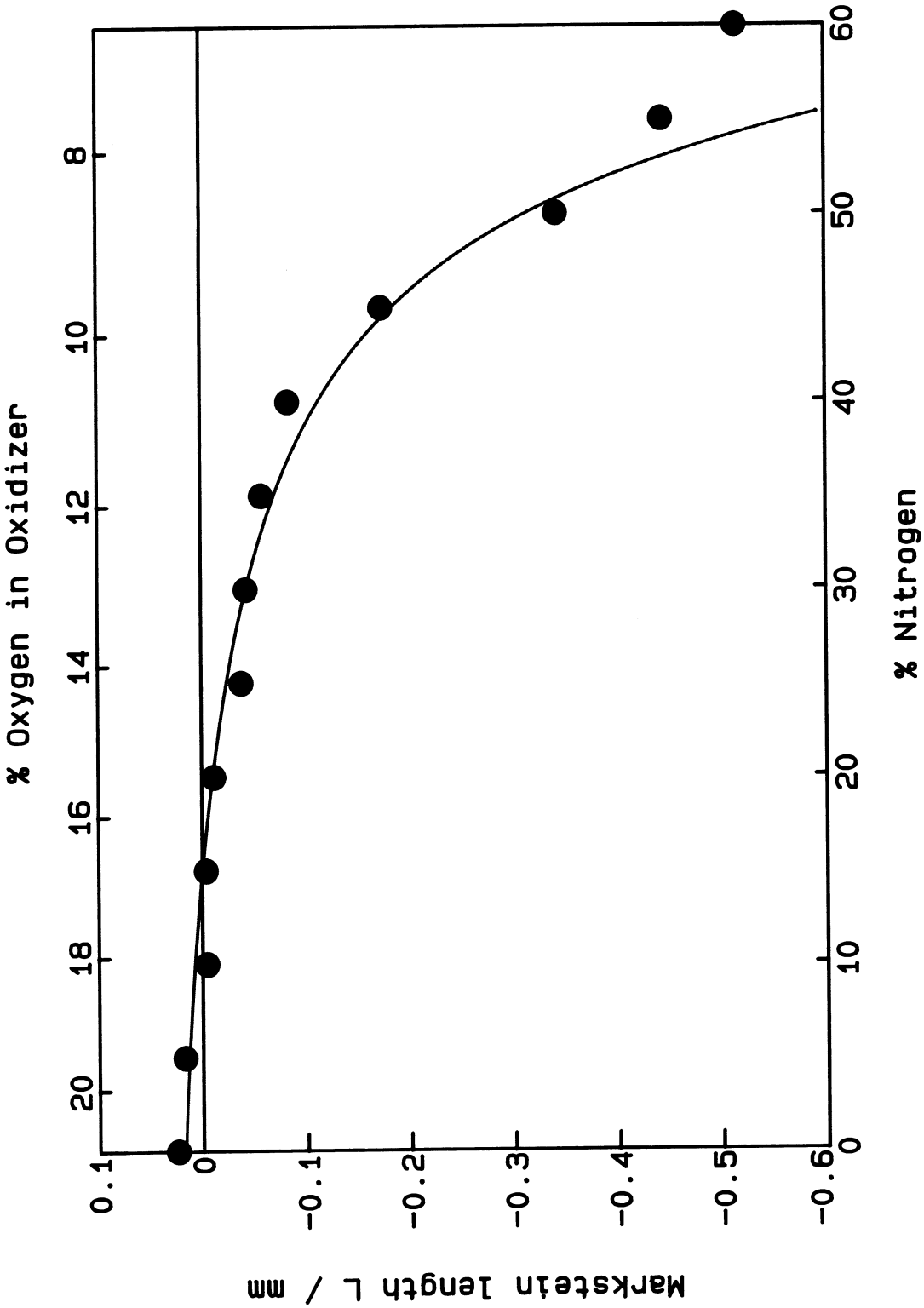

FIGURE 56

Markstein length *vs* stoichiometry for methane/air flames

Points: Experimental results. Curve: Theory of Clavin and Joulin[55] fitted to results.

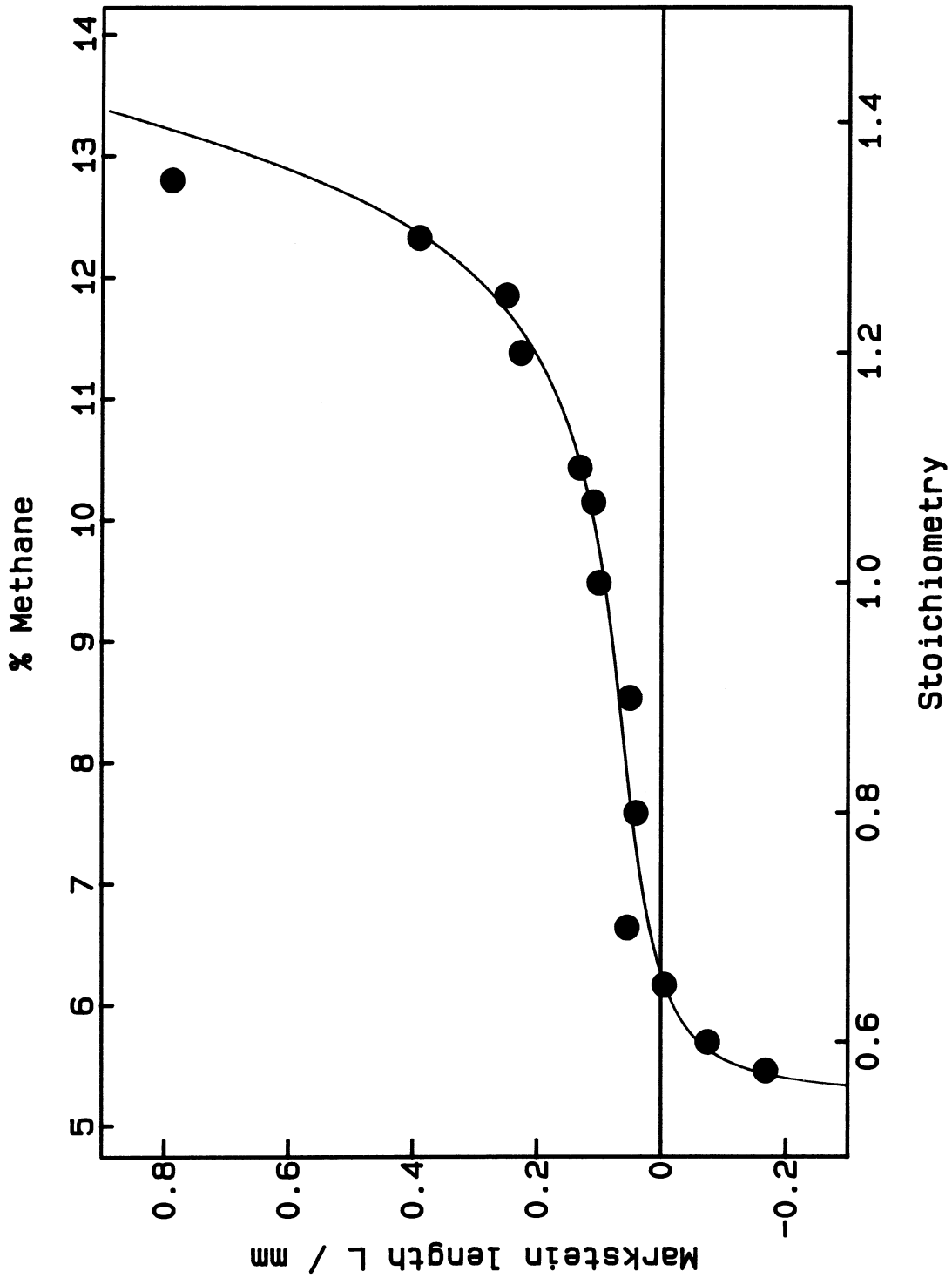

FIGURE 57

Markstein length *vs* pressure for stoichiometric methane/air flames

Points: Experimental results. Curve: $L = L_0 p^x$ fitted to results.

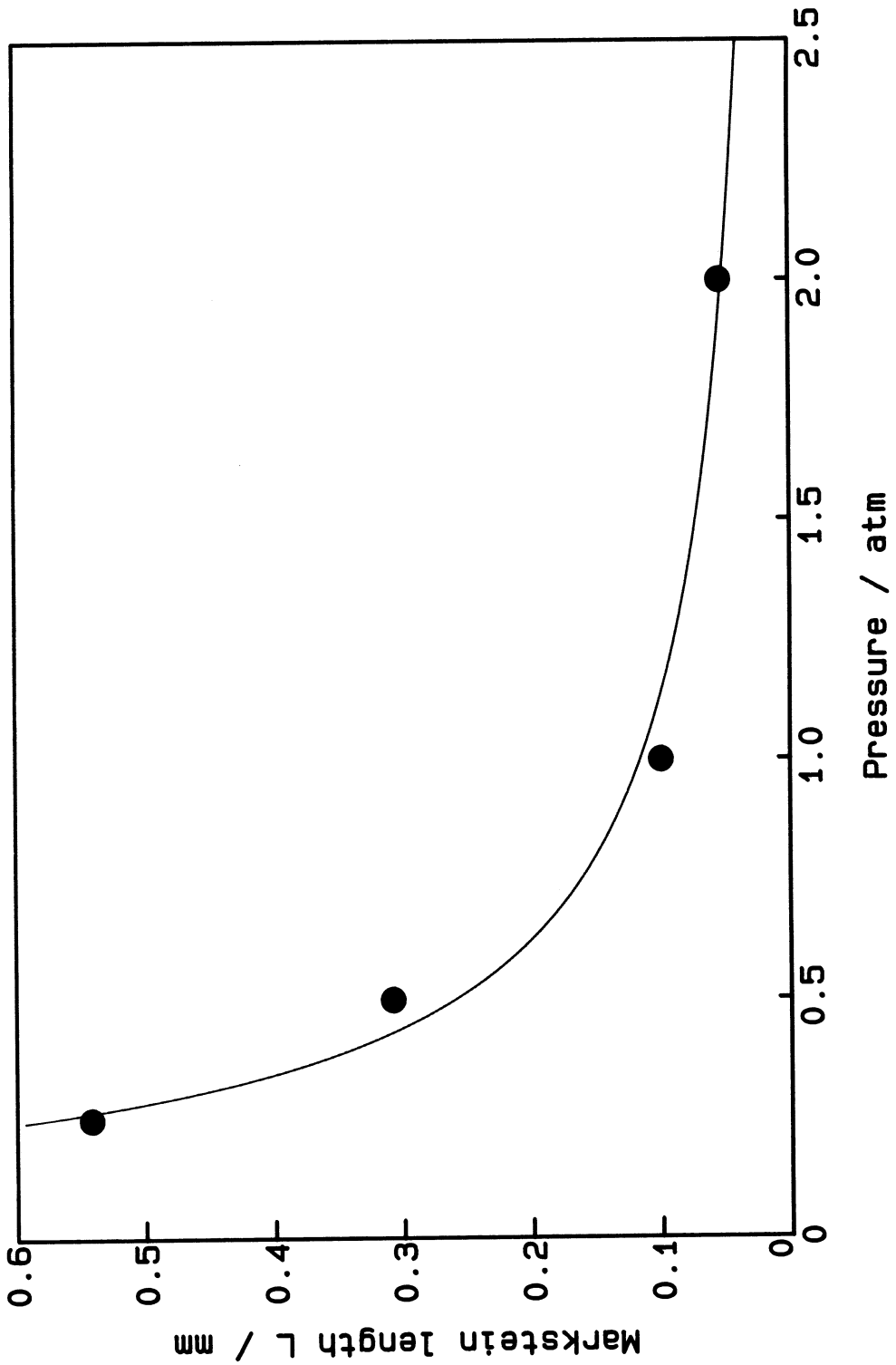

FIGURE 58

Markstein length *vs* stoichiometry for ethane/air flames
Points: Experimental results. Curve: Theory of Clavin and Joulin[55] fitted to results.

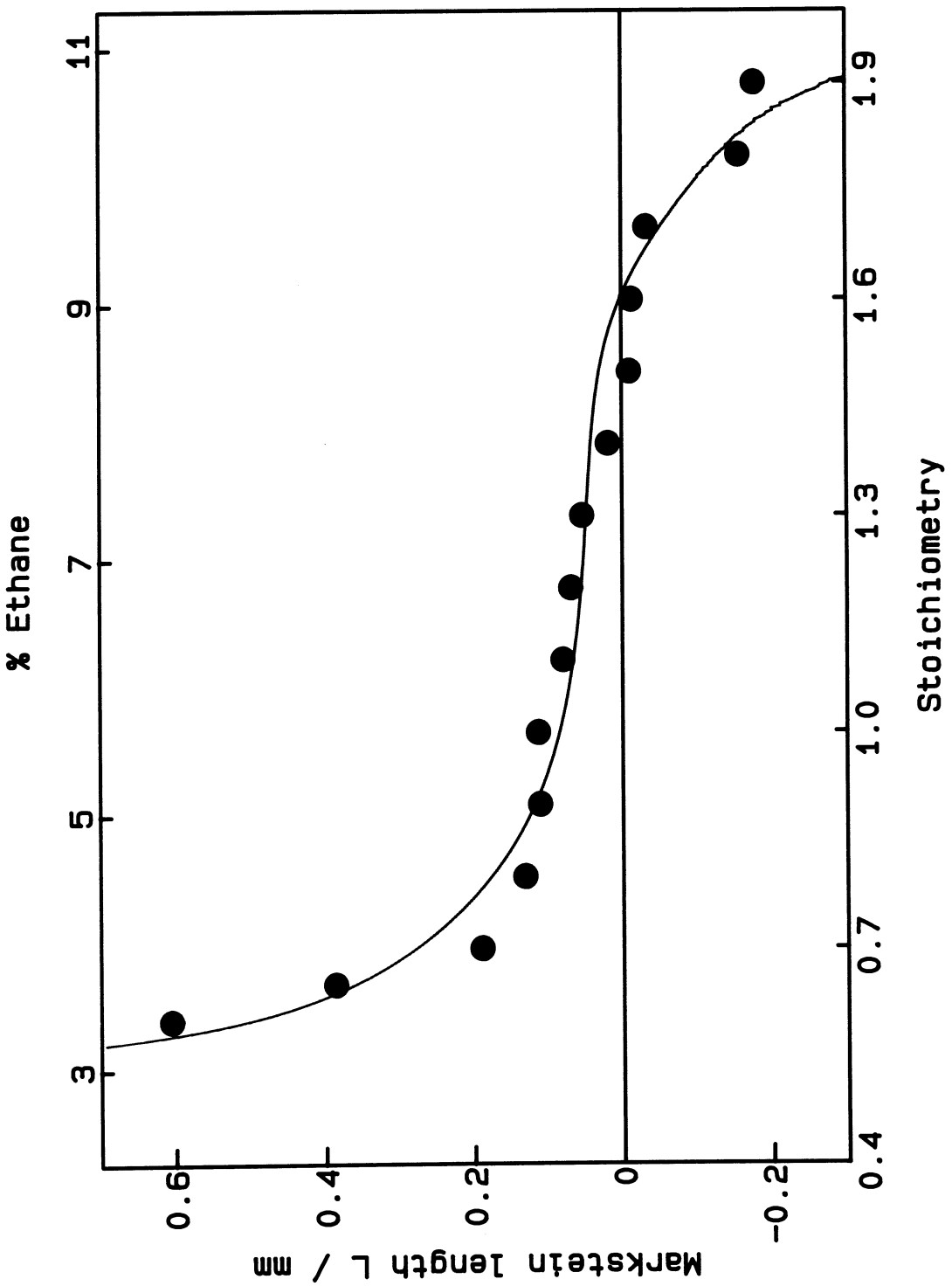

FIGURE 59

Markstein length *vs* stoichiometry for propane/air flames

Points: Experimental results. Curve: Theory of Clavin and Joulin[55] fitted to results.

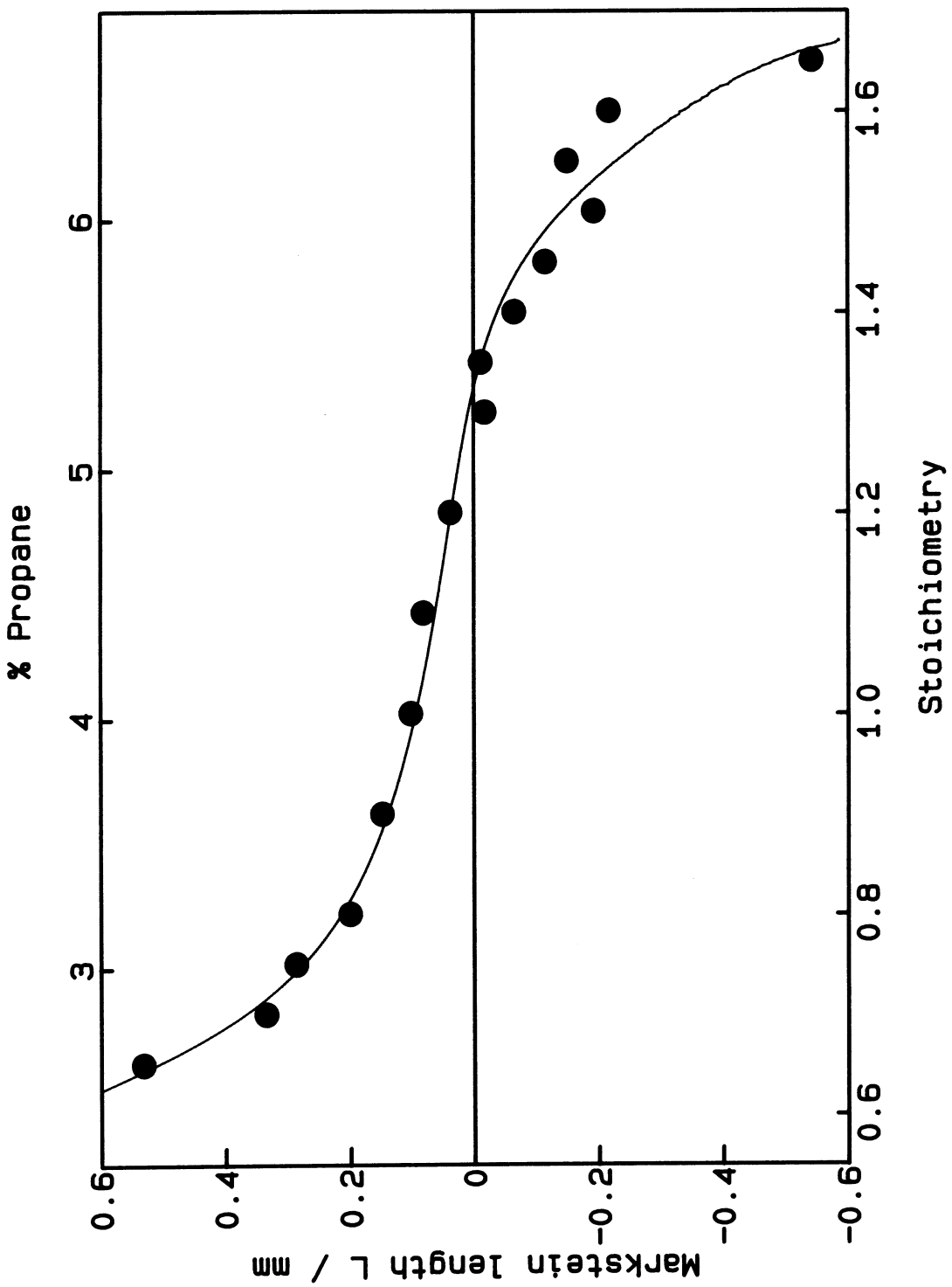

FIGURE 60

Markstein length *vs* stoichiometry for ethylene/air flames

Points: Experimental results. Curve: Theory of Clavin and Joulin[55] fitted to results.

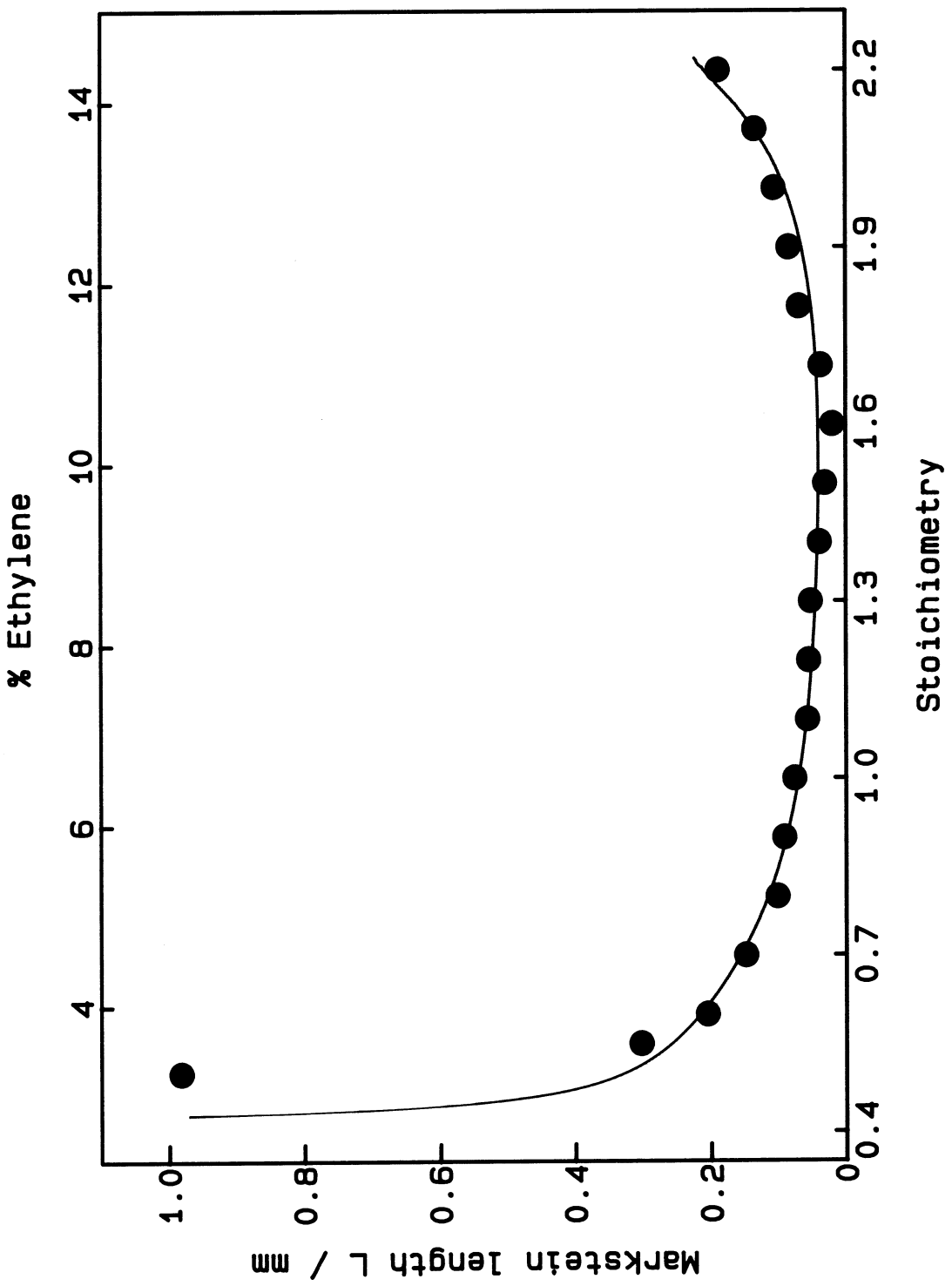

6.4 MODELLING OF EXPANDING SPHERICAL FLAMES

The results of detailed modelling of expanding flames are presented in this section. Attention is focused on the flame speed as a function of radius. The data are exclusively for hydrogen mixtures except for one methane run. They are compared with experimental results in the first section and then used to test the experimental methodology in the second.

6.4.1 **Comparison with experimental results**

The main function of the expanding flame modelling was to test the validity of the experimental methodology. The tests are described in the next section. But for such tests to be valid, it is necessary to demonstrate that the predictions of the detailed model are in accord with the experimental results. Direct comparisons of modelled and experimental flame speeds were performed. In addition, modelled and experimental flame relaxation parameters were compared. The latter procedure must be viewed with some caution since the flame relaxation parameters are obtained using the simple model whose validity is to be tested in the next section. Nevertheless, the comparison does give some measure of the agreement between model and experiment.

Modelled flame speed *vs* radius data for a selection of hydrogen/air mixtures are plotted in Fig. 61 along with corresponding experimental data. Within the experimental uncertainties (which are magnified in such a plot by differentiating the experimental data) the agreement is good: experiment and model show the same general trends.

In the lean mixtures, the measured speeds have been included beyond the onset of cellularity, which occurs at radii of about 19 mm and 24 mm for stoichiometries of 0.6 and 0.7 respectively. This has been done to demonstrate the effect of cellularity on the flame speeds. The modelling, being mathematically one-dimensional, does not predict cellularity. In the region where model and experiment are directly comparable, the experimental speeds fall rather more rapidly than the modelled.

The comparison of modelled and experimental values of the flame relaxation parameter b for hydrogen/air in Fig. 16 shows that there is good agreement over most of the stoichiometric range. In very rich and in lean mixtures, though, differences arise. We will see in the next section that the simple model does not work well in mixtures with negative values of b. In this case, the same systematic

FIGURE 61

Comparison of experimental and modelled speeds
of expanding spherical flames in hydrogen/air mixtures
•: Experimental points (cellular region denoted by ○). Other symbols: Results of detailed expanding flame modelling. Numbers on right denote stoichiometry.

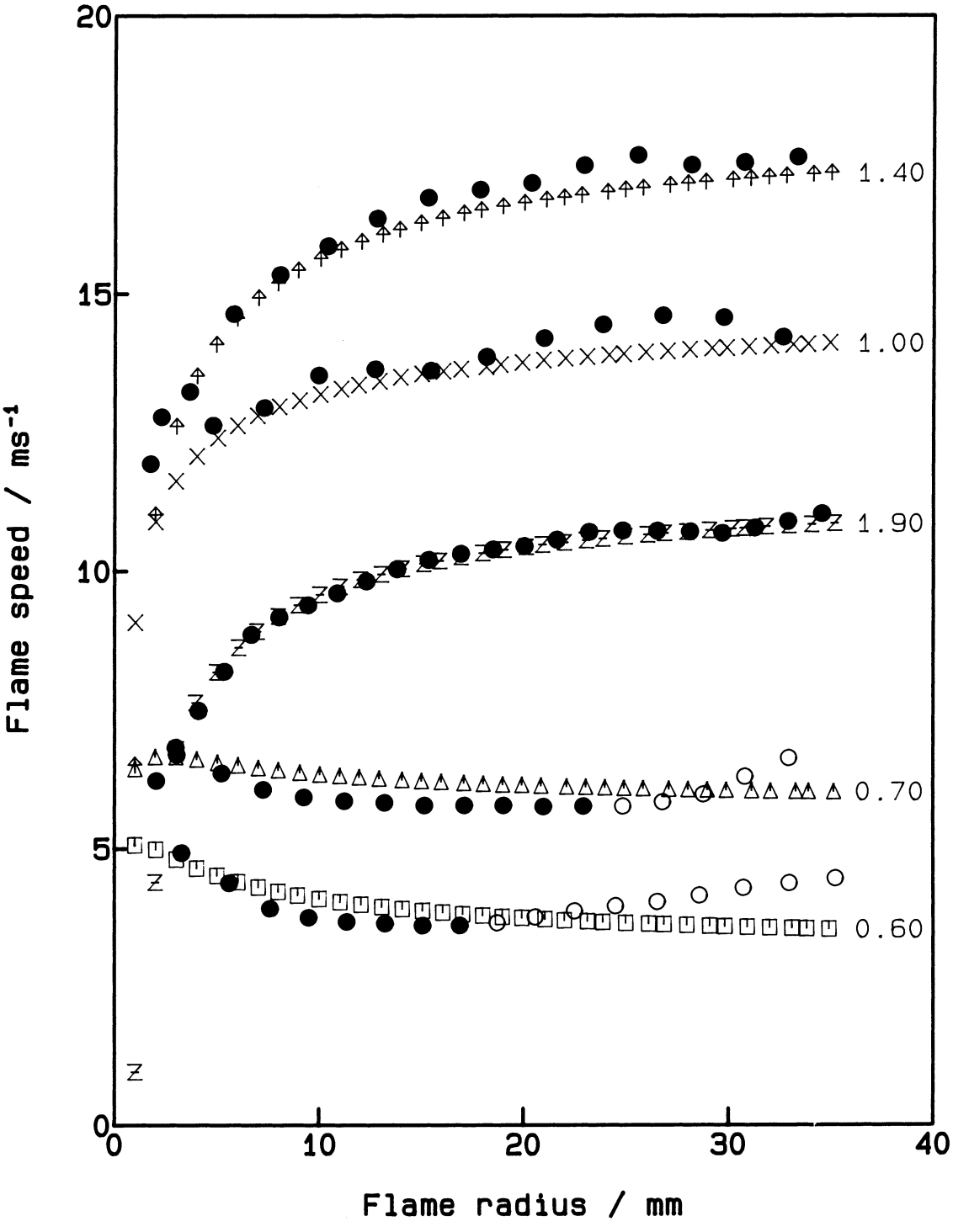

error might be expected in modelled and experimental values of *b* so that they agree, but differ from the theoretical curve. But analysis of the experimental results was limited to radii before the onset of cellularity, which was frequently less than the maximum flame radius of 35 mm used for the modelling results. If the modelling results were analysed over the same range as the experiments, the derived burning velocities and flame relaxation parameters agreed more closely with the experiments.

Modelled values of *b* for nitrogen-diluted stoichiometric hydrogen/air mixtures are plotted in Fig. 19 along with experimental data. Again, agreement between modelling and experimental *b* values is very good. In very dilute mixtures, both experimental and modelled values of *b* drift away from the theoretical trend given by the solid line. This is probably for the same reason as in lean hydrogen mixtures. In the present case, though, the flames did not become cellular, so agreement between model and experiment exists at all dilutions.

The flame relaxation parameter *b* obtained for the methane/air run was 1.868 mm, in good agreement with the experimental value of 1.80 ± 0.18 mm.

6.4.2 **Test of the expanding spherical flame methodology**

An important feature of the expanding flame method of determining burning velocity studied in the present work is that it is testable. A simple model is used to extrapolate flame speed measurements of laboratory-scale expanding spherical flames to infinite radius. As described in Chapter 3, only two assumptions are made in the model, and both appear to be reasonable. But apparently reasonable assumptions can have a limited range of validity or just be plain wrong. It will be argued later that another burning velocity determination method involving extrapolation suffers from exactly this problem, and so gives inaccurate results.

In the present work, the testing was done by applying the simple model to the results of detailed simulations of expanding spherical flames. These simulations were performed using the code described in Section 6.1.2.2. The simple model was applied to the radius *vs* time data predicted by the detailed simulations just as if they were experimental results. The flame speed predicted by the simple model was therefore an estimate of the one-dimensional flame speed. But in this case the true one-dimensional flame speed was already known from previous runs of the planar one-dimensional version of the flame code using the same kinetic scheme. A comparison could therefore be made between the estimated and true values. This gave a good

way of gauging the accuracy of the simple model when applied to experimental radius *vs* time data.

Detailed comparisons were performed for hydrogen flames, for which the computational cost of the expanding flame model was not too great. For these flames, the "ignition energy" was varied until it was at the minimum. This could be done by changing the height or the width (or both) of the initial Gaussian temperature profile at $r = 0$. In the present work the temperature maximum was kept constant at 5000 K and the width at half-height was varied. Typical values were of the order of 0.5 mm.

For hydrocarbon flames, the long execution times (ca. 3 days of CPU time on a VAX 8530) and some problems with ignition meant a successful run was only achieved for a single methane/air mixture. In order to produce this, it was necessary to "ignite" the mixture with a hydrogen/air mixture. In addition, the present C_2 scheme would not run successfully. The only scheme which gave a successful run was an older one containing slightly different rates from those in Section 6.2. The expanding flame program is still under development, and clearly some attention will need to be paid to the ignition behaviour.

Listed in Tables 8 and 9 are the values of the flame relaxation parameter b and the one-dimensional burning velocity S_u° obtained by fitting the simple model equation (3-12) to the radius *vs* time data predicted by the detailed expanding flame model. In order to provide conditions as similar to the experiments as possible, the modelled data consisted of flame radii from 1 to 35 mm in roughly 1 mm steps, along with the corresponding times. The burning velocity was obtained from the one-dimensional flame speed by multiplying by the calculated density ratio. Also included in the tables are the true one-dimensional burning velocities, obtained from planar one-dimensional modelling using the same kinetic scheme. In order to fit in with the experimental results, the initial temperature corresponding to the data in Table 8 was 296 K while in Table 9 it was 298 K.

A selection of the modelled flame speed *vs* radius data for hydrogen flames at different stoichiometries is shown in Fig. 62. Smooth curves representing the best fit of the simple model have been drawn through the modelled points. The simple model follows the detailed results very closely except at small radii where differences would be expected.

FIGURE 62

Hydrogen/air flame speed *vs* radius predicted by detailed modelling and fitted by simple model

Symbols: Results of detailed expanding flame modelling. Curves: Equation (3-10) fitted to modelled results. Numbers on right denote stoichiometry.

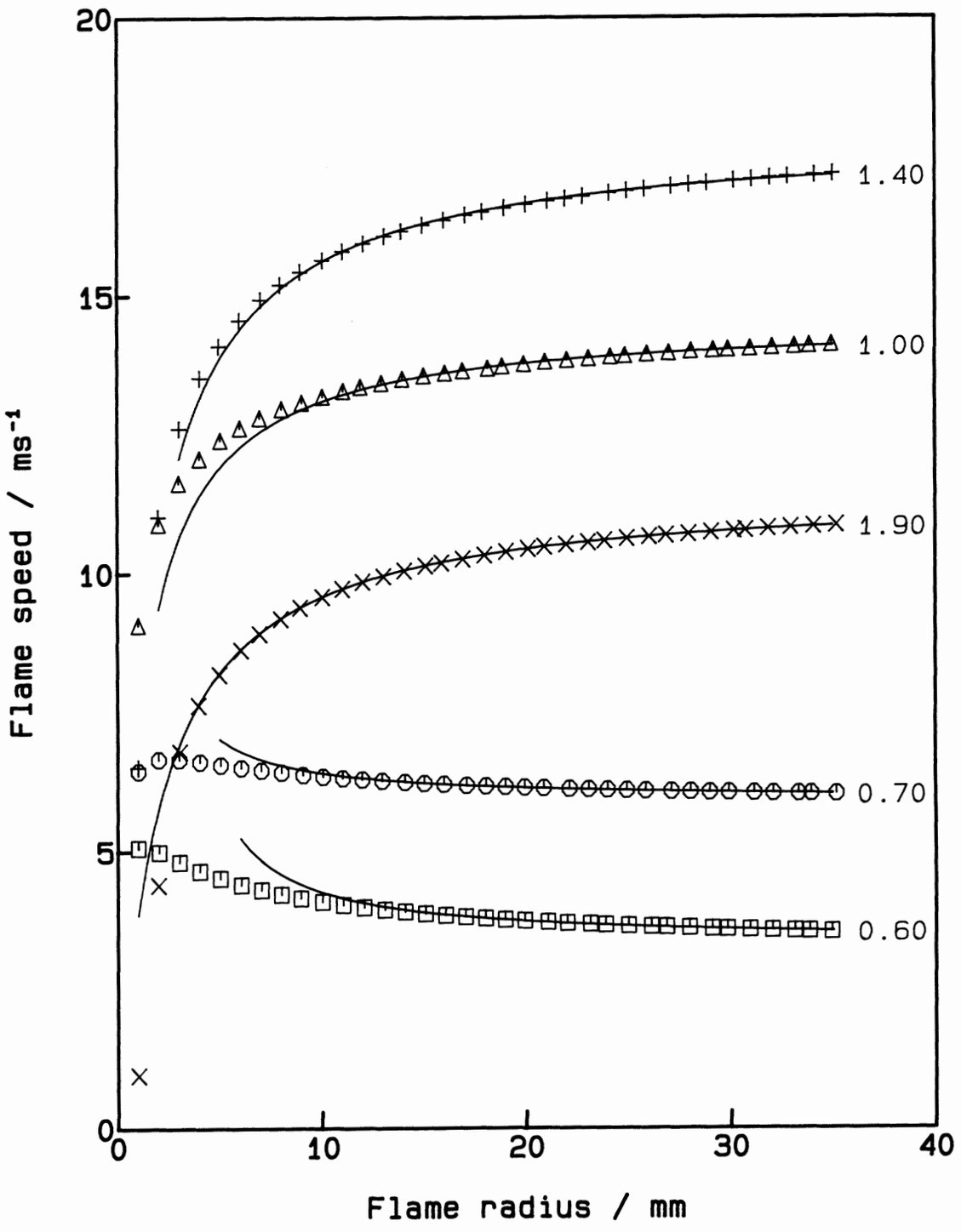

TABLE 8

Comparison of predicted and true burning velocities for modelled hydrogen/air flames

Stoich-iometry	points omttd	b/mm	1-D Burning velocity / ms^{-1} predicted	true	% difference
0.3	27	-12.165	0.035	-	-
0.4	25	-8.148	0.123	0.079	+55.7
0.5	18	-4.486	0.323	0.288	+12.5
0.6	15	-2.194	0.646	0.616	+4.9
0.7	11	-0.809	1.035	1.014	+2.1
0.8	3	0.070	1.426	1.419	+0.5
0.9	6	0.611	1.781	1.795	-0.8
1.0	10	1.108	2.097	2.127	-1.4
1.1	10	1.267	2.371	2.403	-1.3
1.2	7	1.285	2.585	2.617	-1.2
1.3	7	1.351	2.718	2.756	-1.4
1.4	7	1.446	2.769	2.811	-1.5
1.5	7	1.580	2.748	2.785	-1.3
1.6	8	1.675	2.655	2.692	-1.4
1.7	8	1.760	2.513	2.548	-1.4
1.8	3	1.799	2.334	2.368	-1.4
1.9	2	1.976	2.128	2.151	-1.1
2.0	3	2.181	1.906	1.920	-0.7
2.1	3	2.472	1.662	1.666	-0.2
2.2	7	2.864	1.397	1.398	-0.1
2.3	9	3.557	1.128	1.122	+0.5

For stoichiometric methane/air using the earlier kinetic scheme, the planar one-dimensional burning velocity was 0.357 ms^{-1}. When the simple model was applied to the expanding flame run using the same scheme, 10 points were omitted and the results were b = 1.868 mm and S_u° = 0.351 ms^{-1}. The predicted burning velocity is 1.7% lower than the true value.

The results of the test show that for most mixtures the predicted and true burning velocities differ by less than 2.5%. The cases when the disparity is greater correspond to negative values of the flame relaxation parameter *b*. In particular, Table 8 shows that poor results should be anticipated for experiments using very lean hydrogen/air mixtures. The radius at which the optimum fit of the model occurs (indicated by the number of initial points omitted) is so large that a real flame would have become cellular by this stage. Cellularity does not arise in the detailed modelling of expanding flames because the model is one-dimensional.

TABLE 9

Comparison of predicted and true burning velocities for modelled nitrogen-diluted hydrogen/air flames

% N_2	points omttd	*b*/mm	1-D Burning velocity / ms^{-1} predicted	true	% difference
0	8	1.060	2.113	2.149	-1.7
10	4	0.761	1.670	1.709	-2.3
20	10	0.585	1.274	1.294	-1.5
30	6	0.097	0.903	0.907	-0.4
40	10	-0.720	0.575	0.562	+2.3
50	20	-2.809	0.300	0.279	+7.5
60	20	-3.692	0.132	0.090	+46.7

Chapter 7

DISCUSSION

In this chapter we discuss the experimental methods, the results of the experiments and the modelling, and the implications of the work.

In the first section, the two experimental methods used in this work to obtain one-dimensional burning velocities and Markstein lengths are compared. It is shown that results from the expanding spherical flame experiments are superior in every way to those obtained from flames in stagnation-point flow. The rest of the discussion is therefore largely about the expanding flame work.

The second section deals with burning velocities. Some general observations are made on the results, and this is followed by a discussion of the physical meaning of the reference surface. Next, a specification is drawn up for obtaining good burning velocity data, and previous experimental methods are compared with it. Some methods with claims to give true one-dimensional results are looked at in some detail in the last part.

The third section deals with the experimental values of the Markstein lengths for the different fuel/air mixtures. The results are compared with theory and with the few other data available.

The final section deals with some implications of the present work. The effect of stretch on flame properties like flammability limits and its application to practical combustion devices is considered.

7.1 METHODOLOGIES

Before discussing the results themselves, we consider the two main methodologies used in this work. The basis of both techniques is an extrapolation to zero stretch conditions, so this is studied in some detail. The advantages and disadvantages of the two methods are discussed, and a comparison is performed.

7.1.1 **Expanding spherical flames**

7.1.1.1 Accuracy of extrapolation

The test of the expanding flame method described in Section 6.4.2 demonstrates how well the simple model predicts the one-dimensional burning velocity from modelled expanding spherical flames. As described in the previous section, the experimental expanding flames are very close to being one-dimensional, so that from a geometrical point of view the modelling should represent the real flame behaviour extremely well.

Aspects of the real flame that are not included in the detailed model include thermal radiation from the burnt gas and the effect of the electrodes. Thermal radiation was dealt with in Section 3.2.3 where it was shown to have a negligible effect. Effects of the electrodes include the removal of heat leading to flame quenching and also to cooling of the combustion products. There will also be a "volumetric error" in the flame speed: the flame radius will increase at a slightly greater rate than expected because part of the burnt gas volume is occupied by the electrodes. The effects of heat loss are difficult to quantify, but it seems clear that their influence will wane as the flame becomes larger. The use of small electrodes as in the present experiments should also minimize these effects. The magnitude of the volumetric error can be estimated by a simple calculation in which the electrodes are represented by a single rod passing though the centre of the flame. The ratio of rod volume to flame volume is $1.5(r/R)^2$ where r and R are the radii of rod and flame respectively. If r = 0.8 mm as in the present experiments then the flame radius must reach 9.8 mm before the above ratio falls below 0.01. In fact, this overestimates the effect, because the electrodes are tapered near the tips. The effect on the present experiments can therefore be discounted, but it could be sizeable if the electrodes were bigger.

In view of the above, it seems likely that the detailed modelling of expanding spherical flames represents real flames well. The extremely good predictions of the one-dimensional burning velocity obtained in the tests in Section 6.4.2 suggest that true one-dimensional burning velocity results will be obtained from the experiments. This is the first time that such assurance has been available, and is a strong point in favour of the methodology.

But the method does not always give good results when applied to the detailed modelling. The tests in Section 6.4.2 show that the simple model is not a good fit to

the radius *vs* time behaviour of very lean hydrogen flames. Under such circumstances, the flame speed determined by extrapolation is too high. This is reflected in the experimental results where the burning velocities (in Fig. 15) and the Markstein lengths (in Fig. 54) deviate from the trends predicted by modelling and theory respectively. The situation is made worse in lean hydrogen flames by the early onset of cellularity. Cellularity increases the flame area and thereby the speed of propagation. The experimental data in Fig. 61 show that the onset of cellularity changes an initial downward trend of flame speed *vs* radius to an upward one. The modelled trend continues downwards since cellularity cannot arise in one-dimensional modelling. Cellular flames therefore do not conform to the simple model and if used would lead to incorrect results. So it is necessary to restrict the analysis of lean hydrogen flames to small radii, as in Fig. 13.

We now study the consequences of the poor fit of the model to mixtures with a negative flame relaxation parameter b. Particular reference is made to hydrogen because of the limitations imposed by cellularity. It is of interest to consider whether the simple model can be improved or replaced by a better one in this regime in order to obtain better results from the experiments.

First, the reason for the failure of the simple model needs to be understood. The model contains only two assumptions: that the flame is effectively planar and one-dimensional, and that the effect of stretch on the burning velocity is linear. The flame structure is unlikely to differ from that of a flame of the same radius with a positive flame relaxation parameter, for which the simple model works well. It therefore seems likely that the second assumption is the one that is breaking down. To study this further, we will compare the behaviour of the simple model with the theory of Ronney and Sivashinsky[175]. This is an asymptotic analysis of expanding spherical flames with Lewis number less than 1. It therefore applies to exactly the regime of interest. It contains no flame thickness effect, so in order to perform a comparison with the simple model of the present work it is necessary to set $k = 0$, so that, according to equation (3-11), $b = \ell$.

The relationship between the dimensionless flame speed S and the dimensionless radius R in the Ronney-Sivashinsky model is

$$\frac{dS}{dR} + S^2 \ln S^2 = \frac{2S}{R} - 1 \qquad (1)$$

where l is a heat loss term which we will set to zero for the purposes of the comparison, since heat loss effects are not anticipated. The flame speed S is the speed of the expanding spherical flame dr/dt divided by the one-dimensional burnt gas flame speed S_b°. The dimensionless radius is given by

$$R = \frac{r}{\delta \; B \; I(\mathrm{Le}, T_u/T_b)} \tag{2}$$

where r is the dimensional flame radius, δ is the flame thickness given by equation (2-36), B is the dimensionless activation energy E/RT_b and $I(\mathrm{Le}, T_u/T_b)$ is a function which is positive for Le < 1, zero for Le = 1 and negative for Le > 1. Its magnitude decreases slowly with increasing T_u/T_b. At large radii, dS/dR is negligible and S is close to 1. Using these approximations, it is straightforward to show that equation (1) reduces to

$$S = 1 + 1/R. \tag{3}$$

Expressed in the same form, the simple model of the present work is

$$S = \frac{1}{1 - 1/R} \tag{4}$$

and this also equals equation (3) in the limit of large radii. It follows that the denominator of equation (2) is equal to $-l$ so that, since $k = 0$, $R = -r/b$. We now compare the flame speed *vs* radius behaviour predicted by equations (1), (3) and (4).

Since the equations are in dimensionless form, a single comparison is all that is necessary to deduce the relationships between them. Equation (1) was integrated using a Runge-Kutta method[84] with initial conditions of R and S equal to 10^{-4}. The variation of dimensionless flame speed S with dimensionless radius R according to each of these equations is shown in Fig. 63. Equations (3) and (4) both predict higher flame speeds than the full theory, but equation (3) provides a much closer approximation to it than (4).

Since the Ronney-Sivashinsky theory lacks a flame thickness effect, it is not possible to perform a quantitative comparison with experiment or detailed modelling. We will therefore assume for the moment that the effect of stretch is represented correctly in the theory. We first compare equations (3) and (4) with the full theory and then

FIGURE 63

Flame speed *vs* radius predicted by Ronney-Sivashinsky theory
Solid curve: Ronney-Sivashinsky theory[175]. Dot-dashed curve: Equation (7-3).
Dashed curve: Equation (7-4).

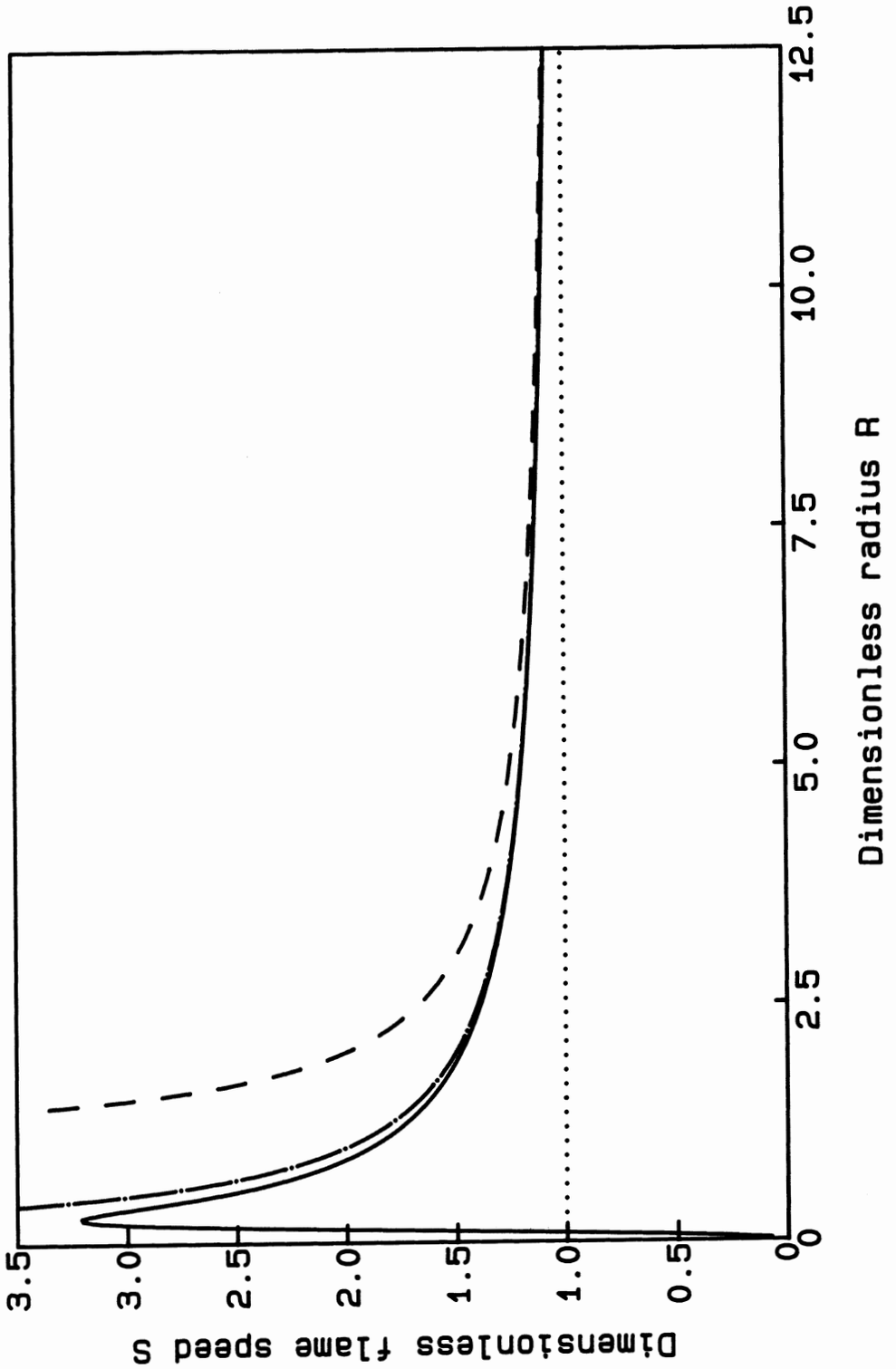

consider whether the replacement of the latter with the former for mixtures with negative b is justified.

It is possible to use the Ronney-Sivashinsky theory to determine the critical radius above which equations (3) and (4) predict the flame speed accurately. It turns out that the dimensionless radius must reach $R_{cr} = 10.188$ before equation (4) predicts a flame speed within 1% of that predicted by the full theory. The corresponding value for equation (3) is $R_{cr} = 2.501$. The dimensional critical radius is

$$r_{cr} = R_{cr}\ \delta\ B\ I(\mathrm{Le}, T_u/T_b). \qquad (5)$$

As a hydrogen/air mixture is made leaner, the last three terms on the right-hand side will all increase. The result is that r_{cr} will increase very rapidly as the mixture becomes leaner. This approach therefore predicts a poor fit of the simple model in lean mixtures of light reactants.

Next, we need to determine how the values of b and S_b° derived using the simple model will be affected when it is not a good fit to the experimental data. A feature of the simple model is that when b is negative the flame speed is infinite at $r = |b|$. An examination of Fig. 63 suggests that the fitting procedure would therefore tend to produce smaller values of b than the correct ones so as to minimize the difference between model and experimental points. The large critical radius for equation (4) suggests that this effect would occur even at large radii. The consequence would be overprediction of the one-dimensional flame speed since the curve would need to level off more quickly to fit the points at larger radius. A check was performed by using the program SBLS9 to analyse the radius *vs* time data corresponding to Fig. 63 with $r/\mathrm{mm} = 10R$ over the range $R = 0.1$ to 3.5 in steps of 0.1. This corresponds to $r = 1$ to 35 mm with $b = -10$ mm and $S_b^\circ = 10\ \mathrm{ms}^{-1}$. The program found no optimum number of points to omit: each time a point was removed, the fit was better. We will consider the case with the arbitrary number of 10 points omitted. The results were $b = -4.596$ mm and $S_b^\circ = 11.277\ \mathrm{ms}^{-1}$. When equation (3) was used in SBLS9 instead of (4), the results were $b = -8.623$ mm and $S_b^\circ = 10.296\ \mathrm{ms}^{-1}$.

It therefore appears that when b is negative, both equations (3) and (4) underestimate its magnitude and overestimate the burning velocity, but the inaccuracies are considerably smaller when equation (3) is used. Two points remain to be discussed: the derivation of a version of equation (3) containing the flame thickness effect, and the justification for using it instead of the standard model given by equation (3-12).

One method of deriving an equation of the form of (3) is to start with an alternative definition of stretch, as was done by Clavin[176]. Use of

$$\Gamma = \frac{2}{r} S_b^{\circ} \tag{6}$$

instead of the standard definition

$$\Gamma = \frac{2}{r} \frac{dr}{dt} \tag{7}$$

in the derivation in Section 3.2.1 leads to the expression

$$\frac{dr}{dt} = S_b^{\circ} \frac{(1 - \ell/r)}{(1 + k/r)}. \tag{8}$$

Integrating equation (8) leads to a new expression relating r and t:

$$r + (k + \ell) \ln (r - \ell) = S_b^{\circ} t + A. \tag{9}$$

There are two disadvantages with this expression. One is that it can only be fitted to a set of experimental results if k is known in advance. But more important is that it was derived from equation (6) which, strictly speaking, is incorrect since it does not conform to the basic definition of stretch.

A better approach is to recall that Clavin's asymptotic expression for the linear variation of burning velocity with stretch is correct up to terms of order ϵ which in the present context means δ/r. It follows that equation (3-10), i.e.

$$\frac{dr}{dt} = \frac{S_b^{\circ}}{(1 + b/r)}, \tag{10}$$

is accurate to the same order since b is roughly the same order of magnitude as the flame thickness δ (in fact it is a little larger). Use of the binomial expansion gives

$$\frac{dr}{dt} = S_b^{\circ} (1 + b/r)^{-1}$$

$$= S_b^{\circ} (1 - b/r) + O(\epsilon^2). \tag{11}$$

The final radius *vs* time expression is obtained by integrating equation (11) to produce

$$r + b \ln (r - b) = S_b^{\circ} t + \text{constant} \qquad (12)$$

which can be compared with the standard simple model equation (3-12)

$$r + b \ln r = S_b^{\circ} t + \text{constant}. \qquad (13)$$

According to the above argument, equations (10) and (11) are equivalent at the level of accuracy at which linearity can be assumed. Use of equation (12) as an alternative to the simple model equation (13) therefore appears to be justified. The main advantage of equation (12) is that when b is negative its behaviour at $r < |b|$ is physically reasonable. So it can be fitted to a larger range of radii than can equation (13), a point of particular importance in lean hydrogen flames where the maximum radius is limited by cellularity.

TABLE 10

Comparison of analyses using standard and alternative models

Mixture stoich or dilution	Analysis based on: equation (13) L/mm	S_u°/ms^{-1}	equation (12) L/mm	S_u°/ms^{-1}	Correct value of S_u°/ms^{-1}
0.6	-0.26	0.646	-0.31	0.639	0.616
0.5	-0.52	0.324	-0.76	0.312	0.288
0.4	-1.05	0.123	-2.04	0.111	0.079
50	-0.38	0.300	-0.46	0.296	0.279
60	-0.53	0.132	-0.71	0.129	0.090

Comparison of equations (12) and (13) shows that they are very similar, so essentially the same fitting method can be used. In order to test whether the new equation provides a better fit than the old to flames with a negative relaxation parameter, equation (12) was fitted to r *vs* t data predicted by detailed modelling, for which the

correct burning velocity is known. The mixtures tested were some very lean and very dilute hydrogen mixtures. The results are shown in Table 10.

It is interesting that the burning velocities are only improved slightly, and the errors generally remain large. By contrast, the Markstein lengths are changed considerably, and in such a way as to yield better agreement with the theoretical trends.

A different picture emerges when the new equation is applied to the corresponding experimental results. First, no optimum fit could be obtained for the leanest mixtures: the uncertainty in the flame speed, which measures the goodness of fit, decreased monotonically as b was made more negative. This suggests that either the model or the fitting procedure is not robust enough to deal with experimental data, since no such problems arose when fitting equation (12) to the modelled radius *vs* time data. Second, in the moderately lean mixtures for which results could be obtained, there were large changes in both Markstein length and burning velocity. In both cases the new data fitted in better than the old with the trends of modelling and theory. The reason for this is connected with the early onset of cellularity in such flames. Cellularity imposes an upper limit on the usable radii, while equation (13) imposes a lower limit since it predicts infinite flame speed at $r = |b|$. The more physically reasonable behaviour of equation (12) at small radii removes this lower limit and greatly increases the range of experimental data included in the fitting process.

It is difficult to know whether the use of equation (12) to analyse all runs with a negative flame relaxation parameter is a good idea or not. On the one hand there are good pragmatic reasons for using such a formulation: the Markstein lengths and burning velocities appear to be more accurate and the flame speed *vs* radius behaviour is more reasonable. On the other hand, an element of arbitrariness is introduced: one hesitates to consider the derived data as final because some other model might give an even better fit. And the justification for exchanging models, that they are equivalent at the level of the claimed accuracy, does not tell the whole story. The large differences in the results of fitting equations (12) and (13) show that the models are being applied beyond this level. This is confirmed by the large magnitudes of the values obtained for b: -10 mm is not uncommon. In this case $b/r = O(1)$ and the expressions are well beyond their stated level of accuracy. It is likely that equation (12) represents the theoretical behaviour of negative b mixtures more accurately than (13), as suggested by the Ronney-Sivashinsky model. But since a higher order analysis has not been performed this can only be a supposition. Finally, equation (12) could not be fitted to experimental data for very lean flames.

For these reasons, the possible use of equation (12) instead of (13) in mixtures with negative b has been introduced as a possible alternative after the standard model has been used to analyse all the data. All of the advantages and disadvantages of introducing the new model are therefore apparent.

A final point about the accuracy of the extrapolation relates to the flame thickness correction. It was pointed out in Section 6.3.3 that the assumed $1/r$ dependence of the density correction function $f(r)$ is only approximately satisfied. This is unimportant because the tests in Section 6.4.2 show that the predicted burning velocity of hydrogen/air flames usually differs from the true value by less than 3%.

But values of k are smaller for hydrocarbons than for hydrogen mixtures. This follows from the position of the reference surface. It is nearer to the hot boundary in hydrocarbon than in hydrogen flames, so less cool gas is included in the calculation of the mean density inside the reference surface, leading to a smaller flame thickness correction. It may be, therefore, that even higher accuracy of the expanding flame method can be anticipated from hydrocarbon flames, since the model would be a better fit to the experiments.

If the error in the burning velocity due to the inaccuracy of the extrapolation is treated as random, then the overall uncertainty in the burning velocity can be obtained by combining this with the repeatability of the results estimated in Section 4.1.3.2. The final uncertainty is about 2.5% when b is positive. The uncertainty of the flame relaxation parameter b was also estimated in Section 4.1.3.2. On the assumption that the random error in the determination of b is the major contribution to the total error, a reasonable estimate for the uncertainty in the Markstein lengths is the same as that in b, namely 10%.

7.1.1.2 Advantages and disadvantages

The fundamental advantage of the expanding flame method is that, alone among laboratory methods, it is truly one-dimensional. The flow is therefore well-defined, to such an extent that there is no need to measure or visualize it. Departures from the ideal geometry are readily detected from the shape of the visualized flame. The stretch rate can therefore be measured with great precision. Another consequence of the flame geometry is that it can be modelled precisely using a one-dimensional expanding flame code. This allows a check to be made on the accuracy of the extrapolation used to obtain the experimental results as described in Section 6.4.2.

Since the flame is freely propagating it is close to being adiabatic: unlike a burner-stabilized flame there is no surface to which heat might be lost. Heat loss to the spark electrodes must occur, but this is expected to be negligible except when the flame is very small. The analysis method is not valid at such small radii.

Another consequence of one-dimensionality is that there is no possibility of interference with the propagation by a secondary flame or by atmospheric entrainment. The system therefore corresponds closely to the one-dimensional definition.

A final advantage, due to the extrapolation method, is that although the importance of the reference surface has been emphasized in the present work, a knowledge of its position is not needed for obtaining burning velocities. This has two advantages. First, the precision of the results is improved by their independence from this poorly-known parameter. Second, it becomes possible to determine the reference surface experimentally as shown in Section 7.2.2.

The disadvantages of the expanding flame method are principally that it is not suitable for all mixtures, that there is an assumption of chemical equilibrium in the burnt gas, and that it is only valid for weak stretch.

Unsuitable mixtures include those with an effective Lewis number much greater than 1 (difficult to ignite), an effective Lewis number much smaller than 1 (the simple model does not fit), and a small flame speed (buoyancy causes nonsphericity). Also, very rich hydrocarbon mixtures are unsuitable because the assumption of thermodynamic equilibrium in the burnt gases becomes unsafe. Moreover, sooting can occur in such mixtures, increasing the radiative heat loss considerably.

Fortunately, all of these conditions occur near the extremes of the stoichiometric range. The method is therefore applicable over most regimes of practical interest. In addition, the effects described above can all be overcome to some extent: higher ignition energies, a more detailed extrapolation technique, a drop tower and direct comparison with an expanding flame code using detailed kinetic modelling respectively would improve the utility of the method in the cases listed.

It would be useful to have an independent check on the validity of the assumption of chemical equilibrium in rich hydrocarbon flames. Possibly a time-resolved laser

method (e.g. degenerate four-wave mixing) could be used through the bomb windows to determine flame temperature.

An alternative constant-pressure expanding flame method in which the spherical flame is ignited in a soap bubble avoids the assumption of equilibrium, at the expense of greater experimental complexity and the necessity of the gases being saturated with water vapour. For accurate work the latter point is probably the most serious restriction. If a different bubble material with a low vapour pressure could be used, this method might be worth developing. If results were only needed at atmospheric pressure then the experiment could be performed in the open laboratory: a bomb would not be needed. This would allow much better optical access for diagnostics or perhaps for a laser ignition system if the influence of the spark electrodes was to be eliminated.

Extension of the expanding flame method beyond the weak stretch regime is unlikely to be successful. High stretch rates correspond to small radii, where nonsphericity of the flame kernel and interference from the spark electrodes have their biggest effect. Also, theoretical work[57] suggests that the effects of extensional and dilatational stretch are likely to differ when the stretch rate is high. Any results obtained would therefore be of limited utility. This is not surprising, because a flame kernel with a radius of the order of the flame thickness is rather different from a planar flame. In fact, the early stages of flame propagation are probably better considered as an ignition problem. Application of the flame stretch concept is qualitatively useful, but perhaps not quantitatively.

7.1.2 **Flames in stagnation-point flow**

7.1.2.1 Accuracy of extrapolation

When Wu and Law introduced the stagnation flow method[23,24,27-30], they claimed that the same one-dimensional burning velocity would be obtained whether the stretched burning velocity was defined on the cold or hot side of the flame. The results in Figs. 41 and 42(a) show that this claim is not correct, at least for the configuration used in the present experiments. In all cases, the one-dimensional burning velocity obtained by extrapolation of $S_{u,r}$ was lower than that obtained from S_{L1}. It now becomes necessary to decide which, if either, of these results is correct.

The one-dimensional burning velocities obtained from the extrapolations have been plotted against stoichiometry in Fig. 43 along with a curve representing the results obtained by the expanding flame method. Since the latter data can be shown to be accurate, a comparison should yield useful information. An examination of the data shows that although the stagnation flow data are scattered, those obtained by extrapolation of S_{L1} are, on average, above the expanding flame data, while those from extrapolation of $S_{u,r}$ are below. The mean deviation of S_{L1} from the bomb curve was +0.021 ms^{-1} while that of $S_{u,r}$ was -0.020 ms^{-1}. While there are insufficient data to allow a firm conclusion to be drawn, it would appear that the one-dimensional burning velocity tends to be overestimated by S_{L1} and underestimated by $S_{u,r}$. Possible reasons for these observations will be discussed next.

We start by recalling the results in Section 3.3.1 dealing with the stagnation-point flow methodology. According to assumptions 1, 2 and 3 or 3a, the variations of S_{L1} and $S_{u,r}$ with the stretch rate should be given by

$$S_{L1} = S_u^{\circ} - L_1\Gamma \tag{14}$$

$$S_{u,r} = S_u^{\circ} - L\Gamma \tag{15}$$

where $\Gamma = -dv_z/dz$. But the experimental results in Figs. 41 and 42(a) show that at least one of these equations is incorrect since S_{L1} and $S_{u,r}$ do not extrapolate to the same value of S_u°, although the extrapolations are reasonably linear.

One-dimensional burning velocities for methane obtained by Law and co-workers[24] using the stagnation flow method are shown in Fig. 43 as a dotted line. They are higher than the expanding flame results of the present work. Both methods rely on a linear variation of burning velocity with stretch, and the assumption appears reasonable in both cases. Fig. 5 shows that the expanding flame data agree with the model derived on the basis of a linear variation, and ref. 24 shows that Law's data also vary quite linearly. Why do the extrapolated burning velocities differ?

In the first paper[23] on the stagnation flow technique, burning velocities measured at the cold boundary of button-shaped methane/air flames were presented. It was suggested that these should approximate to one-dimensional flames because the upstream velocity gradient was so low. And indeed, the one-dimensional results for methane/air obtained by the extrapolation technique and presented in later work[24] agree very well with the button-flame data. But the flow divergence in button-

shaped flames is not negligible. An approximate area ratio of 1.14 was obtained for a stoichiometric methane/air flame in the present work (see Section 5.3). This agrees quite well with a value of 1.2 obtained by back calculation from the data of Günther and Janisch[78]. It would appear, then, that Law's method extrapolates to a value at zero stretch which is 15 to 20% too high.

Essentially, the situation is that there is flow divergence when there is apparently no stretch. This is certainly possible in stationary spherical flames as described in Section 2.1.2.2. But in such a case the divergence is due to the curvature of the flame. In the stagnation flow experiments the flame is nearly flat, and it seems unlikely that there could be flow divergence without stretch in such a configuration: the streamlines would need to diverge within the preheat zone and then straighten up and approach the reaction zone normally. A consideration of equation (14) shows that Law's results could be explained if the stretch experienced by the flame was greater than that determined from the upstream velocity gradient; that is, if there is some "residual" stretch which is not due to the straining flow and therefore not detected by the experimental technique. As shown in Section 3.4, the direct effect on the flame of the extra stretch would be small but the increased flow divergence would have a large effect on the measured burning velocity.

One possibility is that this residual stretch is due to the flame itself. Recent work by Pindera and Talbot[51] suggests that one third of the stretch in a particular experiment of Wu and Law's could have been flame-generated. The basic idea is that, because of the finite size of the flame, not all of the thermal expansion is translated into an increase in the normal gas velocity; some "sideways" expansion occurs, resulting in a radial velocity gradient. The streamlines approaching the reaction zone necessarily diverge as a result of the thermal expansion, leading to an area ratio considerably larger than 1 as described earlier. It was shown in Section 3.4 that the measured area ratio of about 1.2 in a particular button-shaped flame is compatible with the stretch rate measured as a tangential velocity.

Support for the idea of residual stretch is given by Fig. 42(b) where the ratio of the measured to the ideal stream tube area is plotted as a function of distance from the apparent stagnation surface. If the measured flows were ideal then the experimental points would all lie on the horizontal line corresponding to an area ratio of 1. If the only effect of thermal expansion were streamline refraction (as shown in Fig. 10 of ref. 72) then the data would initially be on the area ratio = 1 line but would curve downwards between the cold boundary and the luminous zone. In fact the data all exceed 1 at some point, showing that the flow divergence is larger than that

predicted on the basis of stagnation-point flow. The effect becomes more apparent at low stretch rates where the divergence of the ideal streamlines is smaller. Clearly another effect besides streamline refraction is occurring.

Since there appears to be no other mechanism for inducing stretch in stagnation flow flames, we will assume that this residual stretch is generated by the flame itself and is in addition to that measured by the slope of the upstream velocity profile. We will also assume that the residual stretch is constant for a given mixture and experimental set-up since this is necessary for the extrapolations to be linear. Equations (14) and (15) now become

$$S_{L1} = S_u^{\circ} - L_1(-dv_z/dz + \Gamma_{resid}) \tag{16}$$

$$S_{u,r} = S_u^{\circ} - L(-dv_z/dz + \Gamma_{resid}) \tag{17}$$

The results of the present work and those of Law and co-workers[23,24,27-30] show that S_{L1} for fuel/air mixtures always increases with the stretch rate, i.e. L_1 is always negative. So an extrapolation to the true zero stretch position will always lead to a smaller one-dimensional burning velocity. We therefore have an explanation of why burning velocities obtained by extrapolation of S_{L1} always give higher values than those obtained from the expanding flame method or from extrapolation of $S_{u,r}$.

Residual stretch will affect measurements of $S_{u,r}$ in a stagnation flow in the same way as S_{L1}. In the experiments performed in the present work, the burning velocities always decreased with stretch, giving the positive Markstein lengths in Fig. 44. The one-dimensional burning velocities derived must therefore always be too low. The fact that the straight lines through S_{L1} and $S_{u,r}$ did not extrapolate to the same point is therefore explained, as is the form of Fig. 43, in which the burning velocities obtained from extrapolation of S_{L1} and $S_{u,r}$ are respectively above and below the expanding flame data. In principle, extrapolation of the two lines to the point where they meet should give both the true value of the one-dimensional burning velocity and the value of the residual stretch. But there is too much uncertainty in the present experiments for such a procedure to yield reasonable results.

A final point worth noting is that the slope of the burning velocity *vs* dv_z/dz curves should, according to the above analysis, still be equal to the appropriate Markstein length - residual stretch should cause no error.

All of the foregoing assumed that S_{L1} was the gas velocity measured at the cold boundary. In fact, the quantity measured is the minimum upstream velocity, which does not occur at the same point. For the data in Fig. 40, the temperature starts to rise about 2.1 mm from the burner, while the minimum velocity is at about 2.25 mm. The difference is small, but an asymptotic analysis by Tien and Matalon[72] suggests that it leads to a nonlinear burning velocity extrapolation and high values of the one-dimensional burning velocity. According to Tien and Matalon's work, correctly-measured values of S_{L1} (i.e. at the real cold boundary) should extrapolate to the true one-dimensional burning velocity, as should $S_{u,r}$, provided the measured stretch is the true value.

It would appear from the work in this thesis that the effect described by Tien and Matalon is insufficient to explain by itself the high values of burning velocity obtained by extrapolation of S_{L1}. In particular, the flow divergence in Fig. 42(b) is not predicted by Tien and Matalon. Re-analysis of some of the stagnation flow data using the gas velocity at first temperature rise did produce a steeper variation with stretch, but it still failed to extrapolate to the same point as $S_{u,r}$. In addition, Fig. 43 shows that $S_{u,r}$ does not extrapolate to the one-dimensional burning velocities obtained by the expanding flame method.

The Law methodology has also been modelled by Dixon-Lewis[89], using a finite-domain analysis of the stagnation-point flow. This is a method of determining the flow from the Navier-Stokes equations, instead of imposing it. Like Tien and Matalon, he found that the variation of S_{L1} with stretch was nonlinear, and a linear extrapolation to zero stretch overestimated the true, one-dimensional burning velocity. The physical reason in this case is not clear. It is likely that the effects predicted by Tien and Matalon occur, since Dixon-Lewis also simulated Law's experiments by using the upstream velocity minimum as S_{L1}. There could, however, be extra features due to the different flow model. In particular, when the flame in the Dixon-Lewis model is stressed, it generates more stress of its own. This is reminiscent of the residual stretch described in the present work, but it cannot be the same effect. Residual stretch is considered to be due to the finite size of the flame and therefore cannot be predicted by a mathematically one-dimensional model.

It is worth pointing out that the objections of Tien and Matalon and of Dixon-Lewis are in addition to the residual stretch effect. It is therefore possible that the stagnation-point flow methodology suffers from several serious difficulties.

7.1.2.2 Advantages and disadvantages

On the face of it, the main advantages of the stagnation-point flow method of measuring burning rates are its simplicity and accuracy. The results of the present work suggest that this impression may need to be modified.

An advantage of the stagnation-point flow method is its use in the study of flame extinction at high stretch rates. In this case a counterflow method must be used: a flame blown against a plate either extinguishes or changes to another configuration at stretch rates well below those corresponding to extinction. This is presumably due to heat loss to the plate.

Another advantage is that Markstein lengths are obtained directly from the experiments, without the need for a flame thickness correction.

The main disadvantage of the method is that the extrapolation apparently does not lead to one-dimensional conditions: there appears to be a systematic difference between one-dimensional burning velocities derived from S_{L1} and $S_{u,r}$. It was argued in the previous section that this difference may be due to a systematic error in the measurement of the stretch rate. The experiment could therefore be improved by determining it directly. This could be done by measuring the tangential velocity gradient at the luminous zone using laser-Doppler anemometry.

Use of particle tracking in a stagnation flow brings in a new set of problems. The large uncertainties in the particle tracking measurements used for obtaining $S_{u,r}$ could be reduced by using average area ratios determined from large numbers of streamlines. The time taken to perform such analyses would be large, and an automatic analysis system (e.g. a Particle Image Velocimetry system) might be necessary to deal with all of the information. The calculation of stream tube area errors due to particles not following the flow shows that there are tight constraints on usable stretch rates. The experimental measurements of the product vA of the unburnt gas velocity on the axis with the stream tube area confirm this. Figure 40 shows that vA is constant at low stretch rates, but at higher values it tends to dip close to the flame. It is likely that this is due to error in the stream tube area due to particles not following the flow.

If the explanation of the failings of the stagnation flow methodology in terms of residual stretch is correct then it should be possible to perform the experiment without having to use particle tracking, which is identified above as a serious source

of error. Use of the directly-measured stretch rate should lead to correct extrapolation to one-dimensional conditions if the appropriate burning velocity is used. According to Tien and Matalon, the gas velocity measured strictly at first temperature rise should extrapolate correctly. The data in Fig. 40 show that the position of first temperature rise can be identified without the need for particle tracking. It is the point where the velocity *vs* distance data start to curve up away from the linear downward trend. It could be argued that this point is not well defined, and this is true. But the position of first temperature rise is itself ill-defined, which is another reason for preferring the method advocated in the present work based on the hot side of the flame.

The other piece of information required from the experiment is the Markstein length. If the value based on the hot end of the flame (as measured in the present work) were required then in the absence of particle tracking it would have to be calculated from the unburnt gas value using theory. The relationship between the two Markstein lengths will be considered in Section 7.3.

7.1.3 **Comparison of methods**

In this section we perform a brief comparison of the two experimental methods used in the present work to obtain burning velocities and Markstein lengths.

The burning velocities and Markstein lengths derived using the expanding flame method are plotted in Chapters 5 and 6 and listed in the Appendix. These results show that the method is repeatable and produces data with small uncertainties. The test of the method described in Section 6.4.2 shows that in most cases the method should give burning velocities within about 3% of the correct values. Furthermore, it is possible to determine which mixtures will not give good results.

The main reason for the high quality of the results is that the flow is extremely well-defined. In a truly spherically symmetric system, the flow is only radial and the stretch rate is known precisely. Real expanding flames are very close to being spherical (to the extent that this can be checked), so the flow is very well characterized.

By contrast, the stagnation-point flow method produced widely scattered data with large uncertainties, in spite of very careful work on the part of the experimenter. The scatter in the Markstein length data in Fig. 44 in particular is very large. In

fact, the scatter in the results derived directly from the S_{L1} data is already large, so the $S_{u,r}$ data derived from them are necessarily even worse.

The reason for the large scatter in the S_{L1} data is not clear. Comparable data presented by Law and co-workers do not show the same level of uncertainty. It may be, however, that the Law data have been averaged over repeated runs, whereas the present data are mainly single runs. Also, all of the Law data except for the few in the first paper[23] were obtained using a counterflow system in which two stagnation flow flames are blown against each other. The use of such a system allows data to be collected at a much wider range of stretch rates than in the present system where the flame was blown against a metal plate. The uncertainty in both slope and intercept of the burning velocity *vs* stretch function would be much reduced as a result. A final point is that roughly comparable experiments were performed by Searby and Quinard[177]. They found that the uncertainty in their Markstein numbers (Markstein lengths divided by a flame thickness) were often of the order of 100%. This suggests that they suffered from similar difficulties.

The stagnation flow measurements in the present work performed two main functions. First, the results demonstrate qualitatively the effect of different burning velocity definitions: while one increases with stretch, the other decreases. Second, even when experimental errors are taken into account, the different burning velocity definitions extrapolate to different "one-dimensional" values. This suggests a problem with the methodology.

In view of the above comments, the subsequent discussion in this chapter will refer only to results of the expanding flame work unless otherwise stated.

7.2 BURNING VELOCITY

In this section, points arising from the burning velocity methodology and results are considered.

7.2.1 **General points**

In this section some general points about the experimental results are considered. These include the shapes of the burning velocity *vs* stoichiometry curves and reasons for the gross differences between burning velocities of different fuels.

All of the burning velocity *vs* stoichiometry curves have a similar form, which can be easily explained by means of the following simplification. Any fuel/air mixture other than a stoichiometric one can be considered as a stoichiometric mixture diluted with excess fuel or air. This excess gas acts as a sink for the heat created, so the flame temperature is lower than that of a stoichiometric mixture. The phenomenological and asymptotic theories in Chapter 2 show that the burning velocity depends strongly upon the flame temperature: a small change in the temperature results in a large change in the burning velocity. The burning velocity on either side of the stoichiometric point therefore decreases as the mixture becomes richer or leaner.

This does not explain why the maximum burning velocity occurs at a point slightly (or in the case of hydrogen, very) rich of stoichiometric. On the face of it, one might expect the maximum burning velocity to coincide with the maximum flame temperature. Since this occurs in slightly rich mixtures because of product dissociation, it provides a possible explanation for the position of the maximum burning velocity. In order to examine this point, maximum burning velocities have been obtained from the polynomial curve fits through the experimental data shown in Chapter 5. Mass burning rates were derived from them by multiplying by the unburnt mixture density. Flame temperatures were obtained using the program FTEMP. Stoichiometries at maximum temperature, maximum burning velocity and maximum mass burning rate for the fuel/air mixtures studied in this work are shown in Table 11.

TABLE 11

Stoichiometries at maximum temperature and burning rate

Fuel	Stoichiometry at:		
	T_{max}	$S_u^{\circ}{}_{max}$	M_{rmax}
Methane	1.03	1.07	1.06
Ethane	1.04	1.07	1.07
Propane	1.04	1.08	1.08
Ethylene	1.09	1.10	1.10
Hydrogen	1.05	1.40	1.27

Before considering the physical mechanisms operating, it is worth pointing out that, on the basis of the discussion in Chapter 3, the mass burning rate is the fundamental measure of the flame propagation rate. It is therefore the position of maximum mass burning rate and not maximum burning velocity that should be studied. For most fuels there is no need to make this distinction because the maxima of burning velocity and mass burning rate occur at the same stoichiometry. But for methane there is a small difference and for hydrogen a very large one, in both cases due to the variation in the unburnt gas density with stoichiometry.

It is clear from the table that in all cases the maximum mass burning rate M_{rmax} occurs in richer mixtures than the maximum flame temperature T_{max}. While the shift in T_{max} may contribute to the shift in M_{rmax}, there must be other mechanisms operating.

There has been a range of suggestions for the mechanism responsible for the shift. Dixon-Lewis[40] found that for hydrogen/air flames it was associated with competition between chain branching and terminating steps. The balance between these alters as the composition approaches stoichiometric from the rich side due to increasing concentration of OH radicals.

Sen and Ludford[178,179] claimed that species diffusion alone produced the shift in the maximum burning rate, and an explanation based on kinetics alone is at best incomplete.

It would appear that the burning rate can be shifted by all three effects: product dissociation (via its effect on the temperature maximum), preferential diffusion and chemical kinetics. Sen and Ludford's argument is that preferential diffusion is the fundamental effect in the sense that it always occurs, while at low temperatures there is no product dissociation to shift the temperature maximum and in a simple kinetic scheme there is no competition between chain branching and terminating reactions.

The fastest-burning fuel studied was hydrogen, with a maximum burning velocity of 2.85 ms^{-1}. Next is ethylene (0.66 ms^{-1}), while all the saturated hydrocarbons have similar maximum burning velocities around 0.4 ms^{-1}. The difference between ethylene and the other hydrocarbons can be attributed to its higher flame temperature. This in turn is due to the greater exothermicity because of the presence of a double bond in the molecule. For the same reason, acetylene, with a triple bond, has a higher temperature and a higher burning velocity than ethylene.

The much higher burning velocity of hydrogen is not explained by temperature considerations alone; its flame temperature is similar to that of ethylene, but its maximum burning velocity is more than four times greater. In this case the explanation lies in the detailed kinetics of the combustion process, described earlier.

The variation of the burning velocity of stoichiometric hydrogen/air mixtures with nitrogen dilution is explained by the mechanism described earlier for variations with stoichiometry.

The fall in the burning velocity of the stoichiometric methane/air mixtures with increasing pressure can be understood by reference to equation (2-35). For an overall reaction order less than 2, the burning velocity must decrease with increasing pressure. The best fit of equation (2-35) to the experimental results in Fig. 25 gives a value of the overall reaction order of 1.40 ± .05. The fact that this value is nonintegral shows that the combustion of methane does not proceed by a single elementary reaction. The order is less than 2 because most of the pressure-dependent reactions are chain-terminating steps whose rate increases with pressure.

7.2.2 **Physical meaning of the reference surface**

The reference surface determined by modelling in the present work is essentially an empirical concept which is of use in analysing the experimental results. It could be defined as that surface in an unstretched flame where the mass flux is invariant to

changes in flame curvature. That there is such a surface in a flame implies something about its structure: there must be a thin zone where the burning rate is controlled. A study of the reference surface should therefore provide useful information about flames.

In this section we examine the physical basis of the reference surface using computer modelling of one-dimensional flames. We also consider experimental and theoretical evidence for the reference surface position.

In order to study this in more detail, the temperatures at three points in the flame corresponding to relevant physical processes have been plotted in Figs. 47 to 53 along with the temperature of the reference surface for each parameter range of each fuel. The points chosen were maximum fuel consumption rate, maximum heat release rate and the point at which the radical pool production rate becomes positive. The temperature at the latter point is the "ignition temperature" T_i of Dixon-Lewis[89].

The first point to note is that the reference surface is at high temperature: around 1500 K in hydrocarbons and 1000 K in hydrogen. The notion that the propagation rate is controlled by events in the hot part of the flame therefore appears to be justified. Although the temperature of the reference surface is lower for hydrogen than for the hydrocarbons, it is still high enough to lead to errors in burning velocity measurement due to flow divergence if the gas velocity at the cold boundary is measured.

The second point of interest is that none of the physical surfaces corresponds precisely to the reference surface. But in most cases the reference surface and the other physical surfaces are in the same general temperature range. In fact, the method of representing the positions of surfaces by their temperatures tends to exaggerate any differences; due to the large temperature gradients, the distances between the surfaces tend to be small fractions of the flame thickness. Therefore if any one of the physical surfaces could be located experimentally, it would provide a reasonably accurate measure of the reference surface position for the purposes of burning velocity measurement.

The plots show some interesting behaviour. Figures 47 and 48 show that the reference surface temperature is between those of maximum heat release and H_2 removal rate in most hydrogen mixtures. As the mixture becomes leaner or more dilute, the controlling process appears to change from fuel consumption rate to heat release. This behaviour warrants further study.

Ethane and propane are broadly similar (Figs. 51 and 52) in that the reference surface temperature is slightly higher than that corresponding to maximum fuel consumption but about 200 K lower than the other two surfaces. By contrast, in methane (Figs. 49 and 50) the fuel consumption profile almost coincides with those of heat release and ignition temperature. Ethylene (Fig. 53) is different again in that all the profiles are at similar temperatures.

The ignition temperature T_i defined by Dixon-Lewis is related to the critical temperature of Shebeko et al[180]. In modelling of stoichiometric hydrogen/air and methane/air flames, all chemical reactions were switched off below various temperatures, and the effect on the burning velocity was observed. The critical temperature T_{cr} at which the burning velocity began to be strongly affected was about 1000 K for hydrogen/air and 1600 K for methane/air. These values are similar to those obtained for T_i and for the reference surface temperature in the present work. The implication is that the reference surface is related to where the reaction rate becomes high.

Another source of relevant information is the work by Fukutani and Jinno[181] on modelling of hydrogen/air and methane/air flames. They determined the ratio of the heat release rate due to reaction to the total heat release rate (due to reaction, conduction, diffusion and convection) as a function of position in the flame (specified by the temperature as in the present work). The boundary between the preheat zone and the reaction zone was taken to be when this ratio equalled unity. For hydrogen flames the boundaries were at 900-1000 K, while in methane flames they were at around 1400 K.

In recent theoretical analyses of flame propagation, conditions at the "fuel consumption layer"[32,33,182,183] have played a significant role. In numerical calculations, the fuel consumption layer is roughly where the rate of fuel consumption is a maximum[33]. It can also be considered as the temperature at which the chemistry is switched on[183]. There appears to be a strong connection with the reference surface of the present work. The physical basis of the reference surface may therefore be clarified by further analytical work of this sort.

To summarize, the reference surface appears to be related to the point in the flame where the chemistry becomes active. It is not clear which flame process studied in the present work is most closely related to the reference surface. In fact, there is some evidence that different processes are important under different conditions.

Further study is needed, perhaps including surfaces in the flame corresponding to a wider range of physical processes.

The determinations of the reference surface position in the present work depend solely on modelling which could conceivably be incorrect. We therefore consider experimental evidence for the reference surface position.

First, there is the evidence of the present work. Let us assume, for the sake of simplicity, that "good" one-dimensional burning velocities can be obtained in Bunsen flames by dividing the volumetric flow rate of cold gas V by A_r, the area of the flame it supplies. The one-dimensional burning velocity is then

$$S_u^{\circ} = V/A_r. \tag{18}$$

A range of burning velocities can be obtained depending upon which reference surface is selected. For example, A_r might be measured at the cold boundary, the schlieren or shadow surface, or at the luminous zone. Which surface should be used? Since the correct value for the burning velocity is known from the expanding flame method, it is possible to work backwards to find the correct reference surface. In fact, the good agreement between the results of experiments in the present work on button-shaped and expanding flames supports the use of the base of the luminous zone as the reference surface. The temperature of this region in a stoichiometric methane/air flame[78] is about 1420 K in good agreement with the modelling.

Further support for a hot reference surface is lent by the work of Günther and Janisch[62,63] on flame stabilization. According to their interpretation of the standard view[18], there should be a point near the base of a Bunsen flame where the cold gas velocity is perpendicular to the flame front and equal to the local burning velocity. Günther and Janisch found no such point. They found instead that the part of the flame where the criteria for stabilization were satisfied was the centre of the luminous zone. They considered that this region was the one which controls flame stabilization. This finding is just what would be expected if the reference surface were at the luminous zone.

7.2.3 **Effects causing errors in burning velocity determination**

In this section we consider the implications of the present work for how burning velocity should be measured.

The present work suggests that a good value for the one-dimensional burning velocity will be obtained by measuring the mass flux at the reference surface of an unstretched or weakly stretched adiabatic flame and dividing by the cold gas density.

A good method will therefore minimize the effects of flow divergence, stretch, heat loss and non-one-dimensional effects e.g. atmospheric mixing and interaction with a secondary flame. These effects will now be considered in more detail.

7.2.3.1 Flow divergence

Flow divergence is in a sense a pseudo-effect: it is only necessary to consider correcting for it because a misunderstanding of burning velocity allowed it to give rise to a widespread systematic error in the first place. Its effect is removed by measuring the mass flux at the reference surface, which is likely to be in the hot part of the flame. Currently, there is no direct way of measuring mass flux, so a gas velocity and a density must be determined. It is possible to measure both of these in the hot part of the flame, but a much simpler method is to determine the velocity in the cold gas ahead of the flame. There is then no need to determine the density because it cancels when the mass flux is divided by the cold gas density.

If this technique is used then it is also necessary to know the stream tube area ratio between the point in the flame where the velocity was measured and the reference surface. There are two possible approaches:

1. Particle tracking or a related technique (as in the present stagnation flow work)
2. A flow configuration in which the area ratio varies in a known way and can be extrapolated to a value of unity (this is what the Law method and the present expanding flame method aim to do).

In principle, the use of velocity measurements in the unburnt gas (e.g. by LDA) along with particle tracking gives all the information necessary for determining the mass flux at any point in an axially symmetric flame. In practice, though, the

potential for error is large and great care must be taken. The computation in Section 3.3.2 shows that systematic errors can arise in stagnation-point flows because of the large radial accelerations experienced by the particles.

If particle tracking can be avoided by the use of knowledge about the flow then the results are likely to be more accurate, provided the flow behaves in the expected way. This approach is used by the Law method, but the present work shows that not all of the assumptions are correct. It may, however, be possible to modify the technique so as to obtain good results as described earlier.

An interesting alternative is the use of a closed, stationary flame surface. This has never been used, for obvious reasons: it is geometrically impossible. But an approximation to it is feasible, e.g. the low pressure spherical flame work of Fristrom[184]. In this method, the flame is stabilized around a sphere of sintered brass. The fuel/air mixture is supplied to the brass sphere by a pipe which passes through the flame. If this pipe is narrow and suitably insulated then preheating of the incoming gas should be negligible. The only remaining difficulties are buoyancy and stability. Buoyancy would cause the flame to change from the ideal spherical shape to (roughly) an ellipsoid. But the shape would still be symmetric about a vertical axis, so that the flame area could be deduced from a single photograph.

In order to prevent heat loss to the brass sphere, the flame would need to be stabilized some distance away from it, and it is not clear that the flame would form a stable sphere or ellipsoid under those circumstances. If it did (perhaps under microgravity) then the burning velocity and the reference surface position could be readily determined from a simple experiment. This would consist of photographing the flame at a series of cold gas flow rates V. Suppose (for simplicity) that the flame was spherical. Let the radius of some easily visualized surface (luminous, schlieren or shadow) be r_V. Then it is straightforward to show that r_V varies with V as

$$r_V = [V/(4\pi S_u^{\circ})]^{1/2} + \Delta r \qquad (19)$$

where Δr is the constant distance between the visualized surface and the reference surface. Therefore S_u° and Δr can readily be obtained from a graph of r_V against $V^{1/2}$. If the flame were not spherical then a more complicated expression would replace equation (19). Note that by the mean extensional stretch theorem the burning velocity obtained would still be the one-dimensional value S_u°.

7.2.3.2 Stretch

Low stretch conditions can be obtained in three ways:

1. by selecting a suitable area of the flame with a zero mean stretch (e.g. by using the mean extensional stretch theorem)
2. by selecting a flame or part of a flame with a low stretch rate (e.g. the middle of a button-shaped flame)
3. by measuring burning velocities at a range of stretch rates and extrapolating to zero stretch.

The consideration of stretch effects in burning velocity measurement began only a few years ago. Earlier methods of measuring burning velocity which use one of the above approaches must therefore have done so either completely accidentally or as a by-product of an attempt to attain the conditions specified in the one-dimensional definition. In fact, methods 1 and 2 have both been used for many years. "Total area" methods applied to Bunsen cones started with Gouy[9] in 1879 as described in Chapter 1. According to the mean extensional stretch theorem, such a method should give rise to a result which is affected only slightly by stretch, provided the tip of the cone is not too sharp.

Selection of a part of the flame which has a low stretch rate has been done by several workers[73,185]. Their aim was to obtain average burning velocities for conical flames which were unaffected by cooling at the base and high curvature at the tip. They therefore measured the burning velocity of the frustrum resulting from removal of these sections. According to the mean extensional stretch theorem, such a choice should ensure that the mean stretch rate is quite small. But, as pointed out by Gibbs and Calcote[185], the method does not take account of flow divergence between burner and the combustion region.

Method 3 was used in the counterflow method of Law et al[23,24,27-30] and also in the expanding flame method in the present work. Different values of burning velocity were obtained from the two methods, so clearly at least one of the methods does not work very well. This illustrates the potential dangers of extrapolation methods.

A final point about stretch effects is that, as shown in Section 3.4, they usually have a smaller effect on the burning velocity than flow divergence. It is therefore more important to remove divergence effects than stretch.

7.2.3.3 Heat loss and non-one-dimensional effects

Heat loss has long been recognized as a factor which can affect the result of burning velocity determinations. Non-one-dimensional effects like atmospheric entrainment and the presence of a secondary flame can also cause the burning velocity to deviate from its one-dimensional value.

Heat loss plays a role in flame stabilization, so it follows that any flame on any burner will suffer at least some heat loss. Bunsen flames are stabilized at the base, so effects on the measured burning velocity can be removed by excluding the flame base from the area where measurements are made. This also has the advantage of avoiding any atmospheric mixing effects. The heat loss to porous plate burners is harder to avoid, but in one method[186] the rate of heat loss to the burner at different flow rates is extrapolated to zero to give an adiabatic result.

Atmospheric entrainment can influence the local burning velocity at the edge of a premixed flame. The effect is to make the mixture locally leaner. If it was already lean then the flame burns less intensely; if rich, then it burns more intensely. Either way, the result differs from a one-dimensional flame. The effect can be avoided by making measurements on a region of flame which does not include the edge, or by using a closed flame surface.

The final effect of interest is the presence of a secondary flame. It occurs in rich mixtures when the gas leaving the primary reaction zone contains species which are flammable. Oxygen from the air surrounding the burner diffuses in from the surroundings and forms a diffusion flame around the primary reaction zone. It is therefore a non-one-dimensional effect: in a one-dimensional flame there is nowhere for oxygen to diffuse from. In hydrocarbon flames the main reactant is carbon monoxide. The effect is likely to be an increase in the flame temperature as extra heat is released. The extent to which this perturbs burning velocity measurements is uncertain, but preventing the formation of a secondary flame is probably a good idea. This can be done in two ways. One way would be to use a Smithells separator, which is a narrow tube surrounding the burner-stabilized flame and extending some distance above it. The secondary diffusion flame is induced to sit at the mouth of the tube, separated from the primary zone and therefore not affecting it. The disadvantages due to extra heat loss and instability of the flame probably outweigh the advantage of getting rid of this source of error.

The second way of avoiding the presence of a secondary flame is by using a closed flame surface. This is precisely what is used in the expanding flame method of this work, and is another point in its favour.

It is likely that counterflow methods are also less affected by secondary diffusion flames than ordinary burner-stabilized flames - the proximity of the two reaction zones and the outward flow from between them will delay the formation of diffusion flames so that measurements made near the centre of the flames are unaffected[187].

The general point about heat losses and effects due to the flame not being one-dimensional is that they should be minimized if true one-dimensional, adiabatic results are to be obtained. Heat losses can be minimized in various ways. Excluding the base of a conical flame should work well if the flow rate of gas supplying the rest of the flame can be deduced. Particle tracking is probably needed in order to do this properly.

The counterflow method in which two flames are blown against each other is probably the stationary flame method which is closest to being adiabatic, precisely because the flames do not interact with the burner.

7.2.4 **Review of experimental methods**

The previous section described conditions suggested by the present work for obtaining accurate one-dimensional burning velocities. We now compare previous methods with this specification and pick out those which are likely to give good results. Some results from previous methods are also compared with the present work. Hydrogen/air results are compared with the present data in Fig. 64. Comparisons of some maximum methane/air burning velocities are made in Table 12. Methods with specific claims to one-dimensionality are dealt with in the next section.

7.2.4.1 Burner methods

Methods consisting of a direct gas velocity measurement in the unburnt gas without an area ratio correction will give results which are too high because flow divergence has not been accounted for. The amount by which the results exceed the correct value will depend on the particular circumstances. Dixon-Lewis[40] calculated approximate corrections for conical hydrogen flame methods of up to 40%. For

near-stoichiometric button-shaped methane/air flames the upstream result should be multiplied by a correction factor of about 1/1.2 = 0.83 as shown earlier. We will assume that the same correction is valid for conical flames.

Figure 64 contains results from the button-shaped hydrogen/air flames of Günther and Janisch[78] (curve A) and the conical flames of Wu and Law[23] (curves B and C) along with the present results represented by curve G. Flow divergence between the cold gas and the reference surface is the main reason for the high results. Günther and Janisch's maximum burning velocity was about 25% higher than the present value, in line with the estimated error in methane button-shaped flames.

The effect of divergence in conical flames will vary inversely with burner diameter, explaining why the results of Wu and Law[23] using 5 mm nozzles (curve B) are higher than those using 7 mm (curve C). Wu and Law estimated that their maximum burning velocity would be about 2.8 ms^{-1} if the data were extrapolated to zero curvature, in good agreement with the value of 2.85 ms^{-1} obtained in the present work.

Flame stretch will exert a secondary influence. Its effect can be estimated roughly, using the Markstein length data in Fig. 54 and assuming that stretch rates of 1000 s^{-1} are typical of burner flames. At the maximum burning velocity, the effect is small (compared with divergence) but further out is of the order of 10%. Because stretch affects lean and rich flames in opposite directions, the result is a "tilt" in curves A, B and C of Fig. 64. Button flames are positively stretched. This will increase lean burning velocities and decrease rich, tending to tilt the curve relative to ours to produce better agreement on the rich side. If the velocity measurements in the conical flames were made near the tip where they are negatively stretched[23] then the curves will be tilted in the opposite way to curve A, explaining the better agreement with our data on the lean side.

Any method which consists of measuring the total luminous flame area and dividing by the unburnt gas flow rate should give a result which is free from the effect of flow divergence. Moreover, the mean extensional stretch theorem applied to a conical flame suggests that the mean stretch would be small, since the streamlines near the base of the flame are approximately normal to the luminous zone[62,63].

FIGURE 64

Comparison of hydrogen/air burning velocities measured by different workers Curve A: Günther and Janisch[78] button flame. B: Wu and Law[23] conical flame, 5 mm nozzle. C: Wu and Law[23] conical flame, 7 mm nozzle. D: Michelson[11], total luminous zone area. E: Andrews and Bradley[200] constant pressure expanding flame, uncorrected. F: as E, but corrected to infinite radius. G: present work.

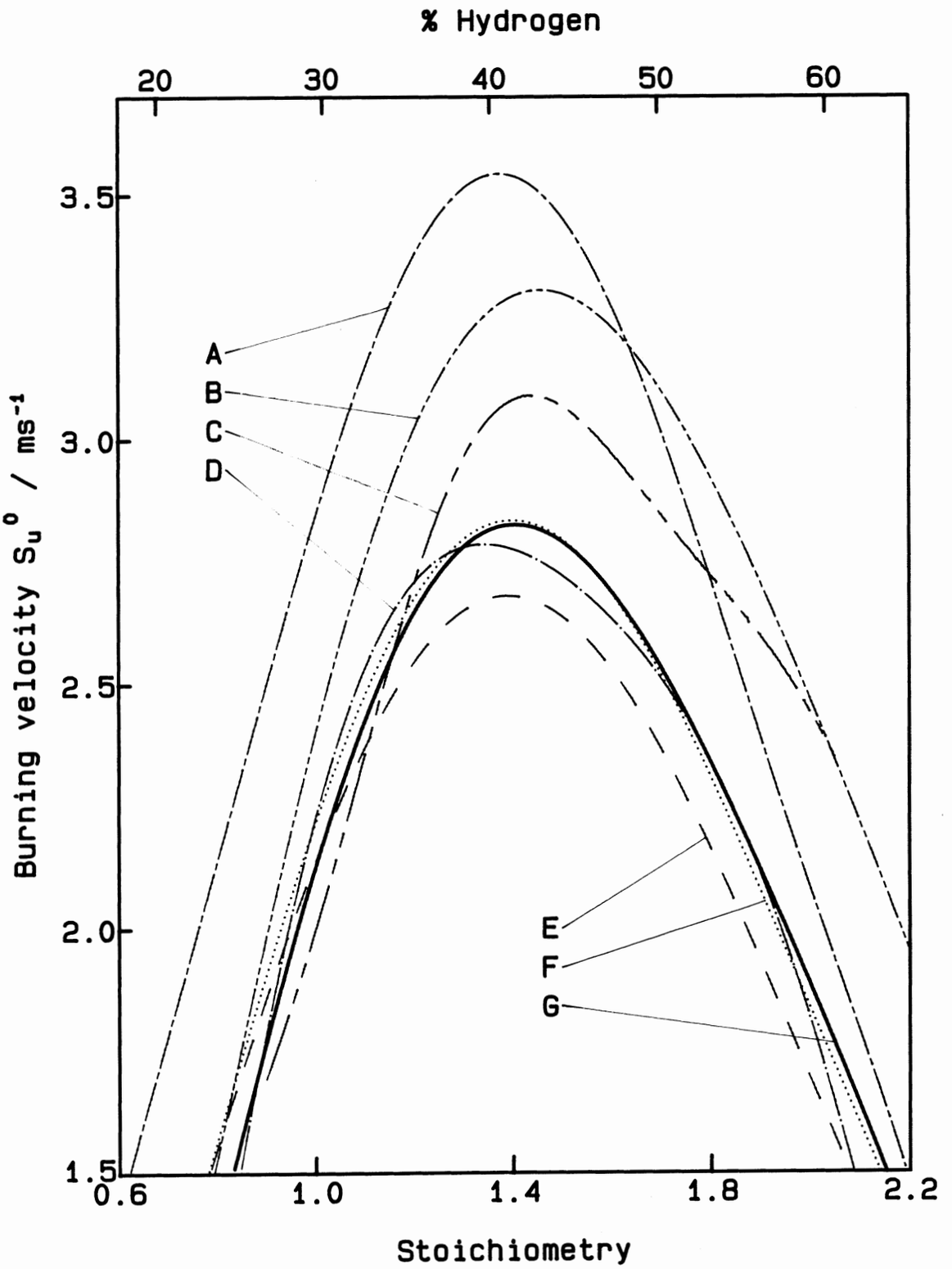

There will be heat losses from the base of the flame, but against this is the inclusion in the total volumetric flow rate of the mixture which passes through the dead space between flame and burner rim.

It is not clear whether the tip of the flame has an effect on the results over and above that accounted for by the mean extensional stretch. Fristrom[20] explained anomalously high upstream burning velocities in the tip as due to "ducting" (i.e. flow divergence). The same argument is used in the present work to explain high burning velocities in button-shaped flames. On the other hand, the work by Lewis and von Elbe[18], using essentially the same burning velocity definition as in the present work, suggested that there is a real increase in the burning velocity at the tip. Even if there were an effect, one might expect it to be very small because of the small proportion of the total flame area affected. But Lewis and von Elbe found that the increase in burning velocity at the tip balanced the decrease at the burner rim. They explained the effects in terms of convergence of heat flow and chain carrier diffusion into the unburnt gas at the tip, and divergence of the same quantities along with heat loss and interdiffusion with the surrounding atmosphere at the base.

In fact, it may be possible to explain the effects in terms of extensional stretch. The fuel mixture used by Lewis and von Elbe[18] was roughly 18% ethane plus some higher hydrocarbons in methane, in a fuel/air mixture with a stoichiometry of 0.88. Fig. 56 shows that the Markstein length of a pure methane/air mixture with this stoichiometry is positive. The addition of ethane and higher hydrocarbons can only make it larger. The effect of the negative stretch at the flame tip will therefore be to increase the burning rate, and positive stretch near the base should decrease it. According to the mean extensional stretch theorem, the effects should balance out over the flame area within the normal streamline near the base, explaining Lewis and von Elbe's finding that the effects at tip and base cancelled out. Also explained is the variation of burning velocity with distance along the flame front shown in Fig. 27 of ref. 18. The experimental points in the central part of the plot where the burning velocity is considered to be constant actually differ in a systematic way from the horizontal line drawn through the data. Such an effect would be expected if stretch were responsible for the changes in the burning velocity.

Overall, it is likely that the burning velocities obtained from the cone area method using the luminous zone to define the cone will be quite accurate, especially if a large burner is used to minimize the effect of heat loss.

It is ironic that this method should give good results: it was introduced by Gouy in 1879. It is therefore no accident that measurements of hydrogen/air burning velocities by this method made over a century ago by Michelson (curve D in Fig. 64) are in close agreement with those obtained in the present work.

TABLE 12

Corrected experimental values of maximum burning velocity for methane/air (after Andrews and Bradley[21])

Authors	Method	Correction factor	Burning velocity / ms^{-1} Experimental	Corrected
Gerstein et al[188]	LA	-	0.333	0.333
Dixon-Lewis and Wilson[189]	LA	-	0.37	0.37
Diederichsen and Wolfhard[190]	LA	-	0.390	0.390
Rosser et al[191]	LA	-	0.386	0.386
Barrasin et al (see ref. 21)	LA	-	0.377	0.377
Dugger (see ref. 21)	ShA	0.94	0.378	0.355
Clingman et al[192]	ShA	0.94	0.405	0.381
Gilbert[193]	ShW	0.94	0.380	0.357
Morgan and Kane[194]	SchA	0.92	0.400	0.368
Natl. Bur. Stds. (see ref. 21)	SchA	0.92	0.381	0.351
Halpern (see ref. 21)	SchA	0.92	0.374	0.344
Fells and Rutherford[195]	SchA	0.92	0.396	0.364
Lindow[196]	SchP	0.83	0.448	0.372
Reed et al[197]	SchP	0.83	0.447	0.371

Key: L inner luminous zone Sch schlieren Sh inner shadow
P particle tracking W wire A total area

Conical flame methods in which the flame area is determined from the schlieren or shadow surface instead of the luminous zone will be too high, but in this case it should be possible to correct the measurements. Andrews and Bradley[21] corrected schlieren, shadow and luminous methods to give cold boundary values by multiplying by factors of 1.11, 1.14 and 1.21 respectively. Therefore it should be possible to do the reverse. To get what are considered in this work to be the correct values, cold boundary values should be multiplied by 1/1.21 = 0.83, shadow by 1.14/1.21 = 0.94 and schlieren by 1.11/1.21 = 0.92. The information in Table 2 of ref. 21 has been

reproduced in Table 12 with these corrections. The mean value of the data in the table is 0.366 ± .016 ms^{-1}, in good agreement with the value of 0.37 ± .01ms^{-1} obtained in the present work.

The other main burner method is that in which a flat flame is stabilized on a porous burner[186,198,199]. The volumetric flow rate of the fuel/air mixture supplying the burner is divided by an area. If the area were that of the flame then, apart from heat loss effects which will be dealt with next, good results would be produced since stretch effects should be minimal. But in fact the burner area is normally used. Whether or not this matters depends on the distance between flame and burner. If it is large then heat loss will be small, but flow divergence will occur[49] and the results will be high. The correction factor is estimated to be the same as for a button flame, viz. about 1/1.2 = 0.83.

If the flame is stabilized close to the burner then flow divergence should be small (since there is not much room for it to occur) but heat losses will be large because the whole of the upstream boundary of the flame is in contact with the burner surface. The usual way of dealing with this[186,198] is to measure the rate of heat loss at different flow rates. The burning velocities, calculated from the flow rates, are linearly extrapolated to zero heat loss to give adiabatic values. An apparent disadvantage of the method is its sensitivity to the surrounding atmosphere. Edmondson, Heap and Pritchard[198] found that ambient oxygen, air, nitrogen and carbon dioxide each led to a different linear extrapolation. They attributed this to edge mixing in their 1 inch (25 mm) diameter burner. However, Botha and Spalding studied the effects of edge mixing by comparing results from burners of different sizes and found that the effect was minimal.

Pritchard, Edmondson and Heap[199] considered that edge effects were responsible for the apparent linear extrapolation. They found that the variation of burning velocity with heat removal rate was nonlinear, but in earlier work[198] had found it to be linear for essentially the same mixtures and conditions. It is therefore necessary to treat their claims with some caution, especially since their stated aim was to bring their results into line with other, higher, burning velocities.

Overall, we conclude that if the linear extrapolation is valid then the method should give reasonable results. In fact, the results of the heat extraction method are quite close to those in the present work. The maximum burning velocities for methane/air[198] and propane/air[186] were 0.365 ms^{-1} and 0.417 ms^{-1} respectively, compared with 0.37 ± .01 ms^{-1} and 0.39 ± .01 ms^{-1} in the present work. Whether

this agreement is due to the linear extrapolation being correct or whether there has been a fortuitous cancellation of errors is not clear.

7.2.4.2 Bomb methods

Constant pressure

The method used in the present work involves an extrapolation of the flame speed to infinite radius. For mixtures with a small value of the flame relaxation parameter b, the radius *vs* time behaviour is close to linear. The slope is therefore close to the limiting (one-dimensional) flame speed and burning velocities derived from the flame speed by multiplying by the expansion ratio should give accurate results. Figures 16, 23, 30, 34 and 39 show that small values of b are found in lean hydrogen and methane and rich ethane, propane and ethylene mixtures.

It is also possible to use the present b values to correct existing expanding flame data for flame thickness and stretch effects. The most recent constant-pressure bomb work is that of Andrews and Bradley[200]. They measured hydrogen/air flame speeds at a flame radius of r_f = 25 mm. If these data are multiplied by the density ratio then the "uncorrected" curve E in Fig. 64 is obtained. The results are considerably lower than curve G on the rich side. However, if we use the experimental values of b (in Fig. 16) to correct these data to infinite radius by multiplying by $(1 + b/r_f)$, then the resulting data, represented by curve F, are in very good agreement with the present results.

Constant volume

A detailed consideration of the constant volume method of measuring the burning velocities of expanding spherical flames[17,201] is outside the scope of the present work. The relevance of the present work for such studies can, however be described. In its usual form, the method involves measurement of the pressure variation inside the combustion bomb following ignition. The pressure rises in the vessel as the flame expands, but at the same time both burnt and unburnt gas are adiabatically compressed. A theoretical model which takes these effects into account is fitted to the pressure *vs* time record and the result is a measure of the variation of the

burning velocity with both temperature and pressure.

The main advantage of the method is the large amount of information obtained from a single run. There are, however, several disadvantages. Initially, the pressure hardly changes (which is why the constant-pressure method described in this thesis works) so there are large uncertainties in the burning velocity at the initial temperature and pressure. Most of the pressure rise occurs in the last few millimetres of flame travel when the flame is only slightly smaller than the combustion bomb, so it is important that the flame conforms to the theoretical model at this stage. In particular, the flame must be smooth and spherical. In the experiments in the present work (using a 600 mm diameter bomb) the flame always wrinkled before it reached the walls of the vessel. Similar behaviour in a 260 mm diameter vessel was reported by Groff[202]. Wrinkling increases the flame area, and therefore increases its speed. Results obtained in a large bomb would therefore be unreliable. Unfortunately, there is evidence that wrinkling may also occur in the smaller 160 mm diameter bombs typically used in this sort of work[202,203].

Flame stretch has not been incorporated into the theoretical models used in such constant volume experiments. The results of the present work suggest that this may not matter a great deal. First, the important data are collected when the flame is relatively large. A flame relaxation parameter b of 2 mm leads to the flame speed differing from the one-dimensional value by about 6% at 35 mm but by only 2.5% at 80 mm. Second, the magnitude of b for stoichiometric methane/air was found to decrease quite strongly with pressure in the present work. If this behaviour is standard (and the analysis in Section 7.3 suggests that it is) then the effect of stretch is likely to be negligible.

It is possible, though, that stretch effects can be manifested in a different way by changes in pressure with time. Clavin and Joulin[204] have postulated a "pressure stretch" equal to $(1/p)(dp/dt)$ with its own Markstein length. This is likely to be connected with the storage rate of mass described in the phenomenological analysis in Chapter 2. The rate of pressure rise in constant-volume bomb experiments becomes large when the flame approaches the vessel walls, so the term could become large. No estimates exist for the magnitude (or even the sign) of the corresponding Markstein length. If it were large, difficulties with burning velocity measurements in a constant-volume bomb would be further increased. Work is needed on this topic, especially in view of its potential importance in internal combustion engines.

7.2.4.3 Other methods

A new tube method was introduced by Fuller et al[205]. In this, a flame was ignited at the top of a vertical tube containing the unburnt mixture. It propagated downwards and remained flat for a considerable distance. The burning velocity was determined directly from multiple exposure photographs. It is not clear why the flames were flat in these experiments but curved in others[16,188,206], although the use of a vertical tube may have helped.

In this technique the flow is (presumably) uniform so the burning velocity should not be affected by flow divergence or stretch. The only likely errors are due to heat loss and the assumption that the flame is perfectly flat. While heat loss will reduce the speed of the flame, any deviation from flatness will increase it. The photographs of the propagating flame shown in Fig. 4 of ref. 205 show that it is slightly curved in the steady state.

Although the relative magnitudes of the effects described above are not known, they should cancel to some extent and the method might give reasonable results. The maximum burning velocity determined for a propane/air mixture was 0.40 ms^{-1}, while the result in the present work was 0.39 ± .01 ms^{-1}.

7.2.5 **Critique of recent "one-dimensional" methods**

Several new experimental techniques have appeared recently which have been claimed to give true, one-dimensional burning velocities. In this section we consider their claims in the light of the results of the present work.

7.2.5.1 Double kernel

Burning velocity measurement by the double kernel method was introduced by Raezer and Olsen[207] and later studied by Andrews and Bradley[200]. It has been claimed to be a clear one-dimensional measurement, so it is important to explain how both flow divergence and stretch effects arise.

The experiment involves the production, in a single combustion bomb, of two expanding spherical flames ignited at the same time at positions typically between 35 and 75 mm apart. As the flames approach each other, the leading surfaces become

flattened. The separation of the two near-planar flames is measured as a function of time until they meet, at which point they are considered to be planar and one-dimensional. It follows that the rate of decrease of the separation with time as the flames meet is twice the burning velocity.

Unfortunately, no particle tracking experiments have been performed in this configuration to show which way the gas is flowing, and therefore how one-dimensional the system is. We can, however, make some good estimates. First, consider the results of particle tracking and computer modelling in bomb experiments[208]. An expanding spherical flame is pushed outwards at several times the burning velocity by the thermal expansion of the burnt gas. A particle ahead of the flame is therefore initially pushed away from it by the flow of cold gas produced by the expanding flame.

There is no reason to think that the situation in a double kernel experiment is any different, so it seems clear that there will be a flow of cold gas from between the advancing flames. The flow pattern in the unburnt gas before the flames become flattened can be calculated precisely. It consists of two source flows in which the flow velocity varies as $1/r^2$. Since the flows are potential, they can be summed[209] giving the flow pattern shown in Fig. 65(a). The region between the advancing flames is magnified in Fig. 65(b) to show the establishment of a stagnation-point flow. Although the flow pattern will change as the flames become flattened, it is likely that its general form will be as in this diagram.

In any case, very general reasoning suggests that the unburnt gas between two advancing flames will acquire a velocity component normal to the line of symmetry; that is, it will flow outwards from between the flames. As the flames continue to burn, they will enter this outward-flowing region. From the point of view of the flame, the cold gas has normal and radial velocity components. Moreover, while the normal component remains roughly constant (because it is due to the flame's movement), the radial velocity component must be zero on the axis of the system (by symmetry) and must increase radially (by continuity). This is just the flow field experienced by a flame in an axisymmetric stagnation-point flow. The only difference is that in the double kernel experiment the flow is time-dependent and the exact form of the radial velocity variation is likely to differ from the stationary case.

It follows that the behaviour of the flames in the double kernel experiment will be qualitatively similar to that of flames stabilized in a counterflow. In particular, the

FIGURE 65

Flow field in a double kernel experiment
(a) general view; (b) close-up of region between flames

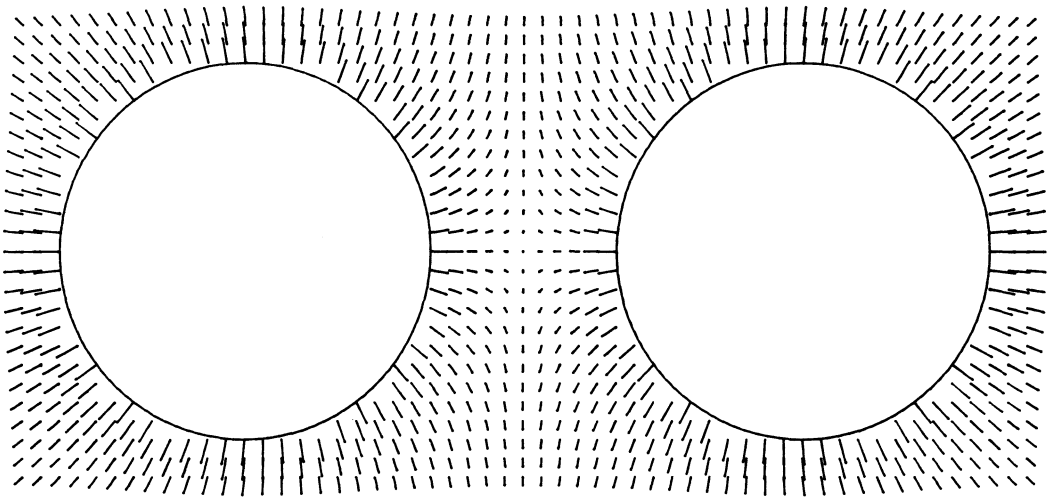

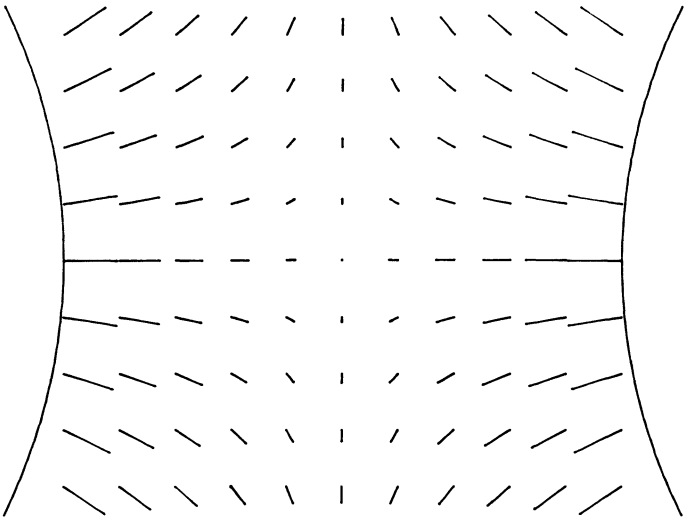

experiments of Law et al[24] show that the upstream gas velocity relative to the flame (which is what is measured in the double kernel experiment) is considerably higher than the one-dimensional value for all gas mixtures, because of the induced flow divergence. Estimating the magnitude of the departure from a one-dimensional burning velocity is not easy: on the one hand, the flow in the double kernel experiment when the flames have become flat is too complex for a simple derivation. On the other hand, comparison via the Law counterflow technique is not advisable, because the results of the present work suggest that the one-dimensional data produced by Law's method are themselves too high. We therefore simply conclude that values of burning velocity obtained using the double kernel technique will be too high.

Using this method, maximum burning velocities of 0.44 ms^{-1} and 0.79 ms^{-1} were obtained for propane/air and ethylene/air by Raezer and Olsen[207], and 0.45 ms^{-1} was obtained for methane/air by Andrews and Bradley[200]. These results are all higher than the values obtained in the present work of 0.39 ± .01 ms^{-1}, 0.66 ± .02 ms^{-1} and 0.37 ± .01 ms^{-1} respectively.

7.2.5.2 Plane counterflow (Law and co-workers)

The essential points about the counterflow method of Law and co-workers[23,24,27-30] have been made in Section 7.1.2.2. Briefly, the evidence suggests that the Law method overestimates the true one-dimensional burning velocity because the true stretch rate is underestimated by the upstream velocity gradient. Extra "residual" stretch causes extra flow divergence, causing the upstream gas velocity to exceed the one-dimensional value even when an extrapolation has been made to apparently zero stretch conditions.

If this suggestion is correct then a comparison between Law's results and the expanding flame data produced in the present work should reveal certain trends. The amount by which Law's apparent one-dimensional burning velocity exceeds the true one must depend on the slope of the S_{L1} *vs* Γ line, i.e. on the Markstein length L_1. This should be closest to zero when the effective Lewis number is greater than unity, i.e. in rich hydrogen and methane and lean ethane and propane. Conversely, L_1 should have a large magnitude when the effective Lewis number is less than unity, i.e. in lean hydrogen and methane and in rich ethane and propane. Law's burning velocities for Le > 1 mixtures should therefore be in closer agreement with the present expanding flame results than those of Le < 1 mixtures.

Figure 43 shows that this prediction is correct for methane/air. The data of Law et al exceed the present expanding flame results (solid line) by a much greater margin in lean mixtures than rich. A more detailed comparison is performed in Fig. 66 by means of cross plots. The present results are plotted as abscissae and those of Egolfopoulos et al[30] as ordinates. The latter were obtained by interpolating between experimental points to find the burning velocities at the same compositions as those of the present work. Points falling on the diagonal line correspond to exact agreement between the two methods. Lean mixtures are represented by open circles and rich mixtures by closed circles. The diagrams correspond to methane (top left), ethane (top right), propane (middle left) and ethylene (middle right).

For methane, results for rich mixtures are in closer agreement than those for lean: the closed circles are nearer to the diagonal. For ethane and propane, the opposite is true. This is precisely the behaviour predicted above on the basis of residual stretch. For ethylene, the Markstein length does not vary monotonically, and a simple comparison of the above type is not possible. But comparison with the Markstein lengths in Fig. 60 shows that the best agreement (in lean and in very rich mixtures) occurs when the Markstein length is large, again in line with predictions. The residual stretch theory is therefore supported by the above comparisons.

Another interesting comparison is with the burning velocities measured by Egolfopoulos and Law[29] of mixtures of hydrogen, oxygen and nitrogen. They found that their experimental burning velocities systematically exceeded the modelled values in very lean hydrogen/"air" mixtures (with various oxygen concentrations in the "air") and in near-stoichiometric mixtures highly diluted with nitrogen. For safety reasons, the only rich mixtures studied were those with 7.7% oxygen in the "air". For these mixtures, the experiments and modelling agreed. Egolfopoulos and Law considered that the discrepancies were evidence of a deficiency in the kinetics at intermediate temperatures.

A comparison with Egolfopoulos and Law's lean hydrogen/air results would not be useful because of the acknowledged inaccuracy of the present results in this regime. The nitrogen-diluted results can be compared, however. The slight difference between the stoichiometries used in the two cases (this work used 1, while Law used 1.044) should not have any effect on the qualitative comparison being performed.

FIGURE 66

Cross plots comparing burning velocity results obtained in this work with those of Law and co-workers[30] and Yamaoka and Tsuji[187]
o: lean mixtures; •: rich mixtures. Abscissa - Present results. Ordinate - Top left: methane[30]; Top right: ethane[30]; Middle left: propane[30]; Middle right: ethylene[30]; Bottom left: methane[187]; Bottom right: propane[187].

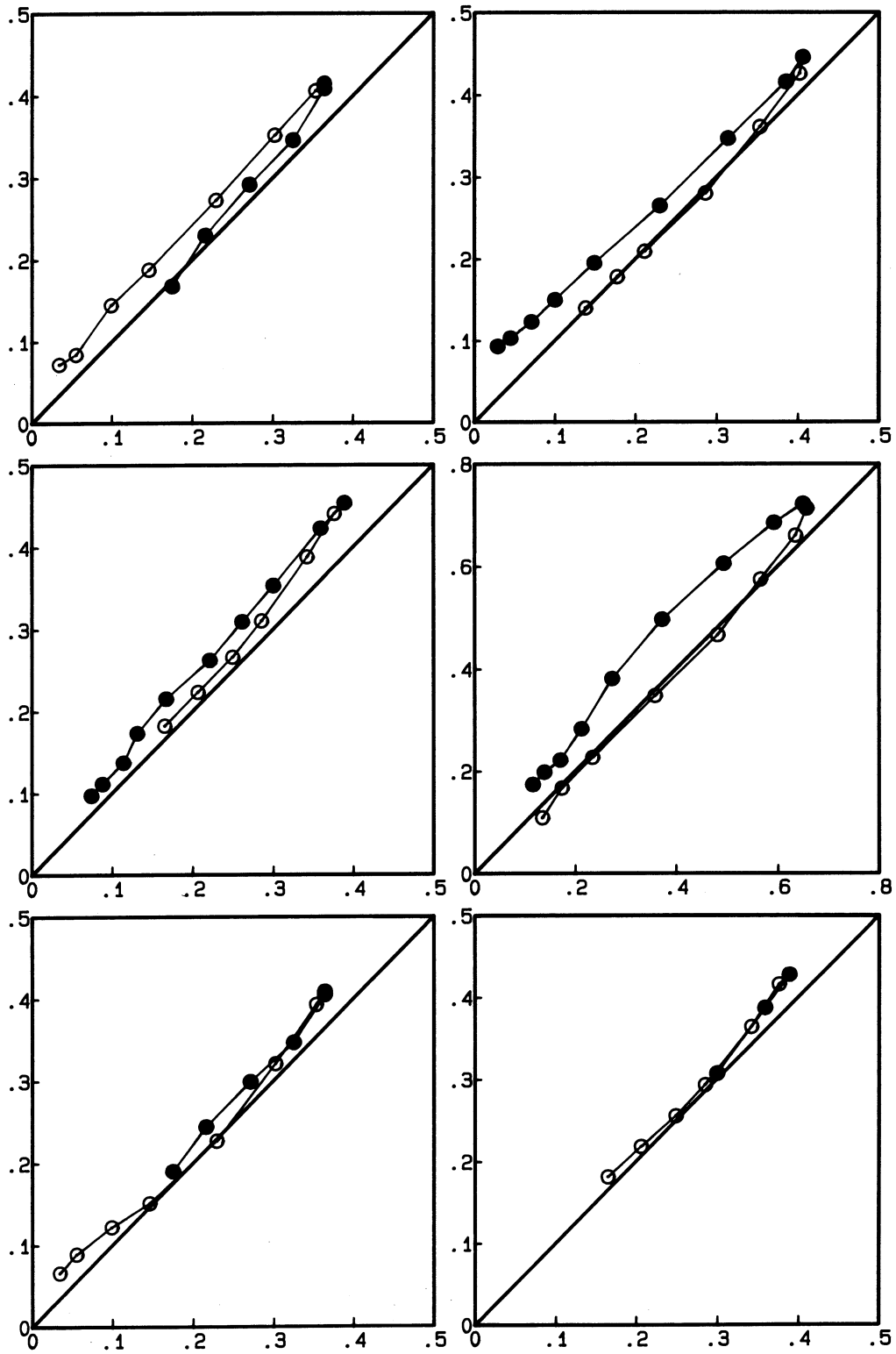

The results at zero dilution agree quite well, but in the range of dilutions for which the Law data are quoted, they exceed those obtained in the present work by about 0.1 ms^{-1}, apart from in the region of 0.6 ms^{-1}, where the results are similar.

A consideration of Fig. 55 shows that the Markstein lengths determined in the present work for nitrogen-diluted mixtures are slightly positive in undiluted mixtures, becoming negative at dilutions of about 15%. According to the earlier arguments based on residual stretch, the counterflow method should give results which are too high for mixtures with Le < 1, which in this case corresponds to dilutions greater than 15%. The differences between the present results and those of Egolfopoulos and Law are therefore explicable on the basis of residual stretch. The explanation can be extended to Egolfopoulos and Law's other results. All the cases where there was a discrepancy between experiment and modelling are ones which would have a negative Markstein length and would therefore lead to high experimental burning velocities. The rich mixtures would have a positive Markstein length, and the counterflow method should be fairly accurate. This explains why no discrepancy was found between experiment and modelling for these mixtures.

To summarize, any discrepancies in the present work between experiment and modelling can be explained by error in the experiments. Where the experiments are known to be accurate, comparisons with the results of Law and co-workers show that the latter are high in mixtures with Le < 1. This finding supports the suggestion of a systematic error in the latter results due to residual stretch. Egolfopoulos and Law's claim that the kinetics of hydrogen oxidation is incomplete is therefore not supported by the present work.

7.2.5.3 Curved counterflow (Yamaoka and Tsuji)

In this method[187], twin flames are stabilized in the counterflow in a Tsuji burner, in which the fuel/air mixture flowing out of a porous cylinder meets a uniform flow of secondary fuel/air mixture, possibly with a different stoichiometry. The flow rate of gas leaving the porous cylinder is reduced until the inner flame gets so close to the cylinder that heat is lost to it. This point is determined by a kink in the flame position *vs* ejection velocity curve. The gas ejection velocity at this point, determined from the volumetric flow rate, is taken to be the burning velocity. Yamaoka and Tsuji assumed that the effect of stretch was negligible, so that their value was the one-dimensional one. Their maximum value for the burning velocity of methane/air was 0.41 ms^{-1} and that of propane air was 0.43 ms^{-1}.

Even if the flow were uniform in this experiment, the burning velocity would still be affected by flow divergence because the flame is curved. The area ratio between luminous zone and cold boundary would be about $1 + \delta/r_{cyl}$ where δ is the distance between these points and r_{cyl} is the radius of the porous cylinder. The latter was 30 mm, while δ for the fastest burning methane and propane mixtures is stated to be about 1 mm. The area ratio is therefore about 1.03 and if this were the only effect then the correct maximum burning velocities for methane and propane would be about 0.40 ms^{-1} and 0.42 ms^{-1}, with larger errors in lean and rich mixtures due to the greater flame thickness.

Since the flame is established in a counterflow, it must be stretched. Residual stretch should be negligible since, as in the case of a flat flame stabilized close to a porous plate burner, there is insufficient space for it to occur. We therefore assume that the stagnation velocity gradient is an accurate measure of the stretch experienced by the flame.

The stretch will have two effects on the burning velocity measurement. One is the extra flow divergence over and above the radial contribution, and the other is the effect on the propagation rate of the flame. It was shown in Section 3.4 that divergence effects have a larger effect than stretch on upstream burning velocity measurements. Nevertheless, if the conditions are sufficiently well controlled, stretch effects can still be seen, as in the different effects of residual stretch on lean and rich mixtures in the Law experiments described in the previous section.

In Yamaoka and Tsuji's work, it is difficult to disentangle the various effects. There will be two contributions to the area ratio between cold boundary and luminous zone. One (the "radial" contribution) depends only on the flame thickness, while the other (due to stretch) depends on both flame thickness and stretch rate. In stoichiometric mixtures the stretch rate is large and the flame thickness small; in lean and rich mixtures the opposite is true. The effect of stretch on the propagation rate will also have its largest effect in lean and rich mixtures since then the Markstein length has the largest magnitude. There is also a further complication. It appears from Figs. 5 and 6 of ref. 187 that the flame thickness depends on both the stoichiometry of the secondary mixture and the stretch rate.

In view of the above, it does not seem possible to make detailed comments about the Yamaoka and Tsuji results. In particular, there is no way to predict whether lean or rich mixtures should agree better with the present work. We therefore conclude that

flow divergence effects will cause the burning velocities of Yamaoka and Tsuji to exceed the present values by an unknown amount. Cross plots of their data against the present work are shown in Fig. 66: methane/air mixtures are at bottom left and propane/air at bottom right. They show that the Yamaoka and Tsuji data are indeed higher than the present results, except in mixtures with burning velocities of about 0.25 ms^{-1}. It may be that accurate burning velocities were obtained for these mixtures because both stretch rates and flame thickness were relatively small.

7.2.5.4 Plane counterflow (Cambray et al)

The counterflow method of Cambray et al[85-87] is chiefly used for the determination of Markstein lengths. But it is implicit in their method that the burning velocities measured at various stretch rates extrapolate to the one-dimensional value at zero stretch. The method will therefore be considered here from the point of view of the burning velocity definition and the likelihood of obtaining true one-dimensional results. We will return to the method in Section 7.3 when we consider Markstein lengths.

The experimental definition of the burning velocity used in the work of Cambray et al is not straightforward. The aim of the experimental work was to measure the burning velocity u_n which appears in the theoretical work of Clavin and co-workers[55,61,176,204]. It is defined[210] as the normal component of the unburnt gas relative to the flame front in the limit $\delta/\Lambda \rightarrow 0$ where δ is the flame thickness and Λ is the hydrodynamic length scale.

There are different opinions on the connection between this definition and a real flame. Eteng et al[211], who used the same definition in their theoretical work, considered that the asymptotic burning velocity is not well defined experimentally. Searby and Quinard[177] stated that u_n in a real flame "is defined as the mass flux at the reaction zone divided by the density of the unburnt gas". They are therefore saying that u_n is the same as the burning velocity $S_{u,r}$ defined in the present work. In order to compare their theoretical stretched burning velocity with experiment, Tien and Matalon[72] derived an expression to correct u_n for the finite flame thickness. In the experimental work by Cambray et al[85-87], u_n was obtained by extrapolating the upstream velocity profile to the reaction zone of the flame.

Measurements of u_n, S_{L1} and $S_{u,r}$ in a rich methane/air flame in a stagnation-point flow were performed in the present work. They are described in Section 5.2 and

plotted in Fig. 42(a). The results contradict Searby and Quinard: it is clear that u_n is not identical to $S_{u,r}$, and this is backed up by the theory. It can be shown from the expressions for the respective Markstein lengths in ref. 55 that the difference between the two burning velocities is

$$S_{u,r} - u_n = \delta\Gamma \ln \sigma. \qquad (20)$$

The $\ln \sigma$ term is a correction for the effect on the mass flux of streamline refraction. In the expanding flame case it accounts for the "storage rate" of mass referred to in Section 2.2.2.2. It does not appear in the unburnt gas Markstein length because the streamlines at the upstream boundary are unaffected by the flame. It seems reasonable, though difficult to justify rigorously, that experimental values of u_n corresponding to its theoretical definition should be produced by Cambray et al's technique of extrapolating the upstream velocity profile to the reaction zone.

Equation (20) does not describe fully the differences between the measured values of u_n and $S_{u,r}$. Figure 42(a) shows that u_n and S_{L1} extrapolate to a higher value at zero stretch than $S_{u,r}$. In the critique of the Law counterflow method in Section 7.2.5.2 it was suggested that the one-dimensional results obtained by extrapolating S_{L1} to zero stretch may be too high because there is residual stretch which is not detected by the measurement method. The values of u_n in Fig. 42(a) were obtained by subtracting $\Gamma\delta$ from S_{L1}, so they extrapolate to the same high one-dimensional value as S_{L1}. If the explanation based on residual stretch is correct then, as described in Section 7.1.2.2, it should be possible to modify the counterflow technique to give correct one-dimensional results. S_{L1} should then extrapolate to the correct one-dimensional value and u_n could be derived from it. The assumption is being made that residual stretch is the only problem with S_{L1}. If the criticisms of Tien and Matalon[72] and Dixon-Lewis[89] were still valid then u_n could be derived from $S_{u,r}$ instead.

Cambray et al also determined u_n from S_{L1}. It is therefore likely that their one-dimensional burning velocities are too high by the same amount as Law's results obtained by extrapolation of S_{L1}.

If the residual stretch explanation is correct then the unburnt Markstein length $\mathcal{L}$ given by the slope of the u_n *vs* Γ function should be unaffected.

7.3 MARKSTEIN LENGTH

In this section the experimental results for the Markstein lengths are discussed and compared with existing values. Unfortunately, no other experimental Markstein length data exist based on the burning velocity definition used in the present work. The present results are therefore compared with theory first of all. Provided the theory is capable of predicting the results, it can then be used for converting experimental unburnt Markstein lengths into the form of the present data for comparison.

7.3.1 Comparison with theory

As described in Section 2.2.3, an appropriate theoretical expression for comparison with the experimental values of Markstein length is equation (2-187), derived from the work of Clavin and Joulin[55] and reproduced below.

$$L = \frac{\delta\sigma}{1 - \sigma}\left[\ln \sigma^{-1} + \frac{\beta(\mathrm{Le} - 1)}{2}\int_0^{(1-\sigma)/\sigma} \frac{\ln(1 + x)}{x} dx\right]. \qquad (21)$$

Most of the terms in this equation can be readily evaluated. The density ratio σ was obtained from flame temperature calculations using the program FTEMP. The integral was performed numerically at various values of σ using Simpson's rule. A polynomial function was then fitted to these values so that the value of the integral at any density ratio could be readily determined.

The terms which are not straightforward to estimate are the flame thickness δ, the Zel'dovich number β and the Lewis number Le. There is considerable uncertainty about each of these quantities since they are all rather ill-defined for a real flame. The methods used to calculate them will be described next. Since precise agreement between asymptotic theory and experimental results is not expected, the general philosophy has been to use data calculated for the appropriate circumstances (e.g. reference surface temperatures rather than unburnt gas temperatures) but in the simplest way. More sophisticated treatments can then be performed if the agreement between theory and experiment warrants it.

The flame thickness δ is given by equation (2-36) and can be expressed as (λ/c_p) divided by the mass burning rate. In the derivation of this expression in Chapter 2

the thermal conductivity and specific heat were stated to be mean values. It is not obvious which values in a real flame should be used, since both composition and temperature are changing in the region that they are intended to characterize. While Clavin and co-workers[61] recommended the use of burnt gas values, Searby and Quinard[177] and Deshaies and Cambray[87] used the thermal conductivity in the unburnt gas. In the asymptotic analysis in Chapter 2, the "flame thickness" δ is actually the distance from the hot boundary to the point at which the temperature is 1/e of its final value. The corresponding region in a real flame is presumably that part of the preheat zone immediately upstream of the reference surface. It therefore seems reasonable that values corresponding to conditions at the reference surface should be used. It would not be appropriate to use burnt gas data; the adiabatic flame temperature would be too high, and the equilibrium composition would differ considerably from that of the preheat zone. In line with the approach described above, we will use a constant temperature of 1600 K for all mixtures since this is an approximately average reference surface temperature, and should therefore characterize the region we are interested in. We will use the expression of Kennel et al[183] for (λ/c_p) and evaluate it at a constant temperature of 1600 K for all flames. The result is 1.267×10^{-4} kg m^{-1} s^{-1} which conveniently cancels with the cold gas density (taken to be that of air) so that the flame thickness in millimetres is given by $1/(10S_u^{\circ})$ when the burning velocity is in metres per second. This procedure was used for all the hydrocarbons, but the densities of the unburnt hydrogen/air mixtures were calculated precisely since they vary strongly with mixture composition.

For the variable pressure case, the flame thickness expression may be extended by putting the pressure in atmospheres in the denominator since its only effect is on the cold gas density. So for constant burning velocity, the Markstein length is predicted by equation (21) to be inversely proportional to pressure. The methane/air results at variable pressure are therefore qualitatively explained.

The Zel'dovich number was determined using equation (2-83). All terms are known except for the activation energy, which was determined from the present experimental burning velocity results and calculated flame temperatures using the method described in Section 2.1.2.1. The results are shown in Table 13.

The data are similar to those determined by Sahay et al[212] but are generally rather lower than the values of Kaskan[213], which were determined using a cooled porous plate burner. The different results for hydrogen/air across the stoichiometric range and for diluted hydrogen/air do not present a problem since the effective activation energy is not a fundamental quantity. In fact, the diluted value is probably a better

estimate for stoichiometric mixtures since the fuel/oxygen ratio remains constant. This probably explains the lower calculated uncertainty.

TABLE 13

Effective activation energies determined in the present work

Fuel	Activation energy / kcal mol^{-1}
H_2/air	23.1 ± 2.9
H_2/air (diluted with N_2)	29.5 ± 0.3
CH_4/air	46.5 ± 2.7
C_2H_6/air	49.7 ± 7.1
C_3H_8/air	45.9 ± 8.4
C_2H_4/air	35.2 ± 4.8

In the simple asymptotic theory of flame stretch effects, the mixtures are considered to be far from stoichiometric such that the effective Lewis number is that of the deficient component[44,55]. In order to compare the theory with results in near-stoichiometric mixtures, a method of estimating intermediate values of the Lewis number is needed. A suitable approach is described by Joulin and Mitani[35]. Their work shows that the effective Lewis number is a function of the Lewis numbers of the fuel and the oxygen. The function depends on the equivalence ratio, Zel'dovich number and assumed reaction orders with respect to fuel and oxidant. It has a particularly simple form when the reaction orders are both equal to 1 so this will be used in all mixtures. For this case, the effective Lewis number of a stoichiometric mixture is simply the mean of the fuel and oxygen Lewis numbers. The use of different reaction orders has a small effect on the value of the effective Lewis number in near-stoichiometric mixtures.

The work of Joulin and Mitani assumes that the Lewis numbers of the reactants remain constant as the composition is varied. In fact, a calculation of Lewis numbers in different mixtures using the CHEMKIN code[111] shows that they change markedly. We will see later that such changes are important in explaining some of the present results, so we will use fuel and oxidant Lewis numbers calculated for each mixture

composition, and combine them according to the method of Joulin and Mitani to give a single effective Lewis number.

The Lewis numbers calculated using CHEMKIN also vary with temperature. In previous work, e.g. refs. 214 and 215, the usual practice has been to use Lewis numbers calculated at room temperature for determining stretch effects. In the present work it is considered more reasonable to use values determined near the reference surface since this is where the relative rates of diffusion of heat and mass have their effect. Accordingly, data were calculated at 1600 K in all cases.

Theoretical Markstein lengths using the above data are plotted as dashed curves in Figs. 67, 68 and 69. Data for hydrogen/air mixtures across the stoichiometric range are plotted in Fig. 67(a) and results for stoichiometric hydrogen/air as a function of nitrogen dilution are in Fig. 67(b). Figs. 68(a), 68(b), 69(a) and 69(b) respectively contain data for methane, ethane, propane and ethylene mixtures with air across the stoichiometric range. Results for stoichiometric methane/air as a function of pressure have not been plotted because the pressure dependence is contained entirely in the flame thickness term. The additional points in the figures are experimental and modelling data which will be described later.

The plots show that the theory accurately predicts the experimental hydrogen and ethylene values but in the other cases fails to follow the trend to negative Markstein lengths. To check the effect of the input data, the theoretical Markstein lengths of these cases were recalculated with higher activation energies. The values used were 70 kcal mol^{-1} for diluted hydrogen/air, 80 kcal mol^{-1} for methane and ethylene, and 110 kcal mol^{-1} for propane. The new data are plotted as dotted curves. These changes were sufficient to provide qualitative agreement with experiment.

The activation energies used are in most cases too high to be acceptable as correct input data. They represent the changes needed to obtain qualitatively correct predictions. Varying the value of (Le - 1) by the same proportional amount would give the same result. But the most satisfactory solution may be to use a more sophisticated version of the theory[204].

The solid curves through the experimental points were obtained by finding the best low-degree polynomial fit to $1 = \beta(\mathrm{Le} - 1)$ calculated from equation (2-187) using experimental values of L. In all cases, these "experimental" values of 1 are qualitatively similar to those calculated for use in the theoretical comparisons. For example, both experimental and theoretical values of 1 are negative in lean hydrogen

FIGURE 67

Comparison of experimental Markstein lengths with other data. (a) hydrogen/air as a function of stoichiometry; (b) stoichiometric hydrogen/air diluted with nitrogen •: Present results. ○: Data derived from modelling of Dixon-Lewis[70]. □ : Data derived from modelling of Warnatz and Peters[67]. △ : Experimental data of Searby and Quinard[177]. Solid curve: best fit through present data. Dashed curve: theory of Clavin and Joulin[55]. Dotted curve: theory of Clavin and Joulin[55] with different data.

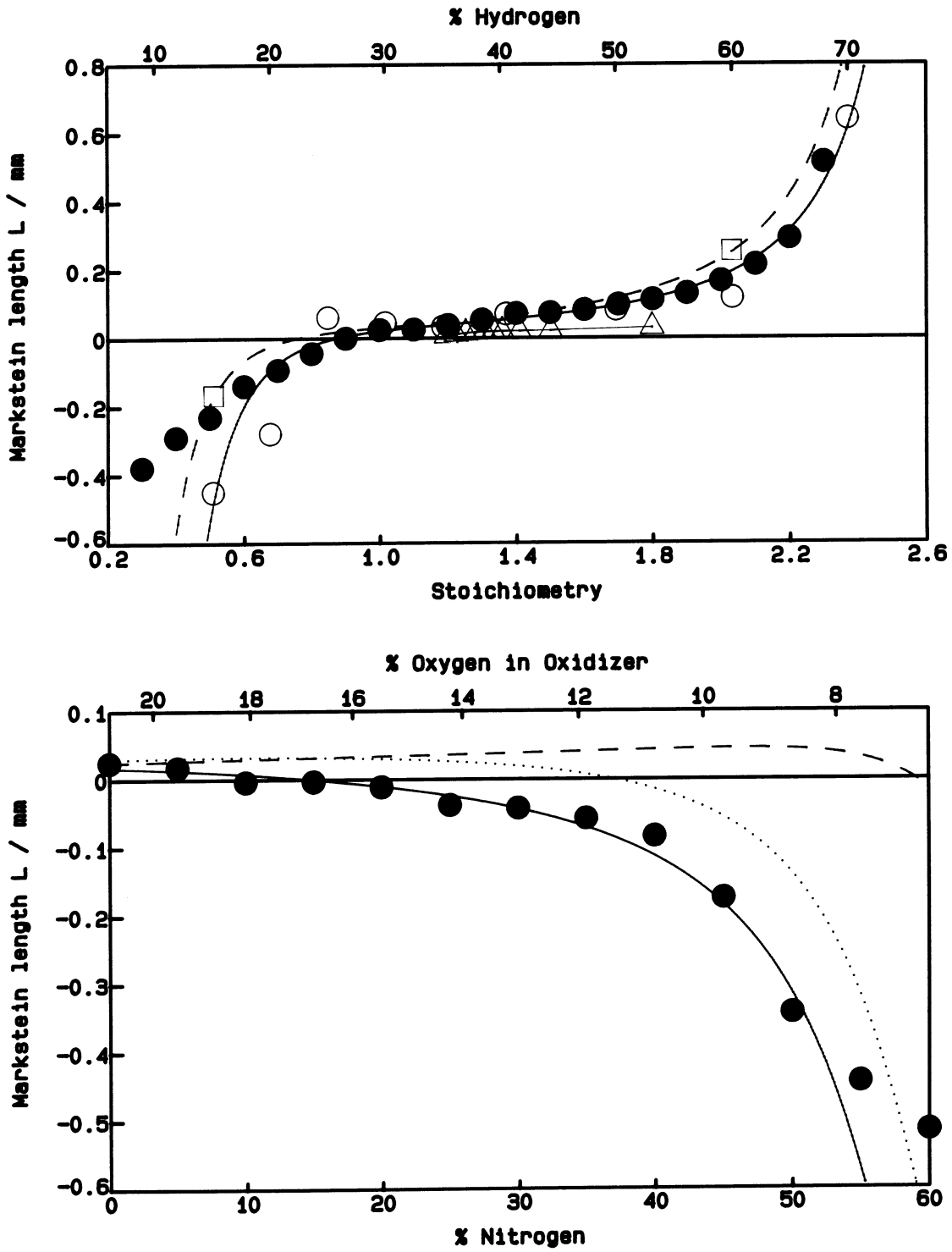

FIGURE 68

Comparison of experimental Markstein lengths as a function of stoichiometry with other data. (a) methane/air; (b) ethane/air

•: Present results. ○: Data derived from modelling of Rogg[68]. △ : Experimental data of Searby and Quinard[177]. □ : Experimental data of Law et al[24]. Solid curve: best fit through present data. Dashed curve: theory of Clavin and Joulin[55]. Dotted curve: theory of Clavin and Joulin[55] with different data.

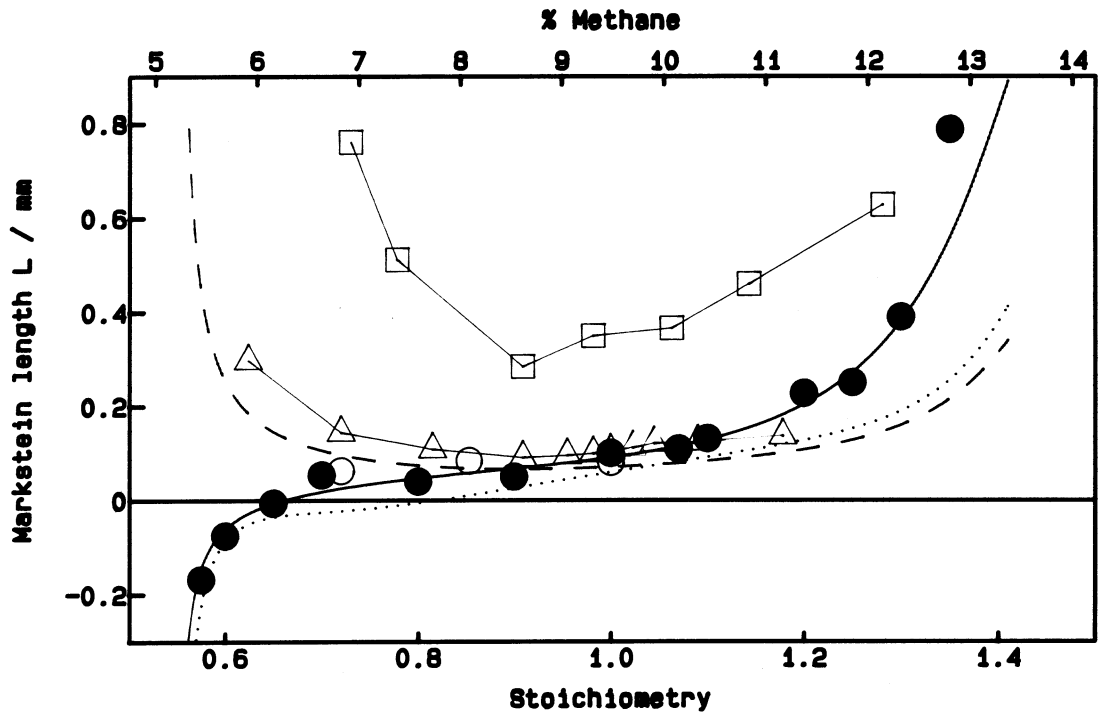

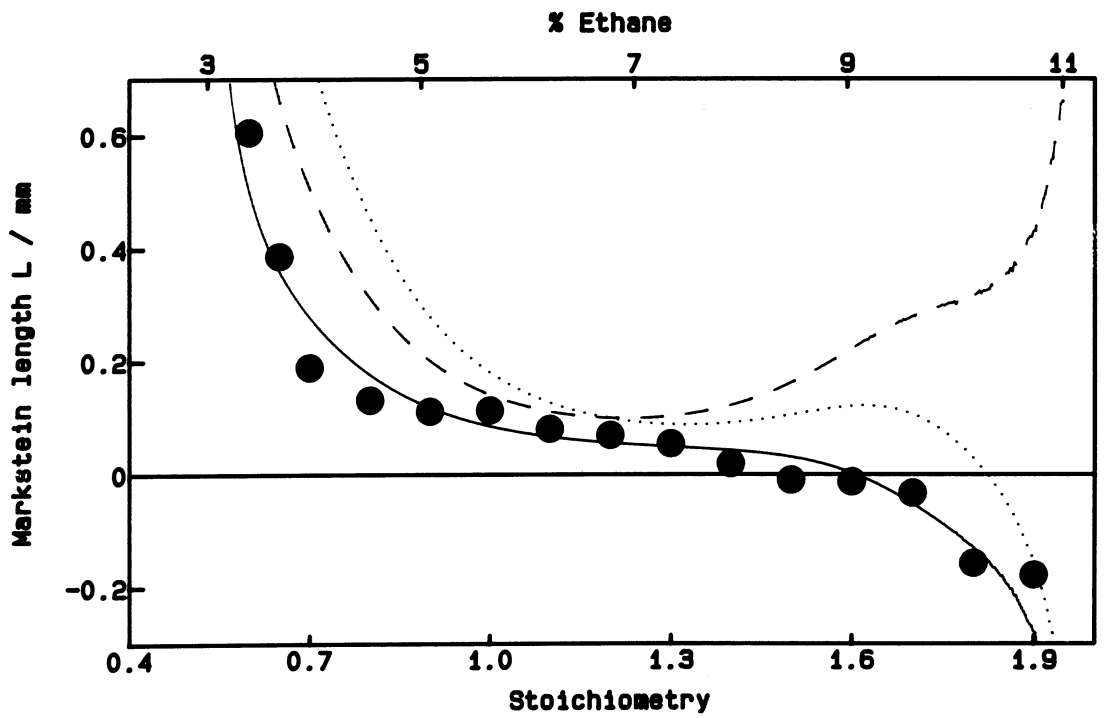

FIGURE 69

Comparison of experimental Markstein lengths as a function of stoichiometry with other data. (a) propane/air; (b) ethylene/air

•: Present results. △ : Experimental data of Searby and Quinard[177]. □ : Experimental data of Law et al[24]. Solid curve: best fit through present data. Dashed curve: theory of Clavin and Joulin[55]. Dotted curve: theory of Clavin and Joulin[55] with different data.

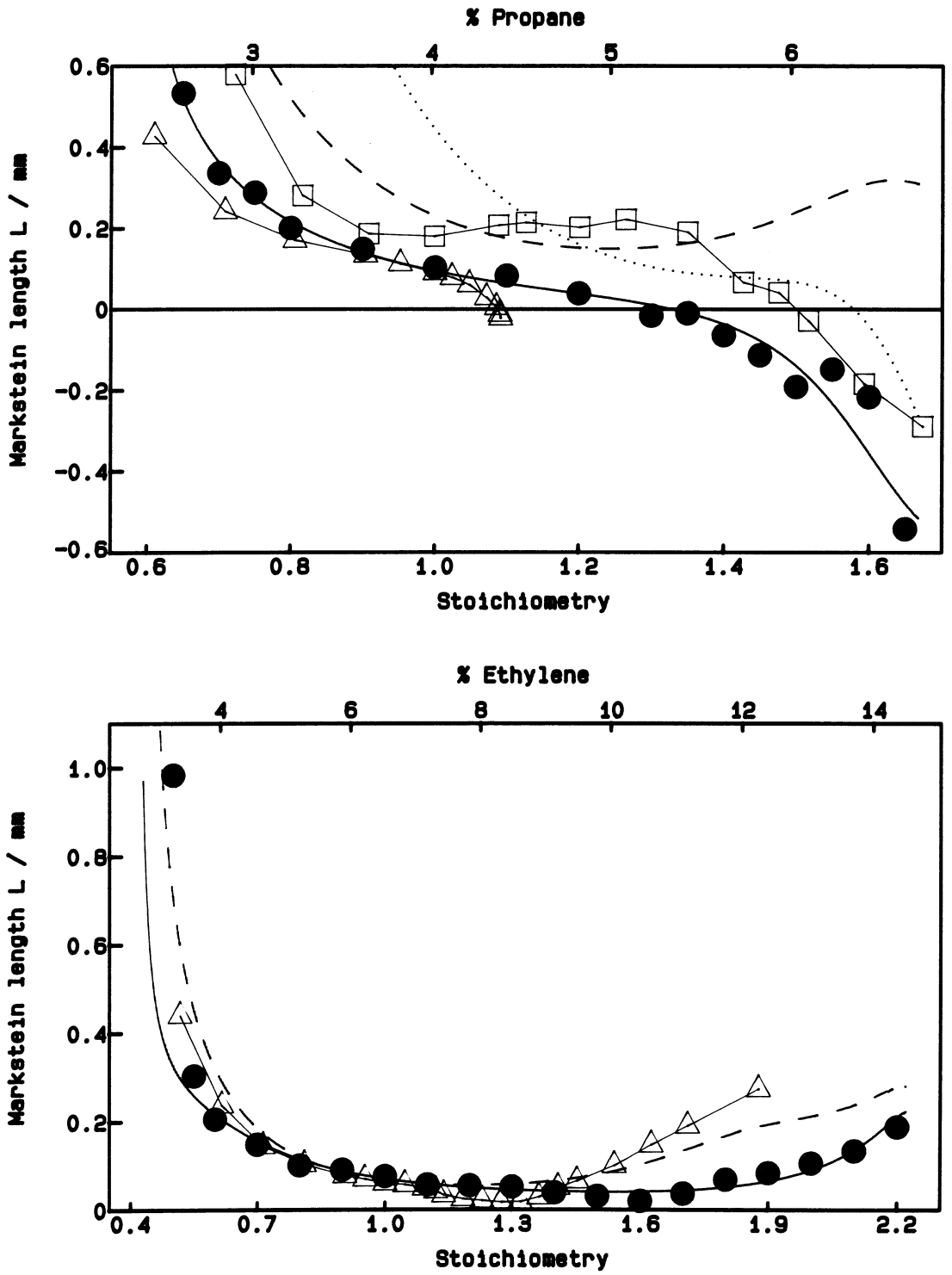

and methane mixtures and positive in rich, while for ethane and propane the opposite is true. For diluted hydrogen/air, l becomes negative as the dilution is increased in both cases. This qualitative agreement is perhaps as much as should be expected from an asymptotic theory.

Overall, we can say that the theory predicts the experimental results moderately well, given some adjustments in the input data. Since the data in question are rather ill-defined, it does not seem unreasonable to make such changes. It is interesting that in the cases where such adjustments were not needed, the theoretical predictions agreed not just qualitatively but quantitatively with experiment.

Since the theory contains no detailed chemistry, the fact that it can make reasonable predictions demonstrates that transport effects dominate, as suggested by the phenomenological analyses of Section 2.2.2. In particular, it can be seen that small variations in the Lewis number are crucial in determining the effect of stretch.

The success of the theory has implications for the comparisons with other experimental work described in the next section. Use of the theory to convert from unburnt Markstein lengths to the present definition can be expected to give reasonable but possibly not precise results. And if the success of the asymptotic theory extends to its predictions of the onset of instability then its use for deriving Markstein numbers[177] should give reasonable results.

A theoretical value for the Markstein length of a stoichiometric methane/air mixture was derived by Rogg and Peters[182]. They used an asymptotic analysis of a systematically reduced three-step kinetic mechanism. The value they obtained was for a burning velocity defined at the fuel consumption layer of the flame (at about 1380 K), so it should be directly comparable with the present work. Their result was $\mathcal{L}/\delta_0 = 2.23$ with δ_0 defined as $(\lambda/c_p)_0/M$ where the subscript 0 denotes conditions at the fuel consumption layer. Because of the way the Markstein number was defined, it turns out that its relationship to that in the present work is $L \approx (300/1380)\mathcal{L} \approx .217\mathcal{L}$. The Markstein length for stoichiometric methane/air at atmospheric pressure was calculated using the data provided in ref. 182 for the burning velocity, the temperature of the fuel consumption zone and $(\lambda/c_p)_0$ and found to be 0.072 mm. The experimental value determined in the present work was $0.10 \pm .01$ mm so the agreement is fairly good.

It has been possible to extract some approximate values of Markstein lengths from detailed modelling of stretched flames. Values for hydrogen/air have been derived from the modelling of Dixon-Lewis[70] and Warnatz and Peters[67]. Methane/air results using a 4-step mechanism and a low strain rate approximation have been taken from the modelling results of Rogg[68]. The stoichiometric value was 0.080 mm which was slightly closer to the experimental result than the asymptotic calculation described earlier. The comparisons are shown in Figs. 67(a) and 68(a). The agreement is generally rather good, when one considers the difficulty of measuring the Markstein length.

7.3.2 **Comparison with other data**

There is a difficulty in comparing the experimental Markstein lengths obtained in the present work with other experimental values. All Markstein length determinations depend on the definition used for the burning velocity. In this work, the definition is equation (3-1): the mass flux at the reference surface divided by the cold gas density. Unfortunately, no other experimental values of the Markstein length have been reported based on this precise definition. But there are three sets of experimental Markstein length data which can be converted to the form of the present results.

The results of Law et al[24] were measured with respect to an upstream burning velocity. Conversion to the present definition of Markstein length can be made approximately as follows. It can be shown[64] that the upstream burning velocity S_{L1} of Law and co-workers is related to the burning velocity u_n of Clavin by

$$u_n = S_{L1} - \Gamma\delta_m \tag{22}$$

where the subscript m denotes a measured rather than a calculated flame thickness. Substituting equation (3-65) for the variation of S_{L1} with stretch in (22) gives

$$u_n = S_u^{\circ} - (L_1 + \delta_m)\Gamma. \tag{23}$$

Comparison with equation (2-180) shows that the term in the brackets equals the unburnt Markstein length $\mathscr{L}$. By using equation (2-186) along with the theoretical expressions for unburnt and burnt Markstein lengths in ref. 55, it can be shown that the relationship between the Markstein length in the present work L and the unburnt parameter $\mathscr{L}$ of Clavin and Joulin is

$$L = \mathcal{L} + \delta \ln \sigma \tag{24}$$

where the flame thickness δ should be calculated using hot gas properties. The relationship between the present Markstein length and that of Law is therefore

$$L = (L_1 + \delta_m) + \delta \ln \sigma. \tag{25}$$

In fact, Law's data were presented as the product of Markstein length and one-dimensional burning velocity. Since the burning velocity data were also presented, L_1 was determined first and then equation (25) was used to determine the corresponding values of L. The measured flame thicknesses used in equation (25) were those of Yamaoka and Tsuji[187]. Unfortunately, the measured thicknesses of propane/air mixtures only extended to moderately rich mixtures, so they were extrapolated to richer values. The results for methane and propane are plotted in Figs. 68(a) and 69(a). The methane data follow the same trend on the rich side as the results of the present work, but are about 0.2 mm larger. The wrong trend is followed on the lean side, possibly due to deficiencies in the theory. The propane data are again around 0.2 mm higher than the present data, but they follow the same trend.

The unburnt Markstein lengths of Deshaies and Cambray[87] were determined using the asymptotic definition of the burning velocity u_n. According to the discussion in Section 7.2.5.4, the unburnt Markstein length associated with it should be valid even if the burning velocity extrapolates to a high value. Deshaies and Cambray presented their results for lean propane/air mixtures at a range of dilutions in the form of a single Markstein number, since they found no systematic trend as the dilution was varied. Their result can be converted to a Markstein length in the present form by substituting the definition of Markstein number, $\mathrm{Ma} = \mathcal{L}/\delta$, in equation (24), giving

$$L = \delta \, (\mathrm{Ma} + \ln \sigma). \tag{26}$$

The use of values of δ and σ for undiluted propane/air with a stoichiometry of 0.8 (near enough to the precise stoichiometry of 0.807) should give a result comparable with the present data. Although Deshaies and Cambray did not state it explicitly, it is clear from ref. 87 that their results were nondimensionalized by dividing by flame thicknesses based on unburnt gas properties. Similar data were therefore used for converting back. The calculated flame thickness was 0.074 mm and the density ratio was 0.1410. The Markstein length calculated from these data was 0.45 ± .09 mm,

compared with 0.20 ± .02 mm for the corresponding mixture in the present work. The reason for the difference is not known, but it may be relevant that Deshaies and Cambray's result, expressed as a Markstein number, also exceeded that of Searby and Quinard[177] by a factor of 2.

Searby and Quinard's work consisted of measurements of Markstein numbers by three different techniques. The direct method was comparable to the stagnation flow method of the present work but with flames of variable curvature. It led to such large uncertainties that the results were meaningless. The other two methods were indirect. One involved measurement of the global response of the flame to a shear flow. Transverse variations were induced in the velocity of the gas approaching a premixed flame by inserting regularly-spaced tubes into the flow. The amplitude of wrinkling in the flame was measured as a function of the amplitude of the variation in the longitudinal gas velocity. This was done for two methane/air and two propane/air mixtures. The Markstein number was determined by comparing the experimental behaviour with that of theoretical predictions at different Markstein lengths.

The final method involved measurement of the critical burning velocity at the onset of instability in a downward-propagating flame. For each mixture, the equivalence ratio was kept fixed and amount of nitrogen was varied until the flame just became unstable. The burning velocity, taken to be the upstream gas velocity, at this point was the critical value required. The Markstein number was determined from this critical velocity using a theoretical expression. This was done for a wide range of fuels and compositions. The results agreed well with those from the other indirect method so, since they cover a wider range, the data from this last method will be compared with the present results.

Since the results were presented as Markstein numbers, the question of converting back to Markstein lengths arises again. This can be done straightforwardly by using equation (26) as in the case of Deshaies and Cambray. But in this case there is a more subtle effect to consider. For the results of Deshaies and Cambray, the effect of using equation (26) is to return to the original dimensional results. This is not possible for the Searby and Quinard data. The Markstein lengths were determined from an expression containing several terms, one of which was a critical Froude number containing a measured burning velocity and a flame thickness based on the unburnt gas. There is no simple way of repeating the calculation using a flame thickness calculated at high temperature, so we have to assume that the parameter used was appropriate. The arguments presented so far in the present work tend to

suggest that it was not. But it may be that the more sophisticated theory used in ref. 177 takes account of this problem.

The results are plotted in Figs. 67(a), 68(a), 69(a) and 69(b). The results for hydrogen follow the correct trend, but are about a factor of 5 lower than the results of the present work. The methane results agree with the present results on the rich side, but follow the wrong trend on the lean side. Again, the deficiencies in the theory may be responsible for this behaviour. The results for propane and ethylene show good quantitative agreement with the present results. Overall, the agreement is rather good, considering the difference between the methods used.

7.4 IMPLICATIONS OF THIS WORK

7.4.1 **Characterizing the flame propagation rate**

Two definitions of burning velocity are considered in the present work. One is the conventional one, namely the gas velocity at the cold boundary of the flame. The other is proportional to the mass flux in the hot part of the flame.

The advantage of the conventional definition is that it is a true gas velocity in the flame, and as such is readily understood. The disadvantage is that it does not reflect the flame's behaviour. For example, in a stationary spherical flame it varies with the flame radius, although the flame itself is unchanged. In a stretched flame, its variation with flow divergence masks the effect of stretch on the flame response.

By contrast, the burning velocity based on the mass flux does not equal any velocity in the flame and its meaning is therefore not obvious, but it does reflect the behaviour of the flame. It is invariant to changes in flame radius in a stationary spherical flame, and in stretched flames it demonstrates the true response of the flame. The Markstein lengths plotted in Figs. 54 to 60 therefore represent the effect of stretch on the rate at which mass is consumed by the flame. An advantage of this is that the present Markstein lengths are consistent with other measures of the flame response to stretch. Examples include flame extinction in stagnation-point flow[214,216] and burning intensity in Bunsen flame tips[217,218].

A way of avoiding the inevitable misunderstandings that must accompany such disparate definitions would be to abolish the term "burning velocity" altogether. The

flame propagation rate would be characterized by the mass burning rate. This would be defined as the mass flux (mass flow rate per unit area) at the reference surface. The reference surface position might be unknown, and discussion would then centre on where in the flame the mass flux should be measured to give the correct value. This would bring to the surface an issue which underlies the present scatter in burning velocity results. The important point is that there would be a measurement of flame propagation rate with a well-defined physical meaning, and the room for misunderstanding would be much reduced.

Workers who have advocated or used the present definition of burning velocity include Lewis and von Elbe[18], Fristrom[20], Dixon-Lewis[22,40], Williams[31], Peters (in the discussion following ref. 24), Rogg[68] and Hoffmann-Berling et al[219].

There is one type of flame for which the definition proposed in this work is not directly applicable. Under certain conditions, the premixed flame in a counterflow can exist on the "other side" of the stagnation point, with reactants supplied solely by diffusion. Such flames are sometimes referred to as having a negative burning velocity. They have been predicted by asymptotic analysis[31] and detailed modelling[220] and have been observed experimentally[221]. As pointed out by Williams[31], the best definition of propagation rate in this case would be the rate of heat release or reactant consumption per unit flame area. The latter definition would, in fact, be consistent with the present one.

7.4.2 **Flame modelling studies**

In the early days of flame theory, prediction of the burning velocity was the sole aim. But with the advent of computer modelling of flames, other comparisons could be made. In particular, the profiles of both major and minor species were predicted and could be compared with experiment. Data were provided by molecular beam mass spectrometry[114] and by laser methods[222]. It was suggested[114,174] that the predicted profiles of radical species provided a much more stringent test of a model than the burning velocity. Also, it was shown[173] that the burning velocity could be predicted well, and the major species profiles fairly well, across the stoichiometric range by flame modelling using a single overall reaction. These arguments suggest that burning velocity may not be a useful parameter in model validation. In this section we discuss this issue and some related ones.

It is clear that accurate prediction of burning velocities and major species profiles is a necessary but not a sufficient condition of a good model. This must be so since these properties can be predicted by a model consisting of a single reaction with a rate bearing no relation to any of the real chemistry[173].

It is not known whether accurate prediction of minor species profiles is a sufficient condition for a good model. It seems unlikely, and in any case the question is premature. Accurate measurement of the profiles of minor species is very difficult, so even where the measurements have been made the data are known only within rather large uncertainties. Clearly where knowledge of flames is incomplete and uncertain, the more accurate data of any sort the better. Thus a role exists for burning velocity measurements in the validation of flame models.

In the present work, the measured burning velocities were used as the sole means of "fine-tuning" the model. Sensitivity analysis was used to find which rates produced the biggest changes in the predicted burning velocity. There were only a few of these for each flame, but different rates became important for different fuels or stoichiometries. This confirms the results of Coffee et al[173,174], but also shows that the burning velocity is actually a sensitive test of the rates of certain reactions in the model.

The new feature in the present work is that the burning velocities can be trusted more than previous results. One can therefore demand that the model should fit the experimental results within, say, 5%. This is rather different from in the past when there was a large spread in burning velocity data and no completely objective way of deciding between them. A modeller with no allegiance to any particular method of measuring burning velocity could plot predicted values through a few sets of experimental data confident of finding one that agreed with the model.

A combination of the present burning velocity method and computer modelling could prove powerful in setting limits on certain reaction rates. There are several ways in which this could be done. One is to use modelling along with sensitivity analysis to "target" those compositions in which the burning velocity is particularly sensitive to a specific rate. Burning velocity measurements in those mixtures could then be performed and compared with the modelled value. Another method is to build reaction schemes in order of complexity. The hydrogen scheme would be developed first, as it was in the present work. Next would come carbon monoxide/hydrogen mixtures where the major additional reaction is $CO + OH \rightleftharpoons CO_2 + H$. The next step would bring in methane, ethane and ethylene in a C_2 scheme. The process would

probably end here since in the present work the burning velocity was not found to be sensitive to any C_3 reactions. The targetting procedure described earlier could be used along with this process.

A third approach, and possibly the most profitable, was described by Gardiner[223]. He pointed out that the traditional approach to combustion modelling is to vary rate constants and perform large numbers of simulations to obtain agreement with experiment. Gardiner described a programme to attack combustion modelling in a new way, using automatic optimization of rate data. The method uses a new mathematical technique to find the set of rate data which best predicts experimental results (burning velocities, species profiles, etc). At the same time, poor data and areas where data are needed are identified. This approach seems to be an efficient way of dealing with a very complex problem. It also highlights the importance of accurate burning velocity data.

Development of the chemical kinetic schemes described in this thesis is not complete, as can be seen from the comparisons between experimental and modelled burning velocities in Figs. 18, 22, 25, 29, 33 and 38. Only in the case of hydrogen/air over the stoichiometric range (in Fig. 15) does the model agree with experiment within the experimental error. In the case of ethylene/air the agreement is particularly poor. The discovery of errors in the C_2 reaction scheme at a late stage in the work (described in Section 6.2) precludes comment on how the fit should be improved. It is worth pointing out, however, that such errors are not important for the present purposes of the modelling. The main aim was to calculate the flame thickness parameter k for each experimental run. It turns out that k is much smaller than b for hydrocarbons, so that the errors in the modelling are unlikely to have any effect on the final values of the Markstein length.

The most direct implication of the present work for flame modelling concerns the magnitude of the measured burning velocities. Current chemical kinetic schemes[30,101] predict burning velocities which are higher (in some cases considerably so) than the present results. If the present results are accurate then those schemes will need to be revised. It is not clear what changes will be necessary to bring the schemes into line. It may be that changing a single reaction rate will be sufficient. In particular, all burning velocities are strongly affected by the rate of the $H + O_2 \rightleftharpoons OH + O$ reaction because it is the major route by which radicals are generated. Any further constraints on this rate would be valuable since, although it is the most important rate in combustion, it is still not well known.

There are also implications for two- and three-dimensional modelling. Use of existing schemes which predict higher burning velocities than those in the present work will lead to predicted two- and three-dimensional velocity fields which differ markedly from the experimental ones. It is possible that some confusion will ensue, because the reason for the discrepancy will not be obvious.

7.4.3 **Magnitude of the burning velocity**

The results of the present work show that the burning velocities of the fuels studied are rather lower than the currently-accepted values. In particular, the maximum burning velocity of methane/air was found to be 0.37 ms^{-1}, about 10% lower than the currently favoured[24,187] value of about 0.41 ms^{-1}. Likely effects on flame modelling were considered in Section 7.4.2. Here we consider other implications.

The main uses of burning velocities for engineering purposes are in burner design and explosion prediction. In both cases, the complexity of the processes being dealt with means that the models used are approximate, and only the differences between burning velocities, rather than their absolute values, are likely to be of importance. But in some cases, the absolute values may matter. The recommended maximum burning velocity for methane/air about 20 years ago[21] was 0.45 ms^{-1}. This is 22% higher than the value obtained in the present work. Such a large difference might have some effect on the predictions of a model using burning velocity. The net effect might only be that the empirical constants need to be changed, but such changes could lead ultimately to a better understanding of the processes involved.

7.4.4 **Flame stabilization**

The standard theory of flame stabilization on burners was introduced by Lewis and von Elbe[18]. The theory rests on a framework, which appears to be generally applicable, involving the concept of a stabilization point. In the diametral plane of an axially symmetric Bunsen flame there should be a single point near the base where the cold gas velocity is perpendicular to the flame front and equal to the local burning velocity. All other gas velocities must exceed the burning velocity. It is this "stabilization point" that controls the stabilization of the flame.

The reasoning is as follows. If the gas velocity were smaller than the burning velocity at any point then the flame would move into the unburnt gas until this was

no longer the case. If a suitable position could not be found then the flame would "light back" into the burner. So for a stable flame $v_u \geq S_u$ where v_u is the unburnt gas velocity and S_u is the upstream burning velocity. If $v_u > S_u$ everywhere then the flame would move away from the burner until this was no longer true. If no suitable position were found then the flame would "lift off". So there must be at least one point in a stable flame where $v_u = S_u$. A consideration of the dynamics of a flame with $v_u > S_u$ moving away from a burner until $v_u \geq S_u$ suggests that the possibility of $v_u = S_u$ being satisfied in more than one part of the flame simultaneously is remote, except for reasons of symmetry. If we confine our attention to conical flames then there are two regions where $v_u = S_u$ is true: at the flame tip, and in a ring near the base of the flame. In the diametral plane, a point marks the position of the ring. It is not obvious a priori which of these two points controls the stabilization of the flame and therefore should be called the stabilization point. A general requirement is that the flow must be divergent as it passes through the flame at the stabilization point - otherwise the flame will not be stable to small perturbations in flow rate or burning velocity. In the present case this does not help since the flow is divergent in both cases. A reasonable criterion for a stabilization point would be that if it disappears then so does the flame. On this basis the stabilization point cannot be at the tip because conical flames which are quenched at the tip remain stable[217]. It must therefore be at the base of the flame. We will see later that this is not just an academic question.

As stated in Section 7.2.2, Günther and Janisch[62,63] found no point at the upstream boundary of a flame with a normal streamline and which could therefore be called a stabilization point. They found instead that the point where the streamline became normal to the flame, and therefore where the stabilization was controlled, was in the luminous zone. From the point of view of the present work this is not surprising since theory, experiment and modelling all suggest that events at the hot end of the flame control its burning rate. The present work therefore supports the Günther and Janisch view of flame stabilization.

Günther and Janisch's description of the flame stabilization process is essentially that of Lewis and von Elbe but with the proviso that the velocities to be compared are at the luminous zone - Lewis and von Elbe were not specific on this point. Günther and Janisch called the normal gas velocity at the luminous zone and relative to it the "combustion velocity". This is equal to the mass burning rate of the present work divided by the local gas density. At the stabilization point the local gas velocity equals the combustion velocity. Everywhere else along the flame (except at the tip), the local gas velocity exceeds the combustion velocity.

Günther and Janisch found that the lift-off behaviour of a Bunsen flame is determined by the behaviour of the stabilization point. As the flow rate is increased, it moves towards the edge of the flame. When it reaches the edge, the flame lifts off.

If the stabilization point concept is sufficiently general then it should apply to a flame in stagnation-point flow. The flow diverges as it crosses the flame, so the stabilization point must be on the axis of the flame: this is the only point where there is a normal streamline. By symmetry, there is nowhere for this point to move to as the flow rate is increased, so no lift-off limit is predicted. This is consistent with the experimental finding that the configuration is stable until the flames are extinguished by stretch or incomplete combustion, but it is not a very useful result.

But reducing the flow rate produces more interesting behaviour since, if a nozzle burner is used, this leads to the production of a button-shaped flame. The stabilization point identified by Günther and Janisch at the base of such a flame differs in an important respect from that at the base of a conical flame. In a conical flame, the angle between the streamline and the flame front above it is less than 90° near the flame tip, as in Fig. 3(c) for example. It increases to 90° at the stabilization point and exceeds 90° near the edge of the flame. The stabilization point is therefore well-defined. But in a button-shaped flame, the angle near the axis of symmetry of the flame is already greater than 90°. It decreases to approach 90° at larger radii and possibly equals 90° at the point near the base of the flame marked by Günther and Janisch as the stabilization point[63]. It then increases again. This general behaviour can be seen in Fig. 6. Unlike in the conical flame, it is not certain that the angle does become 90°. And if it became even marginally less than 90° before increasing again then there would be two stabilization points in close proximity.

It seems very unlikely that the flame could arrange for an angle of exactly 90° at exactly one point under such circumstances. It seems more likely that the stabilization point of a button-shaped flame is in fact the point on the axis of symmetry, as in a stagnation-point flame. This is supported by the lightback mode of this type of flame. As the flow rate is reduced, it is the *centre* of the flame that moves down into the burner and lights back first. Increasing the flow rate also affects the centre of a button-shaped flame. The central part rises until the top surface is nearly flat, and then the flame jumps into a conical shape[66]. The stabilization point is then near the flame base.

Günther and Janisch examined three theories of the lift-off process. These were those of Lewis and von Elbe[18] and of Putnam and Jensen[224] based on the extinction effect of the burner rim, and of Lewis and von Elbe[3] based on the flame stretch theory of Karlovitz et al[41]. All led to similar expressions, namely that the critical boundary velocity gradient for lift-off is inversely proportional to flame thickness divided by the burning velocity. Günther and Janisch found it difficult to conceive how the physical processes of quenching and flame stretch could both describe the lift-off limit correctly using the same formalism. In addition, all led to discrepancies with experimental results.

The current formulation of flame stretch studied in this thesis differs from that of Karlovitz et al, and it may be that a re-examination of stretch effects in flame stabilization would be profitable. According to the arguments presented above, the flow pattern in the neighbourhood of the stabilization point consists of a normal streamline with diverging streamlines on either side. This region must therefore be positively stretched and in fact corresponds to a flame in a stagnation-point flow. Since stretch can increase or decrease the burning rate, it cannot be the fundamental process in stabilization, but it may have some perturbing effect. If so, there should be some qualitative differences in stability behaviour between, say, lean methane and lean propane mixtures. A series of such differences was pointed out by Wohl in the discussion following ref. 225.

If we accept the Lewis and von Elbe model as clarified by Günther and Janisch then stabilization conditions are determined by the existence and behaviour of the stabilization point defined above. Prediction of the dynamics of the stabilization point probably requires detailed modelling of the flow field since so many processes are interacting: heat loss, flame overhang due to the pressure drop, flame stretch, flow recirculation, etc. A simpler view is that the existence of a stabilization point is a necessary condition for a stable flame. Possible reasons for it not existing are quenching by loss of heat or species to the burner (Lewis & von Elbe; Putnam & Jensen), intermixing with secondary air (Günther and Janisch) and flame stretch. All of these processes are likely to have some effect in any given situation. But none of them can claim to be the fundamental process, since physical situations can be conceived in which each of them plays no role. For the above processes, suitable examples are twin flames in a counterflow, inverted flames, and flames with a Markstein length equal to zero respectively. It would therefore appear that a simple, general analysis of flame stabilization is not possible. But if we concentrate on flame stabilization on burners (thus excluding counterflow flames) then flame quenching

(by loss of heat or species or both) must be the fundamental process since it is the only one that necessarily reduces the burning rate as the flame approaches the burner. It may be that theories based on quenching with the inclusion as perturbations of effects due to flame stretch and interdiffusion might be able to predict flame stabilization behaviour adequately.

7.4.5 Minimum spark ignition energies

The stretch in an expanding spherical flame is inversely proportional to its radius, so flames which have just been ignited are strongly stretched. The present work shows that lean mixtures of light reactants (hydrogen and methane) and rich mixtures of heavy reactants (ethane and propane) have negative Markstein lengths. This means that the propagation rate is enhanced by positive stretch. While the ignition process is a complex one that cannot be explained simply in stretch terms, it does seem reasonable that flames with negative Markstein lengths should be easier to ignite than otherwise similar mixtures with positive Markstein lengths.

A simple way of assessing this is to consider the mixture with the minimum spark ignition energy. In the absence of stretch effects, one would expect this to be the stoichiometric mixture. On the basis of the above discussion, a shift in the point of minimum energy would be expected towards mixtures with negative Markstein lengths. Thus hydrogen and methane should have minima in lean mixtures and ethane and propane (and all higher hydrocarbons) should have minima in rich mixtures. The experimental data of Lewis and von Elbe[3] show that this is true in all cases.

A comparison can be performed with the modelled expanding hydrogen flames of the present work which were "ignited" by a region of hot gas with a Gaussian temperature profile. While this is not a precise analogue of a real ignition process, it might be expected to share some of its features[108]. The maximum temperature was kept constant at 5000 K and the minimum ignition energy was determined by changing the radius of the Gaussian profile. The minimum radius (and therefore the minimum energy) corresponded to a hydrogen/air mixture with a stoichiometry of 0.7. The experimental minimum[3] was at a stoichiometry of 0.9, so the results agree qualitatively.

7.4.6 **Flammability limits**

It is found experimentally that flames will not propagate in fuel/oxidant mixtures which are leaner or richer than certain compositions known as the flammability limits. There has been discussion for many years about whether flammability limits are intrinsic properties of flames or occur as a result of external effects like heat loss or flame stretch. The purpose of this section is to consider the relevance of the present work for studies of flammability limits.

A common experimental approach is to observe flame propagation in a flammability tube. A mixture is considered to be flammable if a flame travels a certain distance down the tube. The issue is complicated by different types of propagation near the limit (e.g. cellular flames and small flame caps which only consume a small proportion of the reactants). Different flammability limits are found for upward and downward propagation and for propagation at zero gravity. Strehlow et al[226] concluded that upward propagating flames are extinguished by stretch at the tip, while heat loss to the walls causes extinction in the other two cases. The present work suggests that stretch extinction should only occur in mixtures with an effective Lewis number Le > 1. When Le < 1, combustion should be enhanced by stretch, so the extinction must be caused by some other effect.

Ronney et al[227,228] studied expanding spherical flames in near-limit mixtures at microgravity. A new form of propagation was discovered, known as a Self-Extinguishing Flame. Such flames occurred in sub-limit mixtures with an effective Lewis number smaller than 1. The flame speed followed the solid curve in Fig. 63 (calculated using Ronney and Sivashinsky's theory) but as it decreased a sudden extinction occurred. This was found to be due to radiative heat loss given by the final term in equation (1). The decrease in flame speed with radius can be explained in terms of stretch since the results of the present work show that the Markstein length is negative for such mixtures.

A different approach to flammability limits was used by Law and Egolfopoulos[229]. They considered that flammability limits are kinetic in origin, and depend on the relative rates of branching and termination reactions. A small disturbance, however, like heat loss, is needed to trigger extinction. They measured flammability limits by extrapolating the stretch rate at extinction of near-limit flames as a function of stoichiometry to zero. The stoichiometry at that point was taken to be the true flammability limit.

The analysis of the Law counterflow methodology in Section 7.2.5.2 suggests that the stretch rates are systematically underestimated. Consequently, the experimental flammability limits determined by Law and Egolfopoulos are slightly narrower than they would be if the stretch were measured precisely.

Work by Lloyd and Weinberg[230] on burners which recycle large amounts of heat suggested that the critical requirement for flame propagation in methane/air mixtures is a minimum reaction zone temperature of about 1400 K.

Peters and Smooke[231] analysed flame propagation at the lean flammability limit in terms of competition between chain branching and chain breaking reactions. They found that as the composition approaches the lean limit, the radical concentration in the reaction zone drops to zero. The flame is then extinguished by stretch or heat loss.

Attempts to compute flammability limits have met with mixed success. It appears that in one-dimensional flame modelling there is no clear limit of propagation - the flame simply propagates more and more slowly. But allowing small heat losses within a one-dimensional model does lead to flammability limits[232].

A theoretical framework for dealing with flammability limits is provided by asymptotics. The asymptotic analysis in Chapter 2 of the present work shows that the burning rate is very sensitive to the flame temperature. In lean and rich mixtures the flame temperature is low for thermodynamic reasons as explained in Section 7.2.1, so the burning rate is very low. Williams[31] showed that when there is a nonzero heat loss rate there is no solution for the burning rate at sufficiently low temperature. This explains the finding that heat loss must be included in one-dimensional modelling to allow prediction of flammability limits. It is worth noting that heat loss occurs in all real flames since thermal radiation is unavoidable, so flammability limits can be anticipated for all fuel/oxidant flames. In practical situations, however, convective or conductive losses are more likely than radiative losses to trigger extinction[31].

If the heat release rate fell rapidly as a function of fuel concentration, due to chemical kinetic effects, then whether the heat loss was large or small, extinction would occur at about the same composition. The flammability limits would then be effectively controlled by kinetic processes. Although there no direct evidence for such behaviour, it seems reasonable and is suggested by theoretical work. It would explain how similar values are obtained for flammability limits measured by different

methods. If the rapid change in heat release were directly related to the reaction zone temperature then the findings of Lloyd and Weinberg would be explained.

In addition to the above effects, all real flames are stretched to some extent. Since the Markstein lengths of near-limit mixtures have large magnitudes as shown in Figs. 54 to 60, it appears likely that stretch effects could influence measured flammability limits. But again it is possible that kinetic processes dominate: although stretch might modify the flame behaviour, a rapid fall in the heat release rate with composition would lead to extinction at about the same composition in the absence of stretch.

7.4.7 **Turbulent flames**

One of the main reasons for the current interest in stretch is its application to turbulent flames. The basic idea is that the burning rate of a turbulent flame depends on two factors: the flame area and the stretch rate. The turbulence in the incoming flow, along with contributions due to the flame itself, causes the flame to thicken into a turbulent "brush". Time-resolved pictures show that in fact the area of the flame has increased. The flame resembles a laminar one, but is highly convoluted and moves rapidly around its mean position giving the impression of increased thickness.

If the increase in area were the only effect on the propagation rate then the mass burning rate as defined in the present work would remain constant and the total mass flow rate would increase in proportion to the mean area of the flame. The turbulent burning velocity, which is defined with respect to the *apparent* flame area, therefore increases, and would continue to do so as the turbulence level was increased.

But although the turbulent burning velocity does increase with the turbulence intensity initially, a point comes when it starts to decrease as the turbulence increases. This has been attributed to turbulent quenching due to flame stretch[233].

Given the effects of flame stretch determined in the present work, it is not surprising that such an effect should occur. A positive Markstein length means that stretch reduces the burning rate, so a sufficiently large stretch rate should put the flame out. Since the stretch rates in turbulent flames are likely to be higher than in the present work, and are likely to increase with the turbulent intensity, quenching seems to be a reasonable possibility.

But if the extinction is due to stretch, should there not be mixtures where stretch enhancement occurs? On the basis of the work in this thesis, one would think so. But the present work deals only with weak stretch. Experiments on counterflow flames by Sato[216] showed that flame extinction always occurs at high stretch rates, whatever the mixture. Mixtures with an effective Lewis number which is much larger than 1 (e.g. rich methane, lean propane) are extinguished when they are some distance apart, and this was considered to be a true stretch extinction. It might be predicted qualitatively for any mixture with a Markstein length greater than zero as described earlier.

Mixtures with an effective Lewis number smaller than 1 (lean methane, rich propane) are also extinguished at high stretch rates, but in this case the flames are very close together when the extinction occurs. This was interpreted by Sato as due to incomplete combustion. The burning rates of the flames are enhanced by stretch as shown by the experiments in the present work. They are therefore able to propagate at high stretch rates, and take up positions close to the stagnation plane. The flames therefore get closer and closer together until they start to interfere with each others' chemical processes. Eventually extinction occurs because the flames cannot generate the heat to keep going: there is insufficient time for the reactions to reach completion.

Although quenching occurs in all mixtures at sufficiently high turbulence levels, the experimental results of Bradley and co-workers[234] show that mixtures with an effective Lewis number greater than 1.3 are quenched more readily than the rest. According to the present work, mixtures with Lewis numbers of this magnitude would have large Markstein lengths. The burning velocity would therefore decrease much more rapidly with stretch than mixtures with lower Lewis numbers, in agreement with the results of Bradley et al.

7.4.8 Gas utilization

The work in this thesis demonstrates an advantage of methane as a fuel. It is generally true that burning hydrocarbon fuels in lean mixtures leads to low emissions of oxides of nitrogen, carbon monoxide and unburnt hydrocarbons[235]. Such low emissions are highly desirable for environmental reasons. Of all the hydrocarbons, methane is the only one for which the burning rate is increased in lean mixtures by positive stretch. Since stretch in flames is usually positive (the only common occurrence of negative stretch is at the tip of a flame), it should be possible to design

combustion equipment to take advantage of this property of lean methane mixtures. Possible uses of such an idea are counterflow flame burners (e.g. in domestic central heating boilers) and the use of methane as a fuel in spark ignition engines.

The use of counterflow flames as practical combustion devices would have other advantages besides the enhanced combustion due to stretch. One is that stabilization would be much more straightforward as described in Section 7.4.4. Also, the burners would not be heated at all, so that material degradation would be reduced. All of the heat could be directed into heat exchangers, leading to improved efficiency.

It is possible that a spark-ignition engine using methane could not be run so lean as to be enhanced by stretch. But even if the mixture were only slightly lean, the effect of the stretch would be much smaller than in a conventional petrol engine. A comparison of Figs. 56 and 59 shows that the burning rate of lean propane/air (roughly comparable to petrol) would be reduced much more by stretch than methane. The effects would be important at the ignition stage (as described in Section 7.4.5) and also in the fully-developed turbulent flame as described in the previous section.

Unfortunately, the advantages of methane as a replacement for petrol are vitiated by the high operating pressures. Fig. 57 shows that the Markstein length is inversely proportional to pressure, so compression before ignition is likely to reduce the potential benefits. Similarly, it will reduce the potential ignition difficulties in petrol engines.

A final point is that all of the work in this thesis has dealt with pure fuels. The dependence of the Markstein length on the composition of a fuel mixture is unknown. It is possible that the small quantities of ethane, propane and higher hydrocarbons present in natural gas might make its Markstein length different from that of methane.

7.4.9 **Flame stability (to wrinkling)**

One reason for the interest in flame stretch by theoreticians is its relationship to the problem of the stability of laminar flames. This is the question of whether a flame front will remain smooth and one-dimensional or will wrinkle in response to a perturbation. Such perturbations could be caused by turbulence in the incoming

flow, and flame stability studies therefore relate to the transition from laminar to turbulent combustion.

Early theoretical work by Darrieus and Landau (see ref. 176) suggested that a planar one-dimensional flame is unconditionally unstable. In their treatments the burning velocity was considered to be constant, and the flame to be an interface separating gases of different densities. The hydrodynamic instability that they predicted arises from this density difference. They found that the growth rate σ of the amplitude of a disturbance was proportional to the wavenumber k. Therefore any disturbance of any wavelength would cause the flame to wrinkle. Darrieus and Landau therefore concluded that laminar flames should not exist and that premixed flames must be self-turbulizing.

This result has generally been considered to be contrary to experience, so that a stabilizing mechanism has been sought. In fact, it is not possible to produce a planar, one-dimensional flame in the laboratory because the flow in real flames is divergent, so it could be argued that a test of the theory has never actually been performed. But an examination of the theory shows that the flame is treated as an interface of zero thickness. It follows that one can choose a sufficiently small region on either side of the interface for the divergence to be as small as required; that is, there is no length scale in the problem. The theory therefore applies to a flame in an arbitrarily divergent flow field.

The treatment of Darrieus and Landau neglects any effects of the flame shape and the incoming flow on the structure and propagation rate of the flame. Such effects would be expected to occur, especially at short wavelengths, so that the Darrieus-Landau picture would be modified. Markstein[25] accounted for such influences by introducing a phenomenological dependence of the burning velocity on the curvature of the flame front. At around the same time, Karlovitz et al[41] introduced the concept of flame stretch, in which the burning velocity was affected by nonuniformity in the upstream flow. Later work[42,176] showed that the views of both Markstein and Karlovitz could be accommodated if flame stretch were formulated in the correct way. Flame stretch therefore provides a tool for analysing the stability of laminar flames.

Initially, theoretical studies of flame stability were performed using the thermal-diffusive model in which thermal expansion is neglected (see ref. 176). Later work[54,55] included thermal expansion. The theories in these two papers are equivalent, so we can use the convenient form of the results in the work of Matalon

and Matkowsky[54] to show that the growth rate can be expressed as a series in powers of the wavenumber k. They found that

$$\sigma = A_1 k + A_2 k^2 + O(k^3) \qquad (27)$$

where A_1 depends only on the heat release (this is the Darrieus-Landau result) and A_2 is a function of the heat release and Lewis number. A_1 is strictly positive if the heat release exceeds zero, while A_2 is negative for most mixtures, and is therefore stabilizing. The net result is usually that the flame is stable to small perturbations with wavenumbers greater than some critical value (i.e. wavelengths smaller than a critical value).

The reason for introducing the subject here is to consider the implications of the present work for stability studies. All of the work cited above makes use of the unburnt Markstein length $\mathcal{L}$. Essentially, the stability criterion is something like $\mathcal{L} > 0$. (It is strictly $\mathcal{L} > 0$ in the thermal-diffusive model[176]). Now the unburnt Markstein length is a measure of the effect of stretch on the cold gas burning velocity defined within the framework of these multiscale asymptotic theories. As described in Section 7.2.5.4, the relationship between this burning velocity and that in a real flame is unclear. The physical meaning of the unburnt Markstein length is therefore also unclear.

By contrast, the burnt gas Markstein length has a well-defined physical meaning and the theoretical expression for it, used in the present work in a slightly modified form, is supported by the present experiments. The question therefore arises as to whether the theory needs to be modified.

Essentially, we are asking whether the predictions of the theory would differ if it were developed using the burnt gas Markstein length. I think that the answer to this question is No. To see this, consider that the same model makes predictions of both unburnt and burnt Markstein length. The unburnt Markstein length is defined with reference to a burning velocity which is well-defined within the model, but not readily applied to a real flame. The burnt gas Markstein length is also well-defined within the model, but in addition has a clear physical meaning. Since theoretical predictions of the burnt gas Markstein length are supported by the experiments in this work, we are saying that the model itself is supported by the experimental evidence. We may therefore anticipate qualitatively correct predictions when the model is applied to various phenomena, for example flame stability.

Chapter 8

CONCLUSIONS

In this chapter some issues arising in the present work are considered and conclusions are drawn.

Expanding flame methodology

The expanding flame methodology developed in the present work is easy to apply and gives repeatable results. Most important of all, it is testable: it is possible to demonstrate that true, one-dimensional burning velocities are obtained. This is the first time that this has been possible, and is a strong point in favour of the technique.

Counterflow flame methodology

It is suggested that the counterflow method of Law and co-workers does not extrapolate to zero stretch: there is still some "residual stretch", probably generated by the flame. The predicted consequences are generally high results by the counterflow method, which are worse in Le < 1 mixtures than Le > 1. Comparisons between the present results and those of Law and co-workers agree with this prediction, and therefore support the residual stretch theory. The magnitude of any residual stretch could be determined by measuring the stretch directly, using the radial velocity gradient in the luminous zone, and comparing it with the upstream velocity gradient.

Physical meaning of the reference surface

The reference surface is defined as where the mass flux in a stationary spherical flame equals that of the corresponding planar one-dimensional flame. Theory, experiment and modelling all show that the reference surface is in the hot part of the flame.

The work in the thesis suggests a connection between the reference surface and the flame processes of heat release, fuel consumption and radical production. It was not possible to decide which of these is the most important. Further work is needed to see if a connection exists with any particular flame process.

One-dimensional burning velocity results obtained from extrapolation methods should, in principle, be independent of the reference surface. This is the case for the expanding flame method, but not for the counterflow method of Law and co-workers.

Asymptotic theory

Asymptotic theory predicts that the burning rates of flames in lean mixtures of light gases and rich mixtures of heavy ones should be increased by stretch. The burning rate should be decreased for all other mixtures. These predictions were supported by the present experiments. It is interesting that asymptotic theory is able to predict the experimental Markstein lengths qualitatively, and in some cases quantitatively. It is further evidence that analytical techniques have a role in combustion theory, even when precise simulations are feasible.

Universality of stretch as a description of flames

The question here is whether the same Markstein length is valid for characterizing the effects of both extensional and dilatational stretch. (The phenomenological analyses in Chapter 2 suggest that it should be). Within the admittedly large experimental error, the Markstein lengths for expanding flames and flames in stagnation-point flow are equal. The results of the present work therefore support the general applicability of stretch, at least in the weak stretch regime. The agreement between the Markstein lengths from expanding flames and those derived by Law and co-workers in counterflow flames and by Searby and Quinard in wrinkled flames provides further support.

Importance of defining burning velocity correctly

It is clear from the present work that the effect of stretch on flames in near-stoichiometric mixtures of most fuels is small. Since stretch rates on burners and in

expanding spherical flames are also quite small, it follows that stretch effects are not the cause of the large scatter in reported values of maximum burning velocities. The main reason for this scatter must therefore be flow divergence or, putting it another way, incorrect siting of the reference surface.

Besides the importance of measuring the correct one-dimensional burning velocity, there is another reason for careful definition of burning velocity. The comparisons in Figs. 68(a) and 69(a) between the Markstein lengths determined in the present work and those derived from the work of Law et al demonstrate reasonable qualitative agreement, especially for propane: it is clear that stretch increases the burning rate of rich propane flames and decreases the burning rates of other mixtures. But in their original form, the data give a completely different impression. They were expressed as stretch coefficients which (1) were roughly constant across the stoichiometric range for both methane/air and propane/air mixtures and (2) corresponded to an increase in burning velocity with stretch in all cases. The different impression follows from the definition used for the burning velocity.

It could be argued that the definition is unimportant since it is always possible to convert between different ways of expressing the results. But this misses the point: there is an expectation that measured quantities correctly reflect the underlying physical behaviour. Indeed, Law and co-workers were themselves baffled by the results:

> "... a decreasing trend [in burning velocity *vs* stretch] is predicted for Le > 1 mixtures. This obviously contradicts the present result which shows an increasing dependence for all mixtures... there is no satisfactory explanation for such a behaviour".

We conclude that it is important to measure burning velocity properly in order to understand the effect of stretch.

Meaning of the burning velocity definition

The definition of burning velocity used in this work is the mass flux at the reference surface divided by the cold gas density. It was used because it reduces correctly to the one-dimensional definition and applies to stretched flames in a natural way. The disadvantage is that the connection with a real flow velocity is lost; the burning

velocity only equals a flow velocity in the one-dimensional case, which does not exist except as an abstraction.

Since there are no real flames in which one can identify a flow velocity as the burning velocity, it would appear that there is a good argument for getting rid of the notion of burning velocity altogether. It would be replaced by the mass burning rate, defined as the normal mass flux at the reference surface. Such a change would have the advantage of emphasizing both the physical nature of the measurement being made and the uncertainties involved in determining it (where is the reference surface?). This would lead to much less confusion and to a better understanding of the way flames behave.

Another way of looking at this is as follows. Linnett claimed in 1953 that there is no definition of burning velocity in a divergent flow which is free from all objections. In 1965, Fristrom devised the definition used in the present work which apparently solved all the problems except that it did not correspond to a physical velocity in the flame. However, at that stage (before flame stretch had been considered) it was possible to consider Fristrom's burning velocity to be the physical velocity which would exist ahead of the flame if the flow were one-dimensional. This strong relationship with a physical velocity was enough to justify the definition. Once flame stretch had been discovered, however, no such claim could be made. All real flames are stretched, so that their burning velocities are different from the one-dimensional value (except for the special case of Markstein length = 0). The Fristrom definition therefore does not equal any gas velocity in either the real flame or its one-dimensional counterpart. The only meaning that can be ascribed to this burning velocity ($S_{u,r}$) is that it is proportional to the mass flux at the reference surface. There is no good reason to maintain the connection with gas velocity, and it would be more sensible to express the propagation rate of a flame as the mass burning rate.

In view of the above, Linnett's claim that no definition could be devised that is free from all possible objections is correct: on the one hand, the present work shows that all definitions other than the one used lead to incorrect results; on the other hand, an objection to the present definition is that the burning velocity defined in this work does not equal any gas velocity in the system. This is the price one must pay for obtaining consistent results. It is a consequence of a hitherto little-recognized fact: the speed is not an appropriate parameter for characterizing the propagation rate of a flame.

REFERENCES

1. Gaydon, A.G. and Wolfhard, H.G.: *Flames - their Structure, Radiation and Temperature*, 2nd edition, Chapman and Hall, London, 1960.
2. Chambers English Dictionary, 7th edition, 1988.
3. Lewis, B. and von Elbe, G.: *Combustion, Flames and Explosions of Gases*, 2nd Edition, Academic Press, London, 1961.
4. Bone, W.A. and Townend, D.T.A.: *Flame and Combustion in Gases*, Longmans, 1927.
5. Manson, N.: Combust. Flame 71, 179 (1988).
6. Davy, Sir Humphrey: *On the Fire-damp of Coal Mines, and on the Methods of Lighting the Mines, so as to prevent its Explosion.* Paper read before the Royal Society on 9th November 1815; in Davy's *Collected Works*, (John Davy, Ed.), Volume 6, 1840.
7. Bunsen, R.: Phil. Mag. 34, 489 (1867).
8. Mallard, M.E.: Annales des Mines, 7th Series, Volume VII, 355 (1875).
9. Gouy, G.L.: Annales de Chimie et de Physique, 5th Series, Volume XVII, 27 (1879).
10. Mallard, E. and Le Chatelier, H.: Annales des Mines, 8th Series, Volume IV, 296 (1883).
11. Michelson, W.: Annalen der Physik und Chemie, Volume XXXVII, 1 (1889).
12. Wheeler, R.V.: Trans. Chem. Soc. 105, 2606 (1914).
13. Mason, W. and Wheeler, R.V.: Trans. Chem. Soc. 111, 1044 (1917).
14. Stevens, F.W.: J. Am. Chem. Soc. 48, 1896 (1926).
15. Stevens, F.W.: J. Am. Chem. Soc. 50, 3244 (1928).
16. Coward, H.F. and Hartwell, F.J.: J. Chem. Soc. (Lond.), p. 2676, (1932).
17. Lewis, B. and von Elbe, G.: J. Chem. Phys. 2, 283 (1934).
18. Lewis, B. and von Elbe, G.: J. Chem. Phys. 11, 75 (1943).
19. Linnett, J.W.: *Fourth Symposium (International) on Combustion*, p. 20, Williams and Wilkins, Baltimore, Maryland, 1953.
20. Fristrom, R.M.: Phys. Fluids 8, 273 (1965).
21. Andrews, G.E. and Bradley, D.: Combust. Flame 18, 133 (1972).
22. Dixon-Lewis, G. and Islam, S.M.: *Nineteenth Symposium (International) on Combustion*, p. 283, The Combustion Institute, 1982.
23. Wu, C.K. and Law, C.K.: *Twentieth Symposium (International) on Combustion*, p. 1941, The Combustion Institute, 1985.
24. Law, C.K., Zhu, D.L. and Yu, G.: *Twenty-First Symposium (International) on Combustion*, p. 1419, The Combustion Institute, 1988.

25. Markstein, G.H.: *Nonsteady Flame Propagation*, Pergamon Press, Oxford, 1964.
26. Chung, S.H. and Law, C.K.: Combust. Flame 72, 325 (1988).
27. Yu, G., Law, C.K. and Wu, C.K.: Combust. Flame 63, 338 (1986).
28. Law, C.K.: *Twenty-Second Symposium (International) on Combustion*, p. 1381, The Combustion Institute, 1989.
29. Egolfopoulos, F.N. and Law, C.K.: *Twenty-Third Symposium (International) on Combustion*, p. 333, The Combustion Institute, 1991.
30. Egolfopoulos, F.N., Zhu, D.L. and Law, C.K.: *Twenty-Third Symposium (International) on Combustion*, p. 471, The Combustion Institute, 1991.
31. Williams, F.A.: *Combustion Theory*, 2nd edition, Benjamin, 1985.
32. Peters, N. and Williams, F.A.: Combust. Flame 68, 185 (1987).
33. Seshadri, K. and Peters, N.: Combust. Flame 81, 96 (1990).
34. Chung, S.H.: Transactions of the Korean Society of Mechanical Engineers 9, 655 (1985).
35. Joulin, G. and Mitani, T.: Combust. Flame 40, 235 (1981).
36. Hirschfelder, J.O., Curtiss, C.F. and Campbell, D.E.: *Fourth Symposium (International) on Combustion*, p. 190, Williams and Wilkins, Baltimore, Maryland, 1953.
37. Friedman, R. and Burke, E.: J. Chem. Phys. 21, 710 (1953).
38. Bush, W.B. and Fendell, F.E.: Combust. Sci. Technol. 1, 421 (1970).
39. Mitani, T.: Combust. Sci. Technol. 21, 175 (1980).
40. Dixon-Lewis, G.: Phil. Trans. R. Soc. Lond. A292, 45 (1979).
41. Karlovitz, B., Denniston, D.W., Knapschaefer, D.H. and Wells, F.E.: *Fourth Symposium (International) on Combustion*, p. 613, Williams and Wilkins, Baltimore, Maryland, 1953.
42. Williams, F.A.: in *Analytical and Numerical Methods for Investigation of Flow Fields with Chemical Reactions, Especially Related to Combustion*, M. Barrère, Ed., AGARD Conference Proceedings No. 164, AGARD, Paris, 1975, p. III-1.
43. Williams, F.A.: in *Combustion & Nonlinear Phenomena*, (P. Clavin, B. Larrouturou and P. Pelcé, Eds.), 1985, p. 93.
44. Matalon, M.: Combust. Sci. Technol. 31, 169 (1983).
45. Chung, S.H. and Law, C.K.: Combust. Flame 55, 123 (1984).
46. Candel, S.M. and Poinsot, T.J.: Combust. Sci. Technol. 70, 1 (1990).
47. Buckmaster, J.D.: Quarterly Journal of Mechanics and Applied Mathematics 35, 249 (1982).

48. Daneshyar, H., Mendes-Lopes, J.M.C. and Ludford, G.S.S.: *Nineteenth Symposium (International) on Combustion*, p. 413, The Combustion Institute, 1982.
49. Levy, A. and Weinberg, F.J.: *Seventh Symposium (International) on Combustion*, p. 296, Butterworths, London, 1959.
50. Pindera, M.-Z. and Talbot, L.: *Twenty-First Symposium (International) on Combustion*, p. 1357, The Combustion Institute, 1988.
51. Pindera, M.-Z. and Talbot, L.: Combust. Flame 73, 111 (1988).
52. Law, C.K.: Private communication.
53. Clavin, P. and Williams, F.A.: J. Fluid Mech. 116, 251 (1982).
54. Matalon, M. and Matkowsky, B.J.: J. Fluid Mech. 124, 239 (1982).
55. Clavin, P. and Joulin, G.: J. Phys.-Lett. 44, L-1 (1983).
56. Buckmaster, J.D.: *Seventeenth Symposium (International) on Combustion*, p. 835, The Combustion Institute, 1979.
57. Libby, P.A. and Williams, F.A.: Combust. Sci. Technol. 54, 237 (1987).
58. Frankel, M.L. and Sivashinsky, G.I.: Combust. Sci. Technol. 31, 131 (1983).
59. Champion, M., Deshaies, B. and Joulin, G.: Combust. Flame 74, 161 (1988).
60. Mikolaitis, D.W.: Combust. Flame 63, 95 (1986).
61. García-Ybarra, P., Nicoli, C. and Clavin, P.: Combust. Sci. Technol. 42, 87 (1984).
62. Janisch, G. and Günther, R.: First European Symposium on Combustion, Academic Press, London, p. 689, 1973.
63. Günther, R. and Janisch, G.: Gas Wärme International 24, 489 (1975).
64. Smith, D.B., Taylor, S.C. and Williams, A.: *Problems with Defining and Measuring Burning Velocity.* Paper presented at the Joint Meeting of the British and French Sections of the Combustion Institute, Rouen, France, April 18-21 1989.
65. Dowdy, D.R., Smith, D.B., Taylor, S.C. and Williams, A.: *Twenty-Third Symposium (International) on Combustion*, p. 325, The Combustion Institute, 1991.
66. Fristrom, R.M. and Westenberg, A.A.: *Flame Structure*, McGraw-Hill, 1965.
67. Warnatz, J. and Peters, N.: Prog. Astron. Aeron. 95, 61 (1984).
68. Rogg, B.: Combust. Flame 73, 45 (1988).
69. McAdams, W.H.: *Heat Transmission*, 3rd edition, McGraw-Hill, 1954.
70. Dixon-Lewis, G.: Combust. Sci. Technol. 43, 1 (1983).
71. Mendes-Lopes, J.M.C. and Daneshyar, H.: Combust. Flame 60, 29 (1985).
72. Tien, J.H. and Matalon, M.: Combust. Flame 84, 238 (1991).
73. Andersen, J.W. and Fein, R.S.: J. Chem. Phys. 17, 1268 (1949).
74. Jesch, L.F.: Ph.D. Thesis, University of Leeds, 1970.

75. Durst, F., Melling, A. and Whitelaw, J.H.: *Principles and Practice of Laser-Doppler Anemometry*, Academic Press, London, 1976.
76. Tabor, D.: *Gases, Liquids and Solids*, 2nd edition, Cambridge University Press, 1979.
77. Science Data Book, (R.M. Tennent, Ed.), Oliver and Boyd, 1971.
78. Günther, R. and Janisch, G.: Combust. Flame 19, 49 (1972).
79. Haniff, M.S.: Ph.D. Thesis, University of Leeds, 1982.
80. Haniff, M.S., Melvin, A., Smith, D.B. and Williams, A.: J. Inst. Energy, December 1989, p. 229.
81. Spiegel, M.R.: *Mathematical Handbook of Formulas and Tables*, McGraw-Hill, 1968.
82. Kono, M., Iinuma, K., Kumagai, S. and Sakai, T.: Combust. Sci. Technol. 19, 13 (1978).
83. Weinberg, F.J.: *Optics of Flames*, Butterworths, 1963.
84. Conte, S.D. and de Boor, C.: *Elementary Numerical Analysis*, 3rd edition, McGraw-Hill, 1980.
85. Cambray, P., Deshaies, B. and Joulin, G.: 70th PEP AGARD Symposium, Chania, Crete, 1987, p. 36-1.
86. Cambray, P. and Deshaies, B. *Experimental Investigation of Stretch and Curvature Effects on Premixed Flames Burning Velocity.* Paper presented at the Joint Meeting of the French and Italian Sections of the Combustion Institute, 1987.
87. Deshaies, B. and Cambray, P.: Combust. Flame 82, 261 (1990).
88. Kee, R.J., Miller, J.A., Evans, G.H. and Dixon-Lewis, G.: *Twenty-Second Symposium (International) on Combustion*, p. 1479, The Combustion Institute, 1989.
89. Dixon-Lewis, G.: *Twenty-Third Symposium (International) on Combustion*, p. 305, The Combustion Institute, 1991.
90. Cleveland, W.S.: *The Elements of Graphing Data*, Wadsworth, 1985.
91. Fukutani, S., Yamamoto, S. and Jinno, H.: *Twenty-Third Symposium (International) on Combustion*, p. 405, The Combustion Institute, 1991.
92. Ko, Y., Anderson, R.W. and Arpaci, V.S.: Combust. Flame 83, 75 (1991).
93. Palm-Leis, A. and Strehlow, R.A.: Combust. Flame 13, 111 (1969).
94. Spalding, D.B.: Phil. Trans. R. Soc. Lond. A249, 1 (1956).
95. Dixon-Lewis, G. and Williams, A.: *Ninth Symposium (International) on Combustion*, p. 576, The Combustion Institute, 1963.
96. Bledjian, L.: Combust. Flame 20, 5 (1973).
97. Stephenson, P.L. and Taylor, R.G.: Combust. Flame 20, 231 (1973).

98. Smoot, L.D., Hecker, W.C. and Williams, G.A.: Combust. Flame 26, 323 (1976).

99. Tsatsaronis, G.: Combust. Flame 33, 217 (1978).

100. Westbrook, C.K. and Dryer, F.L.: Combust. Sci. Technol. 20, 125 (1979)

101. Warnatz, J.: *Eighteenth Symposium (International) on Combustion*, p. 369, The Combustion Institute, 1981.

102. Wilde, K.A.: Combust. Flame 18, 43 (1972).

103. Patnaik, G., Kailasanath, K., Oran, E.S. and Laskey, K.J.: *Twenty-Second Symposium (International) on Combustion*, p. 1517, The Combustion Institute, 1989.

104. Smooke, M.D., Lin, P., Lam, J.K. and Long, M.B.: *Twenty-Third Symposium (International) on Combustion*, p. 575, The Combustion Institute, 1991.

105. Peters, N.: *Numerical Simulation of Combustion Phenomena*, (R. Glowinski, B. Larrouturou and R. Temam, Eds.), Lecture Notes in Physics Vol. 241, p. 90, Springer-Verlag, 1985.

106. Paczko, G., Lefdal, P.M. and Peters, N.: *Twenty-First Symposium (International) on Combustion*, p. 739, The Combustion Institute, 1988.

107. Kailasanath, K. and Oran, E.S.: Prog. Astron. Aeron. 105, 167 (1985).

108. Sloane, T.M. and Schoene, A.Y.: *Twenty-Second Symposium (International) on Combustion*, p. 1669, The Combustion Institute, 1989.

109. Kee, R.J., Grcar, J.F., Smooke, M.D. and Miller, J.A.: *A Fortran Program for Modeling Steady Laminar One-Dimensional Premixed Flames*, Sandia Report SAND85-8240, 1985.

110. Grcar, J.F., Kee, R.J., Smooke, M.D. and Miller, J.A.: *Twenty-First Symposium (International) on Combustion*, p. 1773, The Combustion Institute, 1988.

111. Kee, R.J., Rupley, F.M. and Miller, J.A.: *CHEMKIN-II: A Fortran Chemical Kinetics Package for the Analysis of Gas-Phase Chemical Kinetics*, Sandia Report SAND89-8009, 1989.

112. Dowdy, D.R.: The Importance of Mass and Energy Conservation in Finite-Difference Flame Modelling (in preparation).

113. Dowdy, D.R. and Worrell, J.K.: in preparation.

114. Hennessy, R.J., Robinson, C. and Smith, D.B.: *Twenty-First Symposium (International) on Combustion*, p. 761, The Combustion Institute, 1988.

115. Tsang, W. and Hampson, R.F.: J. Phys. Chem. Ref. Data 15, 1087 (1986).

116. Tsang, W. and Hampson, R.F.: J. Phys. Chem. Ref. Data 17, 887 (1988).

117. Pirraglia, A.N., Michael, J.V., Sutherland, J.W. and Klemm, R.B.: J. Phys. Chem. 93, 282 (1989).

118. Natarajan, K. and Roth, P.: Combust. Flame 70, 267 (1987).

119. Michael, J.V. and Sutherland, J.W.: J. Phys. Chem. 92, 3853 (1988).

120. Baulch, D.L.: Private communication.

121. Hsu, K.-J., Anderson, S.M., Durant, J.L. and Kaufman, F.: J. Phys. Chem. 93, 1018 (1989).

122. Baulch, D.L., Drysdale, D.D., Horne, D.G. and Lloyd, A.G.: *Evaluated Kinetic Data for High Temperature Reactions* Vol. 1, Butterworths, 1972.

123. Lightfoot, P.D., Veyret, B. and Lesclaux, R.: Chem. Phys. Lett. 150, 120 (1988).

124. Keyser, L.F.: J. Phys. Chem. 92, 1193 (1988).

125. Warnatz, J.: *Combustion Chemistry*, (W.C. Gardiner, Ed.), Springer-Verlag, New York, 1984.

126. Timonen, R.S., Ratajczak, E., Gutman, D. and Wagner, A.F.: J. Phys. Chem. 91, 5325 (1987).

127. Timonen, R.S., Ratajczak, E. and Gutman, D.: J. Phys. Chem. 92, 651 (1987).

128. Temps, F. and Wagner, H.Gg.: Ber. Bunsenges. Phys. Chem. 88, 415 (1984).

129. Choudhury, T.K. and Lin, M.C.: Combust. Sci. Technol. 64, 19 (1989).

130. Zabarnick, S., Fleming, J.W. and Lin, M.C.: Int. J. Chem. Kinet. 20, 117 (1988).

131. Hsu, D.S.Y., Shaub, W.M., Creamer, T., Gutman, D. and Lin, M.C.: Ber. Bunsenges. Phys. Chem. 87, 909 (1983).

132. Clark, T.C. and Dove, J.E.: Can. J. Chem. 51, 2147 (1973).

133. Cohen, N. and Benson, S.W.: J. Phys. Chem. 91, 162 (1987).

134. Sutherland, J.W., Michael, J.V. and Klemm, R.B.: J. Phys. Chem. 90, 5941 (1986).

135. Bhaskaran, K.A., Frank, P. and Just, Th.: Proc. Int. Shock Tube Symp. 12, 503 (1980).

136. Brouard, M., MacPherson, M.T. and Pilling, M.J.: J. Phys. Chem. 93, 4047 (1989).

137. Slagle, I.R., Gutman, D., Davies, J.W. and Pilling, M.J.: J. Phys. Chem. 92, 2455 (1988).

138. Roth, P. and Just, Th.: *Twentieth Symposium (International) on Combustion*, p. 807, The Combustion Institute, 1985.

139. Fenimore, C.P.: *Twelfth Symposium (International) on Combustion*, p. 463, The Combustion Institute, 1969.

140. Frenklach, M. and Bornside, D.E.: Combust. Flame 56, 1 (1984).

141. Slagle, I.R., Sarzynski, D. and Gutman, D.: J. Phys. Chem. 91, 4375 (1987).

142. Choudhury, T.K., Sanders. W.A. and Lin, M.C.: J. Chem. Soc., Faraday Trans. 2, 85, 801 (1989).

143. Baggott, J.E., Frey, H.M., Lightfoot, P.D. and Walsh, R.: J. Phys. Chem. 91, 3386 (1987).

144. Colket, M.B., Naegeli, D.W. and Glassman, I.: *Sixteenth Symposium (International) on Combustion*, p. 1023, The Combustion Institute, 1977.

145. Wantuck, P.J., Oldenborg, R.C., Baughcum, S.L. and Winn, K.R.: *Twenty-Second Symposium (International) on Combustion*, p. 973, The Combustion Institute, 1989.

146. Wantuck, P.J., Oldenborg, R.C., Baughcum, S.L. and Winn, K.R.: J. Phys. Chem. 91, 4653 (1987).

147. Hoyermann, K., Loftfield, N.S., Sievert, R. and Wagner, H.Gg.: *Eighteenth Symposium (International) on Combustion*, p. 831, The Combustion Institute, 1981.

148. Miller, J.A., Mitchell, R.E., Smooke, M.D. and Kee, R.J.: *Nineteenth Symposium (International) on Combustion*, p. 181, The Combustion Institute, 1982.

149. Tully, F.P., Droege, A.T., Koszykowski, M.L. and Melius, C.F.: J. Phys. Chem. 90, 691 (1986).

150. Herron, J.T.: J. Phys. Chem. Ref. Data 17, 967 (1988).

151. McAdam, K.G. and Walker, R.W.: J. Chem. Soc., Faraday Trans. 2, 83, 1509 (1987).

152. Stewart, P.H., Larson, C.W. and Golden, D.M.: Combust. Flame 75, 25 (1989).

153. Camilleri, P., Marshall, R.M. and Purnell, J.H.: J. Chem. Soc., Faraday Trans. 1, 70, 1434 (1974).

154. Slagle, I.R., Sarzynski, D., Gutman, D., Miller, J.A. and Melius, C.F.: J. Chem. Soc., Faraday Trans. 2, 84, 491 (1988).

155. Weissman, M.A. and Benson, S.W.: J. Phys. Chem. 92, 4080 (1988).

156. Tully, F.P.: Chem. Phys. Lett. 143, 510 (1988).

157. Mahmud, K., Marshall, P. and Fontijn, A.: J. Phys. Chem. 91, 1568 (1987).

158. Cooke, D.F. and Williams, A.: *Thirteenth Symposium (International) on Combustion*, p. 757, The Combustion Institute, 1971.

159. Heinemann, P., Hofmann-Sievert, R. and Hoyermann, K.: *Twenty-First Symposium (International) on Combustion*, p. 865, The Combustion Institute, 1988.

160. Liu, A., Mulac, W.A. and Jonah, C.D.: J. Phys. Chem. 92, 5942 (1988).

161. Mahmud, K. and Fontijn, A.: J. Phys. Chem. 91, 1918 (1987).

162. Frank, P., Bhaskaran, K.A. and Just, Th.: *Twenty-First Symposium (International) on Combustion*, p. 885, The Combustion Institute, 1988.

163. Stephens, J.W., Hall, J.L., Solka, H., Yan, W.-B., Curl, R.F. and Glass, G.P.: J. Phys. Chem. 91, 5740 (1987).

164. Vinckier, C. and Debruyn, W.: J. Phys. Chem. 83, 2057 (1979).

165. Shaub, W.M., Hsu, D.S.Y., Burks, T.L. and Lin, M.C.: *Eighteenth Symposium (International) on Combustion*, p. 811, The Combustion Institute, 1981.

166. Böhland, T. and Temps, F.: Ber. Bunsenges. Phys. Chem. 88, 459 (1984).

167. Böhland, T., Temps, F. and Wagner, H.Gg.: Ber. Bunsenges. Phys. Chem 88, 1222 (1984).

168. Becker, K.H., Engelhardt, B. and Wiesen, P.: Chem. Phys. Lett. 154, 342 (1989).

169. Glarborg, P., Miller, J.A. and Kee, R.J.: Combust. Flame 65, 177 (1986).

170. Hidaka, Y., Shiba, S., Takuma, H. and Suga, M.: Int. J. Chem. Kinet. 17, 441 (1985).

171. Warnatz, J.: Ber. Bunsenges. Phys. Chem. 87, 1008 (1983).

172. Gulati, S.K. and Walker, R.W.: J. Chem. Soc., Faraday Trans. 2, 84, 401 (1988).

173. Coffee, T.P., Kotlar, A.J. and Miller, M.S.: Combust. Flame 54, 155 (1983).

174. Coffee, T.P.: Combust. Flame 55, 161 (1984).

175. Ronney, P.D. and Sivashinsky, G.I.: SIAM J. Appl. Math. 49, 1029 (1989).

176. Clavin, P.: Prog. Energy Combust. Sci. 11, 1 (1985).

177. Searby, G. and Quinard, J.: Combust. Flame 82, 298 (1990).

178. Sen, A.K. and Ludford, G.S.S.: *Eighteenth Symposium (International) on Combustion*, p. 417, The Combustion Institute, 1981.

179. Sen, A.K. and Ludford, G.S.S.: *Nineteenth Symposium (International) on Combustion*, p. 267, The Combustion Institute, 1982.

180. Shebeko, Yu.N., Korol'chenko, A.Ya., Bratov, A.N. and Shamonin, V.G.: Fizika Goreniya i Vzryva 25, 54 (1989).

181. Fukutani, S. and Jinno, H.: in *Notes on Numerical Fluid Mechanics* Vol. 6, Vieweg, 1982, p. 167.

182. Rogg, B. and Peters, N.: Combust. Flame 79, 402 (1990).

183. Kennel, C., Göttgens, J. and Peters, N.: *Twenty-Third Symposium (International) on Combustion*, p. 479, The Combustion Institute, 1991.

184. Fristrom, R.M.: Combust. Flame 2, 103 (1958).

185. Gibbs, G.J. and Calcote, H.F.: J. Chem. Eng. Data 4, 226 (1959).

186. Botha, J.P. and Spalding, D.B.: Proc. R. Soc. Lond. A225, 71 (1954).

187. Yamaoka, I. and Tsuji, H.: *Twentieth Symposium (International) on Combustion*, p. 1883, The Combustion Institute, 1985.

188. Gerstein, M., Levine, O. and Wong, E.L.: J. Am. Chem. Soc. 73, 418 (1951).

189. Dixon-Lewis, G. and Wilson, M.J.G.: Trans. Faraday Soc. 46, 1106 (1951).

190. Diederichsen, J. and Wolfhard, H.G.: Trans. Faraday Soc. 52, 1102 (1956).

191. Rosser, W.A., Wise, H. and Miller, J.: *Seventh Symposium (International) on Combustion*, p. 175, Butterworths, London, 1959.

192. Clingman, W.H., Brokaw, R.S. and Pease, R.N.: *Fourth Symposium (International) on Combustion*, p. 310, Williams and Wilkins, Baltimore, Maryland, 1953.

193. Gilbert, M.: *Sixth Symposium (International) on Combustion*, p. 74, Reinhold, New York, 1957.

194. Morgan, G.H. and Kane, W.R.: *Fourth Symposium (International) on Combustion*, p. 313, Williams and Wilkins, Baltimore, Maryland, 1953.

195. Fells, I. and Rutherford, H.G.: Combust. Flame 13, 130 (1969).

196. Lindow, R.: Brennstoff Wärme Kraft 20, 8 (1968).

197. Reed, S.B., Mineur, J. and McNaughton, J.P.: J. Inst. Fuel 44, 149 (1971).

198. Edmondson, H., Heap, M.P. and Pritchard, R.: Combust. Flame 14, 195 (1970).

199. Pritchard, R., Edmondson, H. and Heap, M.P.: Combust. Flame 18, 13 (1972).

200. Andrews, G.E. and Bradley, D.: Combust. Flame 20, 77 (1973).

201. Rallis, C.J. and Garforth, A.M.: Prog. Energy Combust. Sci. 6, 303 (1980).

202. Groff, E.G.: Combust. Flame 48, 51 (1982).

203. Robinson, C.: Private communication.

204. Clavin, P. and Joulin, G.: in *Turbulent Reactive Flows*, (R. Borghi and S.N.B. Murthy, Eds.), Lecture Series in Engineering, Springer-Verlag, Berlin, 1989, p. 214.

205. Fuller, L.E., Parks, D.J. and Fletcher, E.A.: Combust. Flame 13, 455 (1969).

206. Reynolds, T.W. and Gerstein, M.: *Third Symposium on Combustion, Flame and Explosion Phenomena*, p. 190, Williams and Wilkins, Baltimore, Maryland, 1949.

207. Raezer, S.D. and Olsen, H.L.: Combust. Flame 6, 227 (1962).

208. Rallis, C.J. and Garforth, A.M.: Acta Astronautica 3, 879 (1976).

209. Massey, B.S.: *Mechanics of Fluids*, 4th edition, Van Nostrand Reinhold, 1979.

210. Clavin, P.: *Theory of Flames* in Nato ASI, Ser. E; Disorder and Mixing, (E. Guyon et al. Eds.), p. 293, 1988.

211. Eteng, E., Ludford, G.S.S. and Matalon, M.: Phys. Fluids 29, 2172 (1986).

212. Sahay, R.N., Sharma, S.P. and Gupta, C.P.: Proc. 3rd Natl. Conf. I.C. Engines Combust., 1976, p. 369.

213. Kaskan, W.E.: *Sixth Symposium (International) on Combustion*, p. 134, Reinhold, New York, 1957.

214. Tsuji, H. and Yamaoka, I.: *Nineteenth Symposium (International) on Combustion*, p. 1533, The Combustion Institute, 1982.

215. Mizomoto, M. and Yoshida, H.: Combust. Flame 70, 47 (1987).

216. Sato, J.: *Nineteenth Symposium (International) on Combustion*, p. 1541, The Combustion Institute, 1982.

217. Mizomoto, M., Asaka, Y., Ikai, S. and Law, C.K.: *Twentieth Symposium (International) on Combustion*, p. 1933, The Combustion Institute, 1985.

218. Law, C.K., Cho, P., Mizomoto, M. and Yoshida, H.: *Twenty-First Symposium (International) on Combustion*, p. 1803, The Combustion Institute, 1988.

219. Hoffmann-Berling, E., Günther, R. and Leuckel, W.: *Nineteenth Symposium (International) on Combustion*, p. 433, The Combustion Institute, 1982.

220. Rogg, B.: in Numerical and Applied Mathematics, (W.F. Ames, Ed.), J.C. Balzer AG, 1989, p. 159.

221. Sohrab, S.H., Ye, Z.Y. and Law, C.K.: *Twentieth Symposium (International) on Combustion*, p. 1957, The Combustion Institute, 1985.

222. Bechtel, J.H., Blint, R.J., Dasch, C.J. and Weinberger, D.A.: Combust. Flame 42, 197 (1981).

223. Gardiner, W.C.: Paper presented at AGRE Combustion Workshop, British Gas Midlands Research Station, May 30-31 1989.

224. Putnam, A.A. and Jensen, R.A.: *Third Symposium on Combustion, Flame and Explosion Phenomena*, p. 89, Williams and Wilkins, Baltimore, Maryland, 1949.

225. Harris, M.E., Grumer, J., von Elbe, G. and Lewis, B.: *Third Symposium on Combustion, Flame and Explosion Phenomena*, p. 80, Williams and Wilkins, Baltimore, Maryland, 1949.

226. Strehlow, R.A., Noe, K.A. and Wherley, B.L.: *Twenty-First Symposium (International) on Combustion*, p. 1899, The Combustion Institute, 1988.

227. Ronney, P.D. and Wachman, H.Y.: Combust. Flame 62, 107 (1985).

228. Ronney, P.D.: *Twenty-Second Symposium (International) on Combustion*, p. 1615, The Combustion Institute, 1989.

229. Law, C.K. and Egolfopoulos, F.N.: *Twenty-Third Symposium (International) on Combustion*, p. 413, The Combustion Institute, 1991.

230. Lloyd, S.A. and Weinberg, F.J.: Nature 257, 367 (1975).

231. Peters, N. and Smooke, M.D.: Combust. Flame 60, 171 (1985).

232. Lakshmisha, K.N., Paul, P.J. and Mukunda, H.S.: *Twenty-Third Symposium (International) on Combustion*, p. 433, The Combustion Institute, 1991.

233. Abdel-Gayed, R.G., Bradley, D., Hamid, M.N. and Lawes, M.: *Twentieth Symposium (International) on Combustion*, p. 505, The Combustion Institute, 1985.

234. Abdel-Gayed, R.G., Bradley, D. and Lawes, M.: Proc. R. Soc. Lond. A414, 389 (1987).

235. Weinberg, F.J.: Phys. Bull. 33, 124 (1982).

APPENDIX

Raw experimental data

This section contains the raw data for the experimental work on expanding spherical flames and flames in stagnation-point flow.

For the expanding flame work, the data listed for each run include the initial temperature, the number of points omitted in the analysis and the values obtained for S_b° and b. The value of the burning velocity S_u°, obtained by multiplying S_b° by the density ratio, is also given. These data are given across the stoichiometric range of mixtures with air of hydrogen, methane, ethane, propane and ethylene. Data are also provided for stoichiometric hydrogen/air mixtures diluted with nitrogen and for stoichiometric methane/air mixtures at varying pressure. There are data from at least two runs for each stoichiometry, dilution or pressure. For each set of conditions, average values of the burning velocity S_u° and flame relaxation parameter b are listed, along with the calculated flame thickness constant k. The Markstein length L determined from b and k is also given.

Finally, a typical set of raw radius *vs* time data from an expanding spherical flame run is listed.

For the stagnation flame data the one-dimensional burning velocity and the Markstein length are given with respect to both of the measured burning velocities. In this case the uncertainties from the least squares fit are also listed since they are relatively large.

Expanding spherical flames

Hydrogen/air

Stoich	Run	T_u K	pts omtd	S_b° ms^{-1}	b mm	S_u° ms^{-1}	S_u° ms^{-1}	b mm	k mm	L mm
0.3	h48	297	2	0.267	-2.564	0.082	0.084	-2.46	.010*	-.388
	h49	297	2	0.281	-2.363	0.086				
0.4	h46	295	1	0.746	-2.165	0.190	0.188	-2.16	.113	-.298
	h47	296	2	0.727	-2.159	0.185				
0.5	h43	295	1	1.571	-1.804	0.344	0.340	-1.82	.284	-.232
	h44	296	2	1.524	-1.843	0.335				
0.6	h1	298	0	3.335	-1.023	0.653	0.644	-0.98	.459	-.139
	h2	296	0	3.214	-1.025	0.625				
	h3	297	0	3.348	-0.845	0.653				
	h4	297	0	3.306	-1.036	0.645				
0.7	h5	295	0	5.596	-0.489	0.981	0.980	-0.49	.575	-.091
	h6	296	0	5.570	-0.484	0.979				
0.8	h7	297	0	8.655	0.376	1.403	1.387	0.09	.645	-.044
	h8	295	7	8.429	0.101	1.358				
	h39	296	7	8.685	0.034	1.403				
	h41	295	4	8.591	-0.144	1.384				
0.9	h9	295	2	11.847	0.881	1.782	1.778	0.71	.716	.002
	h10	297	1	11.713	0.534	1.773				
1.0	h11	296	1	14.996	1.162	2.162	2.130	1.09	.753	.027
	h12	297	1	14.512	1.019	2.098				
1.1	h13	298	0	16.573	1.007	2.401	2.416	1.08	.726	.029
	h14	298	1	16.777	1.143	2.431				
1.2	h15	295	1	17.828	1.148	2.612	2.624	1.17	.653	.041
	h16	296	0	17.934	1.194	2.635				
1.3	h17	295	1	18.809	1.599	2.825	2.793	1.31	.602	.056
	h18	296	0	18.124	0.963	2.731				
	h40	296	1	18.741	1.381	2.824				
1.4	h19	298	1	18.353	1.493	2.861	2.850	1.49	.565	.075
	h20	296	2	18.313	1.486	2.839				
1.5	h21	296	1	17.558	1.507	2.806	2.790	1.47	.551	.077
	h22	296	1	17.354	1.427	2.773				
1.6	h23	297	1	16.219	1.588	2.687	2.668	1.51	.519	.085
	h24	295	1	16.084	1.438	2.649				
1.7	h25	295	1	14.830	1.765	2.531	2.535	1.64	.503	.101
	h26	297	2	14.789	1.509	2.539				
1.8	h27	295	3	13.141	1.755	2.333	2.339	1.75	.485	.115
	h28	296	0	13.184	1.746	2.347				
	h45	296	1	13.124	1.736	2.336				
1.9	h29	294	0	11.475	1.927	2.117	2.119	1.86	.462	.133
	h30	297	0	11.398	1.799	2.121				
2.0	h31	296	2	9.768	2.196	1.896	1.895	2.15	.438	.170
	h32	296	4	9.759	2.100	1.894				
2.1	h33	294	3	7.961	2.490	1.614	1.627	2.50	.404	.216
	h34	296	2	8.041	2.517	1.640				
2.2	h35	297	7	6.440	3.233	1.388	1.376	3.09	.379	.295
	h36	294	8	6.379	2.956	1.363				
2.3	h37	294	19	4.707	4.708	1.066	1.098	4.85	.343	.516
	h38	297	19	4.943	4.999	1.129				

* Estimated value

Stoichiometric hydrogen/air at various dilutions

%N_2	Run	T_u K	pts omtd	S_b° ms^{-1}	b mm	S_u° ms^{-1}	S_u° ms^{-1}	b mm	k mm	L mm
0	h11	296	1	14.996	1.162	2.162	2.130	1.09	.759	.024
	h12	297	1	14.512	1.019	2.098				
5	dh24	296	3	12.629	1.147	1.864	1.847	0.97	.744	.017
	dh25	297	1	12.364	0.784	1.830				
10	dh22	298	1	10.596	0.659	1.615	1.609	0.66	.727	-.005
	dh23	296	1	10.581	0.668	1.603				
15	dh26	298	1	9.038	0.586	1.419	1.422	0.66	.711	-.004
	dh27	297	3	9.094	0.738	1.424				
20	dh20	298	2	7.521	0.531	1.222	1.214	0.56	.707	-.012
	dh21	297	3	7.440	0.589	1.205				
25	dh18	298	1	6.233	0.335	1.052	1.034	0.23	.686	-.038
	dh19	297	1	6.032	0.130	1.015				
30	dh16	298	0	4.991	0.134	0.879	0.875	0.18	.668	-.043
	dh17	297	1	4.952	0.229	0.870				
35	dh14	299	2	3.803	-0.062	0.705	0.709	0.03	.660	-.058
	dh15	298	0	3.852	-0.004	0.712				
40	dh5	298	0	2.851	-0.283	0.555	0.561	-0.21	.653	-.084
	dh7	298	3	2.910	-0.139	0.567				
45	dh12	298	4	1.930	-1.189	0.398	0.405	-1.04	.647	-.174
	dh13	298	4	1.993	-0.892	0.411				
50	dh3	299	6	1.263	-2.639	0.279	0.284	-2.48	.632	-.342
	dh4	298	9	1.360	-1.554	0.299				
	dh6	299	15	1.246	-3.247	0.275				
55	dh9	299	11	0.796	-3.156	0.188	0.187	-3.18	.582	-.444
	dh10	298	12	0.788	-3.205	0.186				
60	dh28	298	27	0.437	-3.810	0.111	0.114	-3.54	.498	-.515
	dh29	298	31	0.457	-3.276	0.117				

Stoichiometric methane/air at various pressures

p atm	Run	T_u K	pts omtd	S_b° ms^{-1}	b mm	S_u° ms^{-1}	S_u° ms^{-1}	b mm	k mm	L mm
0.25	mp20	297	12	3.818	8.499	0.512	0.510	8.33	.222	.542
	mp21	297	7	3.779	8.163	0.507				
0.50	mp2	296	11	3.300	4.681	0.439	0.441	4.92	.283	.308
	mp4	294	7	3.347	5.156	0.442				
1.0	s13	295	2	2.640	1.171	0.348	0.353	1.80	.291	.100
	s15	296	0	2.700	2.123	0.357				
	s16	298	1	2.729	2.099	0.363				
	s17	293	4	2.614	1.805	0.342				
	s18	298	1	2.672	1.809	0.355				
2.0	mp14	297	2	2.065	0.785	0.272	0.276	1.05	.222	.054
	mp15	297	5	2.123	1.312	0.280				

Methane/air

Stoich	Run	T_u K	pts omtd	S_b° ms^{-1}	b mm	S_u° ms^{-1}	S_u° ms^{-1}	b mm	k mm	L mm
0.575	m31	298	10	0.171	-2.597	0.032	0.034	-1.65	.132	-.168
	m38	298	6	0.191	-0.612	0.036				
	m47	295	0	0.182	-1.742	0.034				
0.60	m4	298	5	0.293	-0.674	0.054	0.055	-0.68	.144	-.075
	m27	299	3	0.306	-0.677	0.056				
0.65	m3	296	6	0.571	-0.162	0.099	0.099	0.10	.168	-.006
	m29	299	4	0.573	0.363	0.100				
0.7	m22	298	4	0.890	0.740	0.147	0.146	0.86	.204	.054
	m23	296	1	0.881	1.085	0.145				
	m40	298	6	0.871	0.651	0.144				
	m46	295	3	0.889	0.970	0.146				
0.8	m14	298	2	1.513	0.483	0.228	0.229	0.79	.254	.040
	m17	297	1	1.508	0.587	0.227				
	m42	297	1	1.522	0.842	0.229				
	m49	297	1	1.549	1.251	0.233				
0.9	m8	298	0	2.176	1.309	0.305	0.302	1.00	.284	.050
	m9	297	6	2.141	0.695	0.299				
1.0	s13	295	2	2.640	1.171	0.348	0.353	1.80	.291	.100
	s15	296	0	2.700	2.123	0.357				
	s16	298	1	2.729	2.099	0.363				
	s17	293	4	2.614	1.805	0.342				
	s18	298	1	2.672	1.809	0.355				
1.07	m33	297	5	2.727	1.595	0.358	0.364	1.92	.261	.109
	m34	297	2	2.821	2.237	0.371				
	m45	295	5	2.734	1.670	0.357				
	m54	297	2	2.820	2.196	0.371				
1.085	m36	297	7	2.835	2.439	0.373	0.364	2.06	.251*	.119
	m37	297	5	2.745	2.119	0.361				
	m39	296	5	2.724	1.742	0.357				
	m41	299	6	2.674	1.938	0.366				
1.1	m6	298	6	2.792	2.197	0.369	0.364	2.24	.241	.131
	m7	296	4	2.875	2.655	0.378				
	m43	295	4	2.780	2.518	0.364				
	m55	293	8	2.656	1.584	0.346				
1.115	m52	296	5	2.694	1.912	0.355	0.361	2.13	.229*	.125
	m53	298	4	2.765	2.341	0.367				
1.2	m11	297	14	2.420	3.296	0.326	0.325	3.55	.162	.227
	m13	296	6	2.497	4.685	0.335				
	m51	296	10	2.338	2.672	0.314				
1.25	m56	297	9	2.029	4.124	0.277	0.271	3.82	.136	.250
	m59	296	12	1.951	3.520	0.265				
1.3	m16	298	12	1.590	6.251	0.220	0.216	5.78	.118	.390
	m20	298	13	1.521	5.312	0.211				
1.35	m24	297	31	1.225	11.401	0.171	0.175	11.39	.099	.788
	m25	298	25	1.277	11.375	0.179				

* Calculated by linear interpolation

Ethane/air

Stoich	Run	T_u K	pts omtd	S_b° ms^{-1}	b mm	S_u° ms^{-1}	S_u° ms^{-1}	b mm	k mm	L mm
0.6	e14	295	9	0.814	7.979	0.142	0.138	7.12	.188	.605
	e15	295	2	0.765	6.265	0.133				
0.65	e34	297	11	1.062	4.475	0.176	0.177	4.89	.214	.386
	e36	295	8	1.093	5.475	0.180				
	e69	295	14	1.056	4.712	0.174				
0.7	e12	297	7	1.357	3.733	0.213	0.211	2.66	.247	.189
	e13	296	8	1.327	2.853	0.208				
0.8	e10	294	8	2.016	2.268	0.287	0.286	2.12	.286	.131
	e11	296	10	1.995	1.944	0.286				
0.9	e8	295	4	2.669	2.202	0.354	0.353	1.98	.309	.111
	e9	298	7	2.631	1.766	0.352				
1.0	e3	296	0	3.191	2.197	0.403	0.402	2.10	.304	.113
	e4	296	5	3.262	2.504	0.412				
	e5	298	5	3.122	1.822	0.397				
	e6	295	0	3.150	2.044	0.397				
	e7	298	4	3.164	1.908	0.402				
1.1	e16	297	3	3.312	1.634	0.414	0.406	1.54	.254	.080
	e17	298	3	3.231	1.649	0.405				
	e51	294	3	3.218	1.325	0.399				
1.2	e48	297	2	3.046	1.065	0.386	0.385	1.27	.178	.069
	e49	295	4	3.030	1.167	0.381				
	e50	296	1	3.063	1.584	0.387				
1.3	e52	296	8	2.422	0.999	0.311	0.314	0.97	.125	.054
	e53	294	3	2.473	0.938	0.316				
1.4	e45	297	1	1.803	0.908	0.237	0.230	0.40	.103	.019
	e46	297	1	1.731	0.256	0.228				
	e47	297	2	1.711	0.023	0.225				
1.5	e42	296	1	1.175	0.744	0.157	0.149	-0.05	.105	-.010
	e43	295	1	1.089	-0.338	0.145				
	e44	296	4	1.094	-0.599	0.146				
	e54	295	1	1.105	-0.302	0.148				
1.6	e40	295	0	0.726	-0.072	0.099	0.100	-0.09	.096	-.013
	e41	295	1	0.735	-0.036	0.100				
	e55	298	0	0.742	-0.152	0.102				
1.7	e31	296	1	0.514	-0.328	0.072	0.071	-0.37	.094	-.033
	e32	294	1	0.518	-0.047	0.072				
	e57	296	6	0.484	-0.725	0.068				
1.8	e58	296	11	0.316	-2.188	0.045	0.045	-2.09	.098	-.157
	e60	296	6	0.306	-1.987	0.044				
1.9	e38	296	0	0.207	-1.393	0.031	0.029	-2.31	.109	-.178
	e63	296	12	0.173	-3.225	0.026				

Propane/air

Stoich	Run	T_u K	pts omtd	S_b^o ms^{-1}	b mm	S_u^o ms^{-1}	S_u^o ms^{-1}	b mm	k mm	L mm
0.65	t2	296	43	0.850	3.504	0.138	0.165	6.80	.252	.532
	t3	297	44	0.938	5.398	0.153				
	p1	297	21	1.155	9.730	0.188				
	p28	295	36	1.108	8.563	0.180				
0.7	p3	295	8	1.252	3.630	0.193	0.206	4.60	.260	.335
	p4	296	7	1.424	5.983	0.220				
	p7	297	18	1.324	4.192	0.205				
0.75	p29	295	9	1.643	3.732	0.241	0.249	4.18	.283	.287
	p31	295	9	1.741	4.633	0.256				
0.8	p5	297	5	2.151	4.889	0.304	0.285	3.13	.296	.200
	p6	297	9	1.877	1.375	0.265				
0.9	p8	295	7	2.544	2.117	0.332	0.342	2.58	.316	.148
	p9	297	7	2.681	3.044	0.352				
1.0	p10	296	10	3.032	1.870	0.377	0.376	1.95	.312	.102
	p11	296	12	3.016	2.036	0.375				
1.1	p12	296	7	3.219	1.787	0.394	0.389	1.61	.276	.082
	p13	294	9	3.157	1.439	0.384				
1.2	p14	298	8	2.852	0.556	0.355	0.359	0.80	.191	.038
	p17	296	8	2.936	1.043	0.363				
1.3	p16	298	4	2.407	-0.086	0.304	0.300	-0.14	.128	-.017
	p18	297	4	2.342	-0.184	0.295				
1.35	p34	296	0	2.091	-0.089	0.265	0.261	-0.05	.117	-.011
	p35	295	2	2.026	-0.006	0.256				
1.4	p19	298	5	1.764	-0.960	0.227	0.221	-0.92	.102	-.065
	p20	296	4	1.678	-0.882	0.215				
1.45	p30	296	1	1.291	-1.721	0.167	0.167	-1.66	.105	-.114
	p32	296	0	1.291	-1.607	0.167				
1.5	p21	296	6	0.988	-2.313	0.129	0.131	-2.85	.094	-.192
	p22	295	6	0.988	-3.592	0.128				
	p27	295	6	1.028	-2.820	0.134				
	p33	296	6	1.030	-2.682	0.134				
1.55	p23	295	5	0.843	-1.952	0.111	0.114	-2.18	.087	-.149
	p24	297	5	0.901	-2.404	0.117				
1.6	p25	295	4	0.627	-3.613	0.083	0.088	-3.18	.082	-.217
	p26	296	1	0.693	-2.742	0.092				
1.65	p36	294	1	0.537	-2.756	0.072	0.074	-7.99	.075	-.542
	p37	296	8	0.556	-13.216	0.075				

Ethylene/air

Stoich	Run	T_u K	pts omtd	S_b° ms^{-1}	b mm	S_u° ms^{-1}	S_u° ms^{-1}	b mm	k mm	L mm
0.5	ey18	297	2	0.742	11.951	0.141	0.134	10.54	.175	.982
	ey19	296	2	0.667	9.120	0.126				
0.55	ey45	296	16	0.975	3.610	0.173	0.173	3.63	.214	.303
	ey46	295	15	0.974	3.643	0.172				
0.6	ey14	295	9	1.356	1.999	0.226	0.234	2.70	.247	.205
	ey15	295	6	1.399	2.804	0.233				
	ey49	297	6	1.452	3.297	0.243				
0.7	ey12	295	0	2.394	2.344	0.3584	0.358	2.27	.293	.148
	ey13	295	2	2.391	2.203	0.3579				
0.8	ey8	298	6	3.553	1.846	0.492	0.481	1.79	.321	.101
	ey10	296	1	3.408	1.756	0.469				
	ey50	297	4	3.483	1.768	0.481				
0.9	ey7	296	4	4.353	1.665	0.561	0.565	1.74	.320	.091
	ey11	295	3	4.432	1.818	0.569				
1.0	ey2	297	2	5.137	1.584	0.634	0.634	1.53	.299	.076
	ey3	296	4	5.122	1.441	0.631				
	ey4	296	5	5.093	1.383	0.627				
	ey5	298	2	5.199	1.693	0.644				
1.1	ey20	295	1	5.429	1.232	0.652	0.656	1.20	.253	.057
	ey21	297	1	5.462	1.167	0.660				
1.2	ey22	297	0	5.430	1.161	0.654	0.649	1.11	.188	.055
	ey23	297	0	5.339	1.054	0.643				
1.3	ey24	295	1	4.870	0.944	0.588	0.592	0.98	.125	.052
	ey25	295	1	4.933	1.006	0.595				
1.4	ey26	296	1	4.042	0.779	0.495	0.493	0.72	.088	.039
	ey27	296	0	4.062	0.832	0.497				
	ey48	296	5	3.990	0.562	0.488				
1.5	ey28	296	1	2.969	0.637	0.368	0.372	0.58	.087	.031
	ey29	296	1	3.035	0.519	0.376				
1.6	ey30	297	1	2.186	0.393	0.276	0.273	0.42	.097	.020
	ey31	295	1	2.142	0.442	0.269				
1.7	ey32	295	0	1.638	0.511	0.208	0.212	0.68	.093	.037
	ey33	297	2	1.679	0.856	0.215				
1.8	ey34	296	3	1.366	1.801	0.177	0.170	1.15	.092	.069
	ey35	294	0	1.282	0.676	0.165				
	ey47	297	4	1.297	0.971	0.169				
1.9	ey37	297	5	1.049	1.348	0.139	0.138	1.36	.088	.084
	ey38	295	2	1.031	1.377	0.136				
2.0	ey39	296	1	0.872	1.827	0.117	0.115	1.66	.086	.106
	ey40	295	4	0.848	1.501	0.113				
2.1	ey41	295	9	0.679	1.349	0.093	0.096	2.05	.086	.134
	ey42	295	8	0.718	2.749	0.098				
2.2	ey43	297	3	0.594	2.147	0.083	0.084	2.78	.083	.188
	ey44	294	1	0.613	3.421	0.085				

Raw radius *vs* time data for stoichiometric methane/air run s15

t/ms	r/mm
0.5089591	1.641085
1.017662	2.2252
1.529586	3.11528
2.061589	3.908008
2.589974	4.756365
3.107984	5.882872
3.622101	6.814675
4.128246	8.01072
4.63557	8.984244
5.14506	10.16638
5.654717	11.36243
6.164637	12.58629
6.675081	13.78233
7.186222	14.92275
7.698288	16.28568
8.211384	17.32875
8.724481	18.52479
9.237578	19.79037
9.749056	21.12549
10.25933	22.34935
10.77063	23.64275
11.28257	24.97787
11.7975	26.17392
12.3139	27.42559
12.8286	28.69117
13.3427	29.95675
13.85875	31.37532
14.37536	32.59918
14.89171	33.90648
15.40803	35.35286
15.92561	36.60454

Flames in stagnation-point flow

Stoich	from S_{L1}		from $S_{u,r}$	
	$S_{u_1}^{o}$ ms	L_1 mm	$S_{u_1}^{o}$ ms	L mm
0.71	.161 ± .004	-.110 ± .088	.116 ± .003	.084 ± .065
0.81	.269 ± .009	-.052 ± .052	.232 ± .019	.333 ± .105
0.83	.236 ± .007	-.253 ± .037	.230 ± .014	.143 ± .073
1.02	.399 ± .006	-.116 ± .016	.350 ± .030	.198 ± .082
1.06	.366 ± .008	-.249 ± .026	.335 ± .021	.198 ± .071
1.15	.345 ± .006	-.252 ± .021	.322 ± .014	-.009 ± .050
1.22	.342 ± .021	-.233 ± .078	.301 ± .015	.109 ± .056
1.31	.261 ± .003	-.083 ± .024	.236 ± .010	.371 ± .069
1.31	.258 ± .004	-.141 ± .033	.237 ± .011	.309 ± .099